Technical Report
TR-18-14
December 2018

Corrosion morphology of copper in anoxic sulphide environments

Andrew Gordon
Helen Pahverk
Eric Börjesson
Lena Sjögren
Oskar Karlsson
Hans Bergqvist
Fredrik Lindberg
Adam Johannes Johansson

SVENSK KÄRNBRÄNSLEHANTERING AB

SWEDISH NUCLEAR FUEL
AND WASTE MANAGEMENT CO

Box 3091, SE-169 03 Solna
Phone +46 8 459 84 00
skb.se

SVENSK KÄRNBRÄNSLEHANTERING

ISSN 1404-0344
SKB TR-18-14
ID 1706675
December 2018

Corrosion morphology of copper in anoxic sulphide environments

Andrew Gordon, Helen Pahverk, Eric Börjesson, Lena Sjögren
RISE KIMAB AB

Oskar Karlsson, Hans Bergqvist, Fredrik Lindberg
Swerim AB

Adam Johannes Johansson, Svensk Kärnbränslehantering AB

Summary

Copper coupons were exposed to atmospheres containing $H_2S(g)$ or solutions with pre-cultivated sulphate reducing bacteria (SRB) and nutrients in order to examine the magnitude of corrosion and the corrosion morphology of copper in these sulphide environments. For each environment, four different exposure conditions were tested; low or high partial pressures of H_2S gas for either 10 or 30 days, and minimal or rich growth media with SRB for either 10 or 32 days.

The results of the analyses show that the extent of corrosion increases with the partial pressure of $H_2S(g)$, and the richness (level of nutrients) of the SRB growth medium, as well as the duration of exposure.

Inspection of the shapes and morphologies, as well as statistical analysis of the deepest surface defects found on the SRB exposed coupons, suggested that these are not related to the corrosive sulphide exposures but that most of them are due to different types of mechanical damage and wear that occurred before or during preparation of the coupons (cutting and polishing). However, at high sulphide concentrations ($> 10^{-3}$ M) a few observations of increased defect density (number of defects per unit area) are interpreted as possibly caused by localised corrosion during the sulphide exposure.

During the course of the present work a method of evaluating the mass loss due to corrosion was developed as the original method tried for removing corrosion products with a combination of alkaline (20 wt% NH_4OH) and acidic (37 wt% HCl) solutions was found to cause localised corrosion of the copper surface beneath the corrosion film and thus compromised the accuracy of the defect measurements. The outcome of this evaluation was to use only the alkaline solution (20 wt% NH_4OH) for copper coupons with a sulphide corrosion product.

For the $H_2S(g)$ exposures, cross-sections of the corroded copper coupons were examined with SEM-EDS. No signs of localised corrosion were observed, however, the copper surfaces beneath the copper sulphide corrosion films seemed rather roughly corroded.

Contents

Abbreviations

EDS – Energy-dispersive X-ray spectroscopy

LOM – Light optical microscopy

MIC – Microbiologically influenced corrosion

RH – Relative humidity

SEM – Scanning electron microscopy/microscope

SEM/EDS – Scanning electron microscope with energy-dispersive X-ray spectroscopy

SKB – Svensk Kärnbränslehantering AB (Swedish Nuclear Fuel and Waste Management Co)

SRB – Sulphate reducing bacteria

1 Introduction

In the KBS-3 concept for disposal of spent nuclear fuel, the fuel will be encapsulated in copper canisters with a cast iron insert. The canisters will be embedded in compact bentonite clay and disposed in a repository built in a deep granitic formation. The thermal, hydrological, and geochemical development of such repository has been analysed in SKB's safety assessment (SKB 2011).

An important safety function of the system is the corrosion resistance of the copper canister. Examples of processes that contribute to the corrosion are residual oxygen, gamma radiolysis of water, and sulphide in the ground water. While the residual oxygen and gamma radiation are early and finite contributions to the total corrosion, sulphide is an inexhaustible source of oxidants for corrosion and sulphide corrosion is only limited by a low sulphide flux at the canister surface (King et al. 2017).

In the spent fuel repository, there will be circa 6 000 copper canisters, each deposited in individual deposition holes in a granitic formation at Forsmark, Sweden. An important feature of the development of the near-field environment of the canister is the water saturation and swelling of the bentonite clay to a density of ca 2 000 kg × m^{-3}. In the majority of the deposition holes, saturation will be completed in a few hundred years, however, due to the dryness of the chosen site it could take more than one thousand years for the clay to saturate at some locations within the repository. In this report we will refer to this period as the *unsaturated phase*.

On the other hand, there will be some deposition holes at which the ground water conditions after glaciation, a few tens of thousands of years after closure of the repository, could cause partial erosion of the bentonite clay so that advective conditions arise at some canisters after about one hundred thousand years. This scenario, which is described and analysed further in the safety assessment SR-Site, is referred to as the *eroded buffer case*.

While the extent and morphology of sulphide driven corrosion under saturated conditions and in abiotic sulphide solutions have been assessed elsewhere (Chen J et al. 2019, King et al. 2010, 2013, 2017, Martino et al. 2014, 2017, SKB 2010), this report presents experimental studies of the morphology of sulphide corrosion of copper, with relevance to the unsaturated phase and the eroded buffer case.

1.1 Unsaturated phase – $H_2S(g)$ exposure

During the unsaturated phase, sulphide transport might occur through the gas-phase, since sulphide in the groundwater could be in equilibrium with $H_2S(g)$. Thus, even if the near-field of a deposition hole is dry, sulphide in wet regions of the back-filled tunnel could be transported in the gas phase through the bentonite porosity and reach the canister surface.

Earlier studies of copper corrosion in atmospheres containing ~5 ppm H_2S, have shown that the pre-existing oxide film on copper is protective to $H_2S(g)$ in dry atmospheres, but at high relative humidity (RH) the oxide film is replaced by a sulphide film (Sharma 1980). These findings have later been confirmed in several studies of the sulphidation of oxygen containing copper corrosion products, showing that neither cuprite (Cu_2O), tenorite (CuO), or paratacamite ($Cu_2(OH)_3Cl$) are stable in anoxic sulphide solutions (Smith et al. 2007, Höllmark et al. 2012, Kristiansen et al. 2015, Stenlid et al. 2017). A common conclusion from earlier studies of copper in sulphide solutions is that the copper sulphide film formed under repository conditions (e.g. sulphide concentration and flux at the canister surface) is porous, non-passive, and composed mainly of chalcocite (Cu_2S) (Chen J et al. 2011, 2014, Martino et al. 2014, Sharma 1980).

In order to further assess the risk of localised corrosion during the unsaturated phase, the present study aims to quantify the average corrosion depth and any changes in surface morphology (i.e. the occurrence and depth of localised corrosion) as a function of $H_2S(g)$ exposure conditions and duration. The conditions chosen are based on the thermal development of the repository, and sulphide concentrations measured in deep ground water at the Forsmark site (Tullborg et al. 2010).

1.2 Eroded buffer scenario – SRB biofilm exposure

The presence of high-density bentonite prevents the establishment of advective conditions at the canister surface and has a suppressive effect on microbial sulphate reduction in the vicinity of the canister (Stroes-Gascoyne et al. 1997, Bengtsson et al. 2017). However, in the long-term perspective, the possibility of partial erosion of the clay cannot be excluded for all 6 000 deposition holes, meaning that parts of some canister surfaces could become directly exposed to the ground water. Since the groundwater contains sulphate as well as low levels of organic material, a biofilm of sulphate reducing bacteria (SRB) could possibly form at the canister surface. Studies of copper exposed to an SRB biofilm in a medium containing high levels of lactate and yeast have indicated localised as well as general corrosion, albeit with unrealistic levels of nutrients for the Forsmark deep groundwater, and without evaluating the development of localised corrosion over time or in relation to the total average corrosion depth (Chen S et al. 2014). Another study of copper corrosion under an SRB biofilm in highly nutritious solutions also revealed localized as well as general corrosion (Dou et al. 2018). In this study it was found that the deepest localised corrosion features were of the same depth as the average corrosion depth calculated from mass-loss. The work in this report was initiated before the publication of Dou et al. (2018) and aimed at reproducing the exposures made in Chen S et al. (2014), however, with the ambition to evaluate the development of the copper surface topography with time and in relation to the average corrosion depth.

2 Materials and methods

Two types of exposure were performed in order to evaluate the corrosion morphology of oxygen free phosphorous doped copper (Cu-OFP) in: 1) humid H_2S(g) environments, and 2) in media supporting SRB metabolic activity. The exposures in gaseous H_2S environments were carried out by the Institut de la Corrosion, St Etienne, France, while SRB exposures were conducted by Microbial Analytics AB, Gothenburg, Sweden. Examination of the corroded copper coupons consisted of mass loss evaluation, counting and measuring of all sorts of surface defects using light optical microscopy (LOM) and examination of the copper-chalcocite film interface using SEM/EDS. The surface and corrosion examination was carried out by RISE KIMAB AB (previously Swerea KIMAB AB), Stockholm, Sweden.

The gaseous H_2S experiment was designed to evaluate the general and possibly localised corrosion of copper exposed to various partial pressures of H_2S gas at elevated temperature and high relative humidity. The lower partial pressure (10 wt.ppm) was chosen to be representative for a gas-phase in equilibrium with a typical sulphide concentration of the ground water in Forsmark ($\sim 10^{-6}$ M). However, since the consumption of H_2S by copper corrosion is faster than the transport of H_2S through the bentonite buffer, this concentration cannot be upheld at the canister-bentonite interface in the repository. The higher partial pressure (10 000 wt.ppm or 1 %) was used in order to accelerate the corrosion and enhance the possibility of detecting any signs of localised corrosion.

The SRB experiment was designed with the same purpose as the gas experiment, to evaluate general and localized corrosion as a function of the exposure conditions and duration. Coupons of copper were incubated with pre-grown SRB in solution, either resembling Forsmark ground water with respect to sulphate and organic material, or a solution with strongly enhanced sulphate and organic content. The SRB experiment was repeated due to the results of the pickling method evaluation and its unexpected effects on the copper surface topography (see Section 2.4).

2.1 Coupon preparation

SKB-supplied OFP copper was used for the preparation of coupons at RISE KIMAB AB. Coupons with dimensions of ca. 100 × 10 × 5 mm were cut from the bulk material using a bandsaw and electro-discharge machining. The coupons were then ground with abrasive paper to a fineness of P4000. For coupons to be exposed in the H_2S atmospheres, a hole (Ø 5 mm) was drilled at the top of the coupon, so that they could be suspended in the headspace of the exposure chamber. The edges of the coupons were rounded to prevent accelerated corrosion at these locations. To be able to identify each coupon, the corners of the coupons were ground in a systematic way and individually numbered, see Figure 2-1.

The coupons were weighed using a Sartorius Excellence MC 210P scales with an accuracy of ± 0.00009 g before experiments were conducted. The scales were within calibration and checked using reference weights before each weighing. The division of coupons according to sets and numbering can be seen in Table 2-1. An example of a coupon surface before exposure is shown in Figure 2-2.

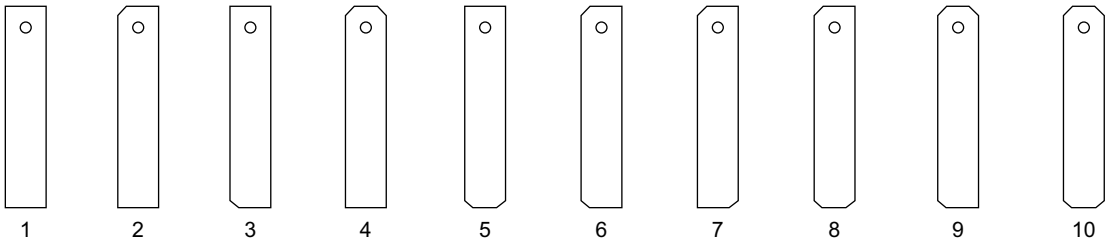

Figure 2-1. *Identification and numbering of coupons.*

Figure 2-2. *Coupon surface before exposure. The scale bar is 100 µm.*

Table 2-1 Coupon sets and numbering of the different coupons for each exposure.

Set	Numbering	Exposure	Planned duration
1	1–5	Gas A 10 wt.ppm H_2S	10 days
2	1–5	Gas B 10 wt.ppm H_2S	30 days
1	6–10	Gas C 10^4 wt.ppm H_2S	10 days
2	6–10	Gas D 10^4 wt.ppm H_2S	30 days
3	1–5	Bio A low nutrient	10 days
4	1–5	Bio B low nutrient	30 days
3	6–10	Bio C high nutrient	10 days
4	6–10	Bio D high nutrient	30 days
5	1–10	Control E, F, G	30 days
6	1–5	Gas A 10 wt.ppm H_2S	10 days (repeat exposure of set 1, coupons 1–5)
7–10	1–10	Bio A–D and Control E, F, G	10/32 days (repeat exposure of sets 3–5)

2.2 Scanning electron microscopy

Scanning electron microscope (SEM) images were obtained with a Zeiss Supra scanning electron microscope with a Field Emission Gun (FEG) as electron source. The electron beam energy was 15 keV and the working distance was about 10 mm. A detector for backscattered electrons was used. The microscope is equipped with a detector for energy dispersive spectroscopy (EDS) which was used for elemental analysis of small areas and for EDS-mapping of the coupon surfaces, carried out to a depth of about 1 µm into the surface. Due to the morphology and filtering effects of corrosion products the analysis results should be interpreted as qualitative only, and as such an accuracy of the measurement values cannot be defined.

2.3 Light optical microscopy

All types of defects on the coupon surfaces were counted and measured using a Nikon Epiphot microscope equipped with a digital camera Kappa DX40. The depths of the defects were measured using the calibrated focus of the microscope, with an accuracy of ± 1 µm. As will be evident further below, various types of defects were found on the surfaces of the copper coupons. Some of the defects might have been caused or affected by corrosion, while others must have been caused by mechanical damage to the copper surface prior to the sulphide exposure. In this report, the term *defect* is used collectively for all types of surface defects of various origins.

2.4 Pickling procedure to evaluate mass loss of coupons

To evaluate the mass loss for the corroded copper coupons the principle method of repeated pickling according to standard SS-EN ISO 8407:2014 was used, although with a different acid solution to those given in the standard. In order to remove the expected corrosion products of Cu_2S and possibly CuS two different solutions were used. The coupons were exposed in 20 wt% NH_4OH for one minute in an ultrasonic bath and weighed between each pickling. This procedure was repeated until the mass-loss curve was considered to be linear (see Appendix A). Thereafter, a 37 wt% HCl solution (50 % HCl 50 % deionized H_2O) was used with pickling intervals of two minutes, again until the mass-loss curve was linear.

During some initial tests, the microscopic examination of the first batch of both SRB and $H_2S(g)$ exposed copper coupons, revealed frequently occurring surface defects of around 20 µm depth, and occasionally occurring defects of about 50 µm, see Figure 2-3 and Figure 2-4. Since this was unexpected for $H_2S(g)$ in comparison with other studies of copper corrosion in sulphide solutions (Chen J et al. 2019), and since there was no correlation between defect depths and mass-loss, it was suspected that the method of film removal (pickling) had affected the observed topography of the underlying copper surface. As part of the pickling procedure unexposed reference coupons are also weighed between each pickling phase. Upon examining the surfaces of the reference coupon used it could be seen that defects had deepened due to the pickling procedure using alkaline (20 wt% NH_4OH) and acidic (37 wt% HCl) solutions sequentially. Before pickling, the five deepest defects on the coupon were 5–9 µm, with a mean value of 6.6 (± 1.5) µm, while after pickling the five deepest defects were 8–18 µm with a mean value of 11.0 (± 3.3) µm, see Table 2-2. A statistical comparison shows that there was no overlap between the 95 % confidence intervals and the mean values when comparing the defects found and measured before and after pickling, meaning that the pickling had a significant effect on the deepest defects (see Figure 2-5). Examples of defects found on the reference coupon before and after pickling are shown in Figure 2-6.

It was decided to evaluate if pickling in only the alkaline solution (20 wt% NH_4OH) would remove the corrosion products sufficiently, to avoid any potential localised corrosion or growth of pre-existing defects during the acidic pickling phase. In order to evaluate the effect and efficiency of pickling in only the alkaline solution (20 wt% NH_4OH), characterization of the defects of an unexposed test coupon was done, which was then repeated after pickling for 6 × 5 minutes in the alkaline pickling solution. Before pickling, the five deepest defects identified on the test coupon were 7–25 µm deep, with a mean value of 14.7 (± 7.1) µm (see Table 2-3). After pickling, the five deepest defects were 7–26 µm, with a mean value of 15.2 (± 7.2) µm. A statistical comparison shows that there was a mutual overlap between the 95 % confidence intervals and the mean values of the deepest defects when comparing the defects found and measured before and after pickling, meaning that there was no significant difference due to pickling (Figure 2-7).

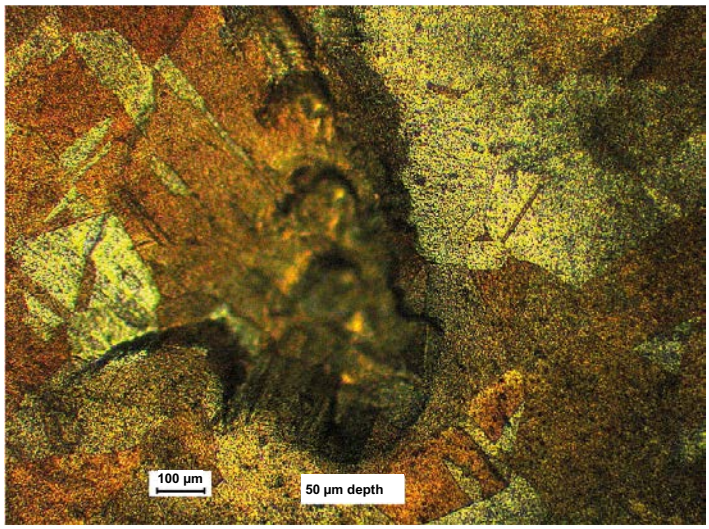

Figure 2-3. *Example of a 50 µm defect found on coupon 2-1 after exposure to Gas B conditions (Table 2.1) and pickling with both 20 wt% NH_4OH and 37 wt% HCl.*

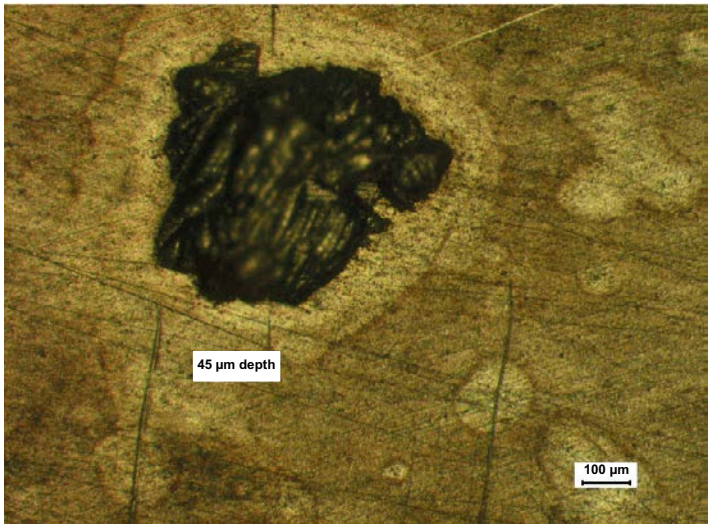

Figure 2-4. *Example of 45µm defect found on coupon 3-2 after initial exposure to Bio C conditions and pickling with both 20 wt% NH_4OH and 37 wt% HCl.*

Table 2-2. Analysis of surface defects found on a reference coupon used during pickling in NH_4OH and then HCl. The observed defects had deepened significantly during pickling.

Coupon	Five deepest defects, side 1 (µm)					Five deepest defects, side 2 (µm)					Deepest defect (µm)	Mean defect depth (µm)		Defect density (defects/cm^2)	
	1	2	3	4	5	1	2	3	4	5		Side 1	Side 2	Side 1	Side 2
Reference before pickling	6	5	5	5	5	9	8	8	7	8	9	5.2	8	4	4
Reference after pickling	18	9	9	8	8	16	12	11	10	9	18	10.4	11.6	0	4

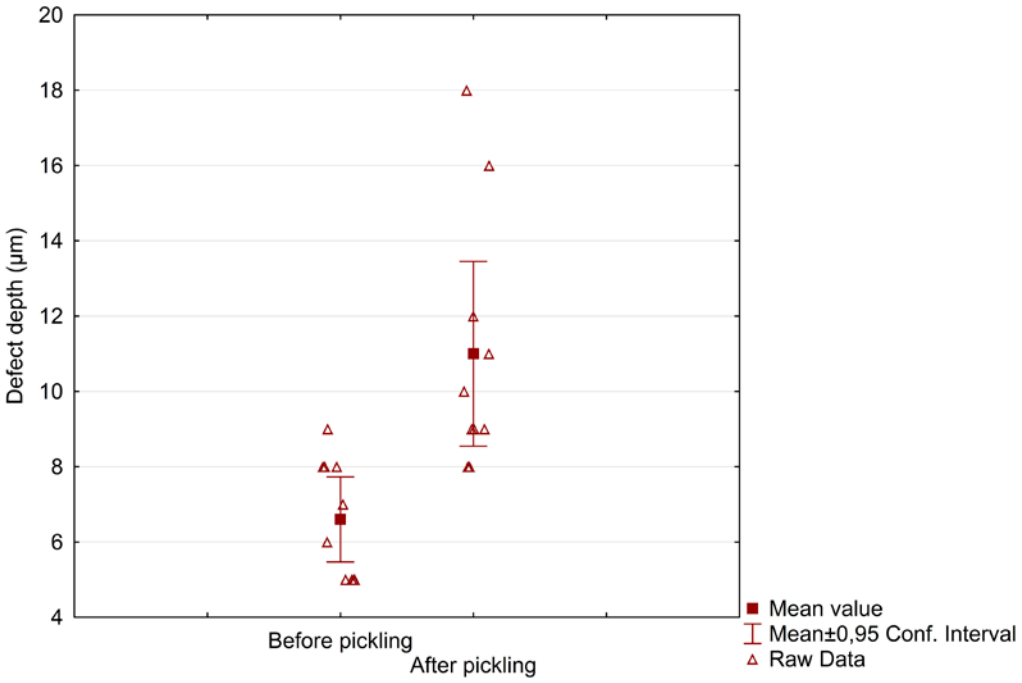

Figure 2-5. *Mean plots of the deepest defects found on the reference coupon before and after pickling with both alkaline and acidic solutions.*

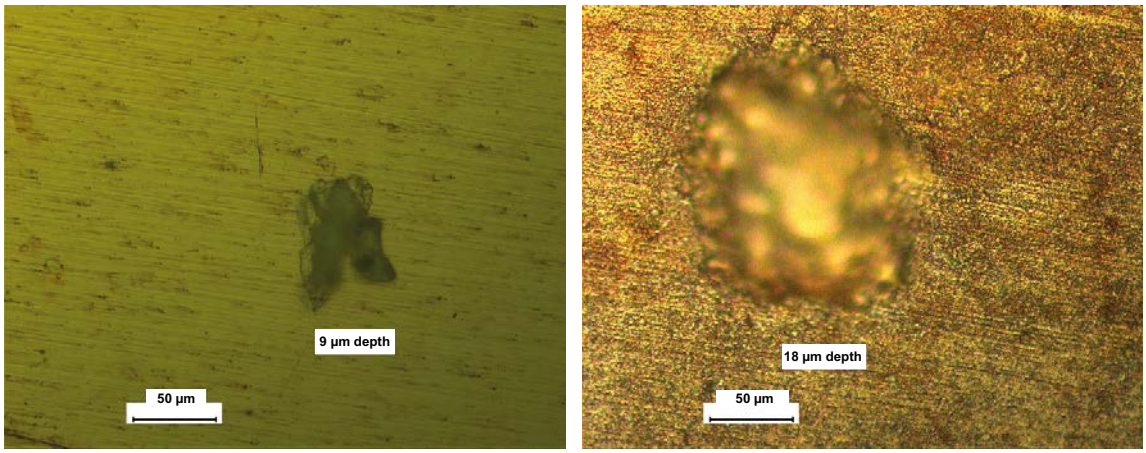

Figure 2-6. *Microscope images of the deepest defects found on the surface of the test coupon before (left) and after pickling (right) with both alkaline and acidic solutions.*

Table 2-3. Analysis of surface defects found on a test coupon used during pickling in only NH_4OH solution. The observed defects had not deepened during pickling.

Coupon	Five deepest defects, side 1 (µm)					Five deepest defects, side 2 (µm)					Deepest defect (µm)	Mean defect depth (µm)		Defect density (defects/cm^2)	
	1	2	3	4	5	1	2	3	4	5		Side 1	Side 2	Side 1	Side 2
Reference before pickling	9	9	8	7	7	25	24	22	19	17	25	8	21.4	14	12
Reference after pickling	11	10	9	8	7	26	26	24	16	15	26	9	21.4	10	12

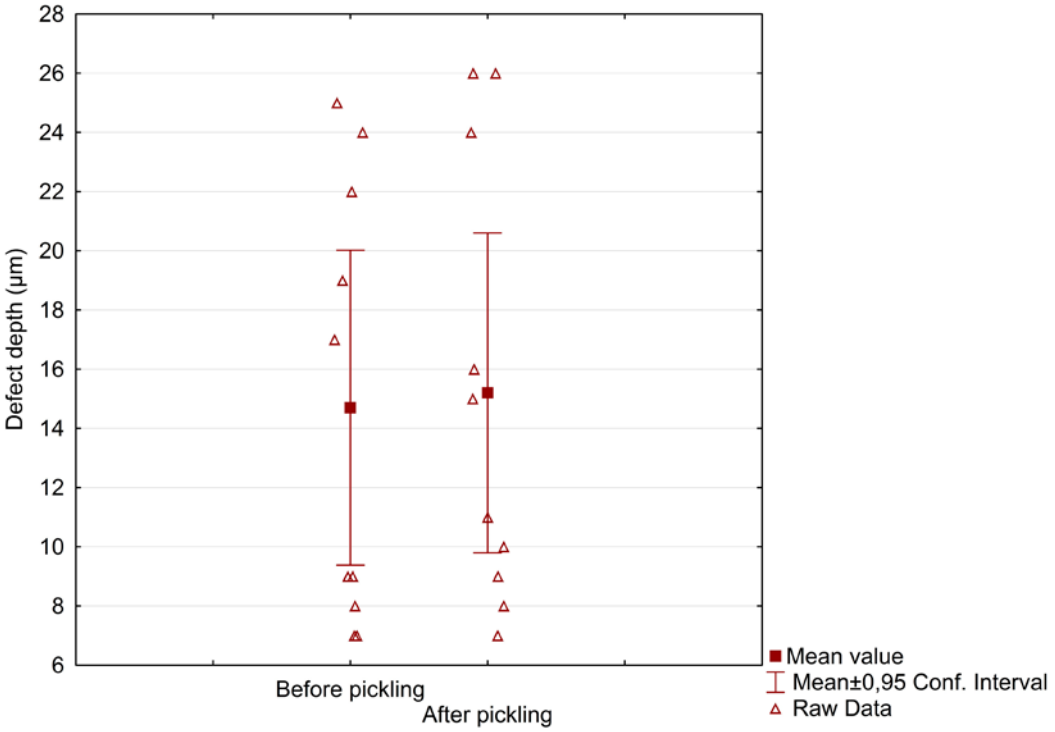

Figure 2-7. *Mean plots of the deepest defects found on the reference coupon before and after pickling with alkaline (20 wt% NH_4OH) solution only.*

Additionally, an extra set of coupons (set 1 coupons 3–5) that had been exposed to the initial 10 wt.ppm H_2S experiments for 10 days, were characterized after exposure but before pickling, as well as after pickling. These coupons were spare as this particular exposure had to be repeated due to the experimental conditions deviating outside of the specification during the exposure period (the Teflon wire holding the coupons had slipped and the coupons were no longer suspended in the test chamber and the H_2S concentration had deviated outside of the specified value). The five deepest defects on the exposed and corroded coupons had depths of 7–17 µm before pickling with a mean value of 9.7 (±1.1) µm and 10–27 µm after pickling with a mean value of 14.3 (±2.2) µm. For these coupons, it should be noted that defect depths measured before pickling included the thickness of any corrosion products present on the surfaces, i.e. there were corrosion products in the defects making them effectively shallower when measured.

The results of these tests indicated that the defects did not increase significantly as a result of the 20 % NH_4OH-only pickling procedure, and that sufficient corrosion products were removed to allow accurate evaluation of corrosion by mass loss. Based on these observations and the results in Figure 2-7, it was concluded that pickling in only 20 % NH_4OH would be used for the remainder of the coupon analyses. Further details of the pickling method development can be found in Appendix A.

2.5 SRB exposures

The SRB exposures were performed by Microbial Analytics AB and the full details of the experimental method and procedure can be found in Johansson (2019). The experimental test matrix with the different media, incubation times, and sterile controls is shown in Table 2-4. The coupons in the group called Bio-A were exposed to pre-grown SRB in a minimal medium for ten days. The minimal medium contained sulphate and lactate at concentrations comparable with the deep ground water at Forsmark. In Bio-B the medium was the same as in Bio-A, but the exposure time was extended to 32 days. The coupons in Bio-C and Bio-D were exposed to pre-grown SRB in a rich medium for 10 and 32 days respectively. The rich medium contained enhanced levels of sulphate, lactate, and in addition yeast extract in order to accelerate the biotic sulphide production and thereby the corrosion process. The

conditions were similar to those in Chen S et al. (2014). The control exposures Control-E and -F had similar conditions to the Bio-B and -D exposures, but without the addition of SRB. Control-G had similar conditions to Bio-D without SRB but with 3×10^{-3} M sulphide added from start. All coupons were removed from the exposure tubes in an anaerobic environment, dried overnight and then put in plastic boxes in plastic bags containing desiccators before being sent to RISE KIMAB AB for further examination.

Table 2-4. Experimental test matrix showing which tests contained SRB, the composition of the media, and which of the sterile controls contained sulphide along with the incubation time.

Group	No. of coupons	SRB	Sulphate (10^{-3} M)	Sulphide (10^{-3} M)	Lactate (10^{-3} M)	Yeast extract (g/L)	Time (days)
Bio-A	6	Yes	4	-	0.1	-	10
Bio-B	6	Yes	4	-	0.1	-	32
Bio-C	6	Yes	20	-	47	1	10
Bio-D	6	Yes	20	-	47	1	32
Control-E	3	No	4	-	0.1	-	32
Control-F	3	No	20	-	47	1	29
Control-G	3	No	20	3	47	1	32

2.6 H_2S atmospheric exposure

2.6.1 Experimental set-up

An experimental set-up was developed to meet the needs of the exposure conditions specified in Table 2-5. Preliminary tests were carried out in order to evaluate the control and stability of the set-up before the first test coupons were exposed.

Table 2-5. Test conditions for H_2S gas exposures.

Temperature	80 – 90 °C
Relative humidity (RH)	70 – 80 %
Duration of exposure	10 days 30 days
Gas environments	10 wt.ppm H_2S 10 000 wt.ppm H_2S

The use of a commercial humidity chamber in conjunction with H_2S was not possible for safety considerations, therefore an alternative procedure was sought. Humidity levels can be accurately controlled in the gaseous phase in equilibrium with salt saturated aqueous solutions. Saturated NaCl solution was chosen as the solution based on previous experience. The effectiveness of the NaCl solution was tested and confirmed through measurements using a commercial RH probe (Testo Model 645) before starting the experimental work. All the preliminary measurements performed in the gas-phase above a saturated NaCl solution were close to 75 % at 80 °C.

The principle of the experiments was to expose copper coupons to $H_2S(g)$ at various concentrations in the head space of a vessel containing a saturated NaCl solution and heated to 80 °C. Figure 2-8 shows a schematic of the test set-up. It consisted of a glass vessel that was partly filled with the deaerated saturated salt solution from an external reservoir using a peristaltic pump or by gravity. Dissolved oxygen was measured with an oxygen sensor (Hach Lange Model K1100) before each solution transfer from the deaeration reservoir to the test vessel. The dissolved oxygen content measured after deaeration was always below 20 ppb. The copper coupons were placed in the headspace where the humidity was generated by the heated salt solution. These coupons were hung on the vessel cap using a Teflon wire as shown in Figure 2-9.

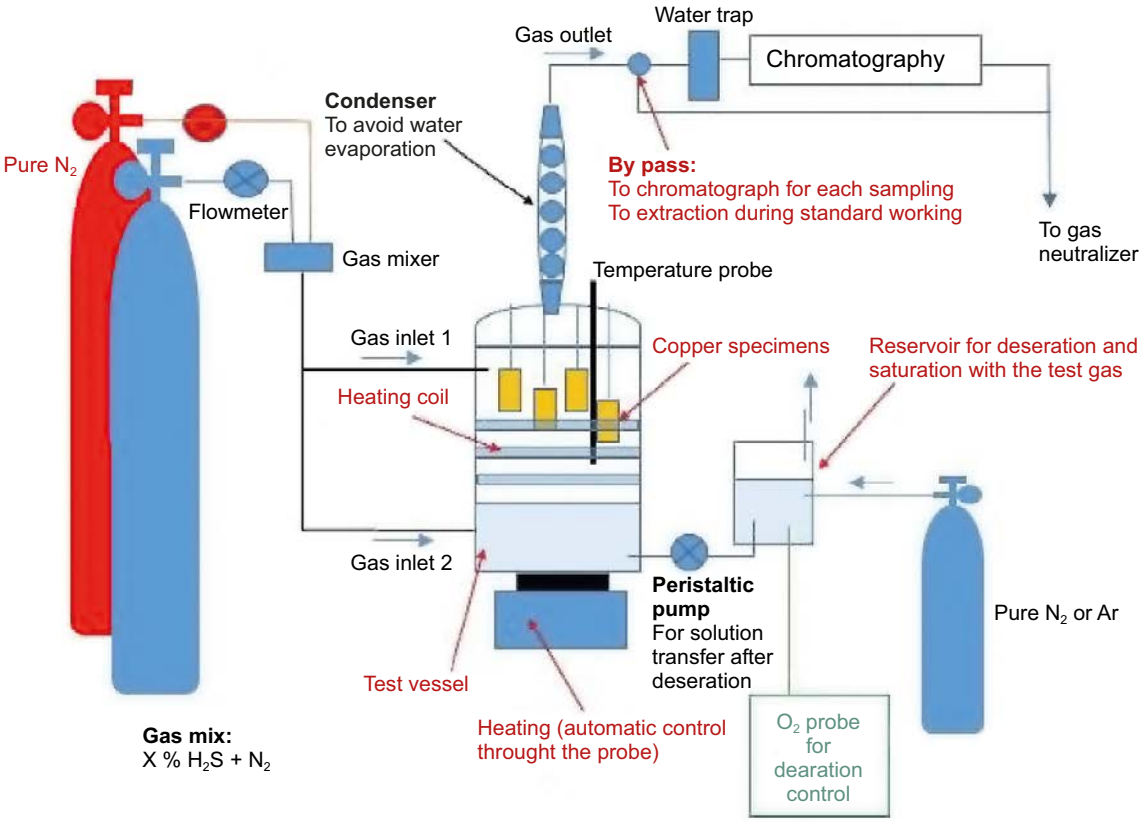

Figure 2-8. *Schematic of the test set-up for the H_2S exposures.*

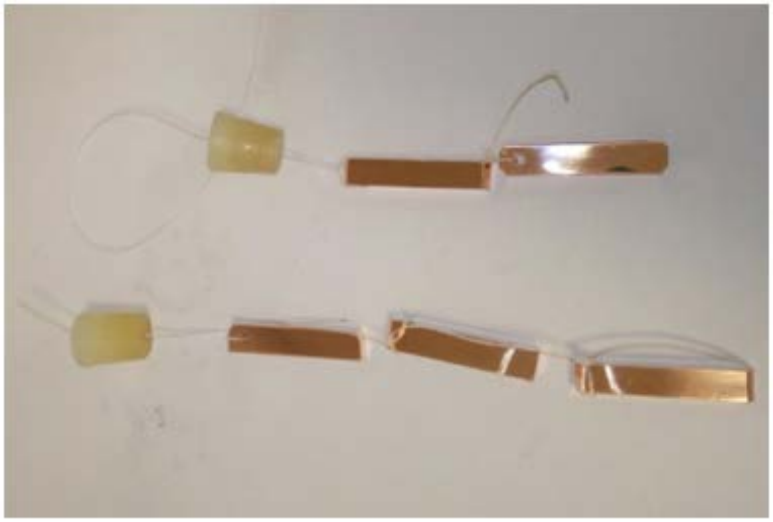

Figure 2-9. *Copper coupons with Teflon thread ready to be hung in the headspace of the exposure chamber.*

It was essential to ensure the target H_2S level in the headspace was achieved because at 80 – 90 °C a vapor pressure is generated in the headspace that dilutes the test gas which in turn decreases the actual H_2S concentration. The saturated vapor pressure at 80 °C was known (0.5 bar) and the expected vapour pressure during the tests was thus around 0.4 bar at 80 % RH, meaning 0.6 bar partial pressure was available for the test gas if the experiments were performed at atmospheric pressure. In such conditions it was thus necessary to use an input gas mix containing 1.7 % H_2S to achieve 1 % in the headspace (or 17 wt.ppm to achieve 10 wt.ppm). At 80 °C, 80 % RH and at atmospheric pressure, the headspace is composed of 0.4 bar of water vapor and 0.6 bar of gas mix (i.e. $0.017 \times 0.6 = 0.01$ bar H_2S which corresponds to a gas mix in the headspace containing 1 % H_2S). The gas mix introduced in the vessel was prepared from two different gas bottles: the first containing pure nitrogen and the second containing nitrogen with x % H_2S (x defined according to the H_2S concentration required in the test). Both gases were then mixed in a bespoke device shown in Figure 2-10. This device consisted of a stainless steel tube containing two inlets and one outlet. Each inlet was supplied from each gas bottle (N_2 in bottle #1 and N_2 + x % H_2S in bottle #2) and each inlet gas flow was controlled using mass flowmeters. These flowmeters were used to adjust the actual composition of the gas at the outlet that was connected to the test vessel.

During the exposures it was decided to use two bottles containing N_2 + 3.4 % H_2S and N_2 + 34 wt.ppm H_2S for the test conditions of 10 000 wt.ppm and 10 wt.ppm H_2S respectively. At the specified concentrations, the same flow rate from each bottle lead to the supply of the test vessel with 1.7 % and 17 wt.ppm H_2S respectively. A photograph of the test bench can be seen in Figure 2-11.

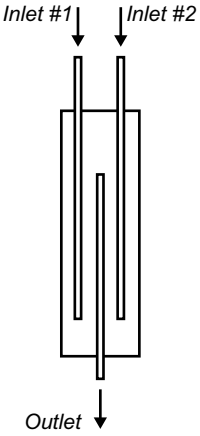

Figure 2-10. *Schematic of the gas mixer.*

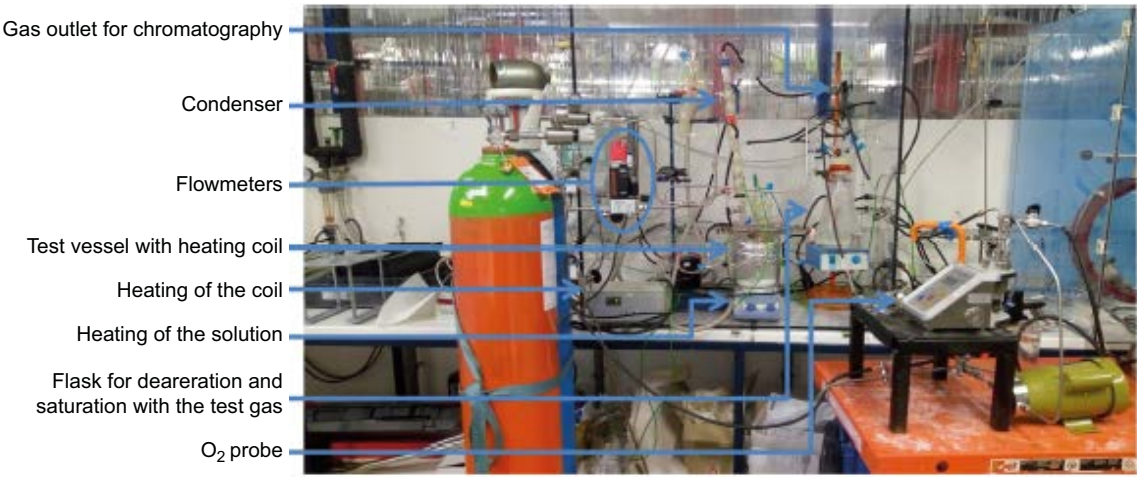

Figure 2-11. *Overview of test set-up.*

2.6.2 Exposure procedure

The experimental procedure was the same for all exposure conditions and is summarized below:

- Deaeration of the NaCl saturated solution in an external reservoir.
- Deaeration of the test vessel containing the coupons. Some NaCl salt was added at the bottom of the vessel to sustain the saturation after salt solution transfer.
- Heating of the solution and pre-heating of the test vessel.
- Transfer of the deaerated solution in the deaerated test vessel, without contamination of the coupons.
- Temperature adjustment.
- Supplying the test vessel with the test gas.
- Controlling the H_2S content using gas chromatography.
- Recording the time when the target H_2S level was reached.
- Periodic chromatographic measurements to adjust the flow rates as needed.

2.6.3 Test performance and monitoring

When the experimental setup described above had been developed and tested, four exposures of copper coupons were performed for which the test matrix is shown in Table 2-6. Using Henrys constant 0.030729 mol/(l × bar) for H_2S at 85 °C, the lower partial pressure of 10 wt.ppm corresponds to a sulphide concentration of 2.13×10^{-7} M in the water film at the coupon surfaces. One percent H_2S in the gas phase corresponds to an aqueous sulphide concentration of 2.14×10^{-4} M. This calculation (as shown in Appendix B) is merely an approximation with several uncertainties, such as the effect of the water film thickness on the surface of the coupons. The exposure times were varied between 10 and 30 days in order to evaluate any development of the corrosion morphology with time.

Figure 2-12 to Figure 2-15 show the gas composition and temperature measurements performed periodically during the test through gas chromatography. As can be seen both the temperature and gas pressure were quite stable during the exposure periods.

Table 2-6. Test matrix for exposures in H_2S atmosphere.

Exposure	No of coupons	Atmosphere	H_2S(g) (wt.ppm)	H_2S/HS^-(aq) (M)	Duration (days)
Gas-A	5	70–80 % RH	10	2.13×10^{-7}	10
Gas-B	5	80–90 °C	10	2.13×10^{-7}	30
Gas-C	5		10^4	2.14×10^{-4}	10
Gas-D	5		10^4	2.14×10^{-4}	30

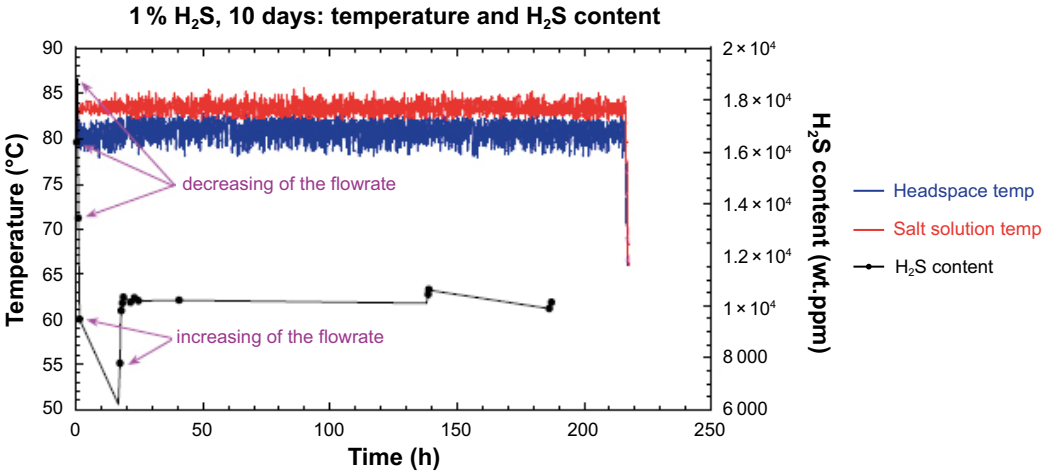

Figure 2-12. *Monitoring data from the 1 % H_2S 10 day exposure.*

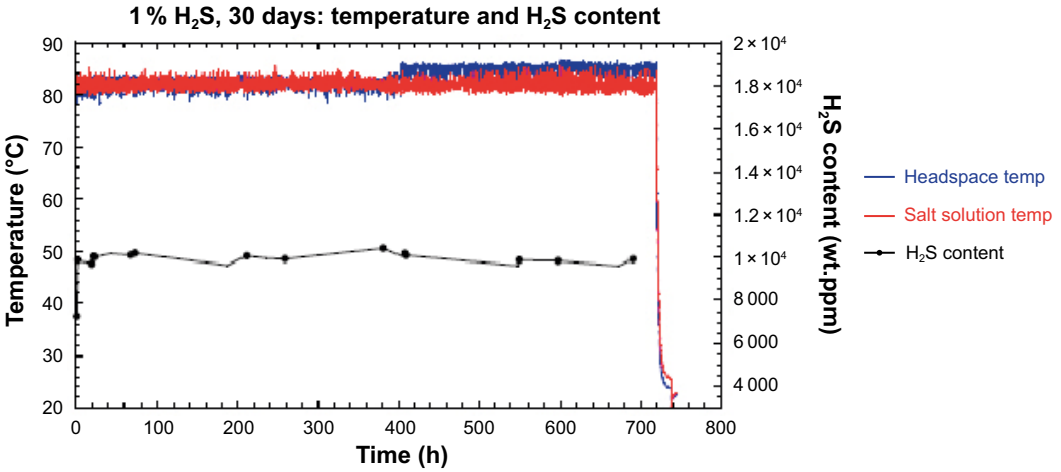

Figure 2-13. *Monitoring data from the 1 % H_2S 30 day exposure.*

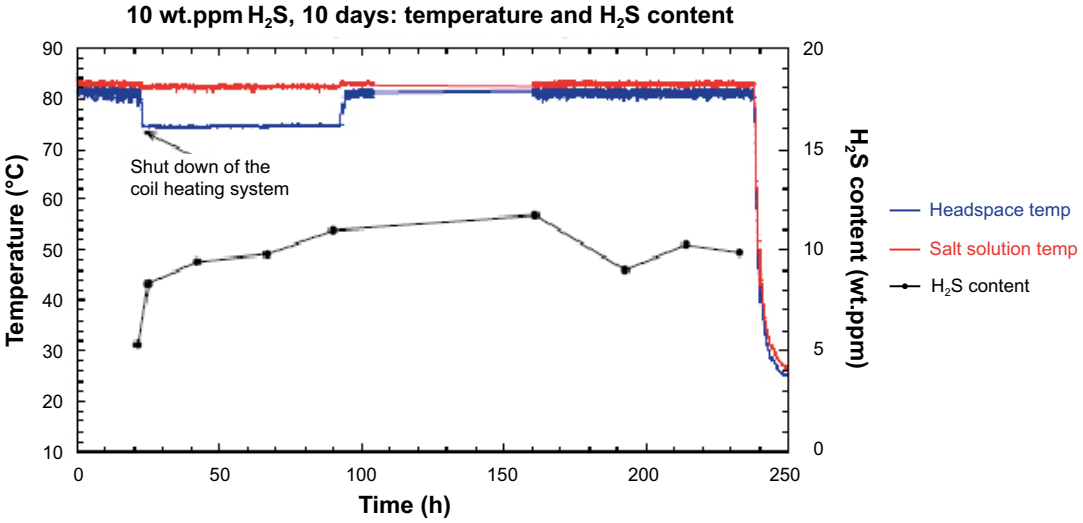

Figure 2-14. *Monitoring data from the 10 wt.ppm H_2S 10 day exposure.*

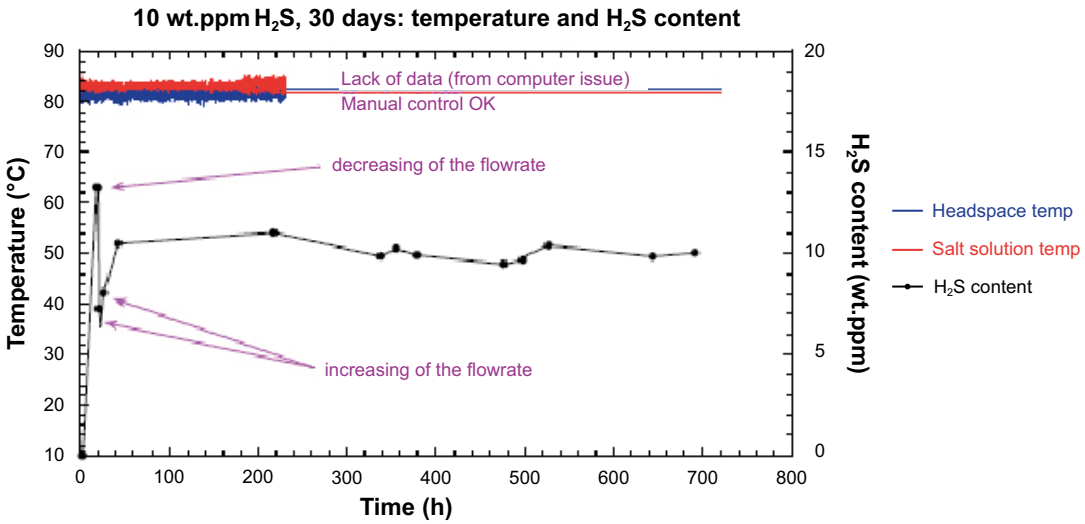

Figure 2-15. *Monitoring data from the 10 wt.ppm H_2S 30 day exposure.*

3 Results and discussion

3.1 SRB exposures

The exposure media were distributed in sterile anaerobic tubes (flushed with 80/20 % N_2/CO_2 gas), each containing 11.5 mL medium and one copper coupon (surface area = 0.0031 m^2), which had been sterilized with UV-light for 20 minutes. After five days of incubation the coupons in the rich medium (Bio-D) had formed a thin black layer on the surface (Figure 3-1). The colour of the coupons in the abiotic Control-G incubated in rich medium with 3×10^{-3} M added sulphide had an irregular discoloration after five days. No discoloration was observed during the exposure of the coupons in minimal medium (Bio-A and Bio-B), see Figure 3-2 and Figure 3-3. Throughout the experiment the black layer on the coupon surfaces became more obvious, see Figure 3-4 for Bio-C coupons after 10 days and Figure 3-5 for Bio-D coupons after 32 days. The sulphide concentrations at the end of the exposures were ca 16×10^{-3} M for Bio-C and 12×10^{-3} M for Bio-D. The formation of a biofilm of *D. aespoeensis* was verified by microscopy for Bio-C and Bio-D, while only a few cells were observed on the copper coupons of Bio-A and Bio-B. After 32 days, the discoloration of the coupons in Control-G became even more pronounced (Figure 3-6). Further details of the SRB exposures are found in Johansson (2019).

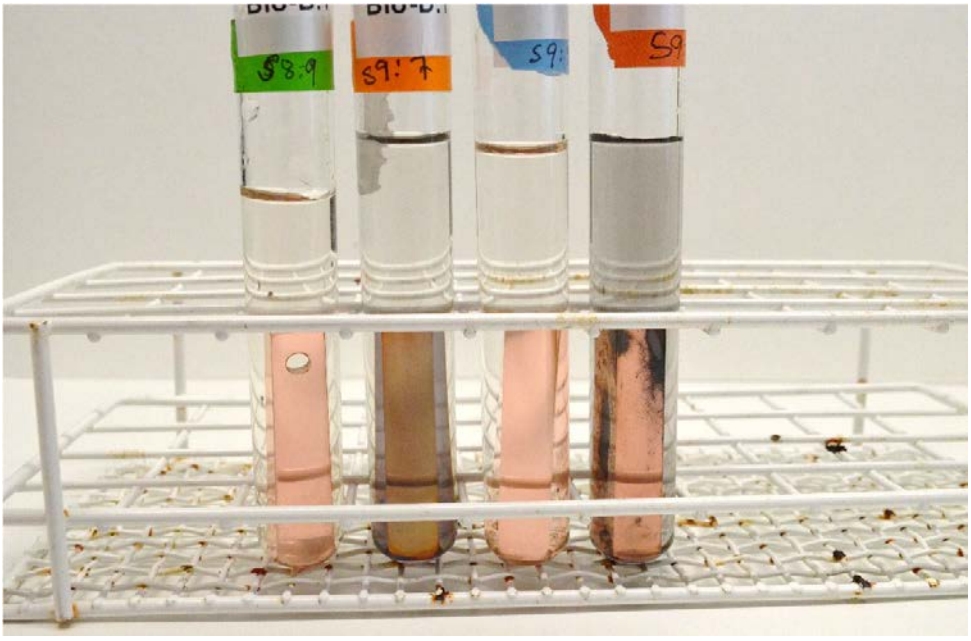

Figure 3-1. *Copper coupons after five days of incubation. From the left: Bio-B (minimal medium with SRB), Bio-D (rich medium with SRB), Control-E (minimal medium without SRB), and Control-G (rich medium without SRB but with added sulphide).*

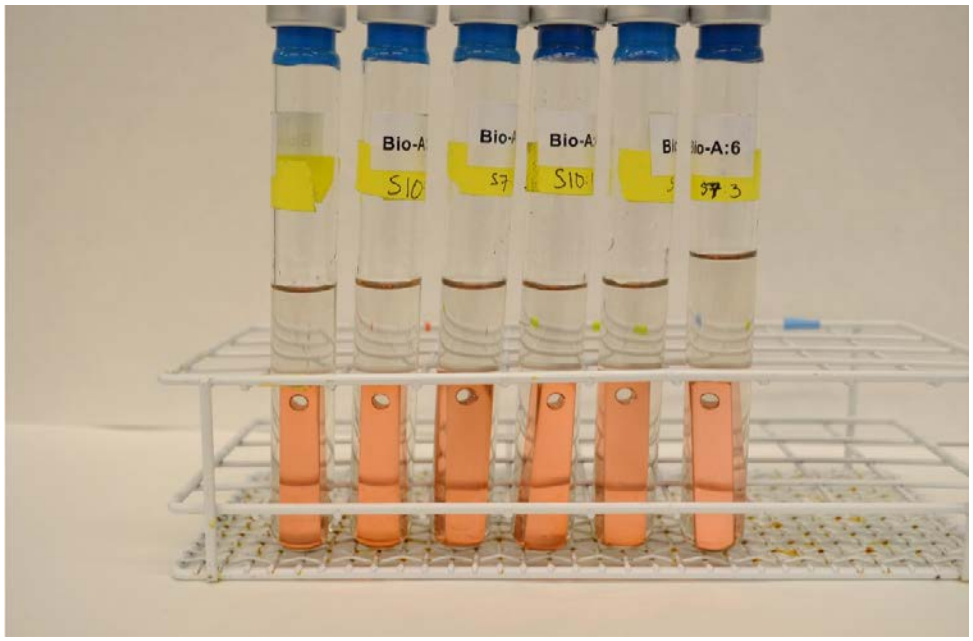

Figure 3-2. *The six replicates of Bio-A (minimal medium with SRB) after 10 days of incubation.*

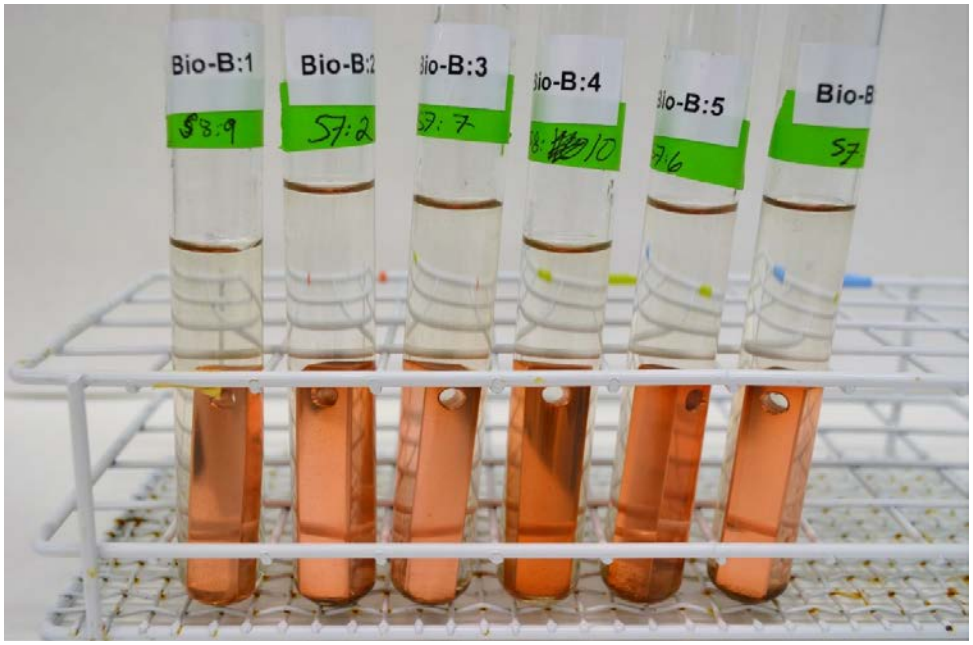

Figure 3-3. *The six replicates of Bio-B (minimal medium with SRB) after 32 days of incubation.*

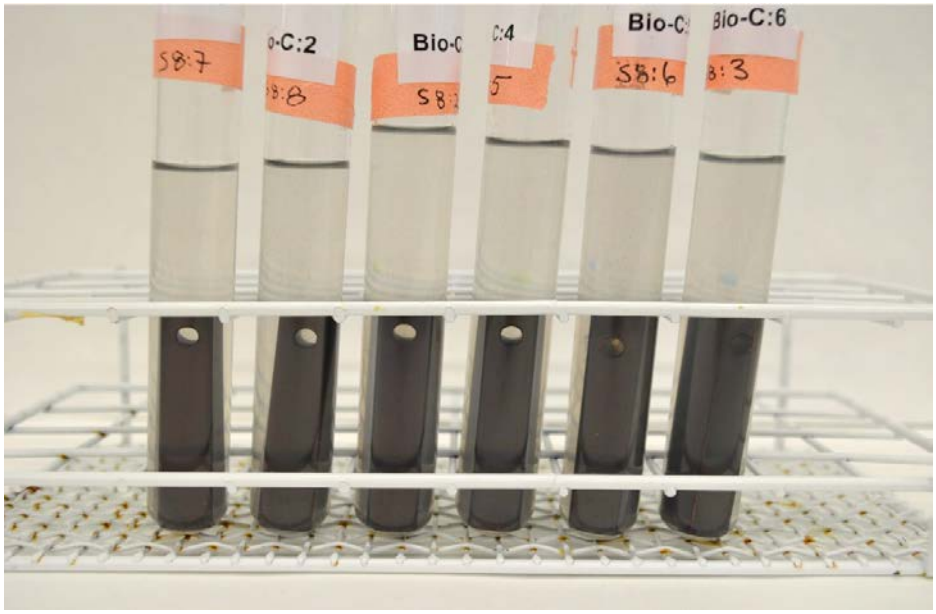

Figure 3-4. *The six replicates of Bio-C (rich medium with SRB) after 10 days of incubation.*

Figure 3-5. *The six replicates of Bio-D (rich medium with SRB) after 32 days of incubation.*

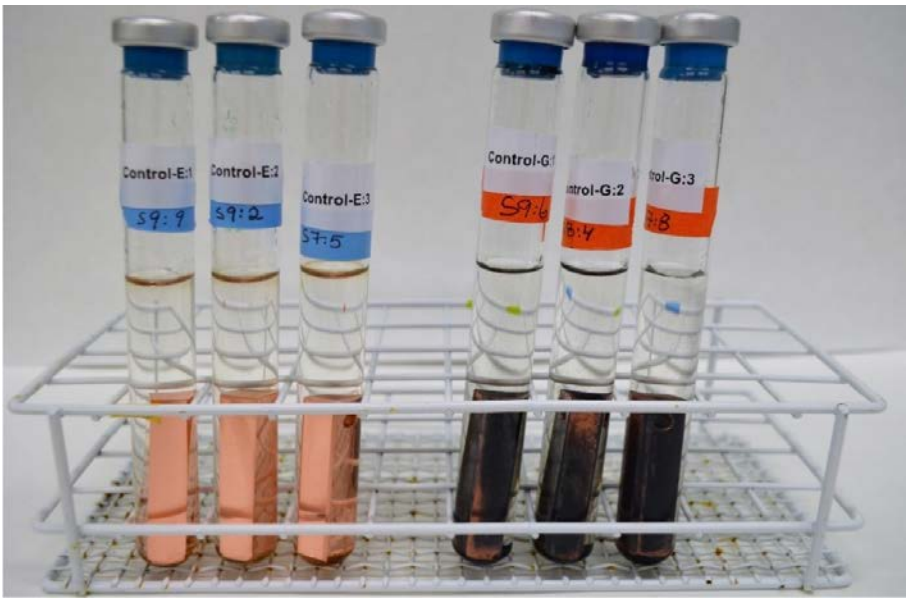

Figure 3-6. *After 32 days of incubation. To the left: The three replicates of Control-E (minimal medium without SRB). To the right: The three replicates of Control-G (rich medium without SRB but with added sulphide).*

3.1.1 Mass loss and average corrosion depth for SRB exposures

Mass loss and the corresponding average depth of corrosion of the coupons are presented in Table 3-1. Triple coupons were used for mass loss evaluation for each exposure group and the corrosion depth is calculated as mass loss per unit area divided by the material density. The mean mass loss with standard deviations is presented in Table 3-2. Two coupons from each exposure were analysed for signs of localised corrosion and the results are shown in Table 3-3. The pickling times for each coupon varied depending on when the pickling was considered complete as compared to the reference coupon used during the pickling. In general, the pickling times were either 30 or 40 minutes for each coupon. The results show in general that an increase in available sulphate and organics (rich medium) in the presence of SRB and a prolonged duration of exposure, results in enhanced mass loss and deeper average corrosion of the copper surfaces. The mass loss on the coupons from the Bio-A exposure were too low to be detected by the method used. For the coupons in the Bio-B series the average corrosion depth was 10 nm, while the average corrosion depth of the coupons in Bio-C and Bio-D were 140 and 210 nm respectively (Table 3-2).

Table 3-1. Mean mass loss and corrosion depth, Group Bio A–D and Control G.

Exposure	Coupon denotation	Mass loss (g/m^2)	Depth of corrosion (µm)	Pickling duration (mins)
Bio-A	S7-11	0*	0	30
Bio-A	S10-3	0	0	30
Bio-A	S7-110	0	0	30
Bio-B	S8-9	0.295	0.03	30
Bio-B	S7-2	0.052	0.006	30
Bio-B	S7-7	0.028	0.003	30
Bio-C	S8-7	0.832	0.09	40
Bio-C	S8-8	1.558	0.18	40
Bio-C	S8-2	1.395	0.16	40
Bio-D	S9-7	2.200	0.25	40
Bio-D	S9-1	1.914	0.22	40
Bio-D	S9-3	1.429	0.16	40
Control G	S9-6	1.008	0.11	40
Control G	S8-4	1.119	0.13	40

* a zero value indicates that corrosion was below the detection limit of the analytical method.

Table 3-2. Mean mass loss and corrosion depth for SRB exposures.

Exposure	Mass loss (g/m^2)	Mass loss Std. Dev. (g/m^2)	Depth of corrosion (μm)	Depth of corrosion Std. Dev. (μm)
Bio-A	0*	0	0	0
Bio-B	0.125	0.1478	0.01	0.017
Bio-C	1.262	0.3808	0.14	0.043
Bio-D	1.848	0.3898	0.21	0.044
Control G	1.063	0.0786	0.12	0.009

* a zero value indicates that corrosion was under the detection limit of the analytical method.

3.1.2 Occurrence and depth of defects on SRB exposed coupons

After removal of the corrosion films the coupons were analysed with light optical microscopy to determine the magnitude and density of any defects in the underlying copper surfaces. This was done on each side of the coupon (the two largest surfaces). To evaluate the density of defects a specific area of 0.5 cm^2 was chosen for analysis. Due to the relatively large number of defects found on the Control-G coupons this area was reduced to 0.1 cm^2.

The depth of each defect was measured by first focusing on the highest point and setting the calibrated focus of the microscope to zero. The focus was then adjusted to the deepest point of the same defect and the depth was determined using the calibration marks of the focus adjuster. This method of depth measurement is described in the ASTM standard G46-94 (ASTM 2013). The results of the analyses can be seen in Table 3-3. Microscope images of the defects measured can be found in Appendix C.

For each side of each coupon, the five deepest defects were identified and the defect density was determined as the number of defects (> 6 μm) per unit area (Table 3-3). Due to the large number of defects present initially (see Section 2.4) it is necessary to compare the coupons statistically. It is important to note though, the aim of the following analysis is not to quantify localised corrosion, but rather to detect any signs of localised corrosion among the defects present on the coupons. The mean values of the 20 deepest defects found on both sides of both coupons for each exposure condition are calculated in Table 3-4, column 4. A direct comparison including all data for all coupons shows no significant difference between the coupons of the Bio-series (Figure 3-7). However, direct comparison is difficult due to a few outliers or extreme values in the data set, e.g. the three defects of ca 50 μm found on Bio-D S9-1 and on References 1 and 2 (Table 3-3). This is reflected by the large standard deviations for the Bio-D and Reference coupons 1–3 in Table 3-4, and it should also be noted that the 95 % confidence interval of Bio-D2 (S9-1) overlaps with the mean values of all other coupons of both the Bio-series as well as the Reference coupons.

If data points corresponding to defects deeper than 30 μm are regarded as outliers or extreme values and are excluded in the analysis, the standard deviations of the Bio-C and Reference groups are reduced and become comparable to the other groups (Table 3-4, column 7). The data points that are removed are the 57 μm defect on Bio-D S9-1, the 49 μm defect on Reference 1, and the 56, 38, and 31 μm defects on Reference 2 (Table 3-3). Again, a statistical comparison reveals no significant difference between the deepest defects found on the coupons of the different exposure groups (Figure 3-8). If the deepest defects were indeed caused by corrosion, the most pronounced difference would be expected between Bio-A and Bio-D, but as shown in Figure 3-8 there is a mutual overlap between the confidence intervals and mean values of the Bio-A and Bio-D series, indicating no significant difference of the deepest defects. Furthermore, no significant difference is found when comparing the coupons of the Bio-C and Bio-D series with the abiotic Control-G that had 3×10^{-3} M added sulphide from start.

Comparing the Bio-series with the reference coupons is not straightforward since the reference coupons had rather deep defects. However, in the complete data comparison (Figure 3-7) Reference 3 is comparable with the Bio-series, and in the analysis without extreme values (Figure 3-8) both Reference 1 and 3 are comparable, and reveal no significant difference when compared with most coupons of the Bio-series. Most importantly, there is no difference between the reference coupons and the Bio-D series, for which a difference would be expected if the deepest defects were related to corrosion. This strongly suggests that the deepest defects found are not related to corrosion, a conclusion that is further supported by inspecting the photos of the defects shown in Appendix C, where the deeper defects appear to show signs of mechanical damage or wear.

Table 3-3. Defects found on SRB exposed coupons and reference coupons. For each coupon the five deepest defects per side are shown, along with mean defect depth and defect surface density per side of coupon.

Exposure	Coupon	Five deepest defects, side 1 (µm)					Five deepest defects, side 2 (µm)					Mean defect depth (µm)		Defect density (defects/cm^2)	
		1	2	3	4	5	1	2	3	4	5	Side 1	Side 2	Side 1	Side 2
Bio-A	S7-11	11	6	6	5	4	8	8	8	7	6	6	7	2	2
Bio-A	S10-3	10	9	9	9	8	10	7	7	6	5	9	7	0	0
Bio-B	S8-9	7	6	6	6	5	7	7	7	6	6	6	7	0	0
Bio-B	S7-2	10	10	10	10	9	13	10	10	9	8	10	10	4	4
Bio-C	S8-7	29	9	7	7	6	8	8	7	7	6	12	7	0	4
Bio-C	S8-8	13	9	8	7	7	8	8	8	7	7	9	8	0	6
Bio-D	S9-7	8	8	8	8	8	10	8	8	7	7	8	8	4	2
Bio-D	S9-1	10	10	10	9	9	57	10	9	9	9	10	19	26	36
Control-G	S9-6	15	10	10	9	9	11	10	9	9	9	11	10	160	140
Control-G	S8-4	9	9	9	9	9	10	10	9	9	9	9	9	200	46
Reference 1	-	10	10	10	9	8	49	18	16	13	12	9	22	6	12
Reference 2	-	38	17	9	9	8	56	31	18	13	11	16	26	10	4
Reference 3	-	25	16	12	11	10	13	9	8	7	7	15	9	6	8

Table 3-4. Statistics of defects found on copper coupons from the SRB exposure groups and corresponding reference coupons. All data are in µm.

Exposure group	All defects			Defects <30 µm		
	Min	Max	Mean (std-dev)	Min	Max	Mean (std-dev)
Bio-A	4	11	7.5 (1.8)	4	11	7.5 (1.8)
Bio-B	5	13	8.1 (2.0)	5	13	8.1 (2.0)
Bio-C	6	29	8.8 (4.9)	6	29	8.8 (4.9)
Bio-D	7	57	11.1 (10.6)	7	10	8.7 (1.0)
Control-G	9	15	9.7 (1.4)	9	15	9.7 (1.4)
Reference 1–3	7	56	16.1 (12.0)	7	25	11.9 (4.2)

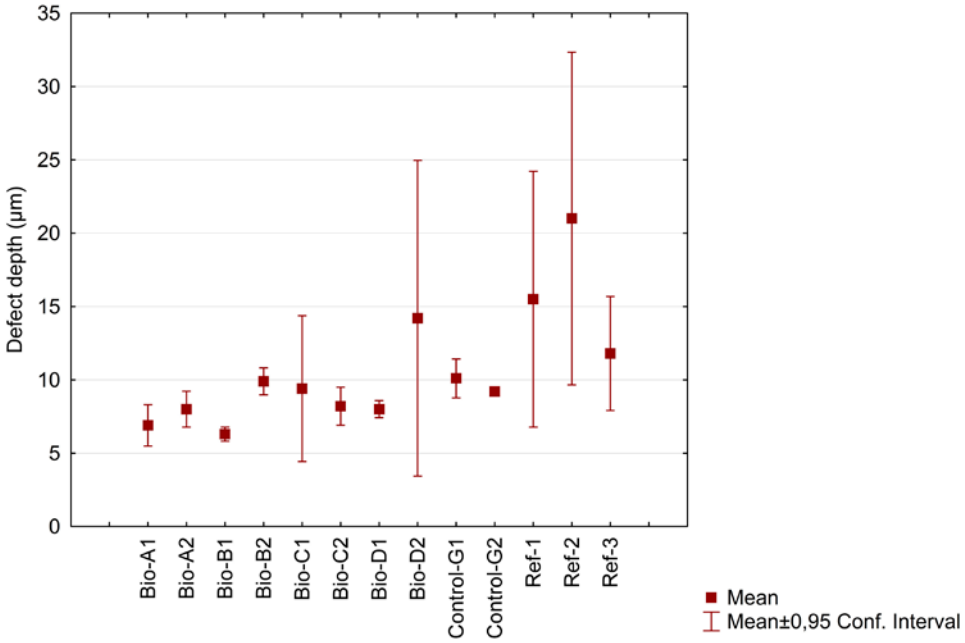

Figure 3-7. *Mean plot of all data collected, i.e. the five deepest defects found on each side for all SRB exposed, control and reference coupons.*

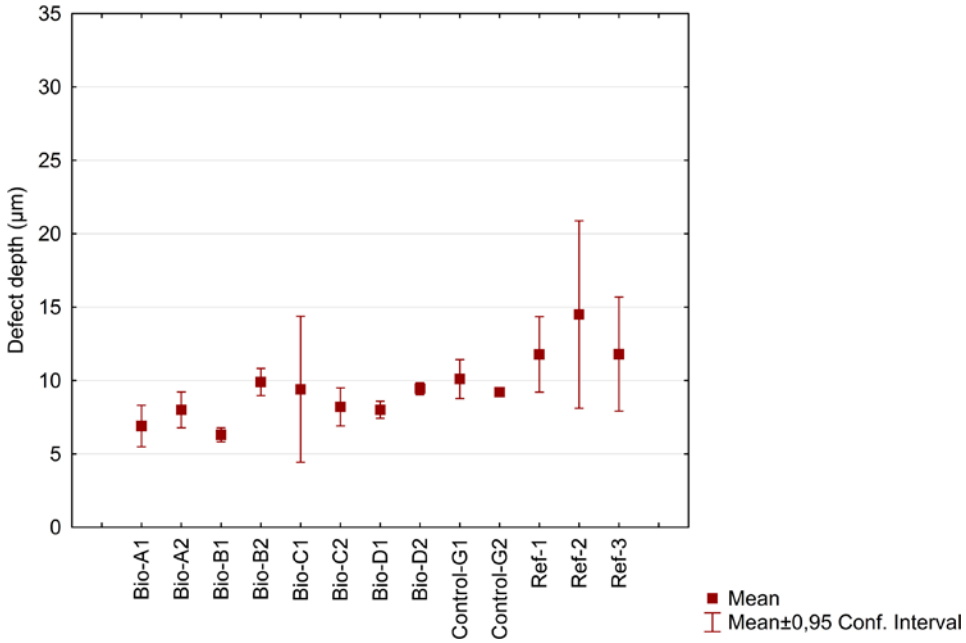

Figure 3-8. *Mean plot with defects > 30 µm excluded from the data set.*

The documented defects can be classified by inspection as belonging to different types of origin. For example, the 4 µm defect shown for Bio-A coupon S7-11 side 1 (Figure 3-9, (a)) seems to be caused by mechanical damage/wear, as several curved ridges following the same pattern suggests that a directed force by some hard object has acted on the surface. Similar defects were found on most coupons, with some examples presented in Figure 3-9. Such marks were found also on the reference coupons, for example the 8 µm deep defect/mark shown in Figure 3-10 (a). Another type of seemingly mechanical damage is exemplified by the notch-like defects (6 and 10 µm respectively) shown for Bio-B coupon S7-2 side 1, see also Figure 3-10 (b) and (c).

The 57 µm deep defect found on Bio-D coupon S9-3 side 2, resembles the 49 µm deep defect found on Reference 1 side 2 (Figure 3-10 (d) and Figure 3-11 (b)), the 38 µm deep defect found on Reference 2 side 1, and the 56 µm deep defect found on Reference 2 side 2 (see Figure 3-10 (e) and (f)) and Appendix C). Both the shape and dimensions of these defects suggest that they are due to removal of crystal grains from the surface, for example during cutting or polishing. It may be noted that the large surface defect shown in Figure 3-11 seems to have been affected by the treatment with 20 wt% NH_4OH, contrary to what was shown in Figure 2-7. This might indicate that the pickling method was still not optimal for examination of corrosion morphology.

However, there are also defects that seem to be caused by corrosion. Coupons from the Bio-D exposure display a number of defects, see for example Figure 3-12 (a), resembling localized corrosion attacks that have been attributed to SRB in a recent work (Dou et al. 2018). In that study it was shown that at a low degree of corrosion (ca 1 µm by mass-loss) the pits attributed to corrosion were deeper than the average corrosion, which might reflect that some defects were present from start also in that experiment. However, with more extensive corrosion (12, 28 and 45 µm average corrosion by mass-loss) the deepest pits found (14, 20, and 44 µm) were of approximately the same depth as the general corrosion. The authors of the paper made the interpretation that general and localized corrosion are equally important processes under the conditions applied (highly nutritious growth media with SRB). Due to the high degree of general corrosion in relation to the localized corrosion attacks, the authors did not describe the localized attacks as due to pitting and a presence of a passive film, but instead suggested that the localized attacks are due to uneven distribution of corrosive metabolites (H_2S/HS^-) under the biofilm.

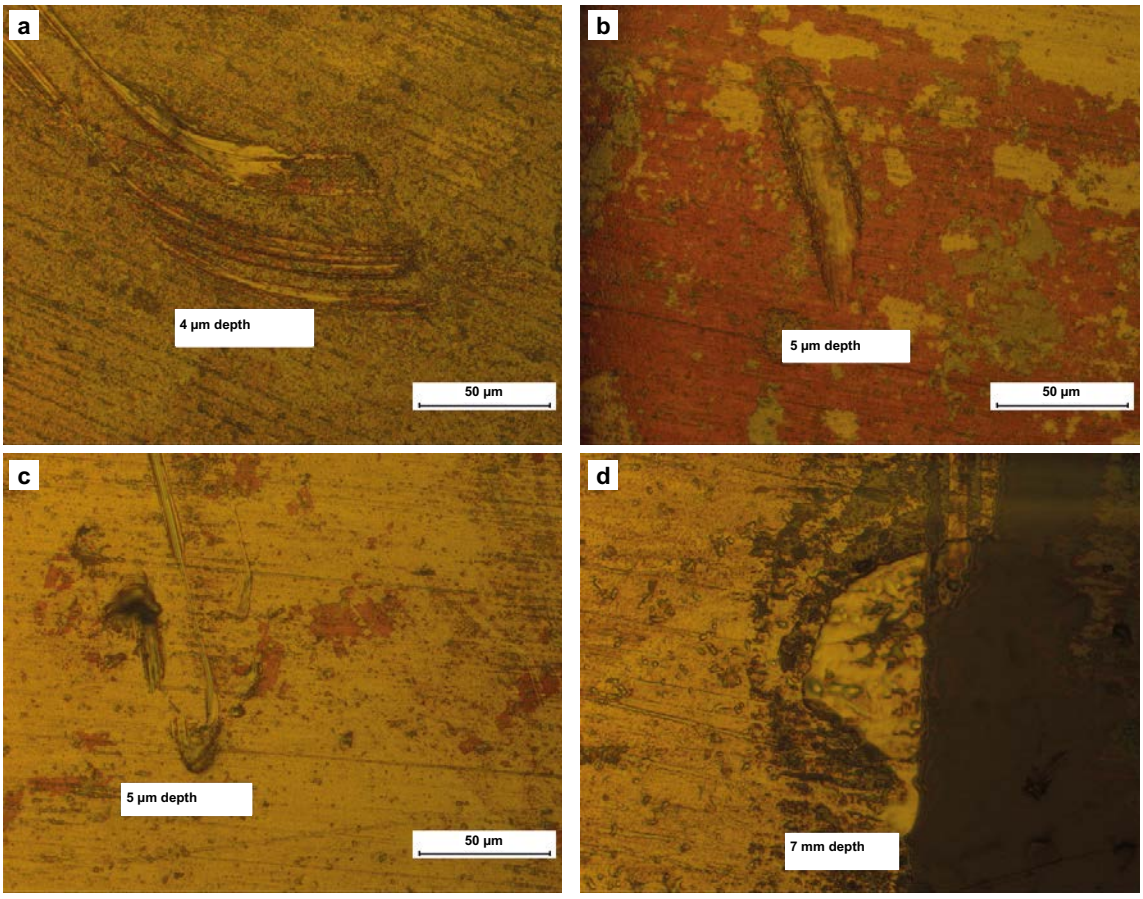

Figure 3-9. *Examples of defects due to apparent mechanical damage. a) Bio-A coupon S7-11 side 1; b) Bio-A coupon S10-3 side 2; c) Bio-A coupon S10-3 side 2; d) Bio-D coupon S9-1 side 2.*

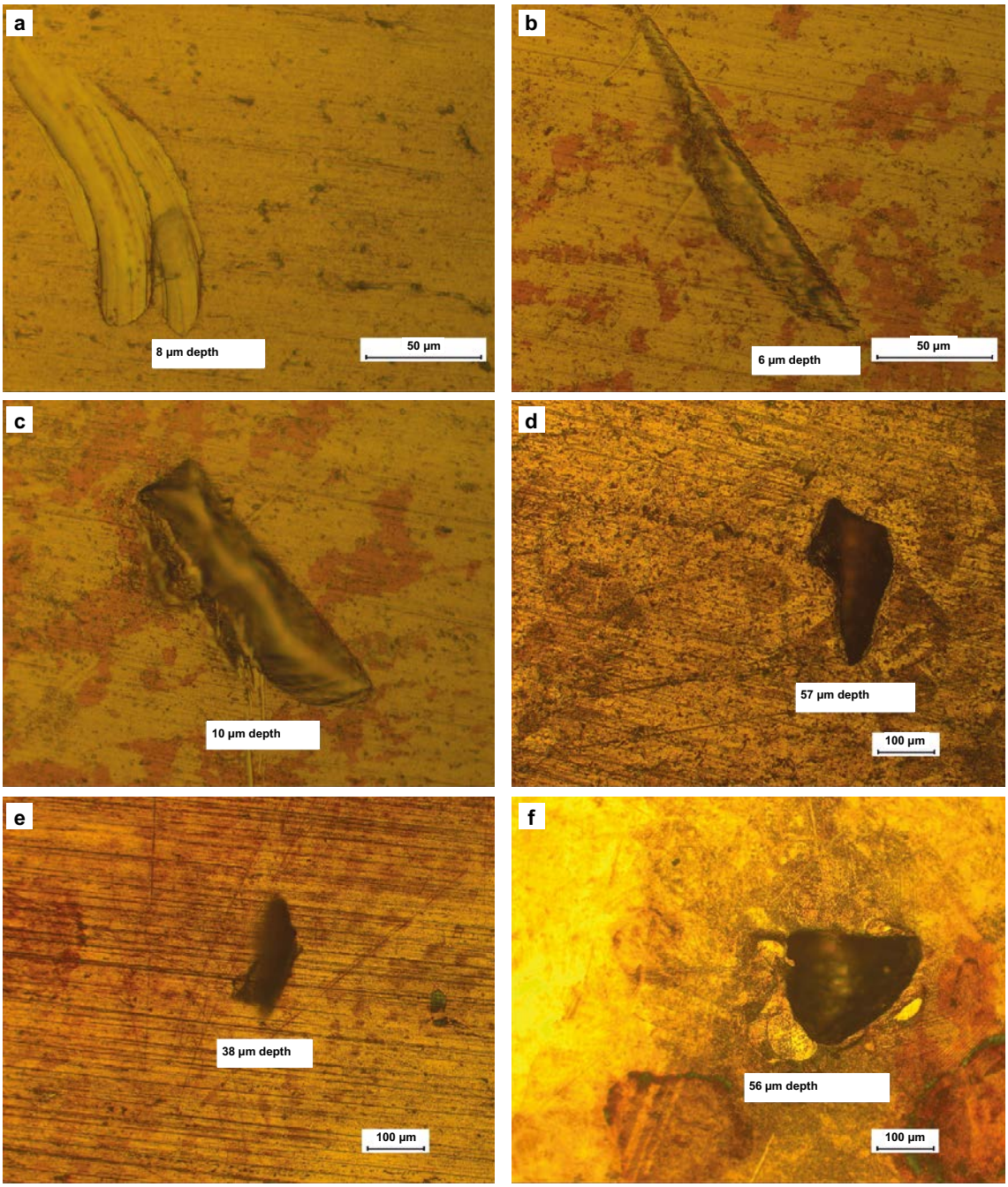

Figure 3-10. *Examples of defects due to apparent mechanical damage on reference coupons. a) Reference coupon 1 side 1; b) Bio-B coupon S7-2 side 1; c) Bio-B coupon S7-2 side 1; d) Bio-D coupon S9-3 side 2; e) Reference 2 side 1; f) Reference 2 side 2.*

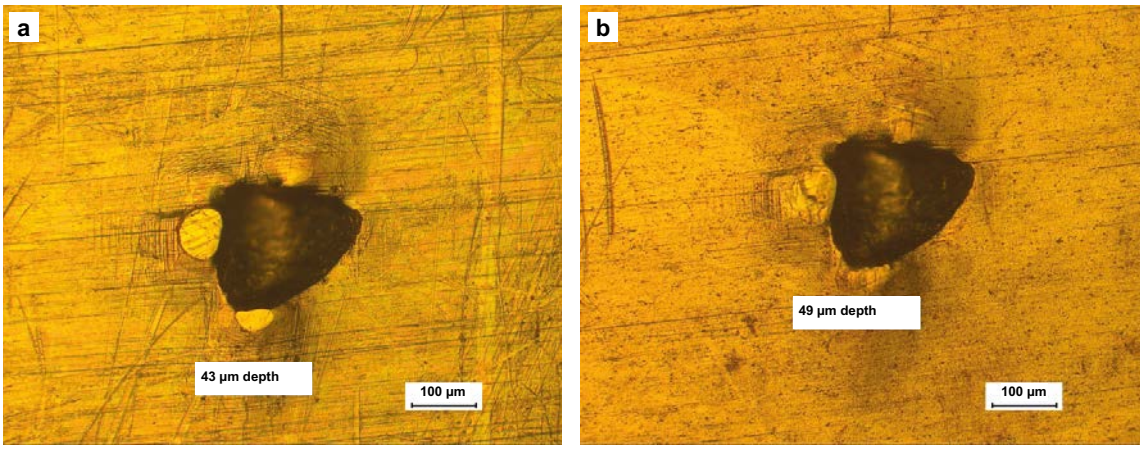

Figure 3-11. *Photographs of deepest defect measured on one of the reference coupons before pickling (a) and after pickling (b) with 20 wt% NH_4OH.*

It is important to note though that localized corrosion described as micro-galvanic corrosion in the vicinity of large crystal grains in the Cu_2S film, has been reported under abiotic sulphide corrosion of copper when the sulphide concentration was 5×10^{-4} M or higher (Chen J et al. 2017, 2019). This type of localised corrosion is thus a possible explanation to the corrosion-like defects observed for example in Figure 3-12 (a), since the sulphide concentration in Bio-D was in the order of 10^{-2} M at the end of the exposure. In addition, there are some features on the Bio-D coupons that could possibly be localized mass-loss due to under-deposit-like corrosion under the biofilm. Several examples of large circular (50–100 µm in diameter) but shallow (7–9 µm) areas are seen on Bio-D S9-3 side 2 (Figure 3-12 (b)).

In the study referred to in the introduction, localized corrosion was also reported for copper under a SRB biofilm in rich medium with lactate and yeast, however, in that study there was no evaluation of mass-loss and general corrosion, meaning that it is not possible to compare the importance of the different corrosion mechanisms (Chen S et al. 2014). Characterization of defects on the reference coupons was not presented in that paper, and the film removal was done using acid (H_2SO_4), which could have had an effect on the surface morphology. It is also worth noting that in both Chen S et al. (2014) and Dou et al. (2018) the sulphide concentration was at least 2×10^{-4} M and in most cases a few mM at the end of exposure, concentrations at which localised corrosion in the form of abiotic micro-galvanic corrosion have been reported, as described above (Chen J et al. 2017, 2019).

The coupons from Control-G had defect densities that were about two orders of magnitude higher than the coupons from Bio-A to Bio-C (Table 3-3), although the depth of the deepest defects was in the same order of magnitude as for the other exposures and the reference specimens (Figures 3-7 and 3-8). The Control-G exposure was abiotic and contained no SRB, although the medium was the same rich medium as in Bio-C and Bio-D, but with 3×10^{-3} M sulphide added from start. The higher surface density of smaller defects in Control-G might indicate that a localised corrosion process was initiated during the abiotic sulphide exposure. As described above, this is not unexpected, since earlier studies of copper corrosion in sulphide solutions have shown that micro-galvanic corrosion can occur when $[HS^-] \geq 5 \times 10^{-4}$ M (Chen J et al. 2017, 2019). A tendency towards higher defect density was also noted for one of the coupons in the Bio-D series (Table 3-3), which had a sulphide concentration of 12×10^{-3} M at the end of the exposure. If correctly interpreted as signs of localised corrosion, one possible explanation for the lower surface density of pits in Bio-D compared with Control-G, could be that it took some time for the sulphide concentration to reach above 5×10^{-4} M in the biotic Bio-D, while Control-G had 3×10^{-3} M from the start. This would also explain why no tendency towards localised corrosion and higher defect density was seen for Bio-C, which contained the same media and SRB as Bio-D but ran only for ten days. It may also be noted that the EDS spectrum for a cross-sectioned coupon from Control-G revealed a film with a higher content of oxygen than most other coupons. This could be due to aerobic exposure after the experiment, however, it can't be disregarded that some oxygen could have been present during the experiment, which could also have affected the observed surface topography.

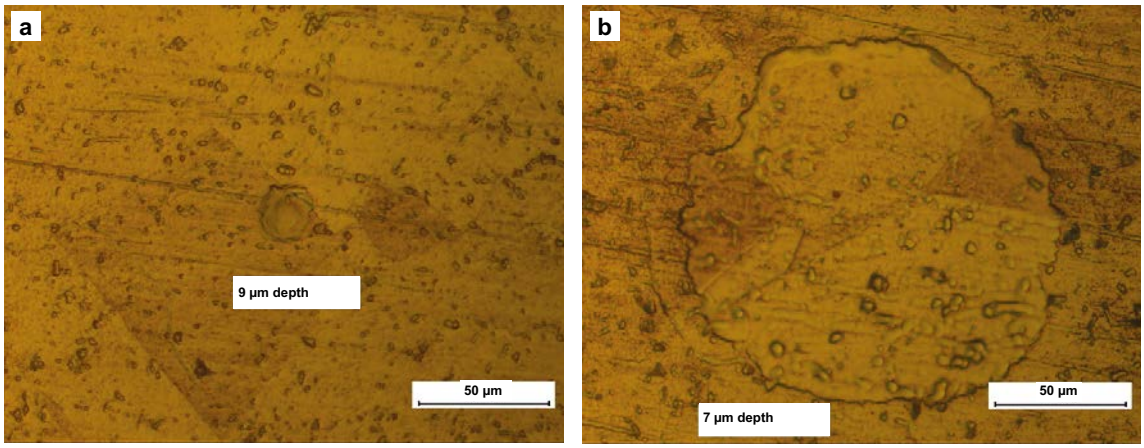

Figure 3-12. *a) Example of a defect found on Bio-D S9-7 side 1 which resembles localized corrosion attacks that have been attributed to SRB in other studies (Dou et al. 2018).b) A wide but shallow defect found on Bio-D S9-3 side 2.*

3.1.3 SEM/EDS results for SRB exposures

One coupon from each exposure was cross-sectioned and analysed using SEM/EDS. The sulphide layer thicknesses were measured at different points on the cross-sectioned coupons (see Table 3-5). The results show a trend of increased thickness with both richness of the medium and exposure duration. Figure 3-13 and Figure 3-14 show the measurement on coupon S10-2 from Bio-A exposure (minimal medium 10 days) and S8-1 from Bio-D (rich medium 30 days).

EDS analyses on the coupons showed that the corrosion product consisted mainly of sulphur, but some amounts of oxygen, calcium, chlorine and silicon were also found. The oxygen content on coupons exposed in Bio-D and Control-G was highest in the outer part of the corrosion film and decreased towards the copper surface (Figure 3-15). The trend of higher oxygen content as the outer surface of the corrosion film is approached might reflect that some air exposure occurred during transportation of the SRB-exposed copper specimens from Micans in Gothenburg to RISE KIMAB AB in Kista, or between opening the glass vials and performing the EDS analysis. The oxygen found could also be due to the plastic used to cast-in the coupons prior to SEM/EDS analysis. Silicon was most likely a residue from coupon preparation, since SiO_2 was used during polishing of the coupons. Results of the EDS analyses for coupon S8-1 from Bio D are shown in Figure 3-15, and complete results from the SEM/EDS analyses can be found in Appendix D.

It may be noted that the Cu_2S film thickness corresponding to weight-loss data (Table 3-2) is always less than the apparent film thickness from SEM cross-sections (Table 3-5). There might be several reasons for this. First of all, weight-loss gives the average corrosion depth over the whole coupon, while the SEM measurements are only carried out at a few points on the cross-sections. Furthermore, film thickness of Cu_2S can't be calculated directly from the copper weight-loss, without making some assumption as regards the porosity of the film.

Table 3-5. Sulphide layer thicknesses measurements on SRB exposed coupons (µm). The numbers 1–4 refer to the number of measurements carried out.

Exposure	Coupon	1	2	3	4	Mean
Bio-A	S10-2	0.16	0.12	0.15	0.09	0.13
Bio-B	S7-6	0.09	0.10	-	-	0.10
Bio-C	S8-6	0.46	-	-	-	0.46
Bio-D	S8-1	1.51	1.53	1.69	-	1.58
Control-G	S7-8	1.21	1.42	1.14	-	1.26

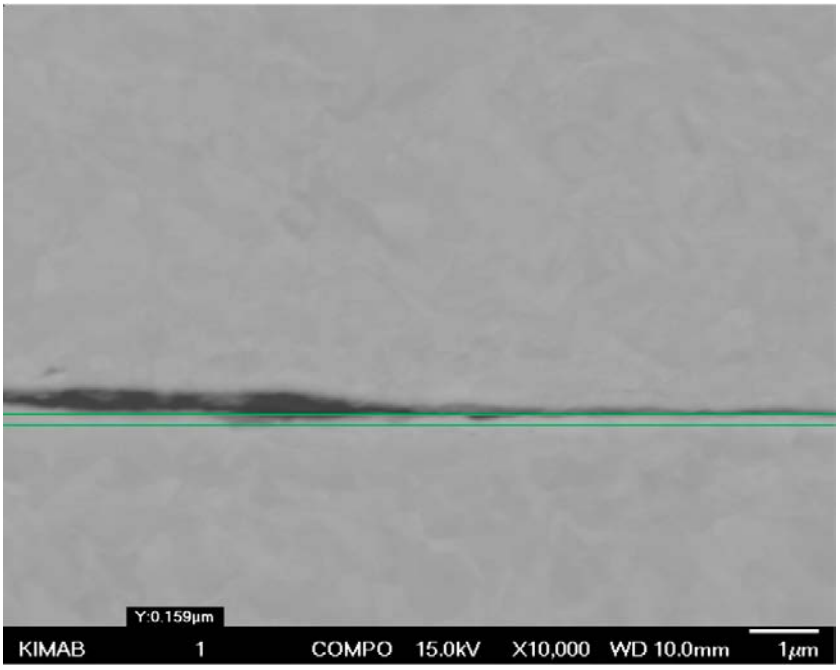

Figure 3-13. *Sulphide thickness measurement on coupon S10-2 (Bio A).*

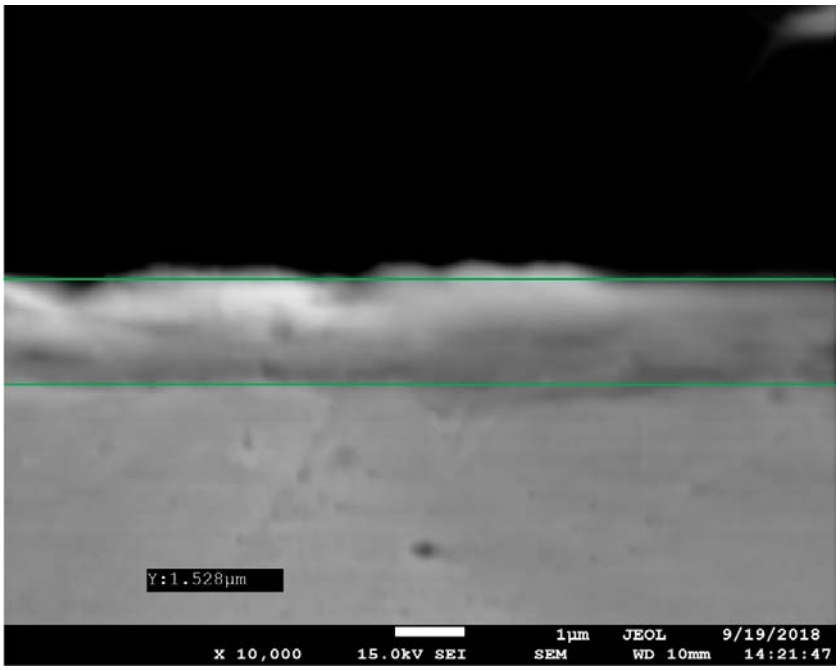

Figure 3-14. *Sulphide thickness measurement on coupon S8-1 (Bio D).*

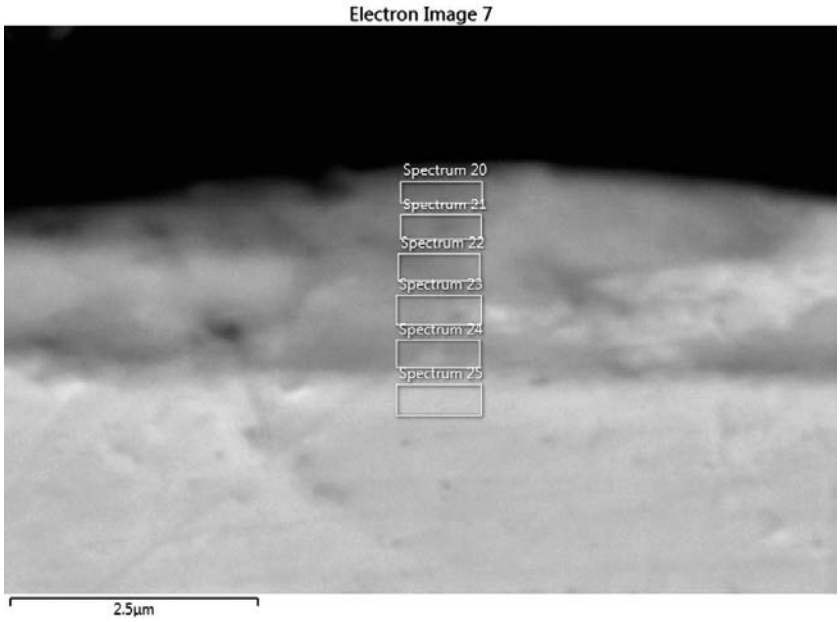

Figure 3-15. *SEM image and EDS analysis on the cross section of coupon 8-1 (Bio D).*

Element (wt%)	Spectrum					
	20	21	22	23	24	25
O	9.41	7.02	5.28	4.23	3.34	1.39
Si		0.52	0.22	0.23	0.8	
S	17.65	20.38	20.48	19.02	14.5	2.63
Cl	0	0.19	0.3	0.2	0.25	0
K	0.48	0.34	0.19	0	0	0
Ca	3.17	2.32	1.54	0.74	0.4	0
Cu	69.29	69.22	72	75.58	80.71	95.99
Total:	100	100	100	100	100	100

3.2 H_2S(g) exposures

3.2.1 Mass loss and average corrosion depth of H_2S exposed coupons

Mass loss and corresponding corrosion depths are presented in Table 3-6 and for each coupon of the gas exposures. Triple coupons were used for mass loss evaluation for each exposure. One coupon was used for SEM/EDS analysis and one coupon was kept as a spare. Mean mass loss and corrosion depth are calculated in Table 3-7. It should be noted that the mass loss results presented herein were obtained with the pickling method using both alkaline and acidic solutions, which, as discussed in chapter 2.4 above, caused localised corrosion attacks of the copper surface. Nevertheless, the effect of the pickling on the mass loss is accounted for due to the use of reference coupons during pickling.

The most extensive corrosion measured was in exposure Gas D (10^4 wt.ppm, 30 days). From the results it can be seen that increasing the H_2S concentration and exposure period increased the corrosion of the coupons. By analysing the average corrosion depths obtained it can be seen that increasing the exposure period by a factor of three gave an increase in corrosion by a factor of approximately five. This trend holds for the exposures of H_2S at both 10 wt.ppm and 10^4 wt.ppm. A possible explanation for this could be that the sulphidation of the pre-existing oxide film ($Cu_2O + HS^- \rightarrow Cu_2S + OH^-$) takes some time and that the actual corrosion process doesn't become efficient before the oxide is completely removed.

Table 3-6. Mass loss and corrosion depth for H_2S exposed coupons.

Exposure	Coupon denotation	Mass loss (g/m^2)	Depth of corrosion (µm)
Gas A	S6-1	1.834	0.21
Gas A	S6-2	1.907	0.21
Gas A	S6-3	1.790	0.20
Gas B	S2-1	9.407	1.06
Gas B	S2-2	10.628	1.19
Gas B	S2-3	10.752	1.21
Gas C	S1-6	4.586	0.52
Gas C	S1-7	4.625	0.52
Gas C	S1-8	4.656	0.52
Gas D	S2-6	19.576	2.20
Gas D	S2-7	22.598	2.54
Gas D	S2-8	21.709	2.44

Table 3-7. Mean mass loss and corrosion depth for coupons exposed to Gas-A to Gas-D.

Exposure	Mass loss (g/m^2)	Mass loss Std. Dev. (g/m^2)	Depth of corrosion (µm)	Depth of corrosion Std. Dev. (µm)
Gas A	1.843	0.0591	0.21	0.007
Gas B	10.262	0.7438	1.15	0.084
Gas C	4.622	0.0351	0.52	0.004
Gas D	21.294	1.5531	2.39	0.175

3.2.2 SEM/EDS results H_2S exposures

One coupon from each $H_2S(g)$ exposure was cross-sectioned and the copper sulphide layer thicknesses were measured using SEM (Table 3-8). As expected, the results show a trend of increased thickness with both sulphide concentration and exposure duration. Figure 3-16 to Figure 3-19 show SEM images of cross-sectioned coupons from Gas-A to Gas-D. From the cross sections analysed for Gas-A, Gas-B and Gas-C it seems that the copper sulphide film formed is not adherent to the underlying copper surface, while the resolution of the SEM images is too low to examine the film morphology (Figure 3-16, Figure 3-17 and Figure 3-18). On the contrary, the copper sulphide film formed on the coupons in the Gas-D series, seems to be adherent to the copper surface (Figure 3-19) and appears to have a compact morphology (Figure 1-14, Appendix D), similar in appearance to what has been observed at high sulphide concentrations in earlier studies (Martino et al. 2014). It should be noted that whether the film appears adherent or not to the underlying copper surface, might be affected by the coupon preparation in order to examine cross sections, however, even if this is the case, the film formed in the Bio-D series has not been detached by the preparation. Although localised corrosion could be expected at the higher sulphide concentration in Gas-C and Gas-D (2.14×10^{-4} M), for which micro-galvanic corrosion has been reported (Chen J et al. 2017, 2019), the cross-sections reveal no obvious signs of localised corrosion, but rather a roughly corroded copper surface beneath the copper sulphide film.

The EDS analyses showed that the corrosion product layer consisted mainly of copper and sulphur, but some amounts of oxygen, calcium, chlorine and silicon were also detected. The relatively small amounts of oxygen in the film could be due to atmospheric exposure during transportation and handling after the exposure. The silicon was most likely residue from coupon preparation (SiO_2 is used during polishing of the coupons). All results from the SEM/EDS analyses can be found in Appendix D.

Table 3-8. Sulphide layer thicknesses measured on H_2S exposed coupons, (µm).

Exposure	Coupon	1	2	3	4	Mean
Gas-A	S6-4	0.28	0.28	0.27	0.35	0.30
Gas-B	S2-4	0.71	0.91	0.68	0.69	0.75
Gas-C	S1-10	1.52	1.57	1.05	1.50	1.41
Gas-D	S2-10	4.60	6.10	4.55	5.19	5.11

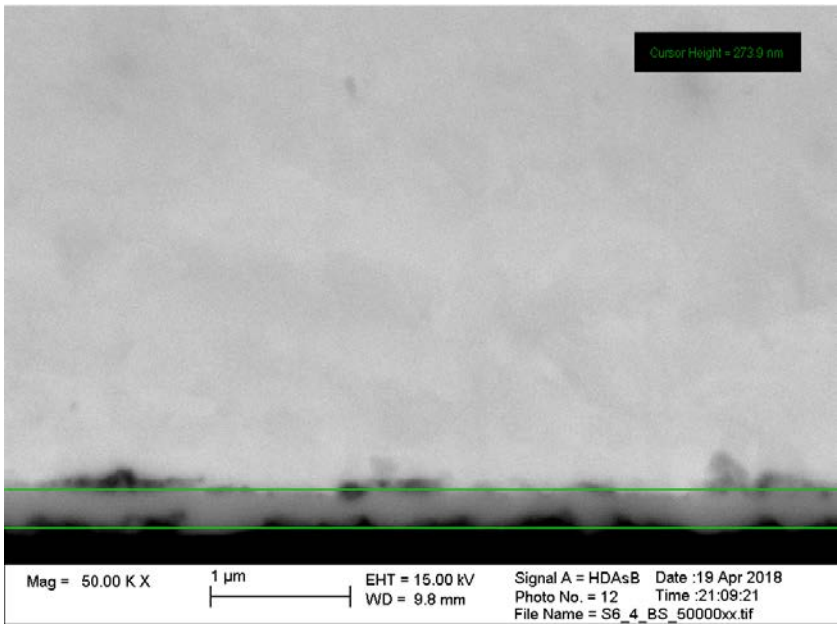

Figure 3-16. *SEM image of the cross section of coupon S6-4 (Gas-A) showing the sulphide layer thickness of 0.27 µm on the surface of the coupon.*

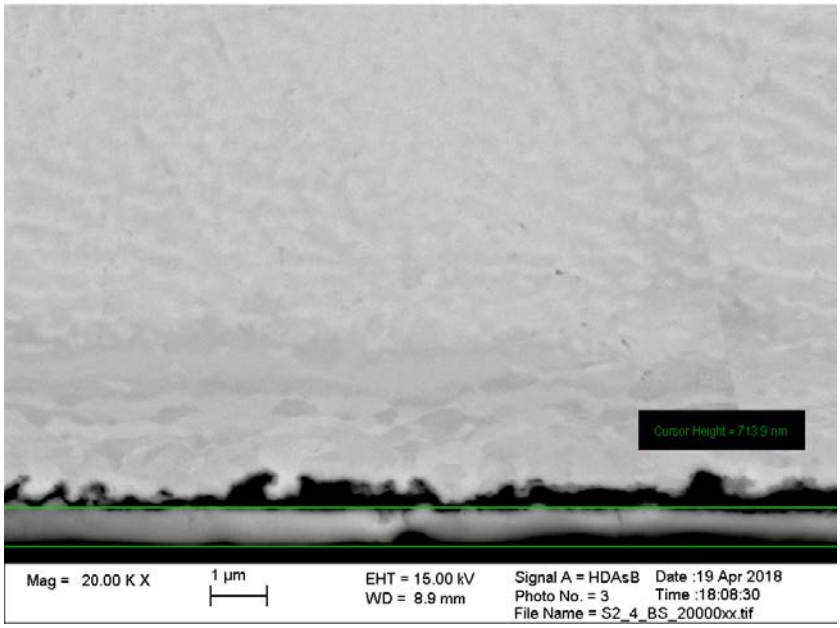

Figure 3-17. *SEM image of the cross section of coupon S2-4 (Gas-B) showing the sulphide layer thickness of 0.71 µm on the surface of the coupon.*

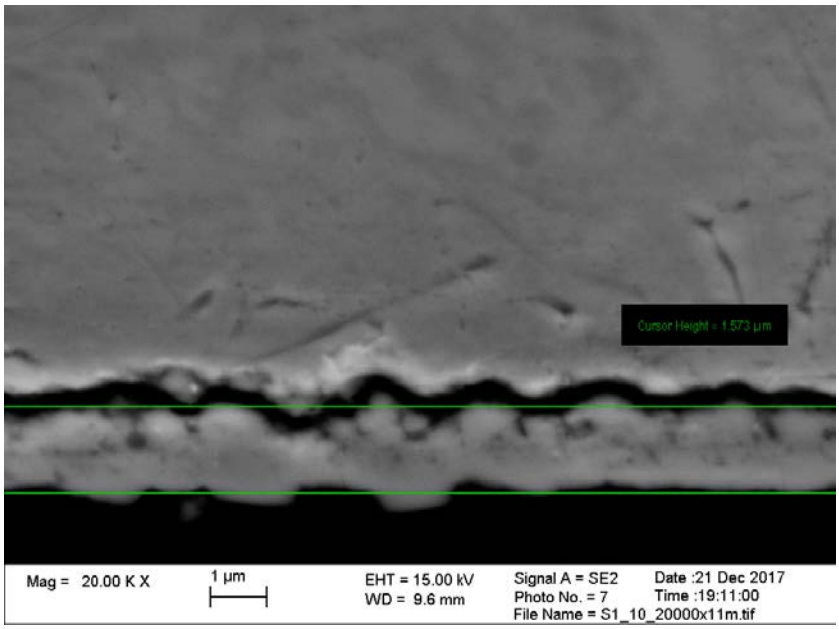

Figure 3-18. *SEM image of the cross section of coupon S1-10 (Gas-C) showing the sulphide layer thickness of 1.57 µm on the surface of the coupon.*

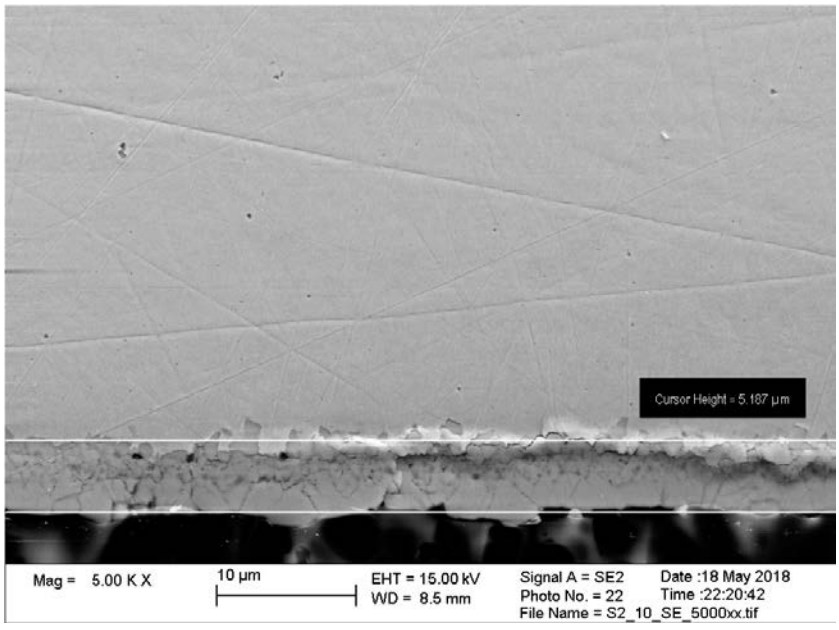

Figure 3-19. *SEM image of the cross section of coupon S2-10 (Gas-D) showing the sulphide layer thickness of 5.2 µm on the surface of the coupon.*

4 Conclusions

Copper coupons were exposed to either $H_2S(g)$ or solutions with sulphate reducing bacteria (SRB) in order to examine the corrosion morphology of copper in relation to the magnitude of corrosion in these sulphide environments. In each environment, four different exposure conditions were tested; low and high partial pressures of H_2S gas for 10 and 30 days each, and; minimal and rich growth media with SRB for 10 and 32 days each.

The formation of a biofilm of *D. aespoeensis* was verified by microscopy for Bio-C and Bio-D (rich medium), while only a few cells were observed on the copper coupons of Bio-A and Bio-B (minimal medium comparable to Forsmark ground water). The average corrosion depth, calculated from mass-loss, in the SRB exposures did not change significantly for the minimal medium between 10 to 32 days of exposure, but in the rich medium the corrosion depth increased from 0.1 µm to 0.2 µm.

In the H_2S exposures the average corrosion depth increased from 0.2 µm to 1.2 µm in the lower H_2S partial pressure, and from 0.5 µm to 2.4 µm for the higher partial pressure between the 10- and 30-day exposure periods.

Surface defects on the copper coupons were counted and measured by light optical microscopy, both for SRB-exposed coupons after removal of the corrosion film and for reference coupons. Statistical analysis of the deepest defects found suggested that these are not related to the corrosion exposures. Inspection of the shape and morphologies of the deepest defects further suggests that most of these are due to different types of mechanical damage and wear that occurred before or during preparation of the coupons (i.e. cutting and polishing).

The defect density (number of defects per unit area) was evaluated for the SRB-exposed coupons, along with abiotic controls and reference coupons. While most of the corroded coupons and reference coupons showed only a few defects per cm^2, the abiotic Control-G with 3×10^{-3} M added sulphide had hundreds of defects per cm^2. This could be interpreted as a sign of initiation of a localized corrosion process. This result is not unexpected, since the concentration of sulphide (3×10^{-3} M) in the abiotic Control-G series was higher than what is typically required to induce micro-galvanic corrosion on copper in anoxic sulphide solutions (5×10^{-4} M). A similar tendency of higher defect density, possibly a sign of localised corrosion, was also observed for one of the coupons of the Bio-D series, for which the sulphide concentration at the end of the exposure was 12×10^{-3} M.

For the $H_2S(g)$ exposures, cross-sections of the corroded copper coupons were examined with SEM-EDS. The conditions of the Gas-C and Gas-D exposures (10 000 wt.ppm $H_2S(g)$ in the gas-phase, corresponding to 2.14×10^{-4} M sulphide in the aqueous phase) would, according to earlier studies, be supportive to micro-galvanic corrosion provided that the water film on the copper surface was thick and conductive enough. However, no obvious localised corrosion was observed, instead the copper surfaces beneath the copper sulphide corrosion films seemed rather roughly corroded.

During the course of the present work the method of evaluating the mass loss due to corrosion was developed as the original method of removing corrosion products with a combination of alkaline (20 wt% NH_4OH) and acidic (37 wt% HCl diluted by 50 %) solutions was deemed to have caused localised corrosion of the coupon surfaces and thus compromised the accuracy of the defect measurements. The outcome of this evaluation was to use only the alkaline solution (20 wt% NH_4OH) for copper coupons with a sulphide corrosion product.

While the present analysis of defects before and after corrosion exposure relies on statistical comparison of the corroded coupons with uncorroded reference coupons, it might in principle be possible to make the analysis deterministic by full characterisation of selected areas of individual coupons before and after corrosion exposure. In the present work this was done only for selected reference coupons used during the evaluation of the pickling methods. It is therefore recommended for any future experiments that full characterization of coupons is performed. This may be achieved in an efficient way by selecting a small coupon surface subarea of ca 0.5 cm^2, which may be characterized on each coupon.

References

SKB's (Svensk Kärnbränslehantering AB) publications can be found at www.skb.com/publications. SKBdoc documents will be submitted upon request to document@skb.se.

ASTM, 2013. ASTM G46-94: Standard guide for examination and evaluation of pitting corrosion. West Conshohocken, PA: ASTM International.

Bengtsson A, Blom A, Hallbeck B, Heed C, Johansson L, Stalén J, Pedersen K, 2017. Microbial sulphide-producing activity in water saturated MX-80, Asha and Calcigel bentonite at wet densities from 1 500 to 2 000 kg m^{-3}. SKB TR-16-09, Svensk Kärnbränslehantering AB.

Chen J, Qin Z, Shoesmith D W, 2011. Long-term corrosion of copper in a dilute anaerobic sulfide solution. Electrochimica Acta 56, 7854–7861.

Chen J, Qin Z, Shoesmith D W, 2014. Key parameters determining structure and properties of sulphide films formed on copper corroding in anoxic sulphide solutions. Corrosion Engineering, Science and Technology 49, 415–419.

Chen J, Qin Z, Martino T, Shoesmith D W, 2017. Non-uniform film growth and micro/macro-galvanic corrosion of copper in aqueous sulphide solutions containing chloride. Corrosion Science 114, 72–78.

Chen J, Guo M, Martino T, Ramamurthy S, Noël J J, Shoesmith D, Lilja C, Johansson A J, 2019. The distribution of corrosion damage to copper surfaces exposed to aqueous sulphide solutions. SKBdoc 1706406 ver 1.0, Svensk Kärnbränslehantering AB.

Chen S, Wang P, Zhang D, 2014. Corrosion behaviour of copper under biofilm of sulfate-reducing bacteria. Corrosion Science 87, 407–415.

Dou W, Jia R, Jin P, Liu J, Chen S, Gu T, 2018. Investigation of the mechanism and characteristics of copper corrosion by sulfate reducing bacteria. Corrosion Science 144, 237–248.

Höllmark H M, Keech P G, Vegelius J R, Werme L, Duda L-C, 2012. X-ray absorption spectroscopy of electrochemically oxidized Cu exposed to Na_2S. Corrosion Science 54, 85–89.

Johansson L, 2019. Exposure of copper to sulphate reducing bacteria and verification of a biofilm. Batch 2. SKBdoc 1701933 ver 1.0, Svensk Kärnbränslehantering AB.

King F, Lilja C, Pedersen K, Pitkänen P, Vähänen M, 2010. An update of the state-of-the-art report on the corrosion of copper under expected conditions in a deep geologic repository. SKB TR-10-67, Svensk Kärnbränslehantering AB.

King F, Lilja C, Vähänen M, 2013. Progress in the understanding of the long-term corrosion behaviour of copper canisters. Journal of Nuclear Materials 438, 228–237.

King F, Chen J, Qin Z, Shoesmith D, Lilja C, 2017. Sulphide mass-transport control of the corrosion of copper canisters. Corrosion Engineering, Science and Technology 52, 210–216.

Kristiansen P T, Massel F, Werme L, Lilja C, Duda L-C, 2015. Sulfidation of single-phase oxide on copper and as powder studied using soft x-ray spectroscopy. Journal of The Electrochemical Society 162, C785–C791.

Martino T, Partovi-Nia R, Chen J, Qin Z, Shoesmith D W, 2014. Mechanisms of film growth on copper in aqueous solutions containing sulphide and chloride under voltammetric conditions. Electrochimica Acta 127, 439–447.

Martino T, Chen J, Qin Z, Shoesmith D W, 2017. The kinetics of film growth and their influence on the susceptibility to pitting of copper in aqueous sulphide solutions. Corrosion Engineering, Science and Technology 52, 61–64.

Sander R, 1999. Compilation of Henry's law constants for inorganic and organic species of potential importance in environmental chemistry. Mainz, Germany: Max-Planck Institute of Chemistry. Available at: https://www.ft.unicamp.br/~mariaacm/ST405/Lei%20de%20Henry.pdf

Sharma, 1980. Reaction of copper and copper oxide with H_2S. Journal of The Electrochemical Society 127, 21–26.

SKB, 2010. Corrosion calculations report for the safety assessment SR-Site. SKB TR-10-66, Svensk Kärnbränslehantering AB.

SKB, 2011. Long-term safety for the final repository for spent nuclear fuel at Forsmark. Main report of the SR-Site project. SKB TR-11-01, Svensk Kärnbränslehantering AB.

Smith J M, Wren J C, Odziemkowski M, Shoesmith D W, 2007. The electrochemical response of preoxidized copper in aqueous sulfide solutions. Journal of The Electrochemical Society 154, C431–C438.

SS-EN ISO 8407:2014. Corrosion of metals and alloys – Removal of corrosion products from corrosion test specimens (ISO 8407:2009). Stockholm: Swedish Standards Institute.

Stenlid J H, Johansson A J, Leygraf C, Brinck T, 2017. Computational analysis of the early stage of cuprous oxide sulphidation: a top-down process. Corrosion Engineering, Science and Technology 52, 50–53.

Stroes-Gascoyne S, Haveman S A, Hamon C J, Delaney T-L, Pedersen K, Arlinger J, Ekendahl S, Hallbeck L, Jahromi N, Dekeyser K, Daumas S, 1997. Occurrence and identification of micro-organisms in compacted clay-based buffer material designed for use in a nuclear fuel waste disposal vault. Canadian Journal of Microbiology 43, 1133–1146.

Tullborg E-L, Smellie J, Nilsson A-C, Gimeno M, Augué L F, Brüchert V, Molinero J, 2010. SR-Site – sulphide content in the groundwater at Forsmark. SKB TR-10-39, Svensk Kärnbränslehantering AB.

Appendix A

Pickling procedure

A1 Introduction

Following the results obtained from the H_2S exposures and from the first SRB exposures, it was decided that the method of removal of corrosion products on copper coupons should be examined in order to avoid detrimental effects of pickling solutions, i.e. that the pickling solution initiates localized corrosion or increases the depths of defects observed on the exposed surfaces.

Initially, pickling solutions of 20 wt% NH_4OH and 37 wt% HCl were used to remove Cu_2S and CuS corrosion products from exposed coupons and it was observed that defects on unexposed reference coupons (used in the pickling procedure) had increased in depth. Therefore, a new pickling procedure where only 20 wt% NH_4OH was tried in order to investigate if this was a more suitable method for examining surface topography and localized corrosion on copper coupons.

The coupons used for this investigation were named S1-3, S1-4, S1-5, see Figure A-1, and had been exposed for 10 days in nominally 10 wt.ppm H_2S gas. These coupons were chosen for this investigation as they were spare coupons as this test had to be repeated due to the concentration of H_2S being out of specification during the exposure period as well as the teflon wire suspending the coupons failing so that the coupons were not correctly positioned in the test chamber. The exact exposure conditions for the three coupons are not known, but this was not of concern for the evaluation of the pickling method. Instead, the aim was to investigate if using the alkaline solution only was efficient enough to remove the corrosion products to allow determination of mass loss, while still gentle enough not to affect the topography of the underlying copper surface, as to initiate or enhance the depth of any defects. One unexposed copper coupon was used as a reference during the pickling and during the investigation of defects on the surfaces. This reference coupon was of the same material and had been prepared in the same manner as the other three coupons.

A1.1 Investigation

The coupons were first characterized under a metallographic microscope in order to quantify defect depths and the density of defects on the surface. Due to the presence of corrosion products it is possible that not all defects were measured in this phase, as they may have been covered by the corrosion film. The coupons were then pickled in NH_4OH solution at 5 minute intervals until all corrosion products were removed (see pickling curves in Figure A-4 and Figure A-5).

The coupons were then examined once again under the microscope in order to quantify defect depths and density. Here, defect density is defined as the number of defects deeper than 6 μm for a chosen area.

SEM/EDS analysis of cross-sections of the coupons was carried out in order to investigate the presence of corrosion products after pickling and their elemental composition.

A comparison of mass loss calculated after pickling with the previous NH_4OH + HCl and the current NH_4OH method was also performed.

A1.1.1 Coupon preparation

The coupons were prepared in the same way as is described in the main body of this report.

A1.1.2 Coupon analysis

Microscope analyses were carried out using the equipment described in the main body of this report.

A1.1.3 Repeated pickling method

Initial weights of each coupon were obtained with an accuracy of ± 0.00009 g before exposure. After exposure each coupon was weighed again. In order to remove corrosion products the pickling was performed in 20 % NH_4OH in an ultrasonic bath. The coupons were weighed between each pickling time of 5 minutes. The pickling was repeated until the pickling curve was considered to be linear.

A2 Results

A2.1 Defect measurements

Table A-1 and Table A-2 show the results of the defect depth measurements on reference coupons before and after exposure to the pickling solution. As can be seen the depths of the defects increased during the pickling using both alkaline and acidic solutions but did not increase after pickling in only the alkaline solution.

Table A-3 to Table A-5 below show the results of the defect depth measurements for coupons S1-3 to S1-5, before and after pickling in only NH_4OH. The defects had increased in depth on the exposed coupons after pickling but this could be due to that the depths measured before pickling included the corrosion product layer, and after pickling this thickness of material is removed.

See Figure A-1 for the appearance of the coupons after pickling. Although some surface deposits remain after pickling, the pickling curves (see Figure A-4 and Figure A-5) appear linear and so the pickling can be considered complete. Figure A-6 and Figure A-7 show the pickling curves for coupons S6-1 to S6-3, the repeated test in 10 wt.ppm H_2S for 10 days, pickled in both alkaline and acidic solutions. Figure A-2 and Figure A-3 show the appearance of the defects as seen through the microscope, before and after pickling. Further images are presented in Figure A-14 to Figure A-16.

Figure A-1. *Appearance of the exposed coupons after pickling, coupon S1-3 (left), S1-4 (middle), S1-5 (right). Coupon S1-3 had the least surface deposits remaining after the pickling. The black square marked on the coupons denotes the area used for analysing defect density on the coupons.*

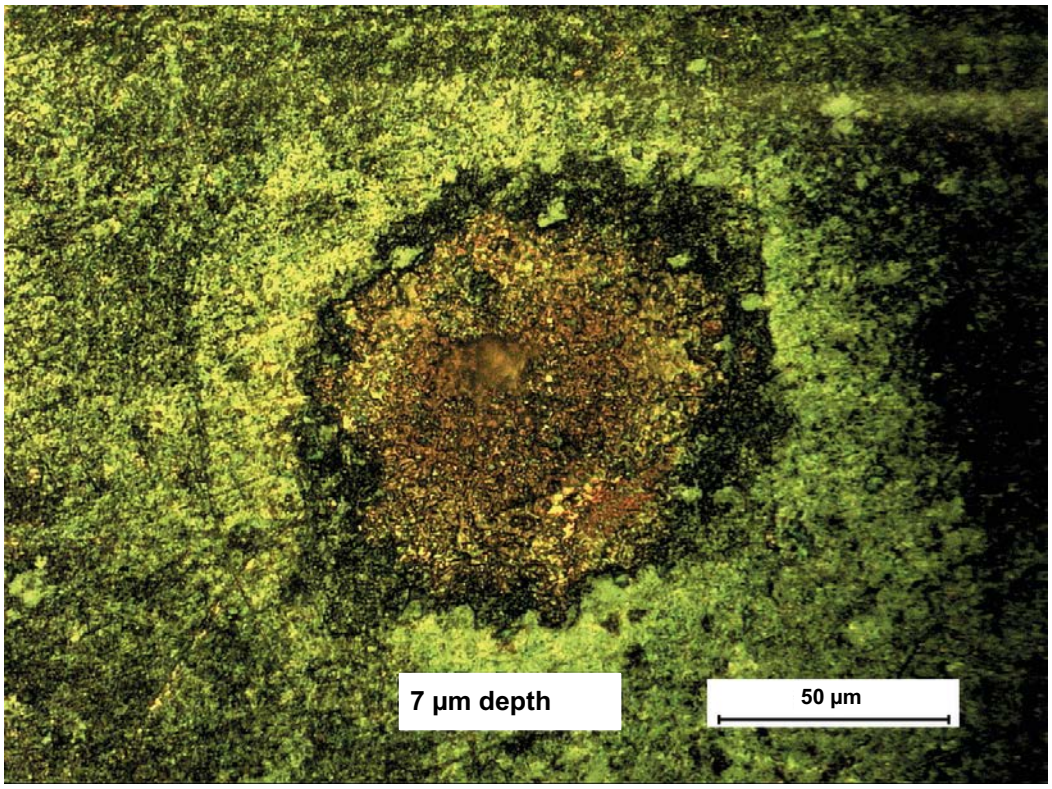

Figure A-2. *Example of defect found on coupon S1-4 after exposure before pickling. The surface deposits can be seen around the defected area.*

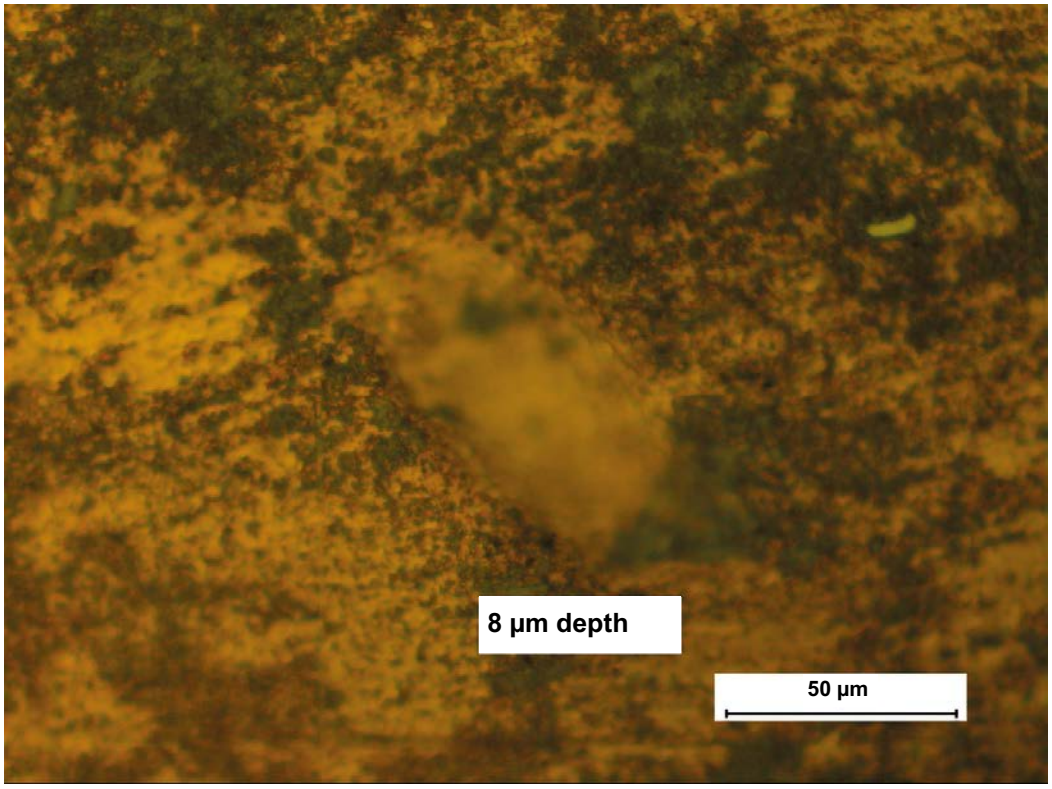

Figure A-3. *Defect found on coupon S1-5 after pickling. The darker areas around the defect are corrosion products that have remained after the pickling.*

Table A-1. Analysis of surface defects found on a test coupon used during pickling in NH_4OH + HCl. The observed defects had deepened significantly during pickling.

			5 deepest defects, side 1					5 deepest defects, side 2						Side 1			Side 2		
Reference coupon	**Corrosion (g/m^2)**	**Corrosion (µm)**	**1**	**2**	**3**	**4**	**5**	**1**	**2**	**3**	**4**	**5**	**Deepest defect (µm)**	**Area (cm^2)**	**No. of defects**	**Defect density ($defects/cm^2$)**	**Area (cm^2)**	**No. of defects**	**Defect density ($defects/cm^2$)**
Before pickling	–	–	6	5	5	5	5	9	8	8	7	8	9	0.5	2	4	0.5	2	4
After pickling	0.0008	0.3406	18	9	9	8	8	16	12	11	10	9	18	0.5	0	0	0.5	2	4

Table A-2. Results after pickling in NH_4OH of reference coupon.

			5 deepest defects, side 1					5 deepest defects, side 2						Side 1			Side 2		
Reference coupon	**Corrosion (g/m^2)**	**Corrosion (µm)**	**1**	**2**	**3**	**4**	**5**	**1**	**2**	**3**	**4**	**5**	**Deepest defect (µm)**	**Area (cm^2)**	**No. of defects**	**Defect density ($defects/cm^2$)**	**Area (cm^2)**	**No. of defects**	**Defect density ($defects/cm^2$)**
Before pickling	–	–	9	9	8	7	7	25	24	22	19	17	25	0.5	7	14	0.5	6	12
After pickling	0.7145	0.08	11	10	9	8	7	26	26	24	16	15	26	0.5	5	10	0.5	6	12

Table A-3. Results after pickling in NH_4OH of coupon S1-3.

			5 deepest defects, side 1					5 deepest defects, side 2						Side 1			Side 2		
Coupon S1-3	**Corrosion (g/m^2)**	**Corrosion (µm)**	**1**	**2**	**3**	**4**	**5**	**1**	**2**	**3**	**4**	**5**	**Deepest defect (µm)**	**Area (cm^2)**	**No. of defects**	**Defect density ($defects/cm^2$)**	**Area (cm^2)**	**No. of defects**	**Defect density ($defects/cm^2$)**
Before pickling	–	–	17	16	11	9	9	14	10	8	8	8	17	0.5	4	8	0.5	1	2
After pickling	5.29	0.59	22	20	16	13	12	14	11	11	11	10	22	0.5	10	20	0.5	1	2

Table A-4. Results after pickling in NH_4OH of coupon S1-4

			5 deepest defects, side 1					5 deepest defects, side 2						Side 1			Side 2		
Coupon S1-4	**Corrosion (g/m^2)**	**Corrosion (µm)**	**1**	**2**	**3**	**4**	**5**	**1**	**2**	**3**	**4**	**5**	**Deepest defect (µm)**	**Area (cm^2)**	**No. of defects**	**Defect density ($defects/cm^2$)**	**Area (cm^2)**	**No. of defects**	**Defect density ($defects/cm^2$)**
Before pickling	–	–	16	8	8	7	7	14	8	8	7	7	16	0.5	1	2	0.5	1	2
After pickling	2.39	0.27	20	13	12	11	10	27	25	16	16	16	27	0.5	6	12	0.5	3	6

Table A-5. Results after pickling in NH_4OH of coupon S1-5.

			5 deepest defects, side 1					5 deepest defects, side 2						Side 1			Side 2		
Coupon S1-5	**Corrosion (g/m^2)**	**Corrosion (µm)**	**1**	**2**	**3**	**4**	**5**	**1**	**2**	**3**	**4**	**5**	**Deepest defect (µm)**	**Area (cm^2)**	**No. of defects**	**Defect density ($defects/cm^2$)**	**Area (cm^2)**	**No. of defects**	**Defect density ($defects/cm^2$)**
Before pickling	–	–	11	10	10	8	7	11	10	9	8	8	11	0.5	1	2	0.5	1	2
After pickling	2.94	0.33	14	13	12	11	10	14	14	11	12	12	14	0.5	4	8	0.5	9	18

A2.2 Mass loss

The mass loss results as calculated using the modified pickling method are presented in Table A-6 below. Comparing the mass loss between the reference coupon and the exposed coupons it can be seen that the reference coupon lost 0.7 g/m^2 due to pickling and removal of the native oxide film, whilst the sulphide exposed coupons lost between 2.4 g/m^2 and 5.3 g/m^2.

Table A-7 below shows the results from the mass loss analyses of the repeated test carried out for 10 days in 10 wt.ppm H_2S (i.e. similar conditions) using the initial pickling method.

As mentioned above, coupons S1-3 to S1-5 were exposed to slightly higher concentrations of H_2S than specified, which might explain their slightly larger weight loss, and why their exposure was repeated. This means that a comparison between these coupons and the coupons S6-1 to S6-3 is not completely representative, but this is the best data available for such as comparison.

The mass loss measured on the two sets of coupons is of the same order of magnitude. This implies that pickling with only 20 % NH_4OH is a suitable method for determining mass loss and subsequently defect depth of copper exposed in such environments.

Table A-6. Mass loss results after 10 day exposure to nominally 10 wt.ppm H_2S (exposure conditions deviated from the specification), (70 – 80 % RH, 80 – 90 °C) and pickling in NH_4OH.

	Mass loss	
Coupon	g	g/m^2
Reference (unexposed)	0.0012	0.7145
S1-3	0.0122	5.2926
S1-4	0.0055	2.3948
S1-5	0.0068	2.9424

Table A-7. Mass loss results after 10 day exposure to 10 wt.ppm H_2S (70 – 80 % RH, 80 – 90 °C) and pickling in NH_4OH + HCl.

	Mass loss	
Coupon	g	g/m^2
Reference (unexposed)	0.0008	0.3406
S6-1	0.0040	1.8339
S6-2	0.0042	1.9066
S6-3	0.0038	1.7896

A2.2.1 Pickling curves

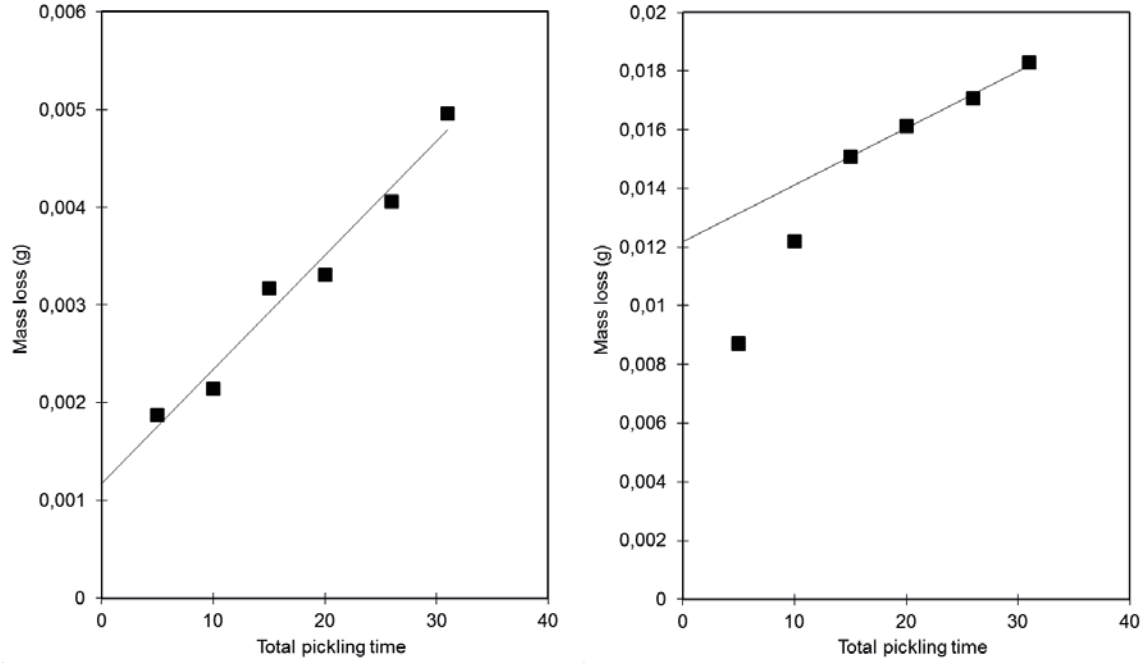

Figure A-4. *Pickling curve for reference coupon (left), pickling curve for coupon S1-3 (right).*

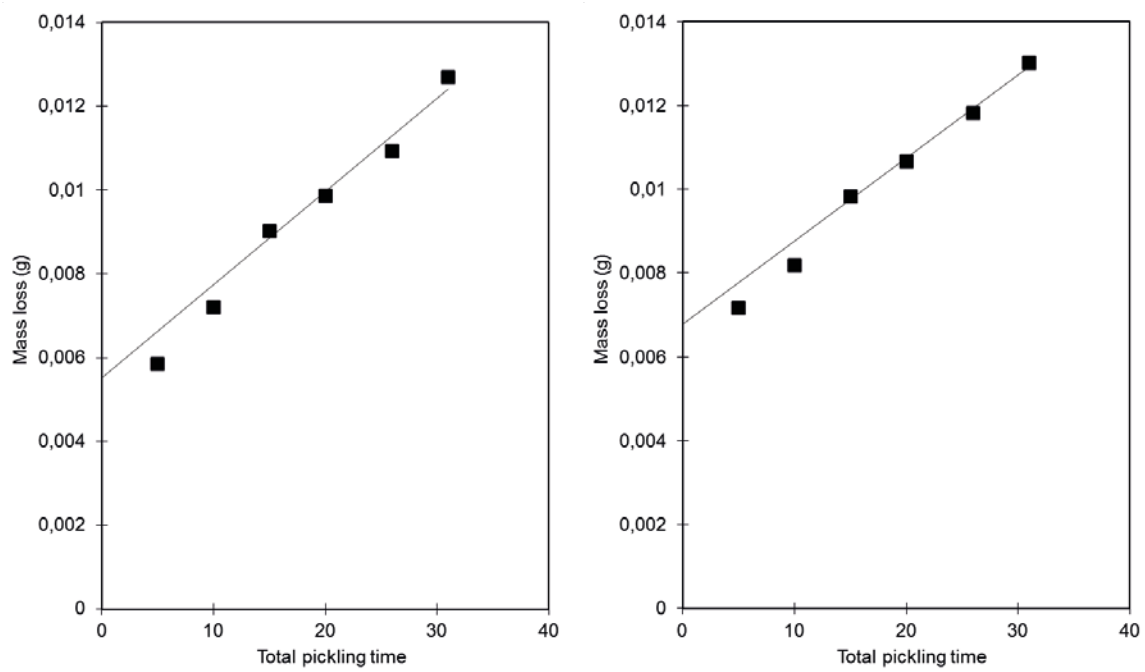

Figure A-5. *Pickling curve coupon S1-4 (left), pickling curve coupon S1-5 (right).*

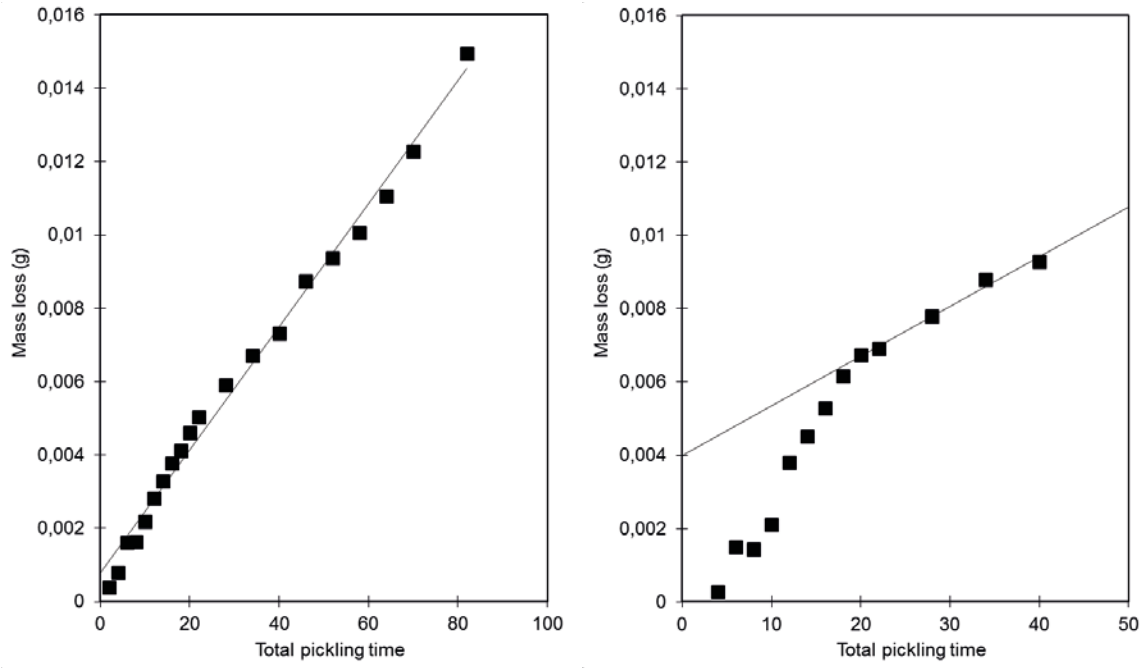

Figure A-6. *Pickling curve for reference coupon (left), pickling curve coupon S6-1 (right).*

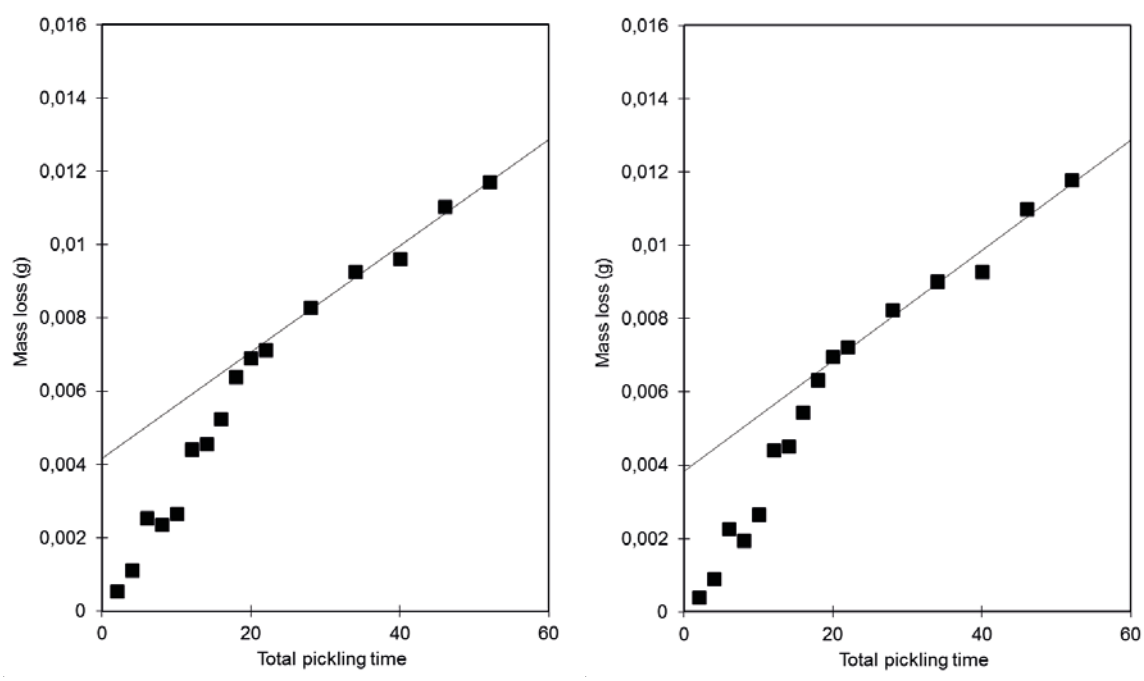

Figure A-7. *Pickling curve coupon S6-2 (left), pickling curve coupon S6-3 (right).*

A2.4 SEM/EDS analyses

The SEM/EDS analyses showed that some darker areas found on the coupons after pickling consisted mainly of Cu and S, meaning that the pickling procedure used had not completely removed all corrosion products after the exposures. However, on coupon S1-3 only a very few small darker surface areas were observed after pickling, so it may be that the duration of pickling or the number of cycles may need to be adjusted for individual coupons rather than the pickling solution itself.

For the cross section coupons no sulphide layer could be seen in the SEM, except on coupon S1-4, where thicknesses in the order of 3 µm were measured (Figure A-8 to Figure A-10). In the surface analyses (Figure A-11 to Figure A-13) some sulphur was detectable, in the order of 0.30 to 2.1 wt%. However, the remaining surface deposits were not consistent and as such these analyses are representative only of the positions analysed.

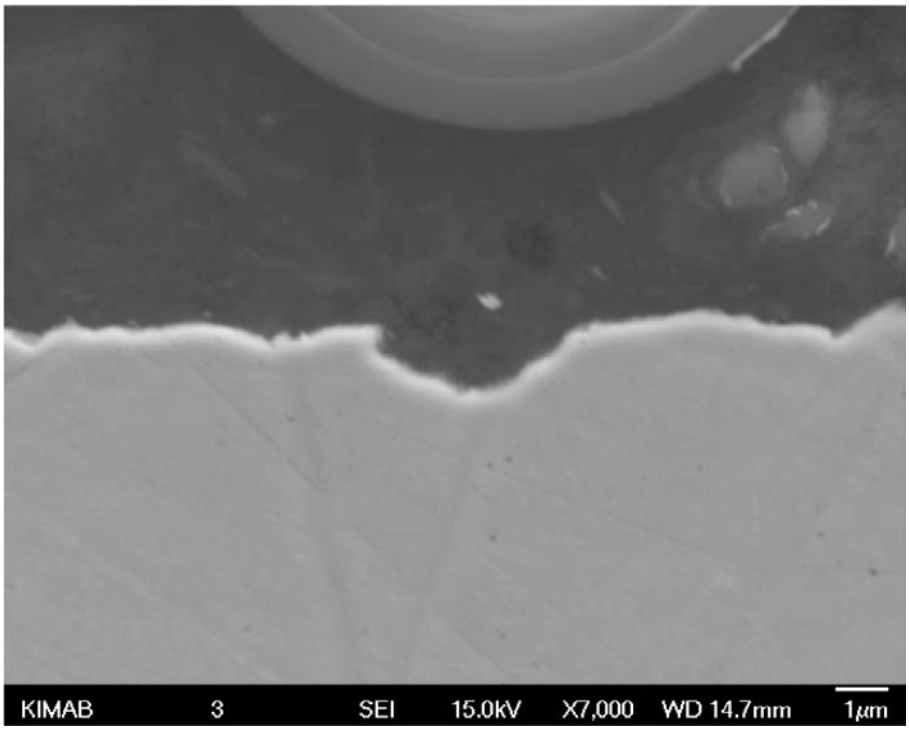

Figure A-8. *Cross-section of coupon S1-3 after pickling. No sulphide layer could be seen.*

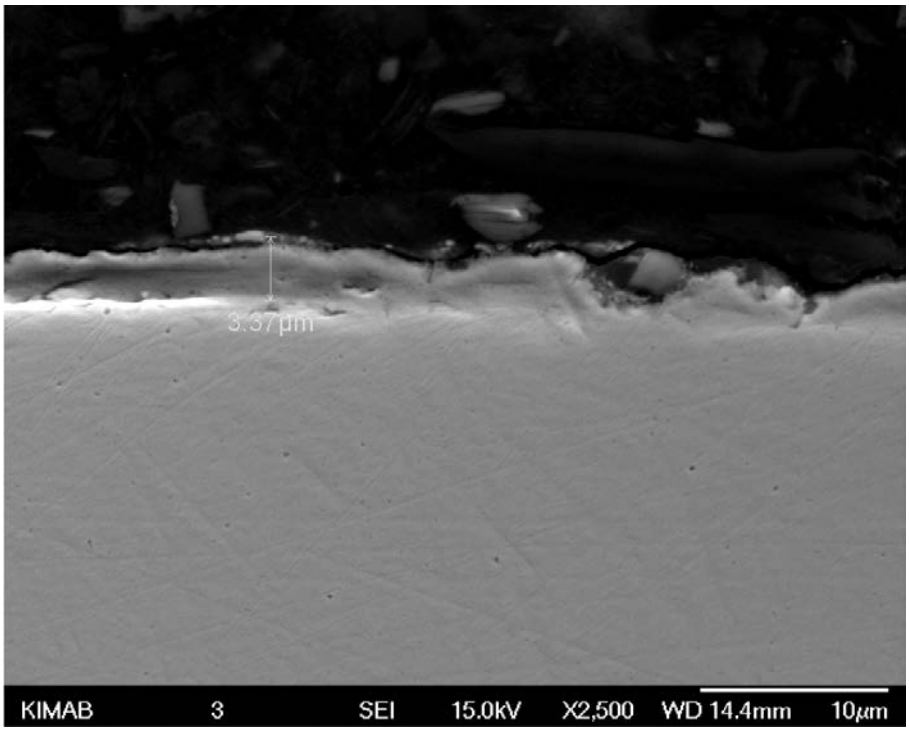

Figure A-9. *Cross-section of coupon S1-4 after pickling. A sulphide layer of approximately 3 um thickness can be seen.*

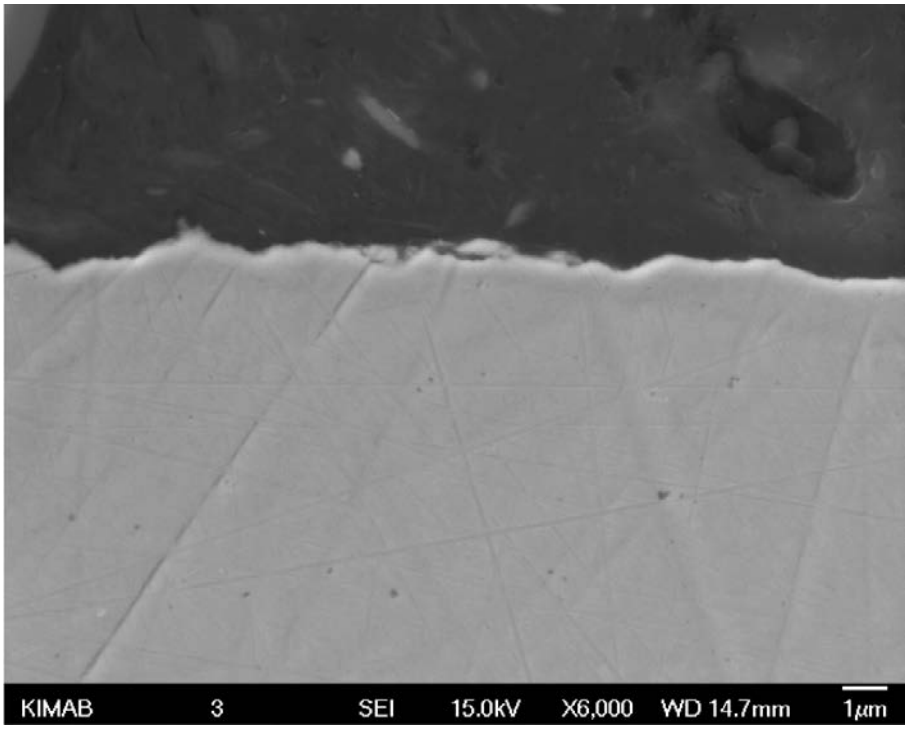

Figure A-10. *Cross section of coupon S1-5 after pickling. No sulphide layer could be seen.*

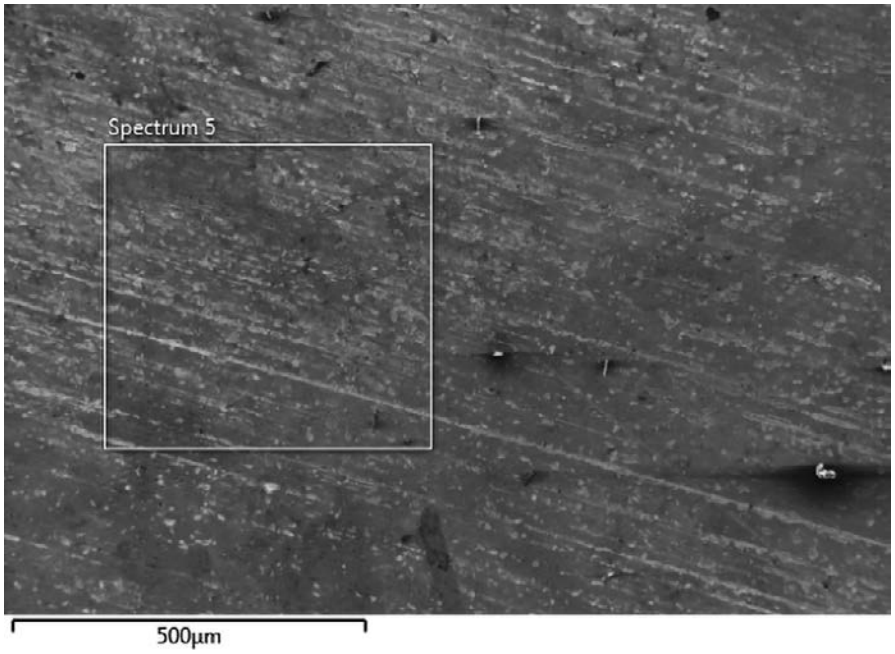

Figure A-11. *SEM/EDS analysis of the surface of coupon S1-3.*

Element	Wt (%)
S	0.3
Cu	99.7
Total:	100

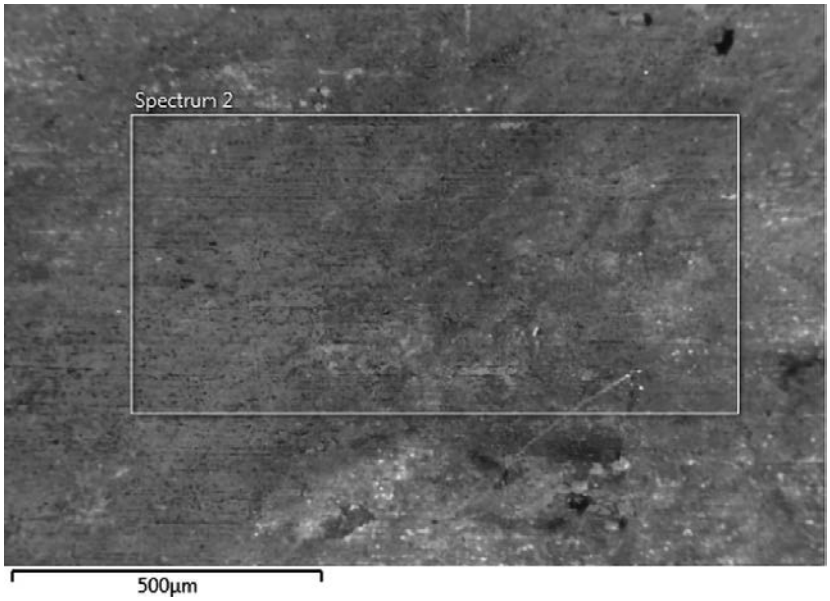

Figure A-12. *SEM/EDS analysis of the surface of coupon S1-4.*

Element	Wt (%)
S	0.87
Cu	99.13
Total:	100

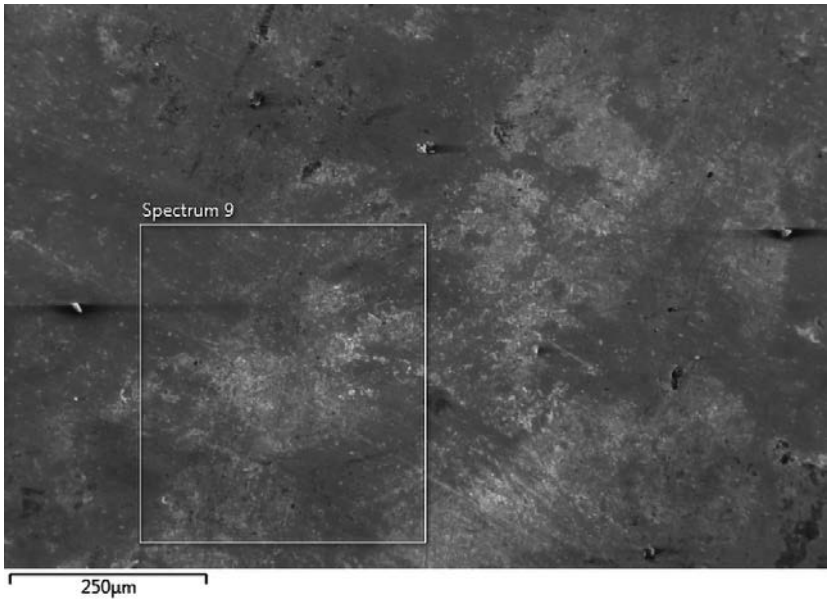

Figure A-13. *SEM/EDS analysis of the surface of coupon S1-5.*

Element	Wt (%)
S	2.61
Cu	97.39
Total:	100

A2.5 Microscope images of defects present on the coupon surfaces before and after pickling

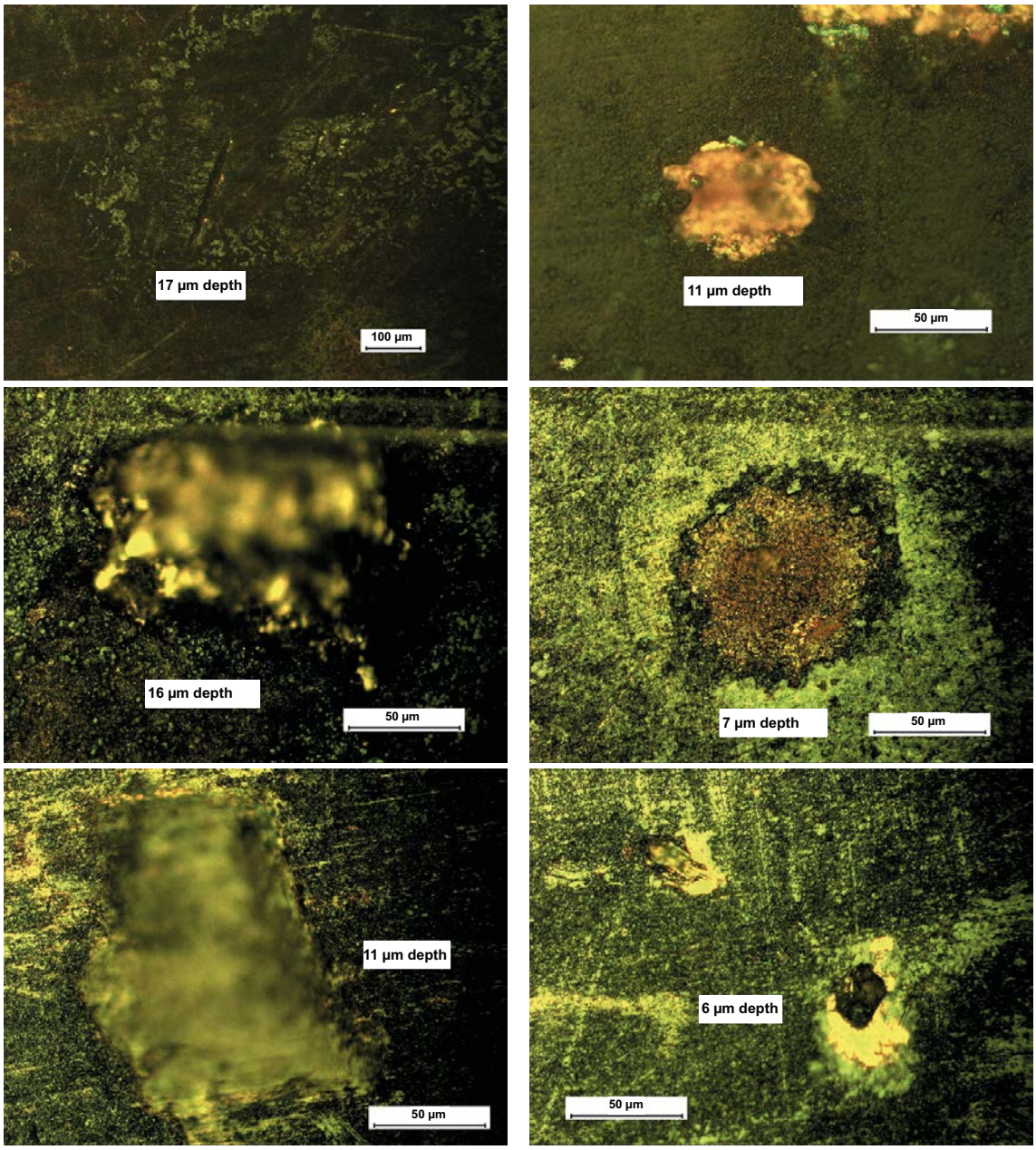

Figure A-14. *Examples of defects found on the coupons before picking. Top row: S1-3; middle row: S1-4; bottom row: S1-5.*

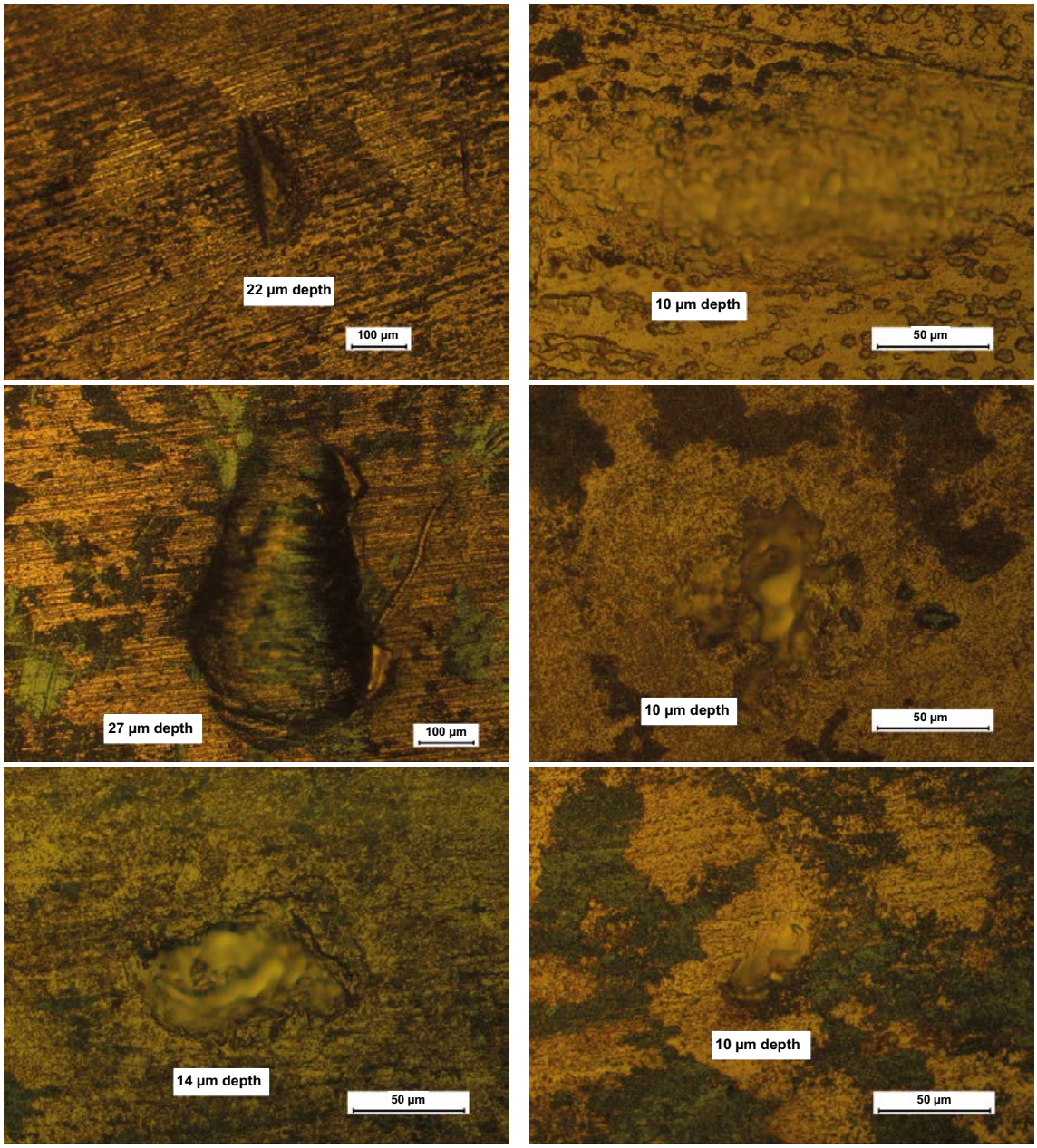

Figure A-15. *Examples of defects found on the coupons after picking. Top row: S1-3; middle row: S1-4; bottom row: S1-5.*

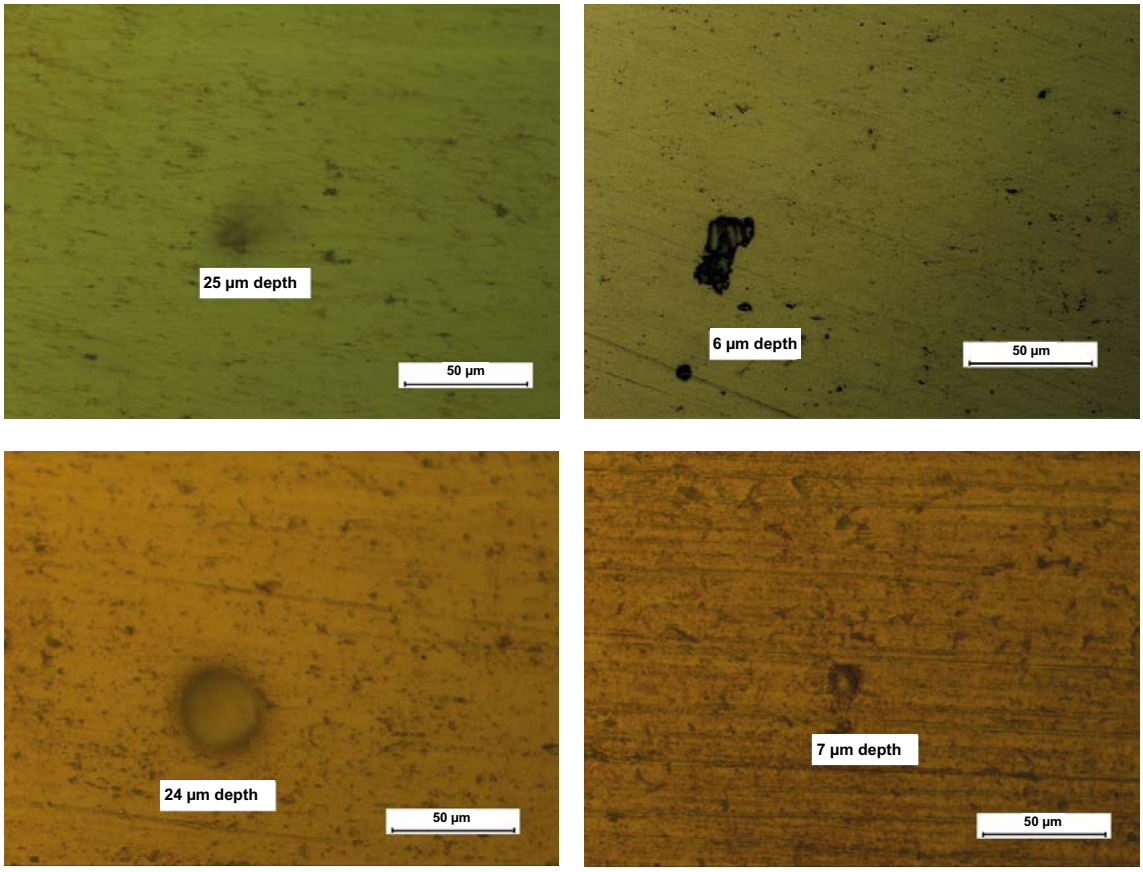

Figure A-16. *Examples of defects found on the reference coupon before and after picking. Top row: before pickling; bottom row: after pickling.*

A3 Conclusions

The investigation has found that using a pickling solution of NH_4OH allows sufficient removal of sulphide corrosion products from copper coupons that have been exposed in H_2S environments, without adversely affecting the defects on the coupon surfaces. It has been possible to analyse mass loss and localised corrosion on the coupons after pickling in only NH_4OH.

SEM/EDS analyses of the surface deposits in cross-section and on the surface revealed that although the pickling was considered complete from a mass loss perspective, some corrosion products remained after the pickling. The surface deposits consisted of mainly copper and sulphur.

Appendix B

Calculation of sulphide concentration

B1 Introduction

In order to estimate the sulphide concentration present on the coupon surfaces in the $H_2S(g)$ experiments a calculation was made according to Henry's law. The calculation assumed that the water film on the surface of the coupons behaves in the same way as a larger volume of water. Whilst this may not be the case, at the time of writing this calculation is the best approximation of the concentration for these experiments available using the available data and resources.

B2 Calculation

Assumptions:

Temperature = 85 °C = 358.15 K

Pressure = 1 bar

RH = 80 %

Gas phase $H_2S + N_2 + H_2O$ => $Ptot = P(H_2S) + P(N_2) + P(H_2O)$

Water partial pressure $P(H_2O) = 0.4$ bar

Water mole fraction = $X(H_2O) = 0.4$

Nitrogen partial pressure $P(N_2) = 1 - 0.4 - P(H_2S) = 0.6 - P(H_2S)$ bar

Nitrogen mole fraction = $X(N_2) = 0.6 - X(H_2S)$

Case 1: Concentration of H_2S = 10 wt.ppm H_2S in N_2 i.e. 1.00×10^{-5} g H_2S/g total

Case 2: Concentration of H_2S = 10 000 wt.ppm H_2S in N_2 i.e. 1.00×10^{-2} g H_2S/g total

Calculation of $X(H_2S)$

Mole fraction $X(H_2S) = n_1(H_2S)/(n_1(H_2S) + n_2(N_2) + n_3(H_2O))$

$n_3 = 0.4$

$n_2 = 0.6 - n_1$

Mass fraction $C = n_1 \times MW(H_2S)/(0.4 \times MW(H_2O) + (0.6 - n_1) \times MW(N_2) + n_1 \times MW(H_2S))$

Solve for n_1

$n_1 = C \times (0.4 \times MW(H_2O) + 0.6 \times MW(N_2))/((1 - C) \times MW(H_2S) + C \times MW(N_2))$

Molecular mass (MW)

$MW(N_2)$ = 28 g/mol

$MW(H_2S)$ = 34.1 g/mol

$MW(H_2O)$ = 18 g/mol

Henrys constant for H_2S at 85 °C (Sander 1999)

$K_{H\theta}$(at 25 °C) = 0.1 mol /(l × atm)

$\ln K_{H\theta} = -2.302585093$

Temperature dependence = $-d(\ln(K_H))/d(1/T) = (\ln K_{H\theta} - \ln K_H(85\ °C))/(1/358.15 - 1/298.15) = 2\,100$ K

=> $\ln K_H(85\ °C) = 2\,100 \times (1/358.15 - 1/298.15) - 2.3026$

=> $\ln K_H(85\ °C) = -3.4826$

=> $K_H(85\ °C) = 0.030729$ mol /(l × atm)

Henrys constant converted to bar

1 atm = 1.01325 bar

$K_H(85\ °C, [mol/(l \times bar)]) = K_H(85\ °C [mol/(l \times atm)])/1.01325 = 0.030327$ mol/(l × bar)

B2.1 Case 1: 10 wt.ppm H_2S

$C = 1.00 \times 10^{-5}$ g H_2S/g total

Converted to mole fraction $X(H_2S)$:

$X(H_2S) = n_1(H_2S)/(n_1(H_2S) + n_2(N_2) + n_3(H_2O))$

$n_1 = 24 \times C / (34.1 - 6.1 \times C) = 7.04 \times 10^{-6}$ mol H_2S/mol gas

Since $n_1 + n_2 + n_3 = 1$ mol

$X(H_2S) = n_1$

$P(H_2S)$, Partial pressure for $H_2S = X(H_2S) \times Ptot = 7.04 \times 10^{-6}$ bar

Concentration of H_2S in water phase = $K_H \times P(H_2S) = 2.13 \times 10^{-7}$ mol/l

B2.2 Case 2: 10000 wt.ppm H_2S

$C = 1.00 \times 10^{-2}$ g H_2S/g total

Converted to mole fraction $X(H_2S)$:

$X(H_2S) = n_1(H_2S)/(n_1(H_2S) + n_2(N_2) + n_3(H_2O))$

$n_1 = 24 \times C / (34.1 - 6.1 \times C) = 7.05 \times 10^{-3}$ mol H_2S/mol gas

Since $n_1 + n_2 + n_3 = 1$ mol

$X(H_2S) = n_1$

$P(H_2S)$, Partial pressure for $H_2S = X(H_2S) \times Ptot = 7.05 \times 10^{-3}$ bar

Concentration of H_2S in water phase = $K_H \times P(H_2S) = 2.14 \times 10^{-4}$ mol/l

Appendix C

Microscope images of defects on SRB coupon surfaces

The surfaces of the SRB exposure coupons were characterized for defects after pickling. The reference coupons were characterized before and after pickling. The images contained in the appendix show all the defects that have been measured on the coupons in the microscope. The criterion for measurement was defect depth greater than 6 µm. Only the two largest surface areas of each coupon were analysed, and were denoted side 1 and 2.

There is a Swedish word in all pictures, djup, which means depth.

SRB exposures – Bio A coupon S7-11 side 1

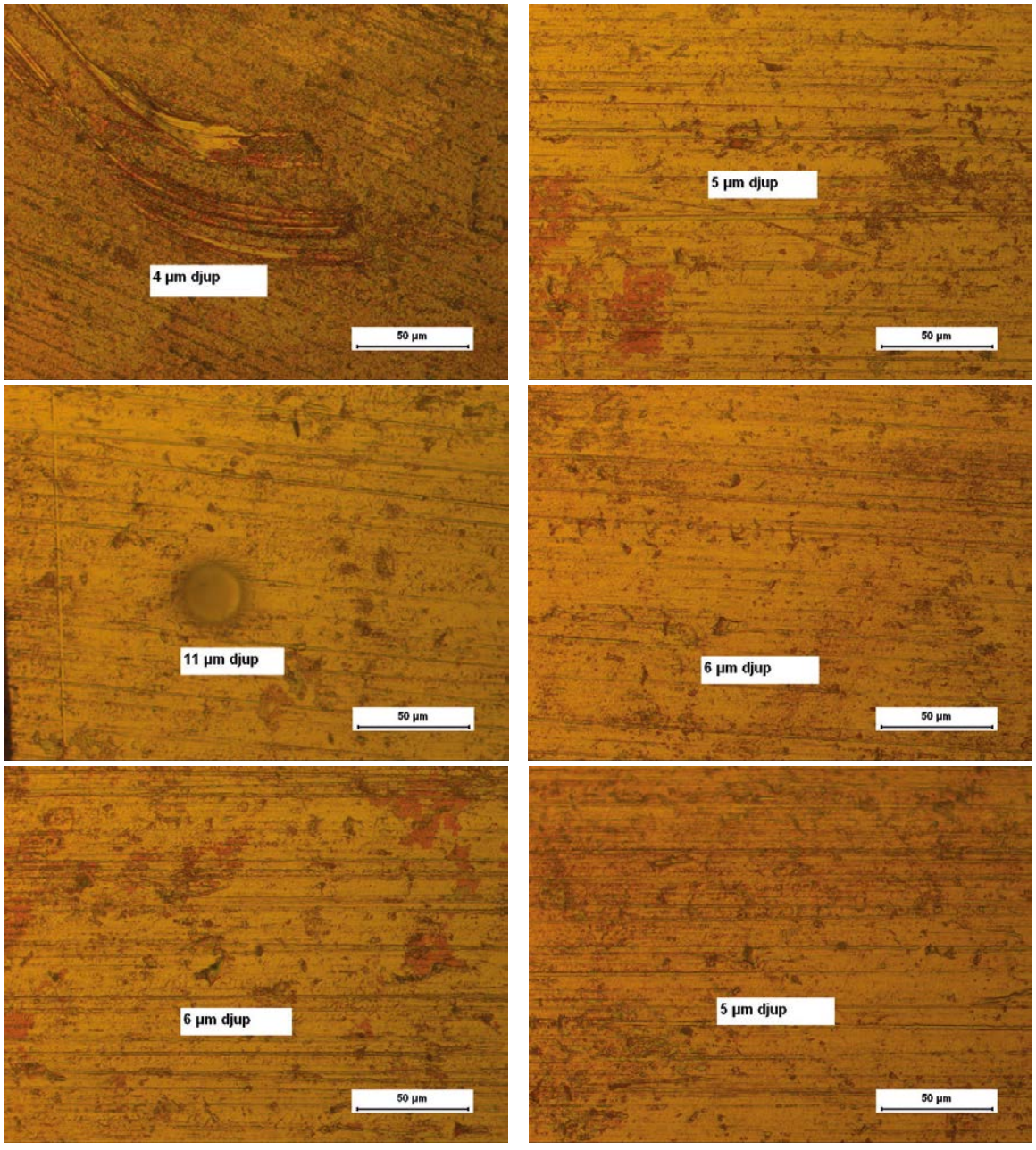

SRB exposures – Bio A coupon S7-11 side 2

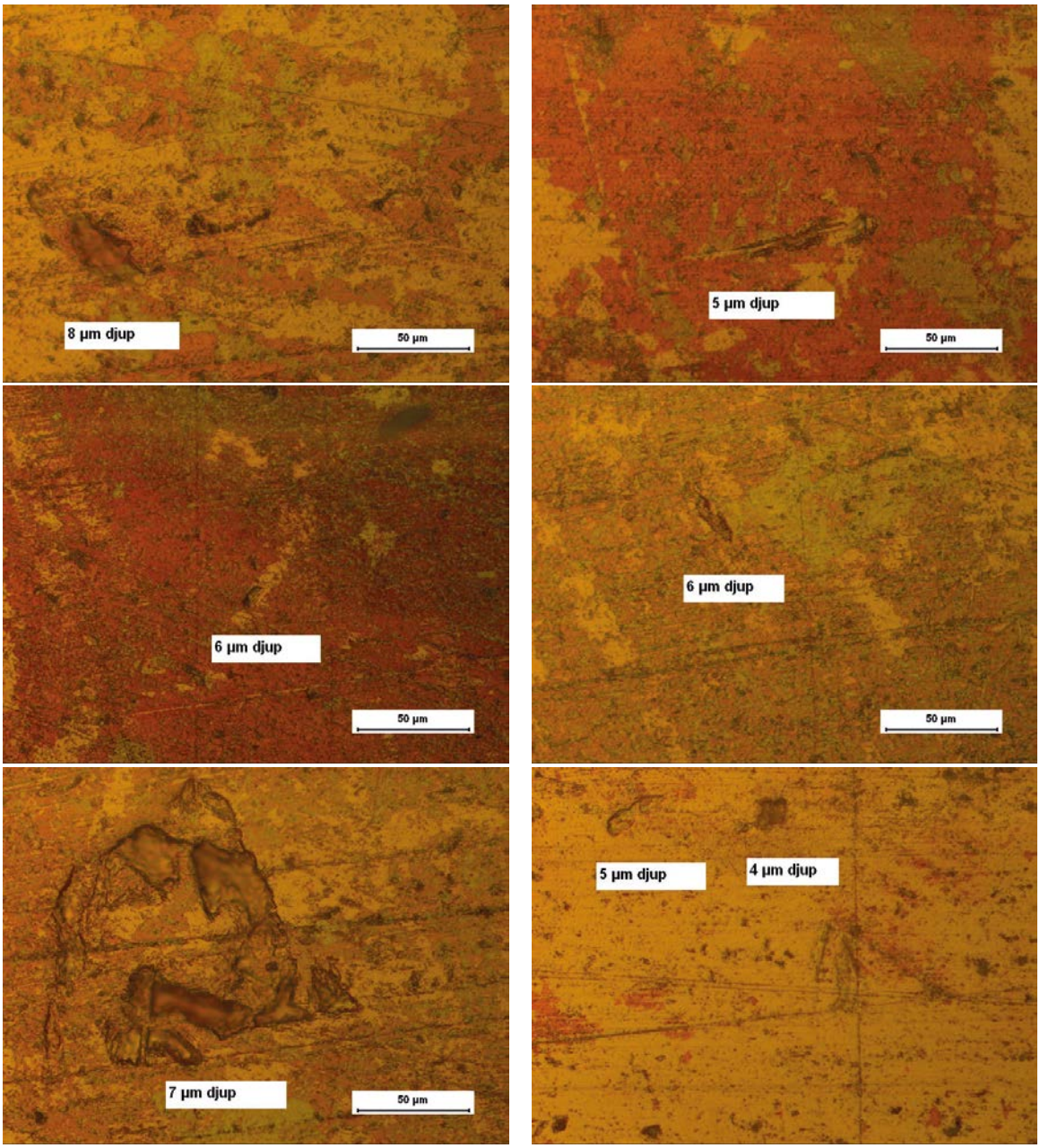

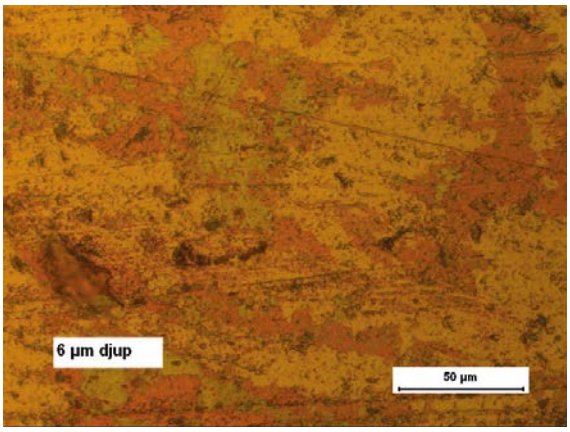
6 µm djup
50 µm

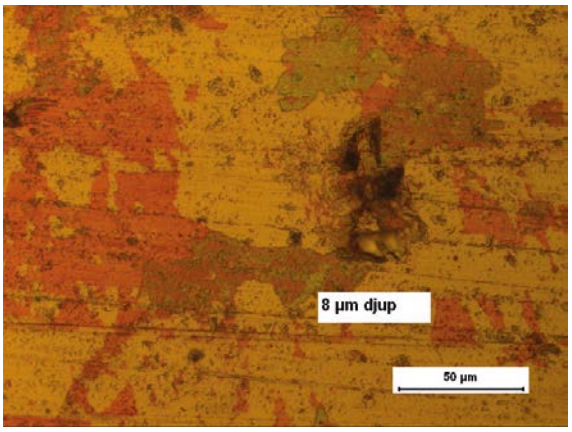
8 µm djup
50 µm

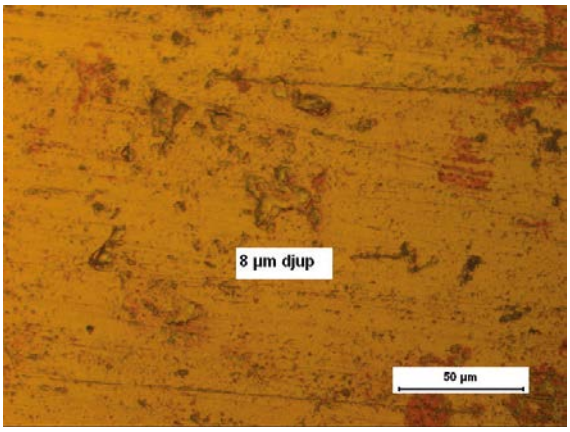
8 µm djup
50 µm

SRB exposures – Bio A coupon S10-3 side 1

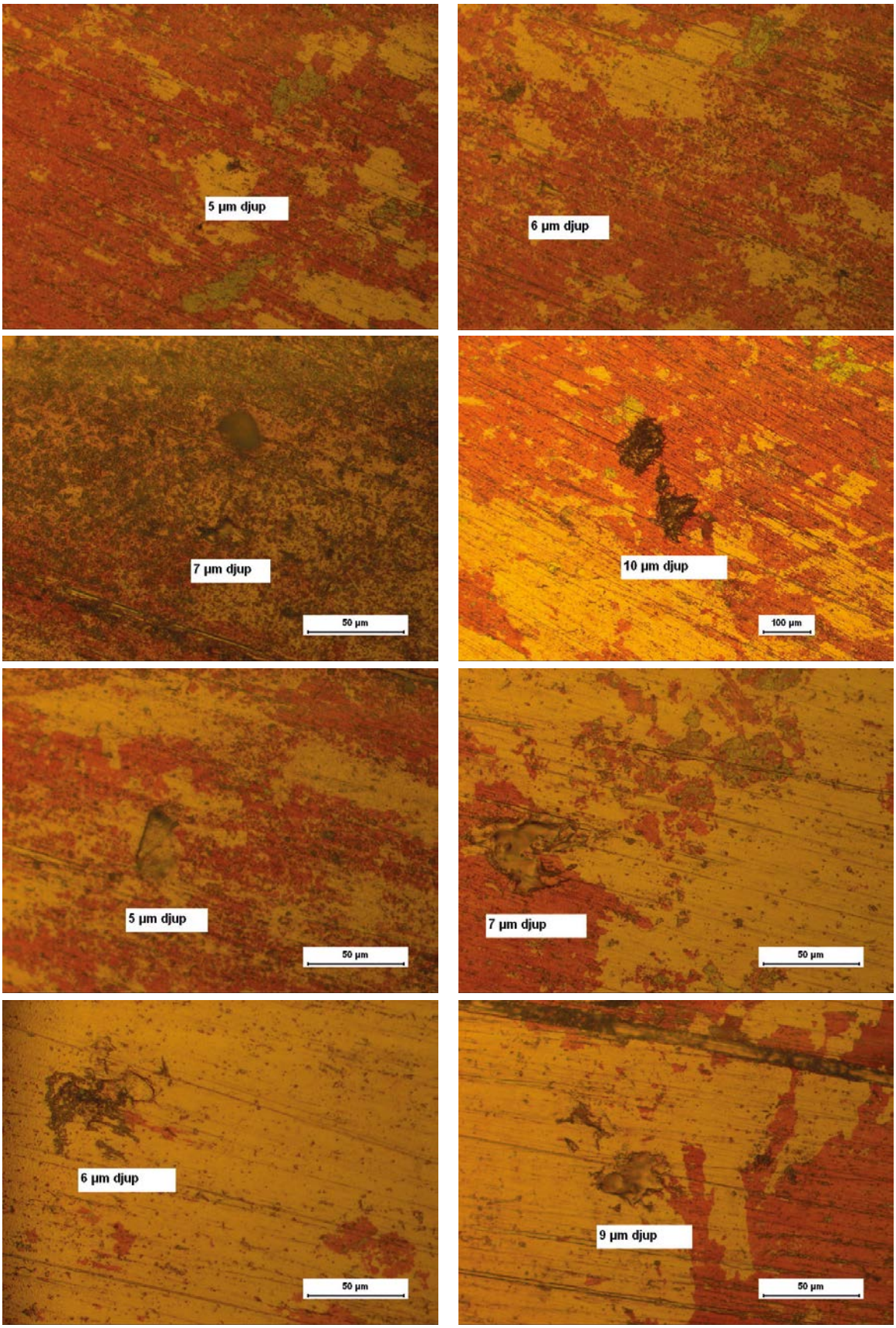

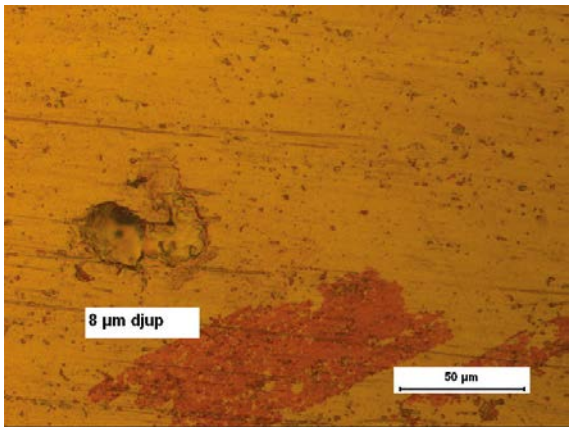
8 µm djup
50 µm

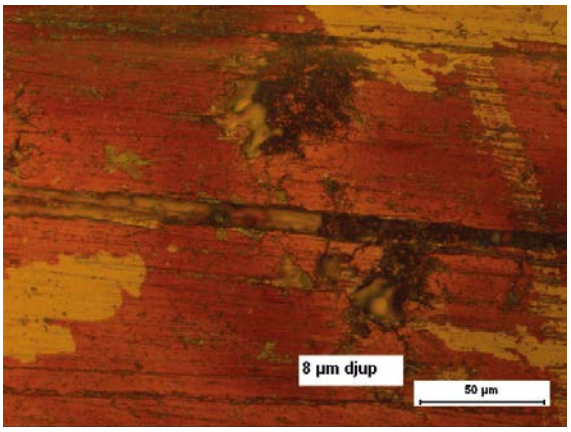
8 µm djup
50 µm

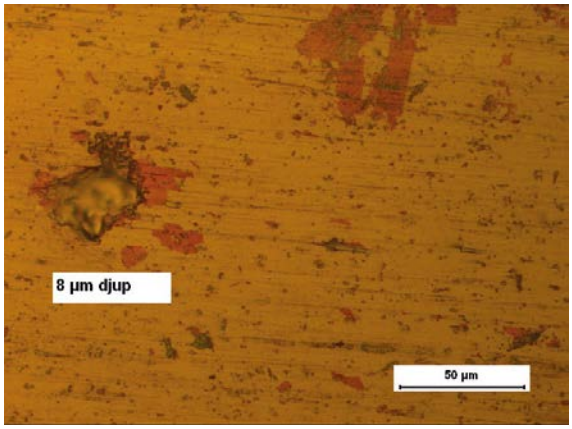
8 µm djup
50 µm

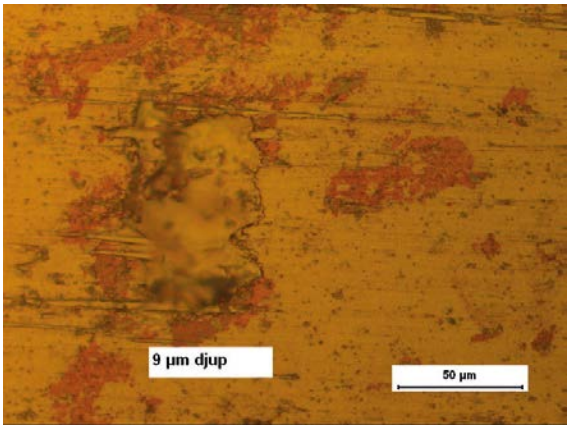
9 µm djup
50 µm

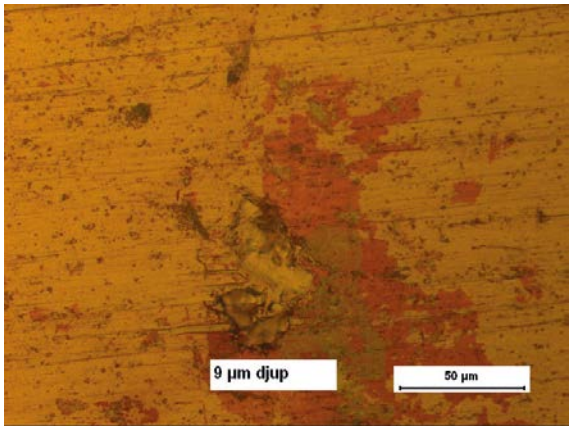
9 µm djup
50 µm

SRB exposures – Bio A coupon S10-3 side 2

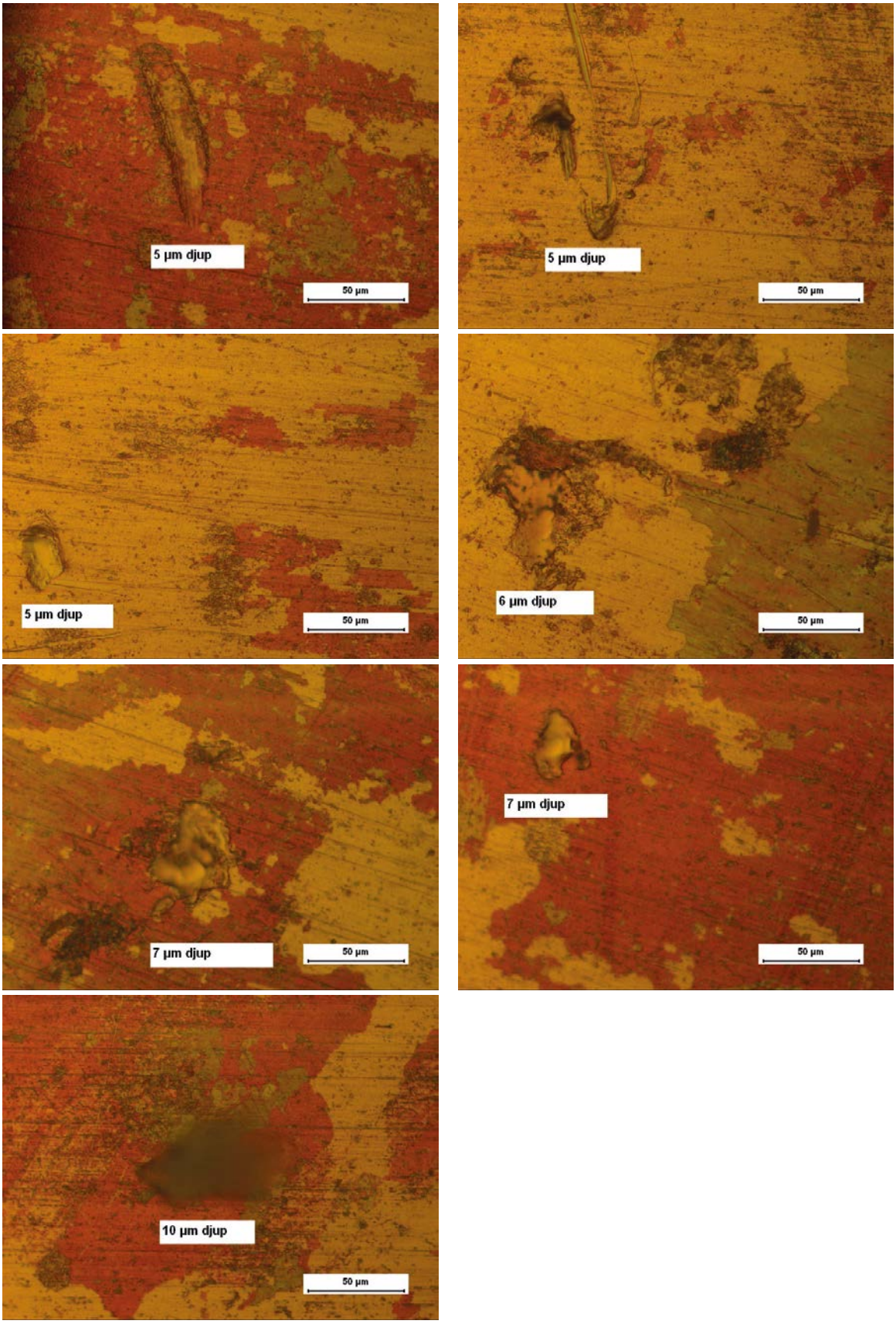

SRB exposures – Bio B coupon S8-9 side 1

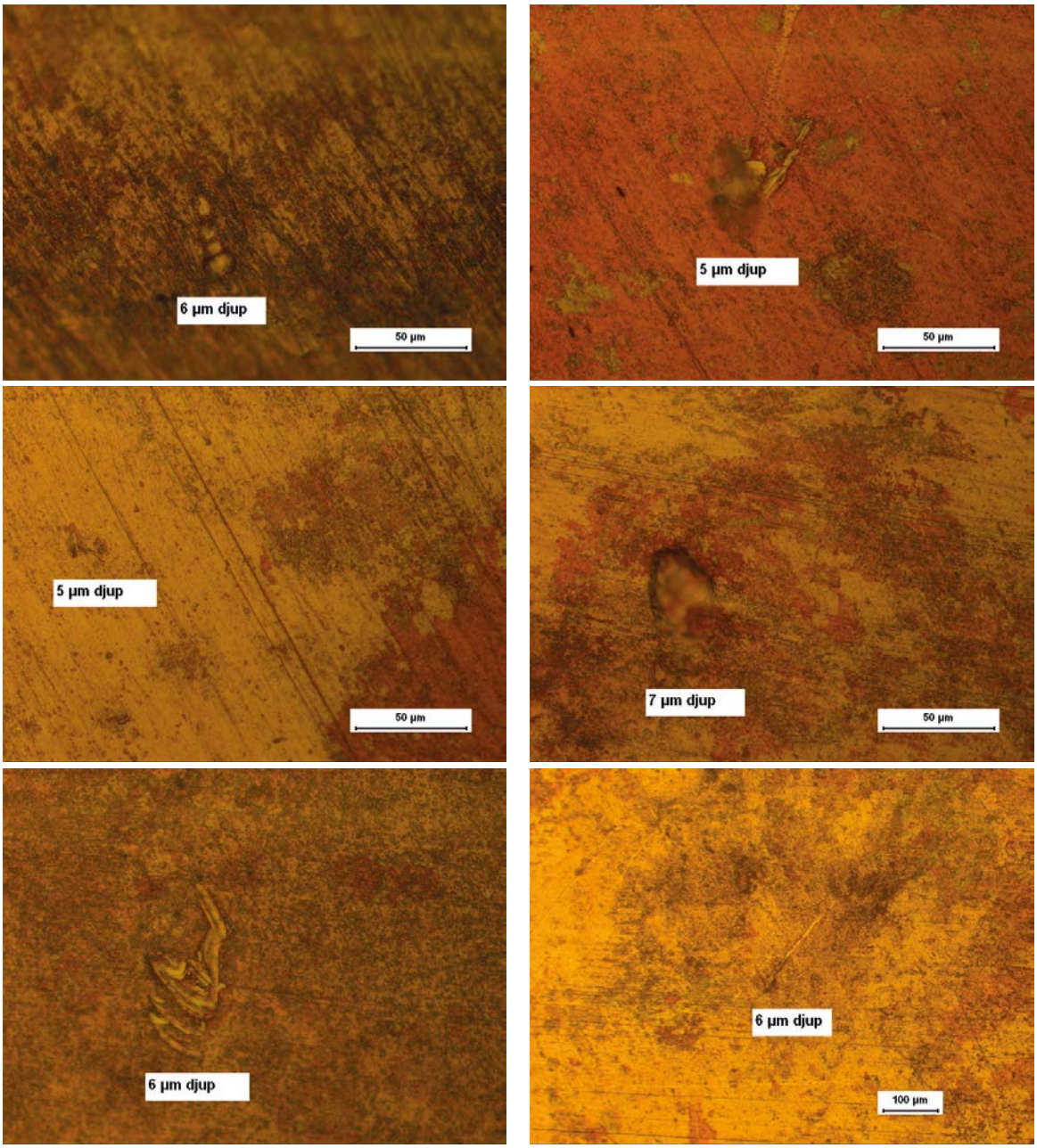

SRB exposures – Bio B coupon S8-9 side 2

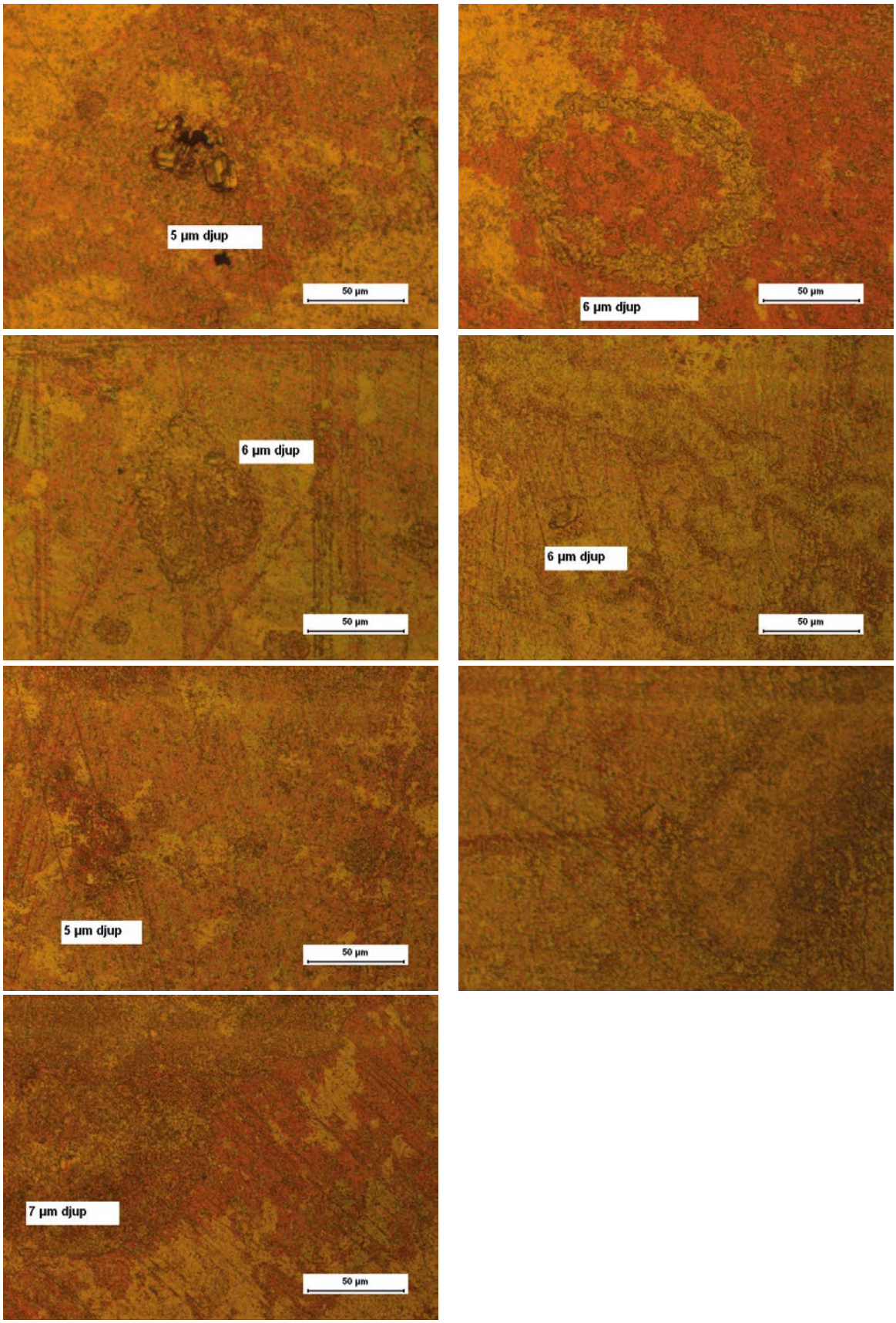

SRB exposures – Bio B coupon S7-2 side 1

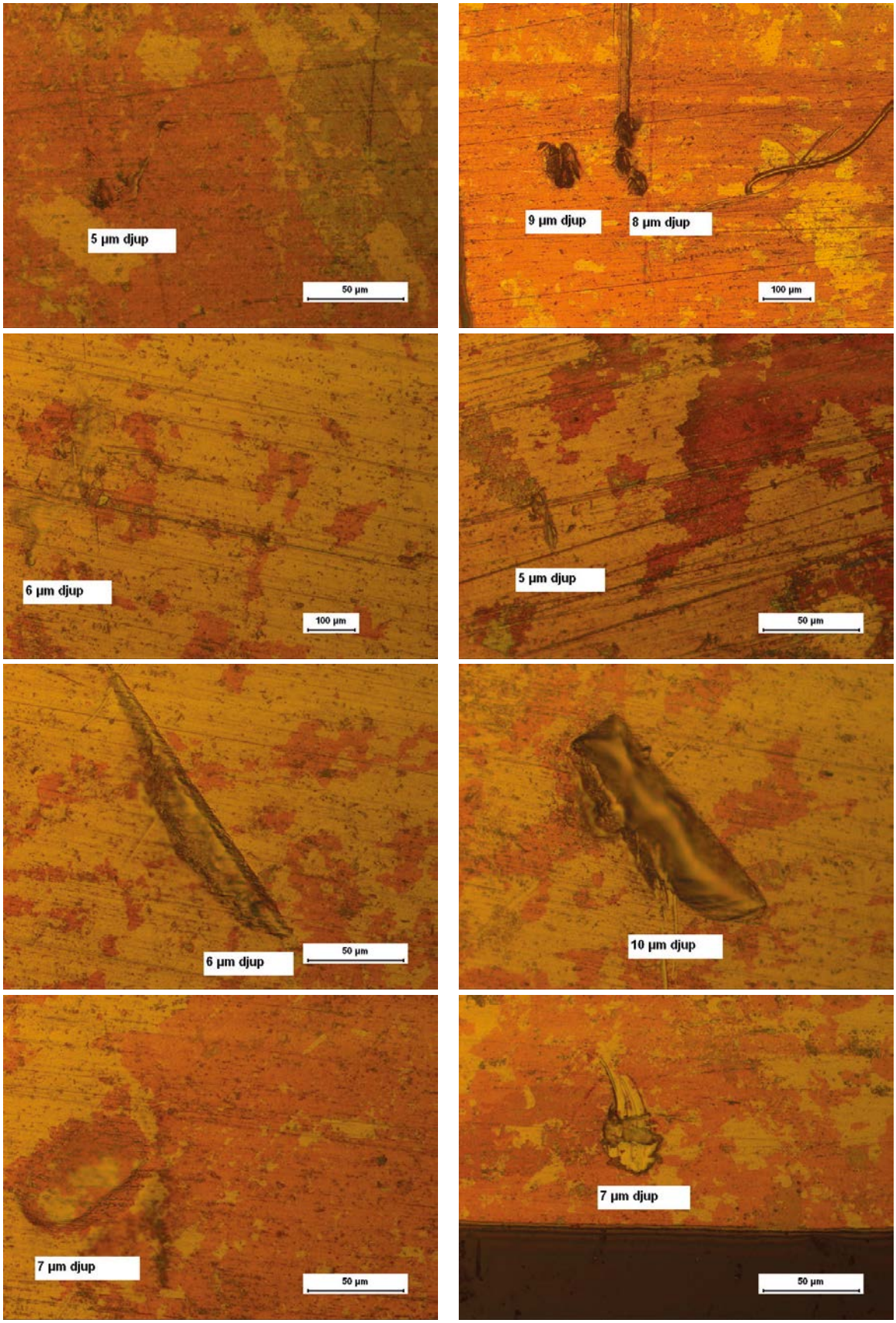

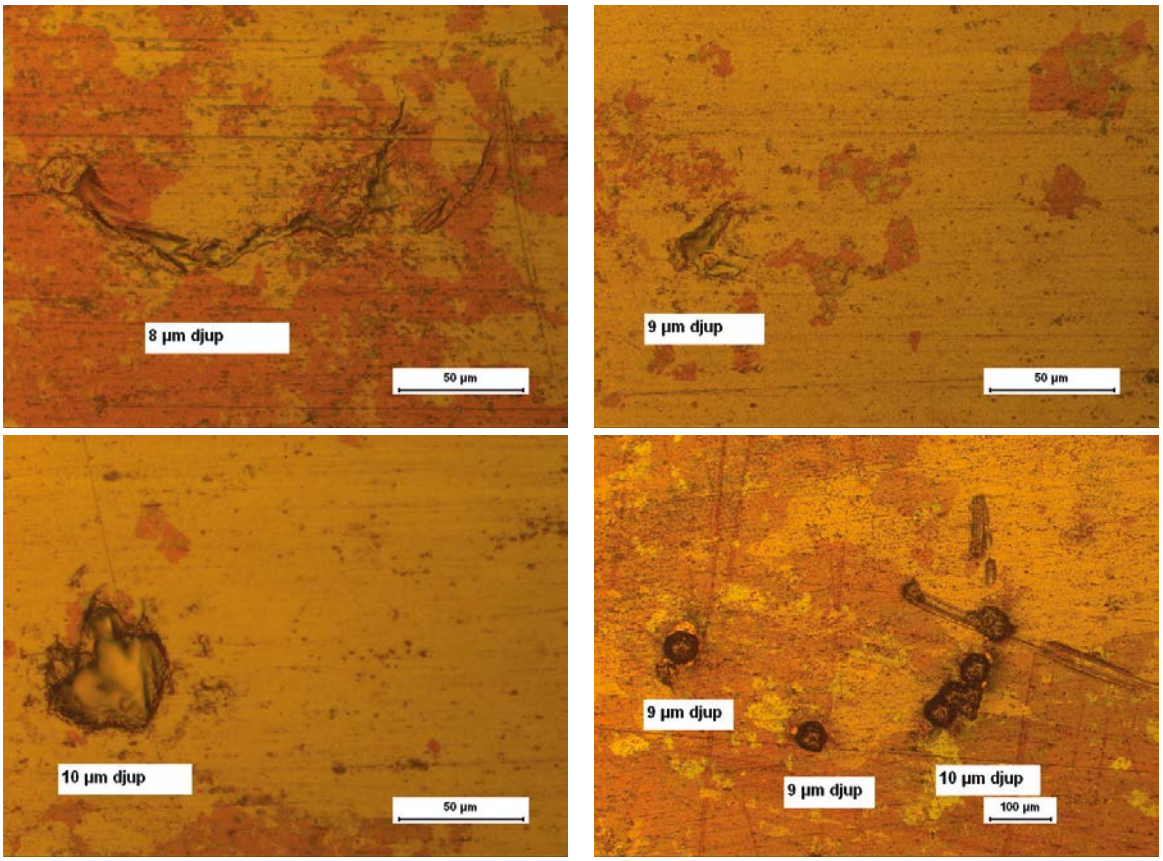
8 µm djup
50 µm
9 µm djup
50 µm
10 µm djup
50 µm
9 µm djup
9 µm djup
10 µm djup
100 µm

SRB exposures – Bio B coupon S7-2 side 2

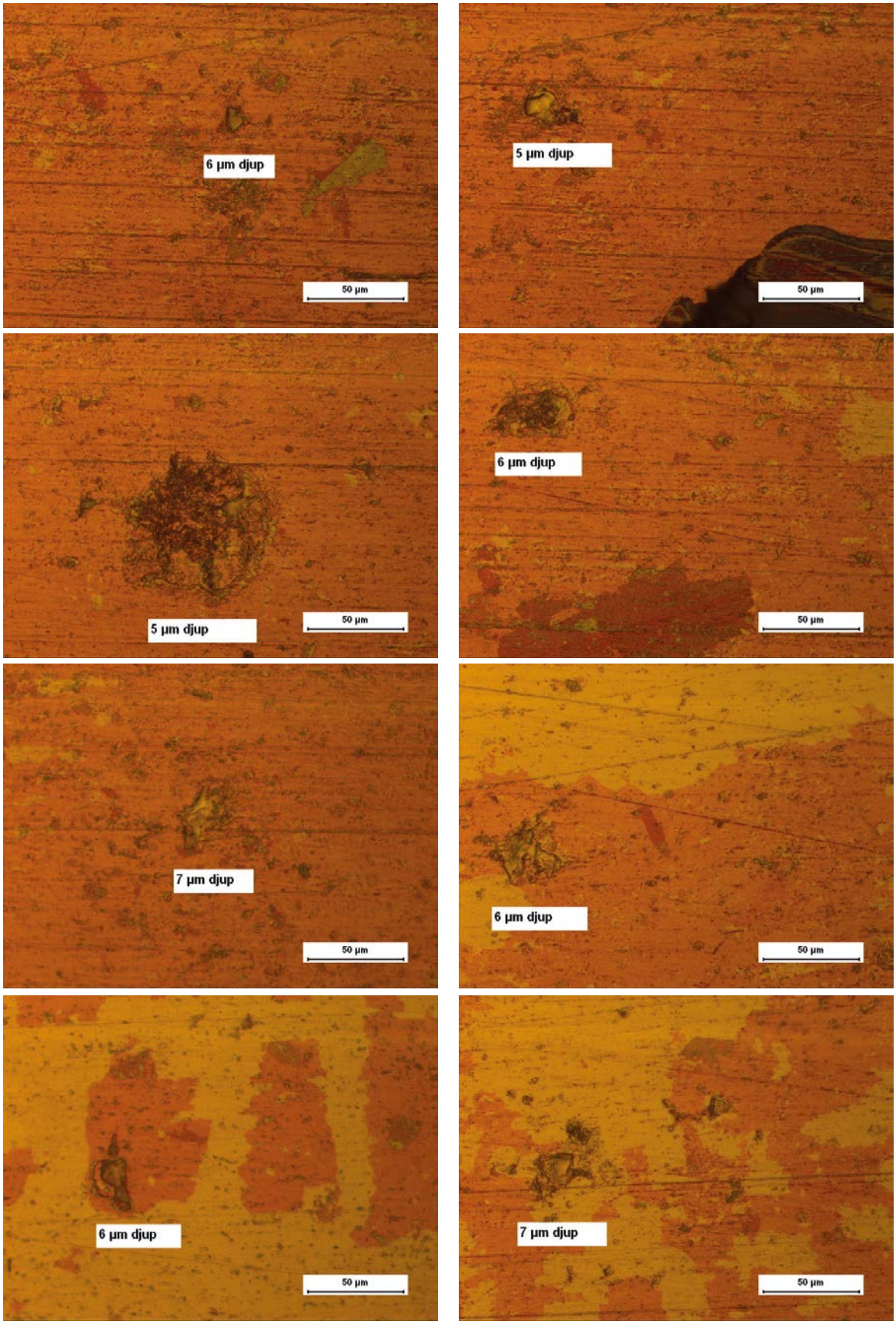

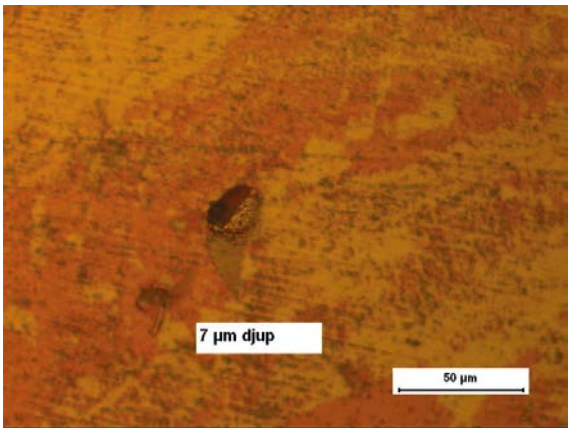
7 µm djup
50 µm

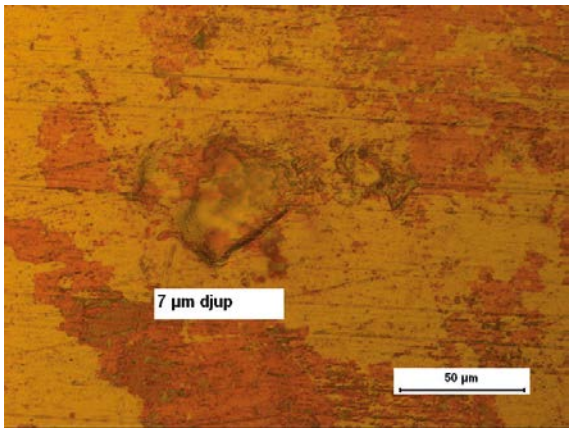
7 µm djup
50 µm

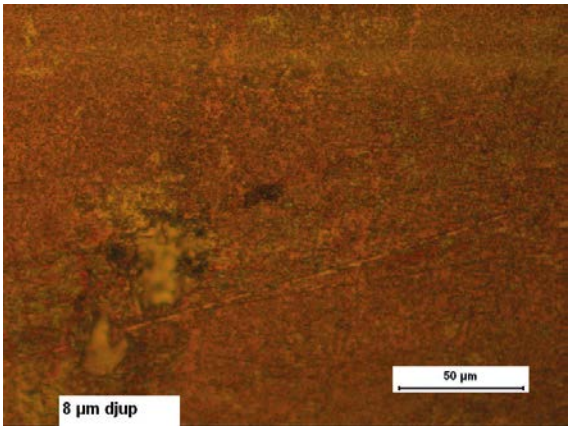
50 µm
8 µm djup

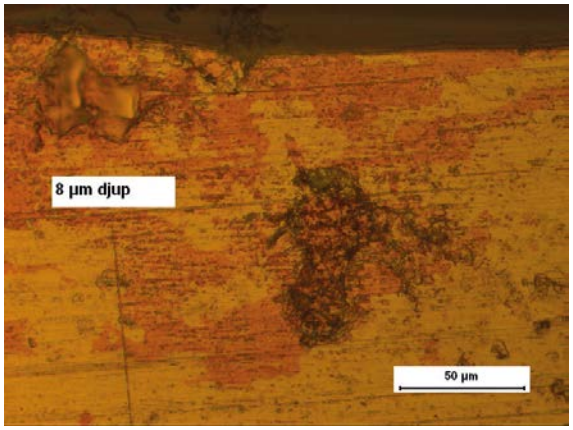
8 µm djup
50 µm

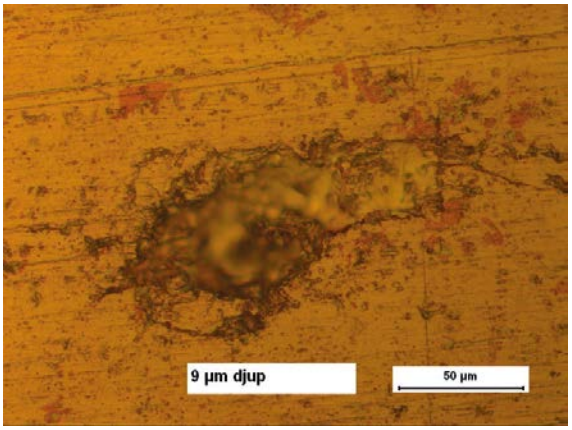
9 µm djup
50 µm

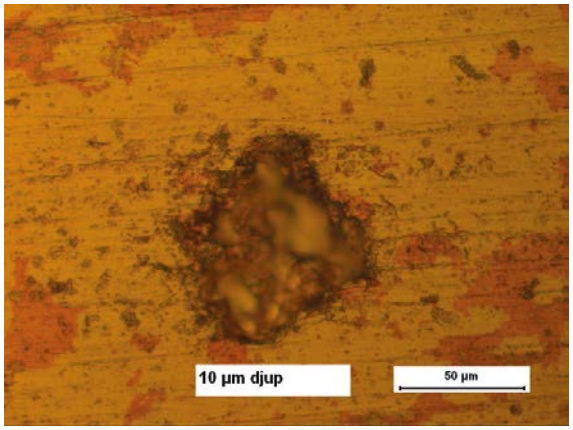
10 µm djup
50 µm

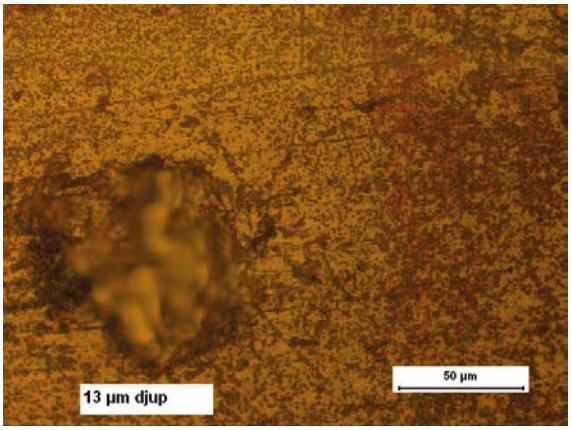
50 µm
13 µm djup

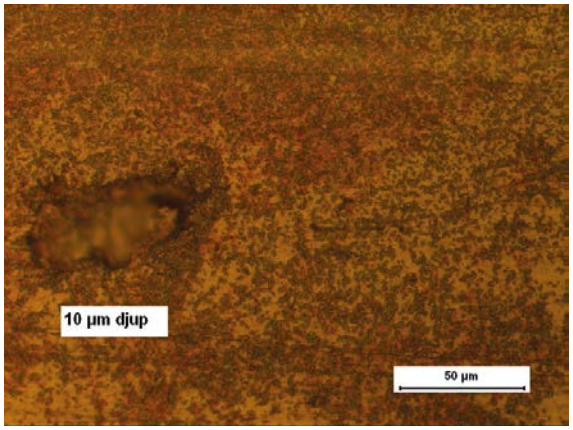
10 µm djup
50 µm

SRB exposures – Bio C coupon S8-7 side 1

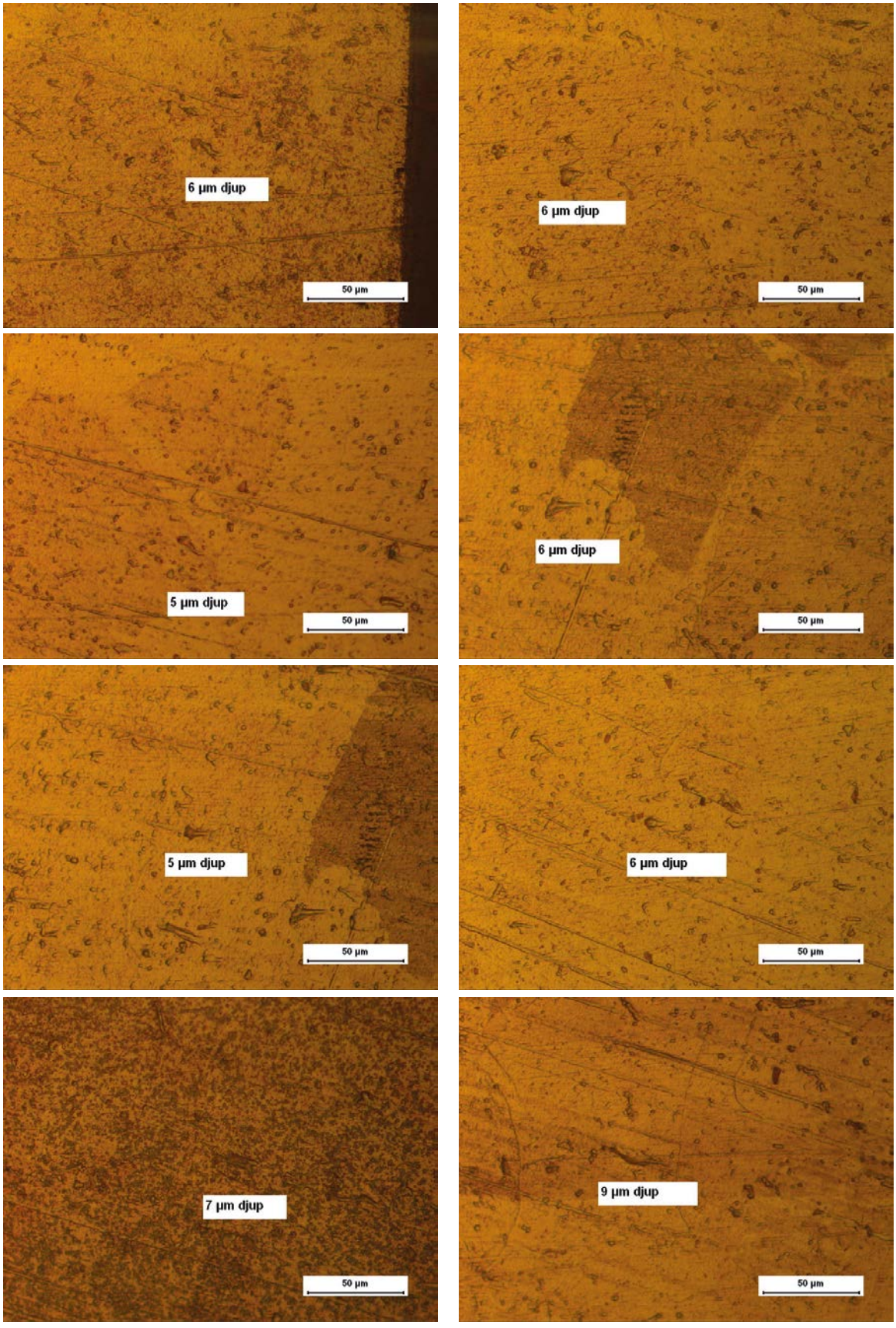

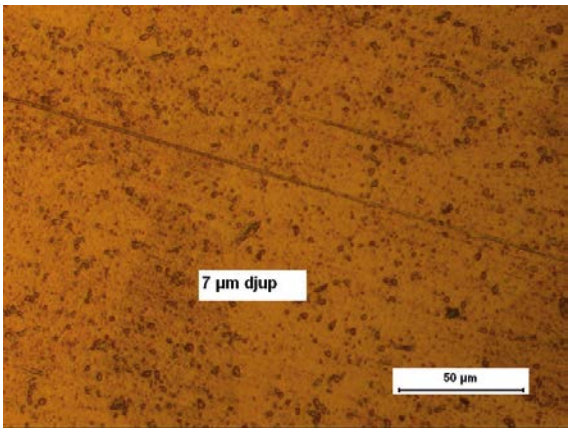
7 µm djup
50 µm

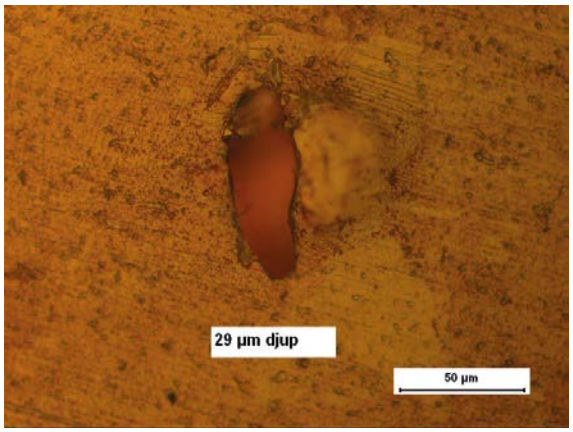
29 µm djup
50 µm

SRB exposures – Bio C coupon S8-7 side 2

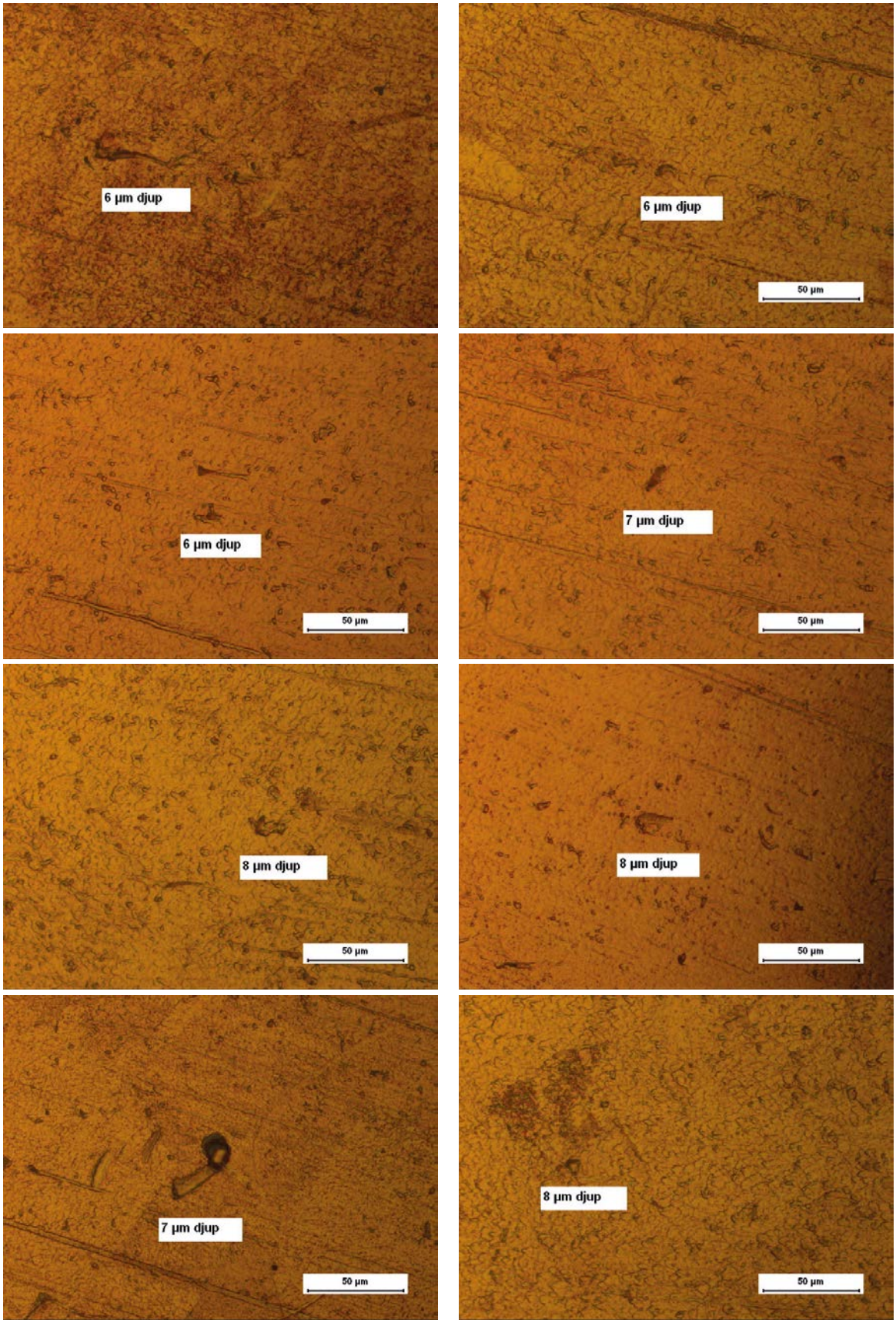

SRB exposures – Bio C coupon S8-8 side 1

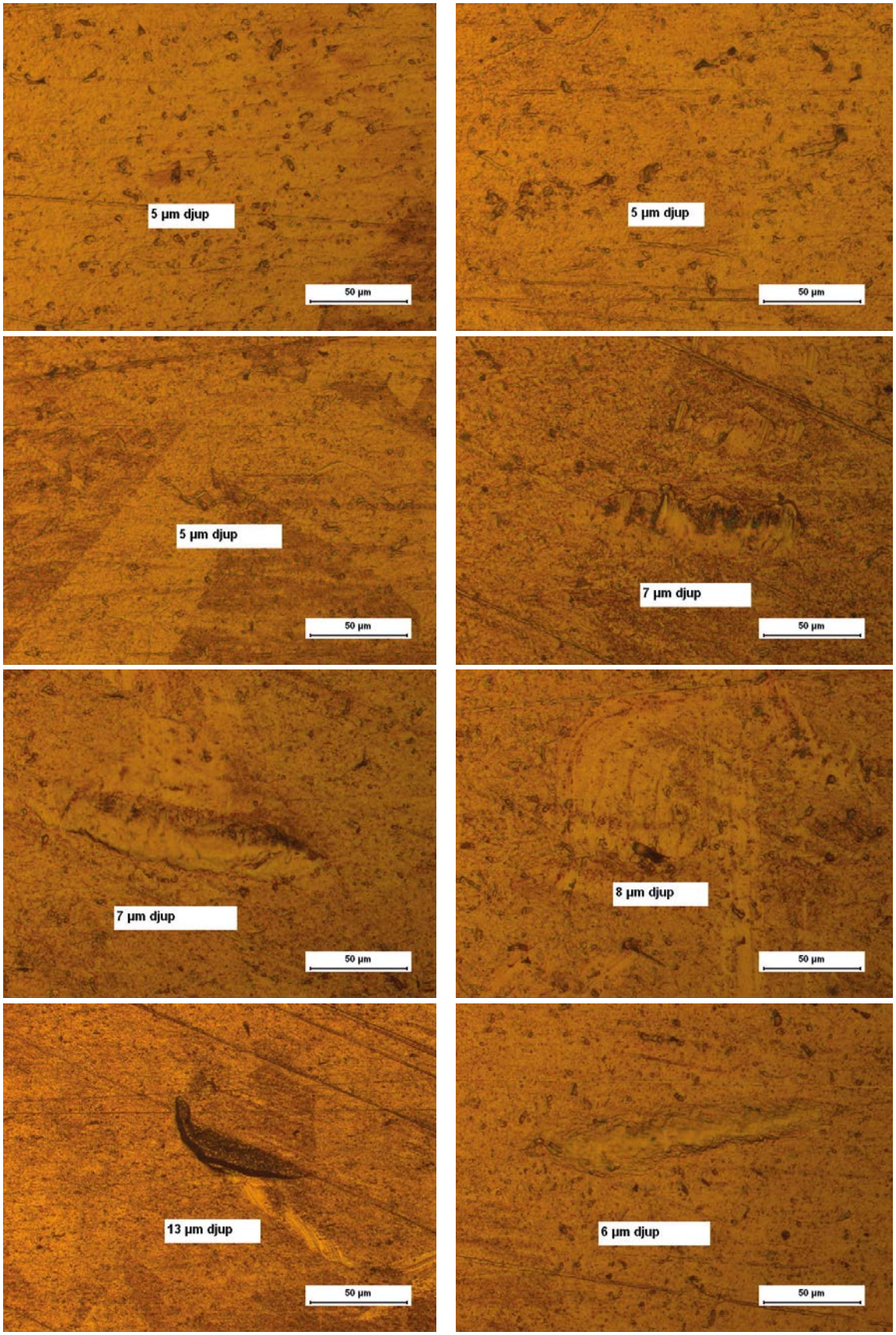

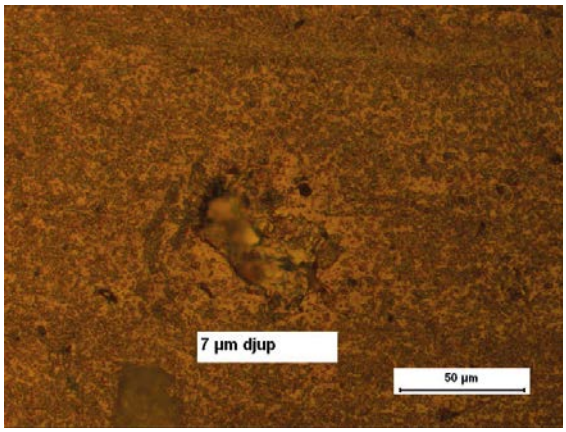
7 µm djup
50 µm

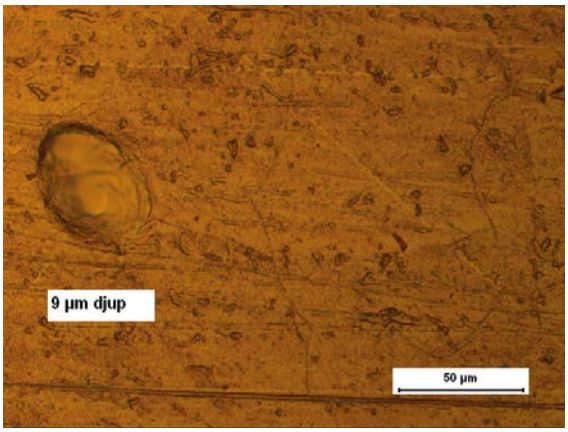
9 µm djup
50 µm

SRB exposures – Bio C coupon S8-8 side 2

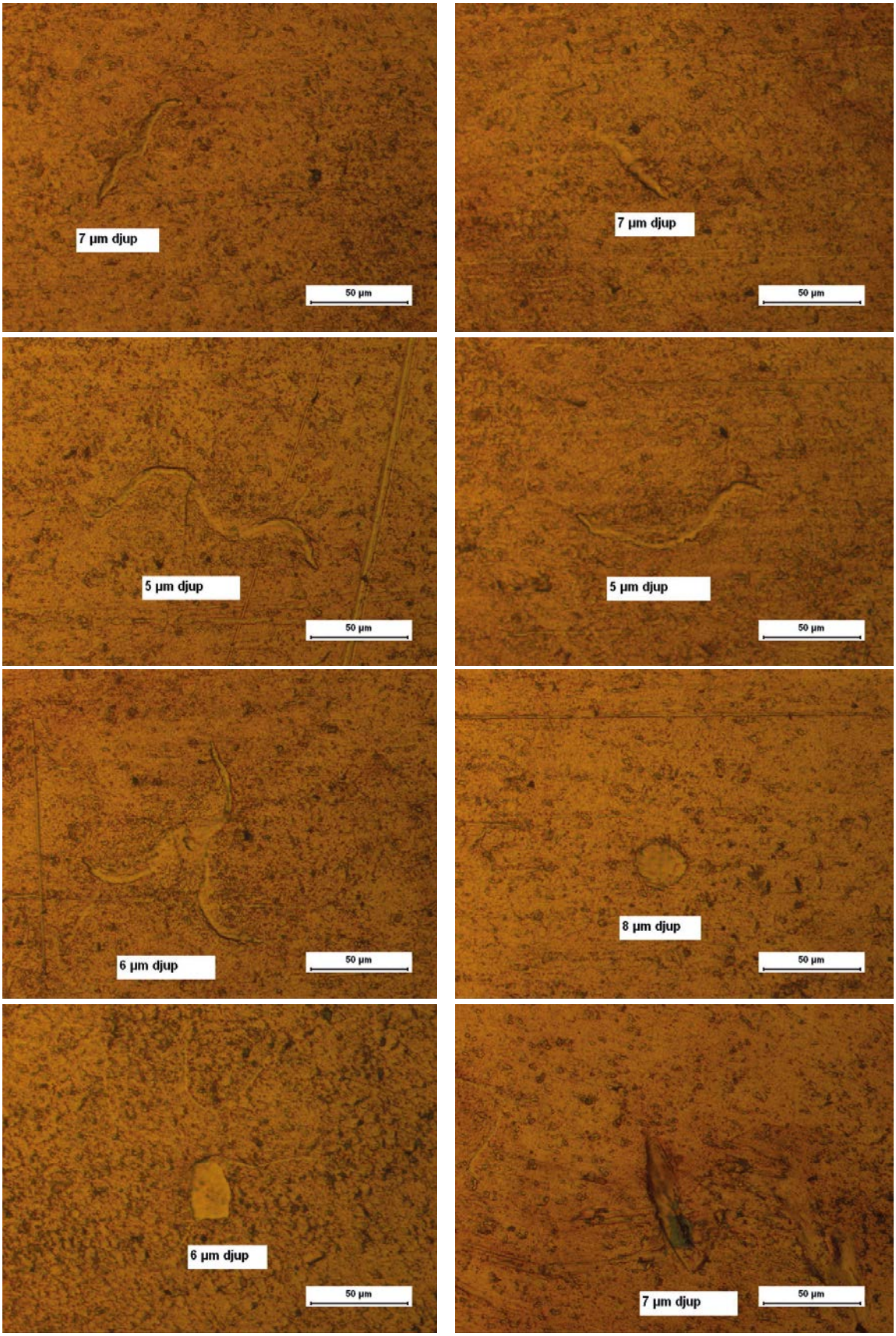

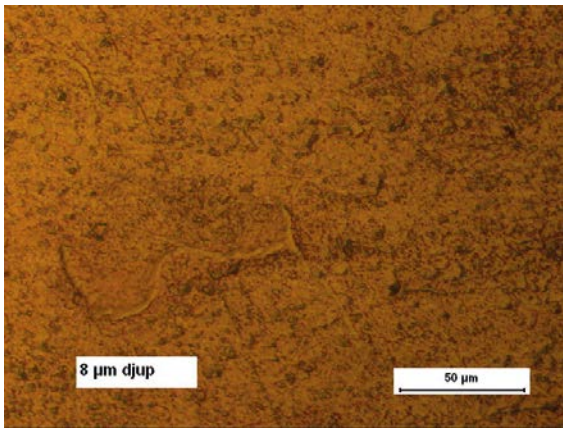
8 µm djup
50 µm

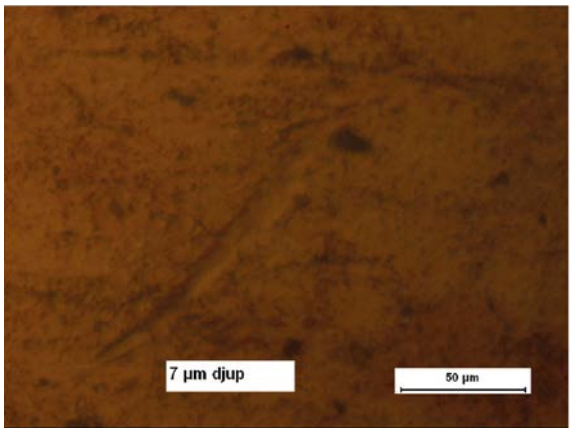
7 µm djup
50 µm

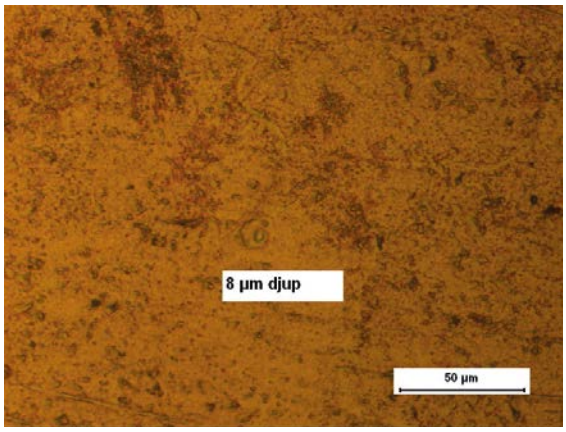
8 µm djup
50 µm

SRB exposures – Bio D coupon S9-7 side 1

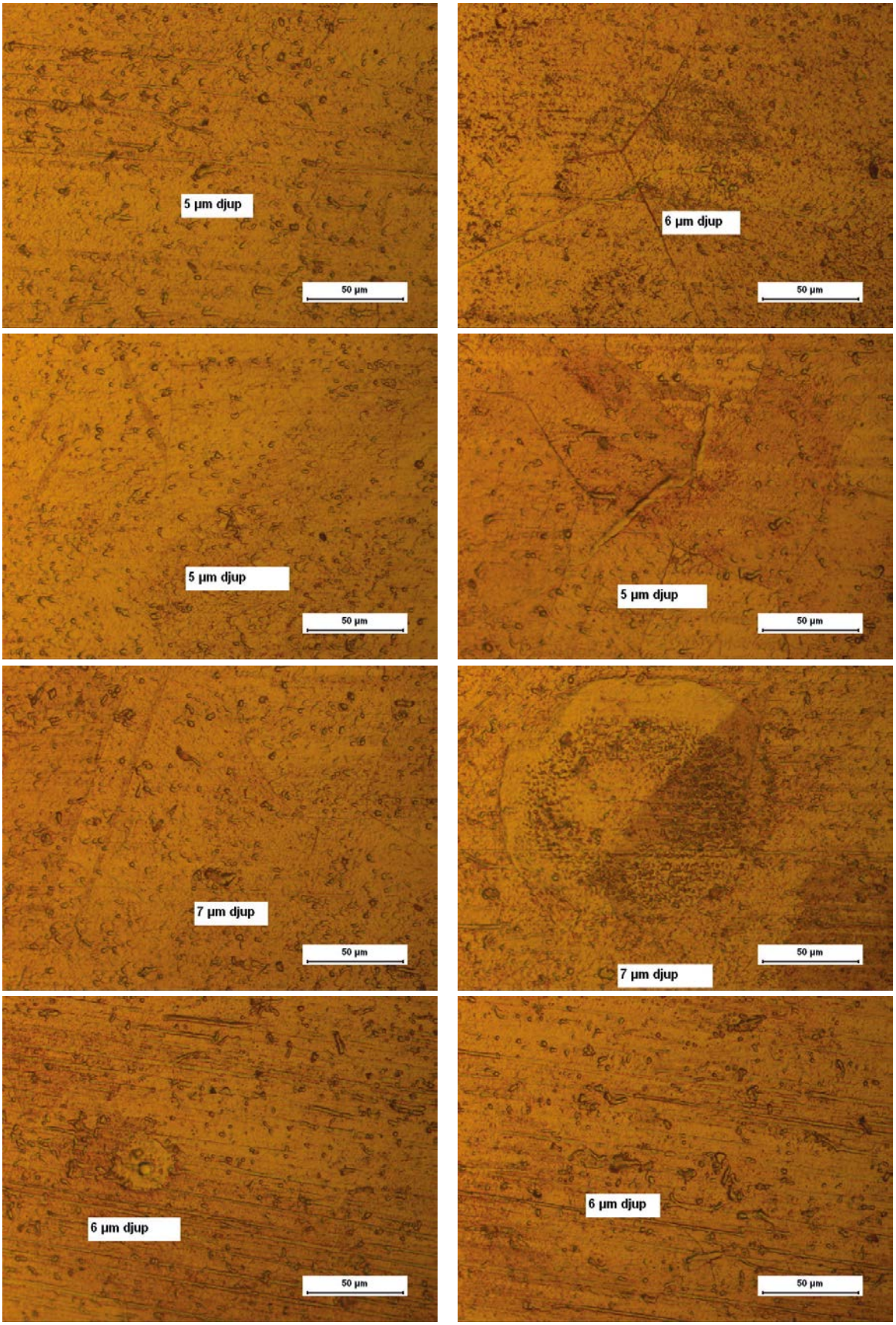

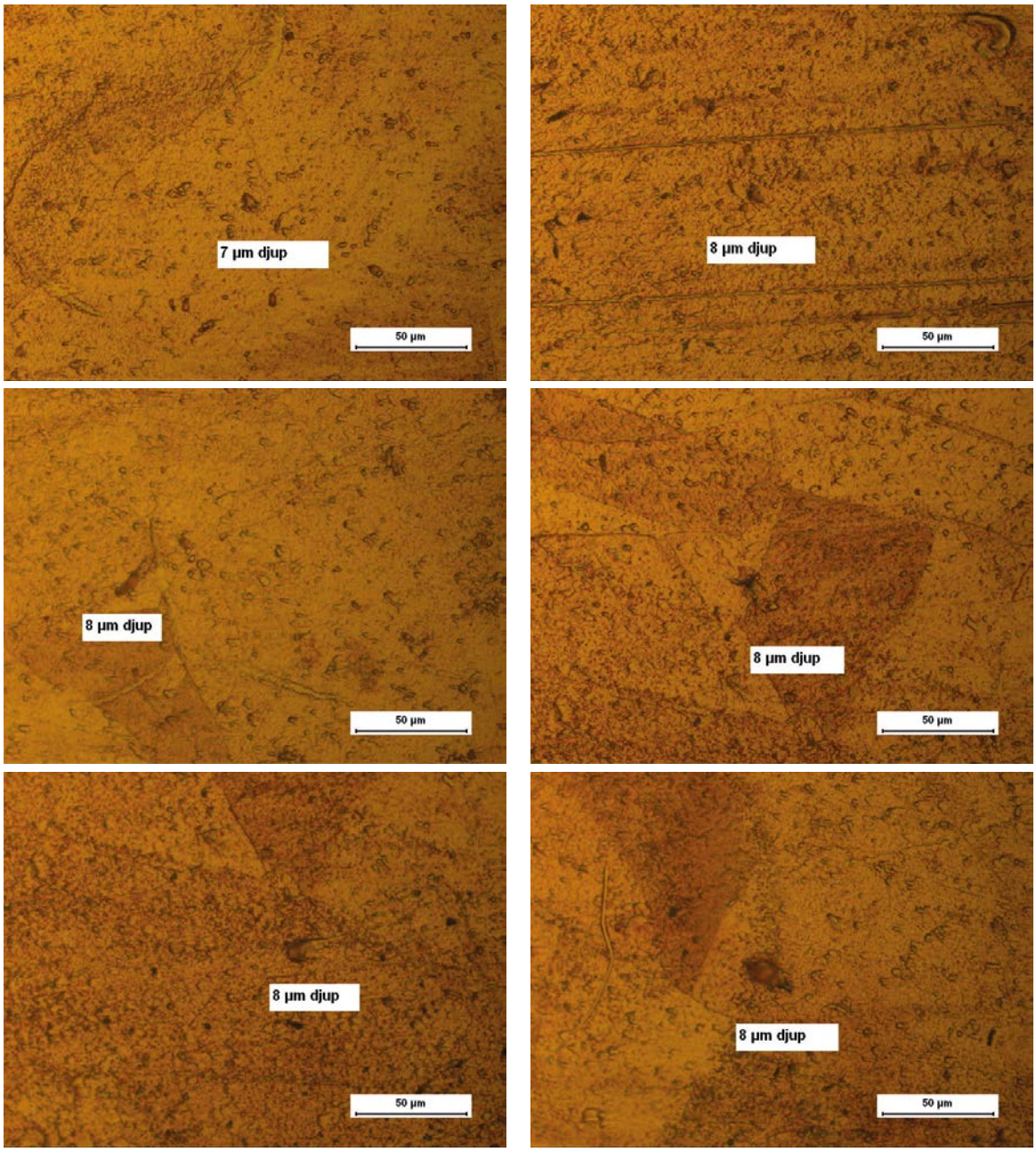
7 µm djup
50 µm
8 µm djup
50 µm
8 µm djup
50 µm
8 µm djup
50 µm
8 µm djup
50 µm
8 µm djup
50 µm

SRB exposures – Bio D coupon S9-7 side 2

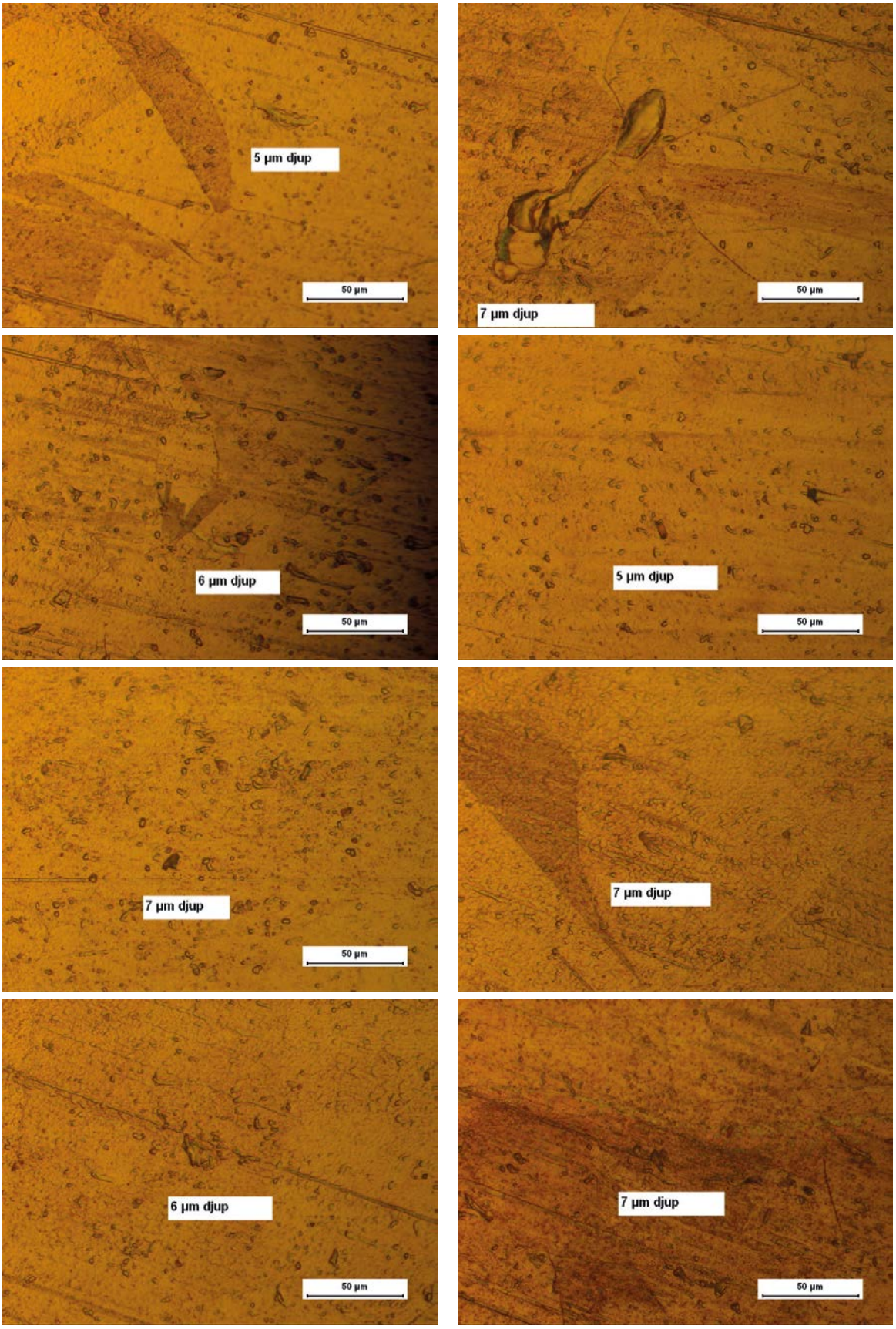

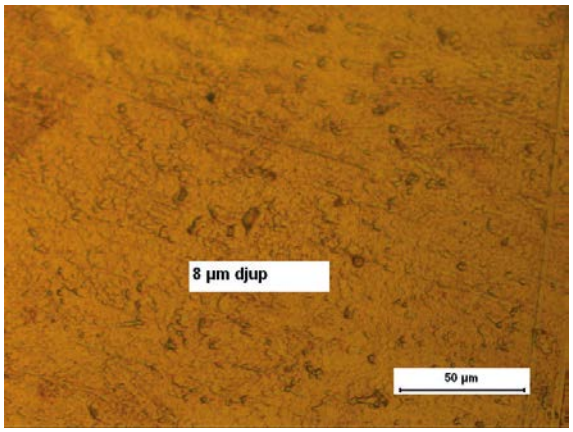
8 µm djup
50 µm

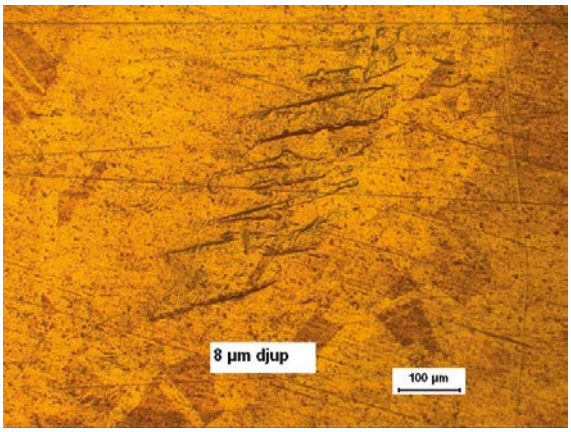
8 µm djup
100 µm

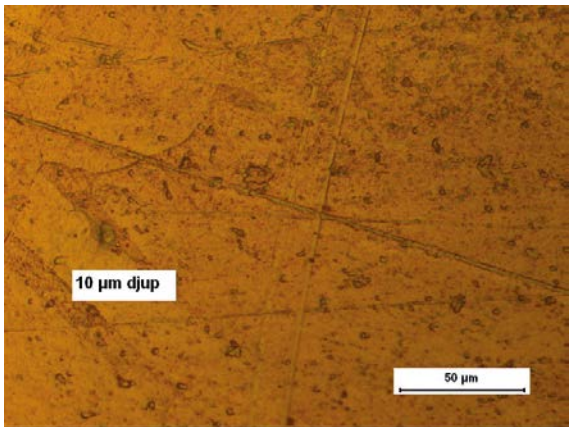
10 µm djup
50 µm

SRB exposures – Bio D coupon S9-1 side 1

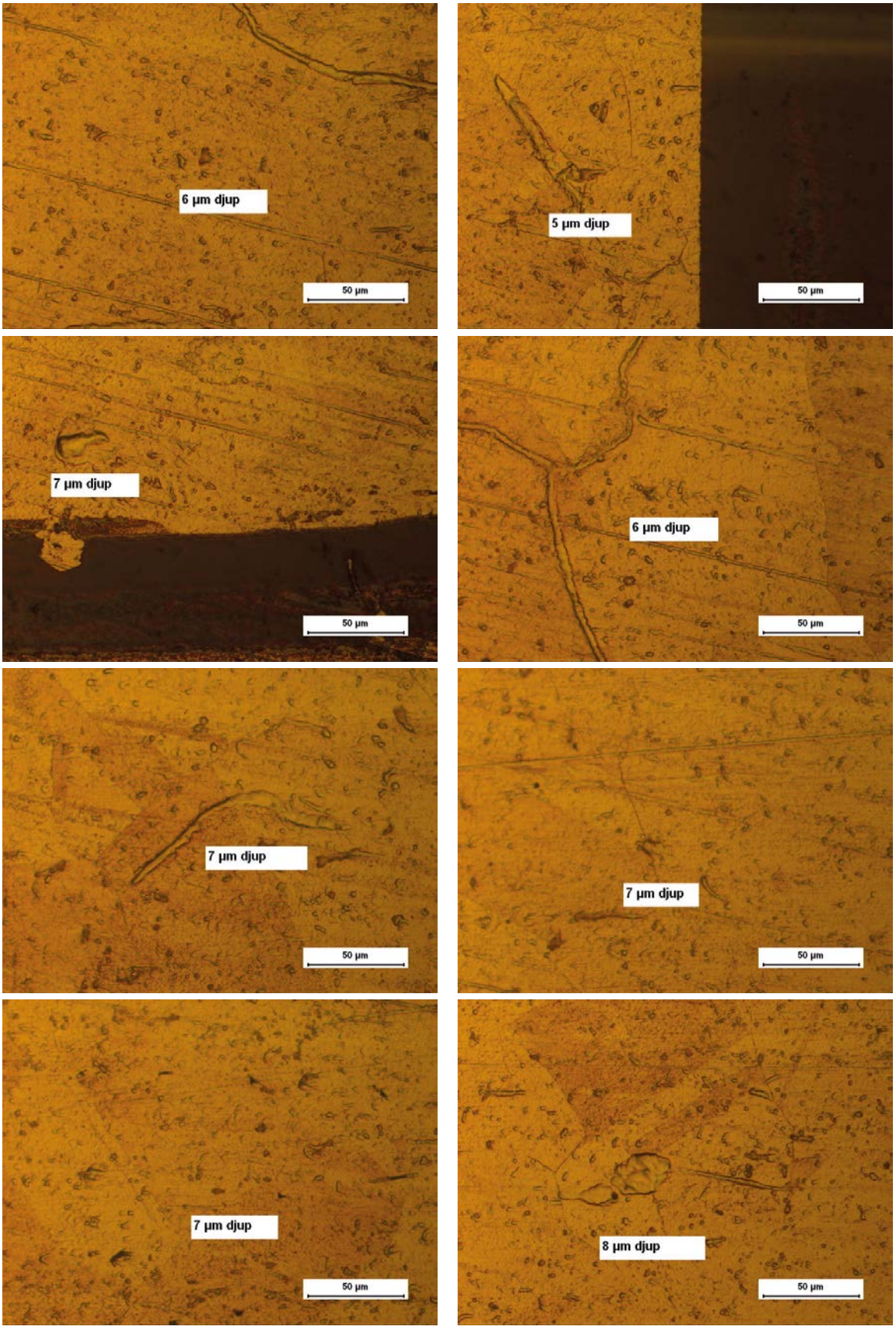

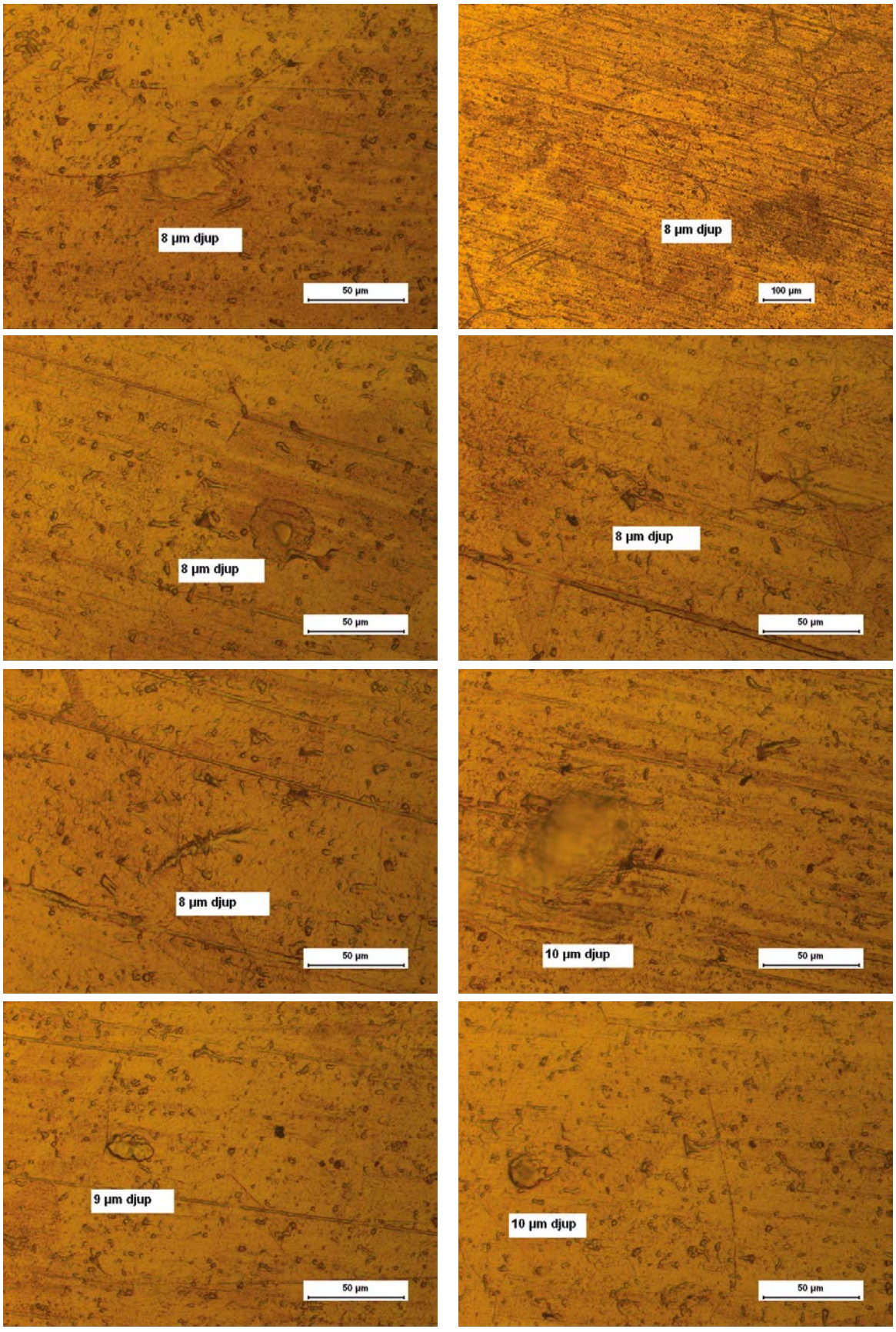
8 µm djup
50 µm
8 µm djup
100 µm
8 µm djup
50 µm
8 µm djup
50 µm
8 µm djup
50 µm
10 µm djup
50 µm
9 µm djup
50 µm
10 µm djup
50 µm

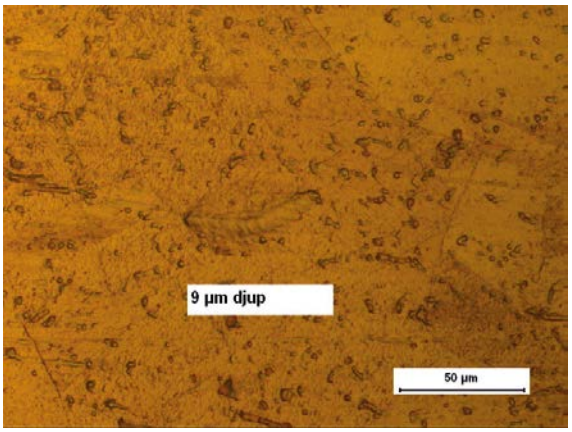
9 µm djup
50 µm

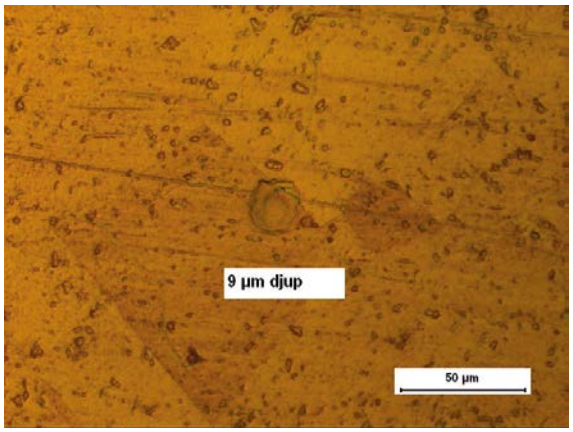
9 µm djup
50 µm

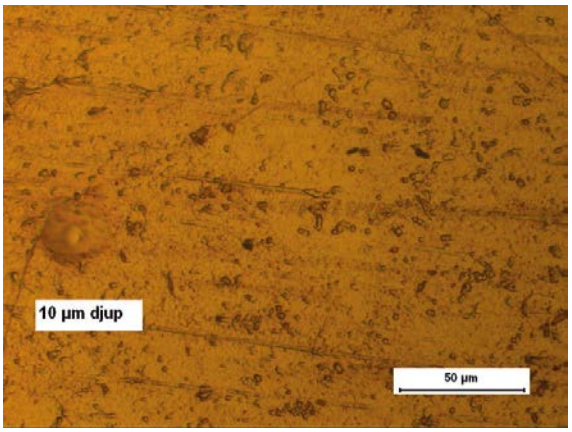
10 µm djup
50 µm

SRB exposures – Bio D coupon S9-1 side 2

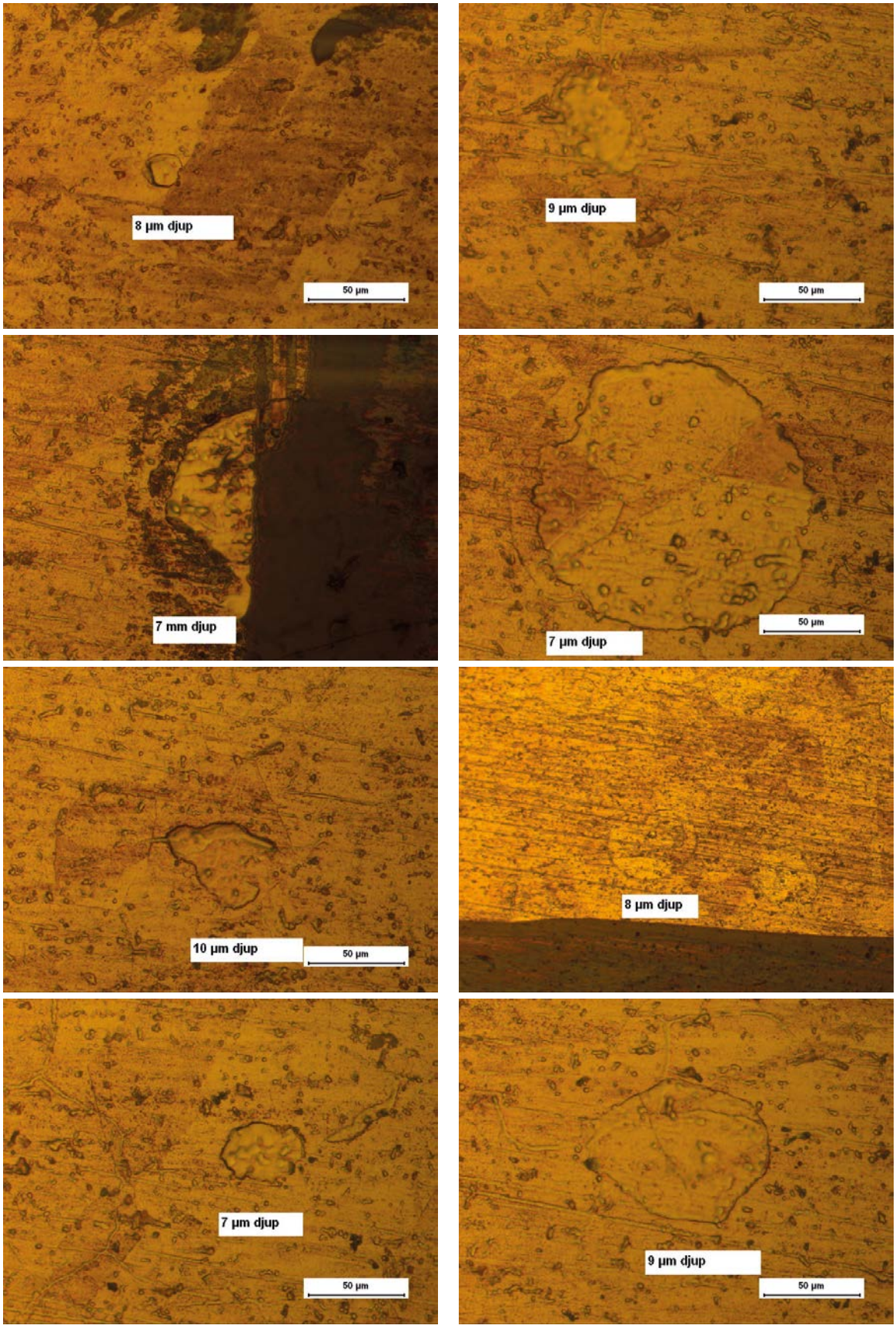

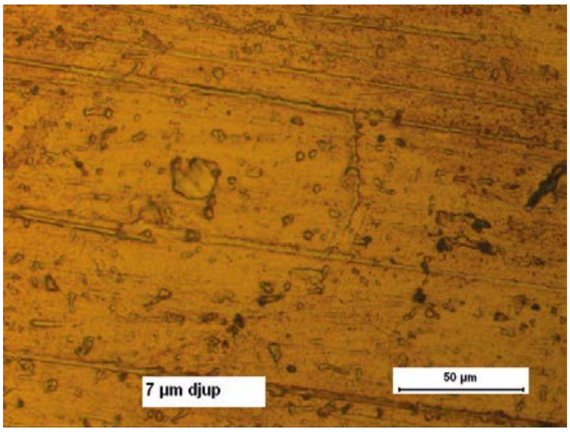
7 µm djup
50 µm
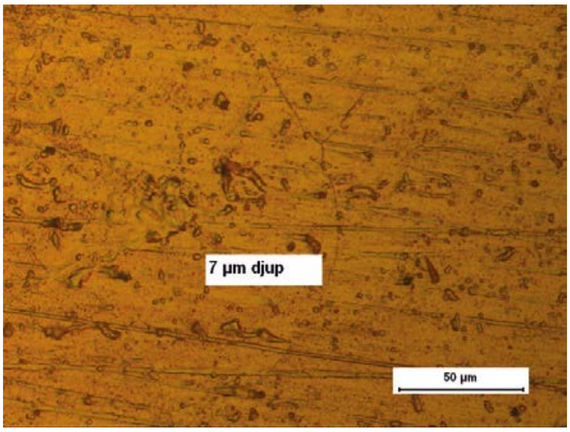
7 µm djup
50 µm
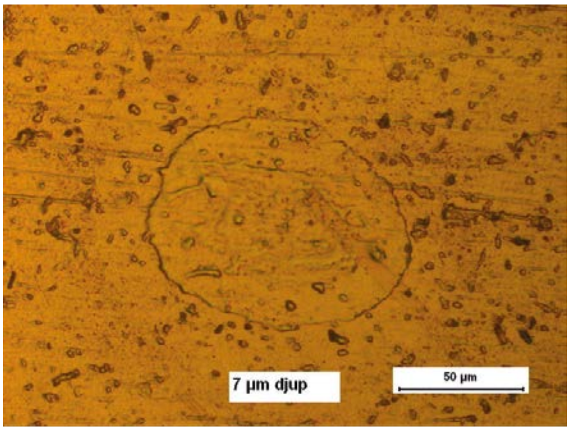
7 µm djup
50 µm
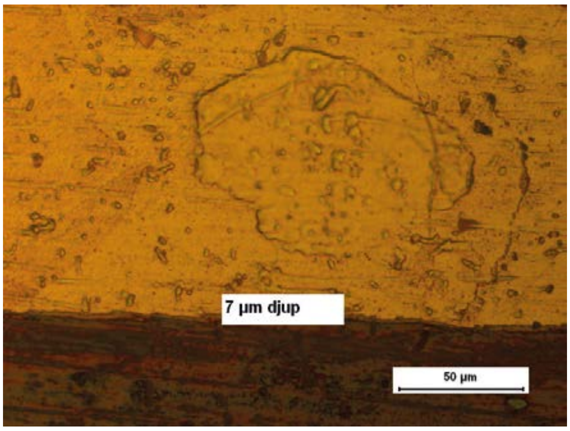
7 µm djup
50 µm
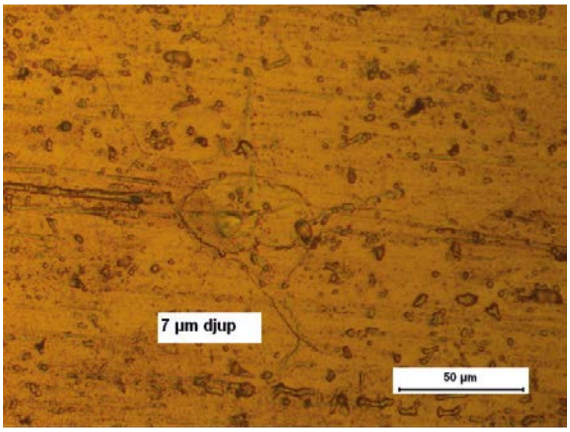
7 µm djup
50 µm
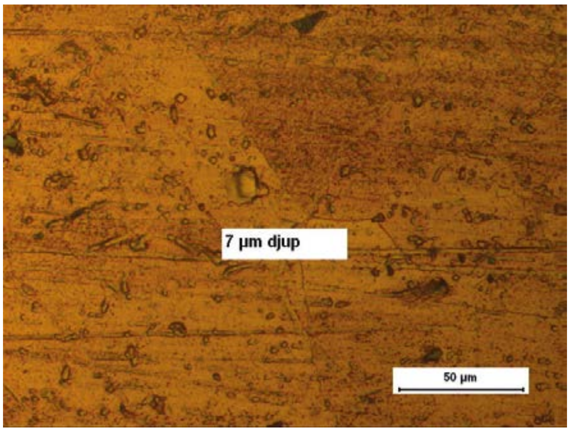
7 µm djup
50 µm
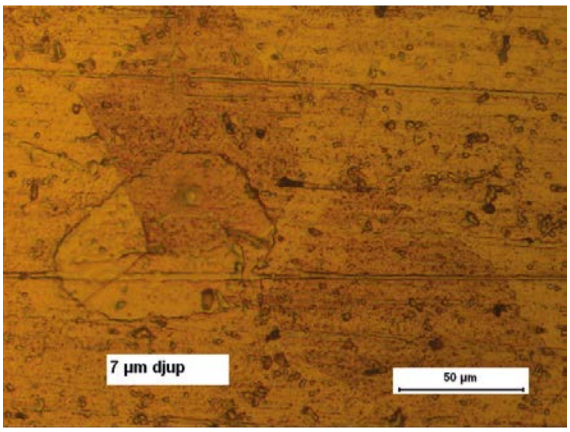
7 µm djup
50 µm
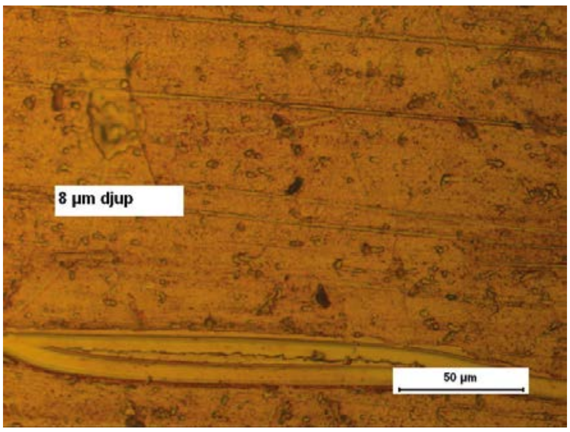
8 µm djup
50 µm

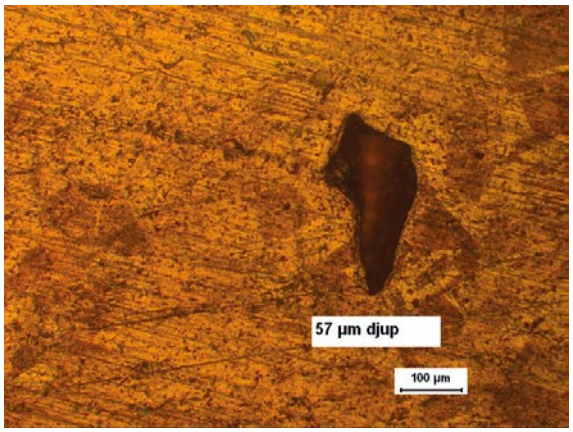
57 µm djup
100 µm

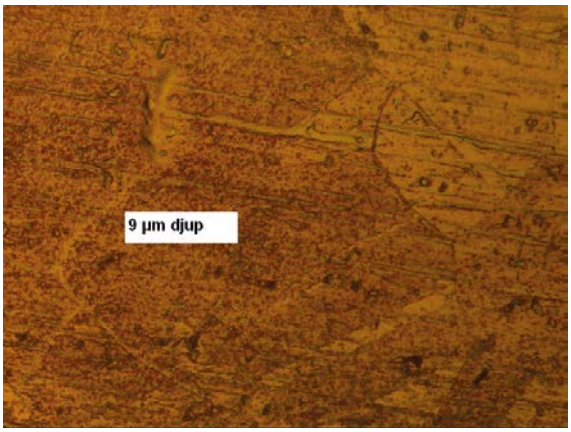
9 µm djup

SRB exposures – Control G coupon S9-6 side 1

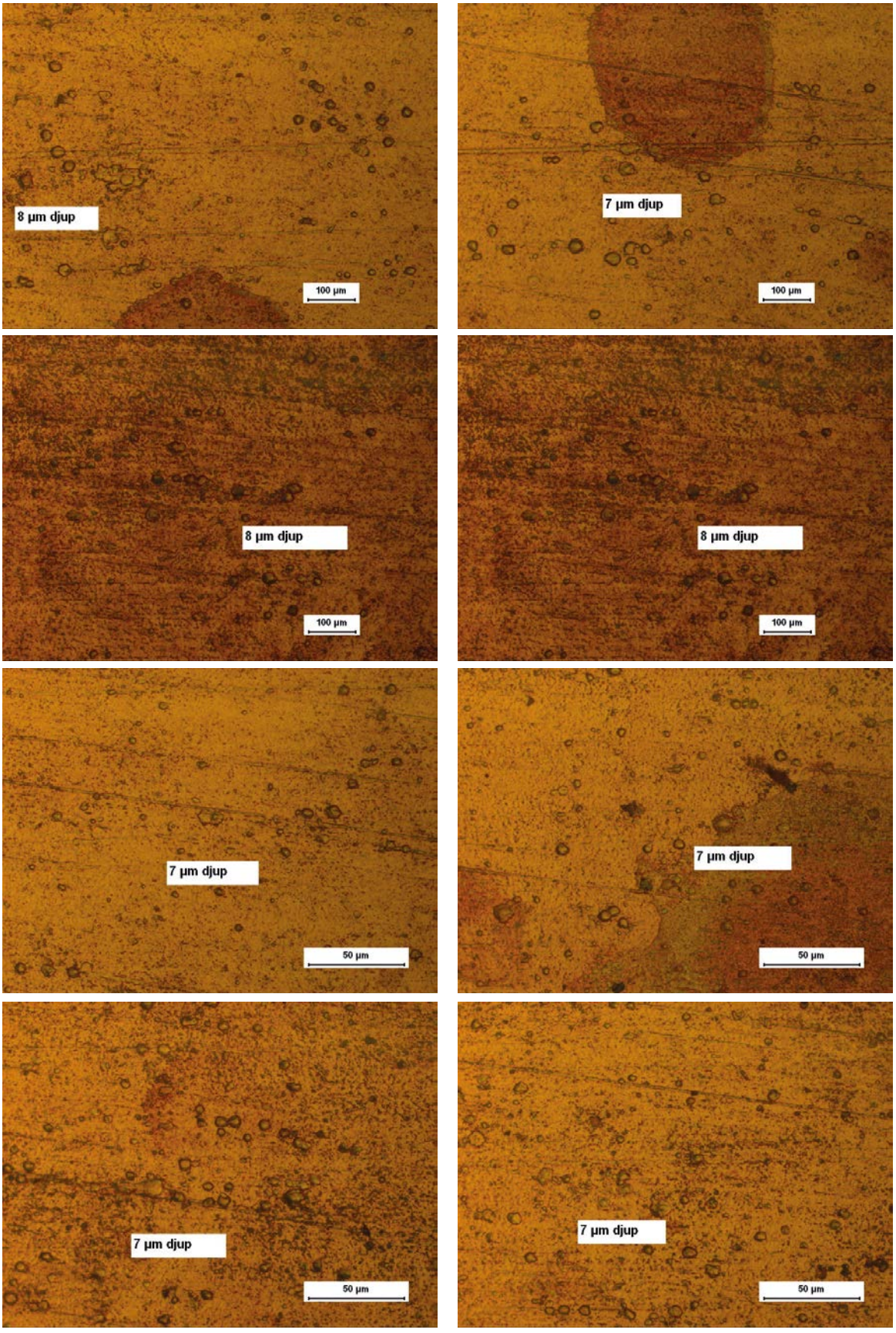

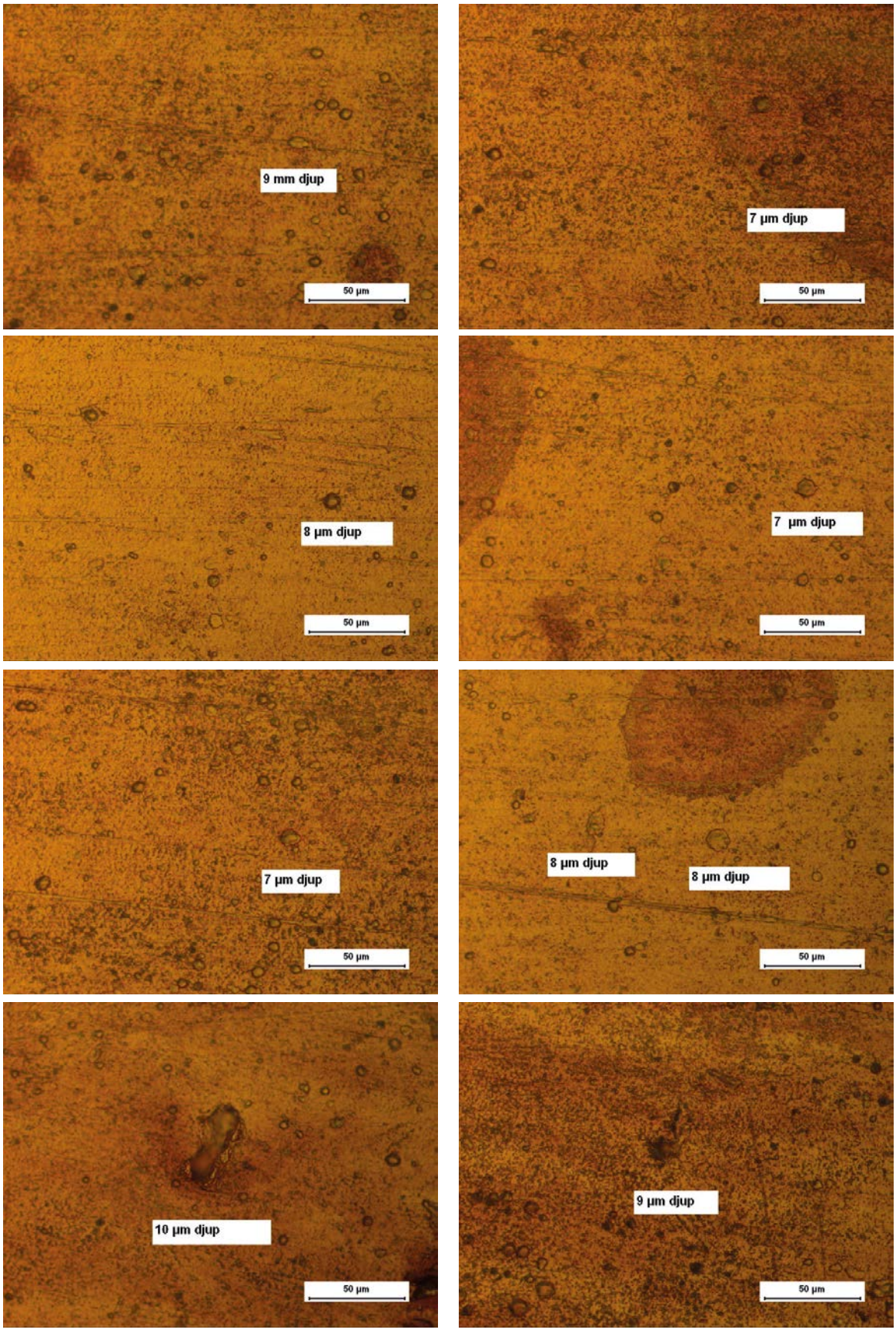
9 mm djup
50 µm
7 µm djup
50 µm
8 µm djup
50 µm
7 µm djup
50 µm
7 µm djup
50 µm
8 µm djup
8 µm djup
50 µm
10 µm djup
50 µm
9 µm djup
50 µm

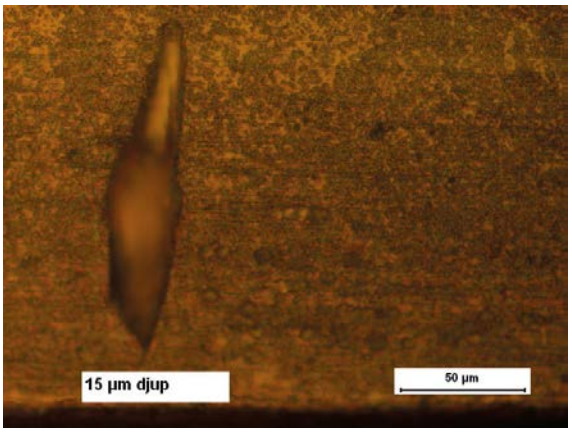
15 µm djup
50 µm

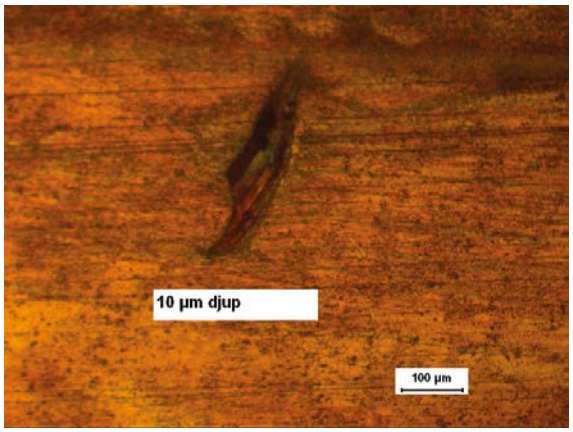
10 µm djup
100 µm

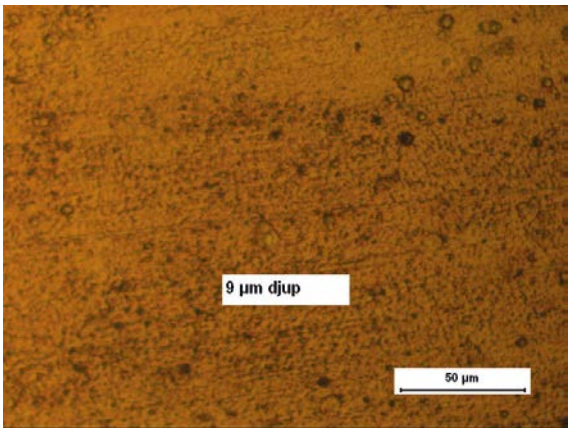
9 µm djup
50 µm

SRB exposures – Control G coupon S9-6 side 2

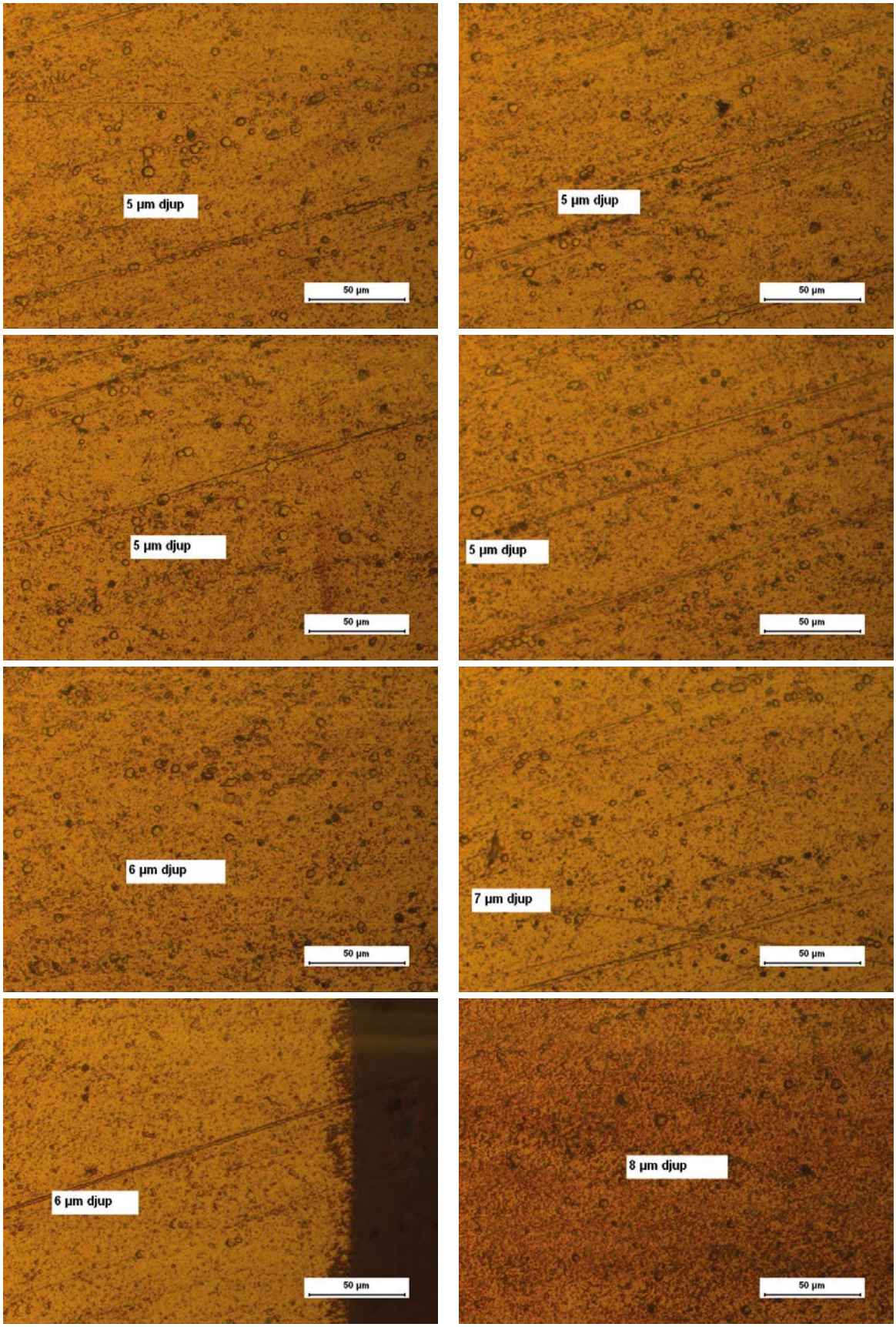

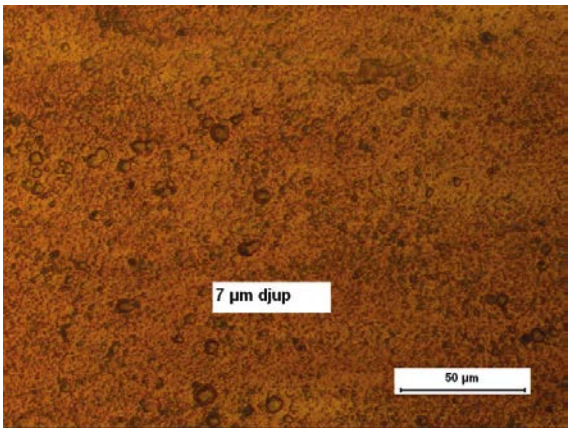
7 µm djup
50 µm

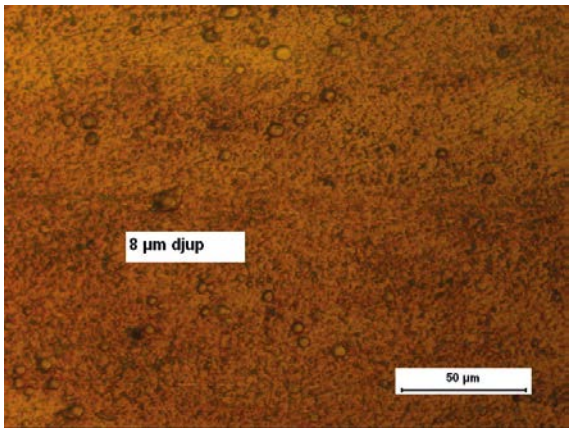
8 µm djup
50 µm

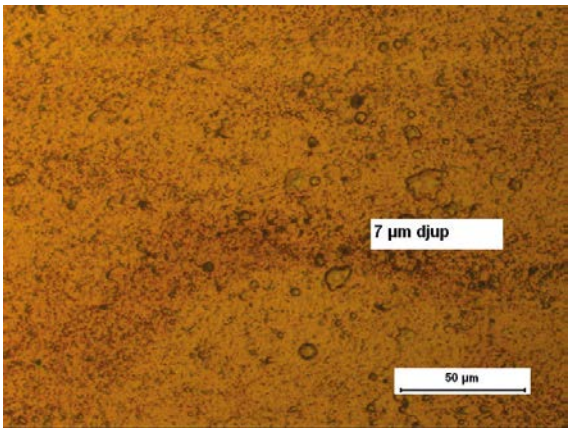
7 µm djup
50 µm

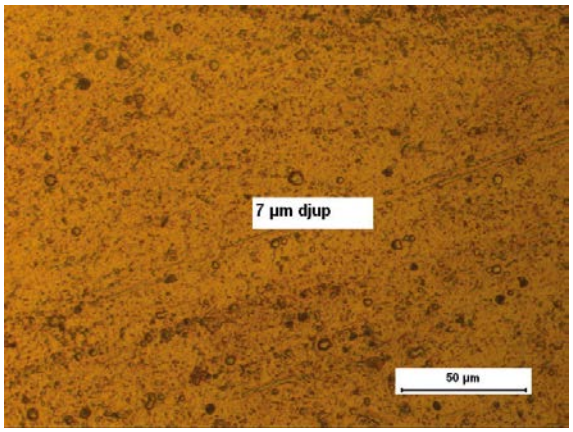
7 µm djup
50 µm

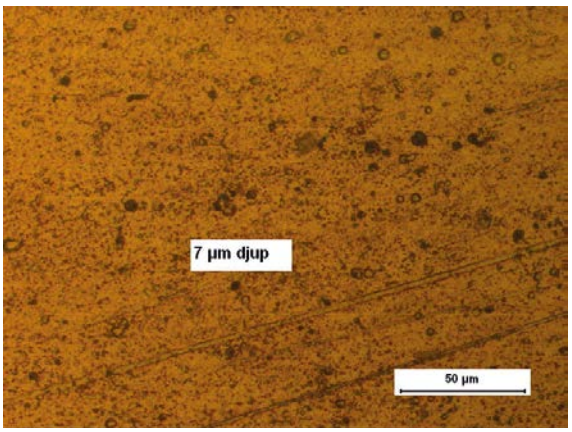
7 µm djup
50 µm

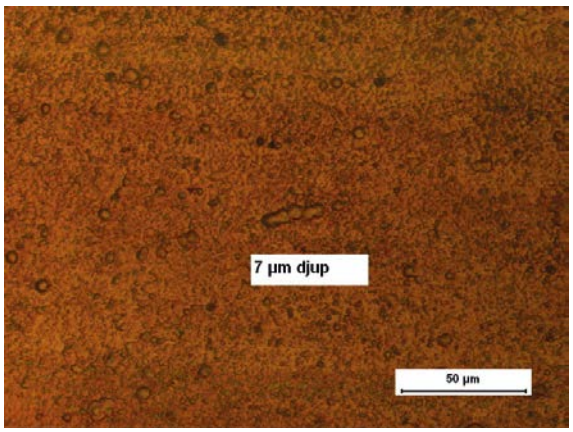
7 µm djup
50 µm

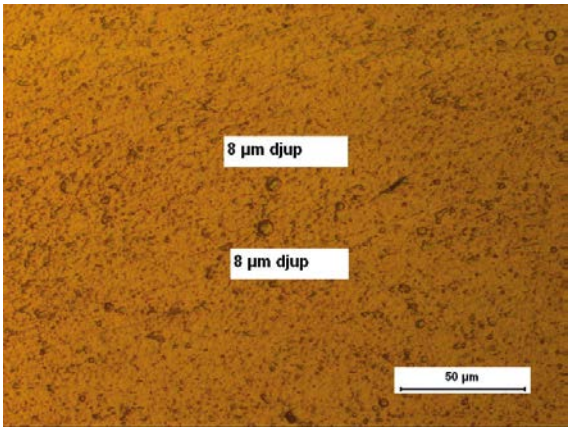
8 µm djup
8 µm djup
50 µm

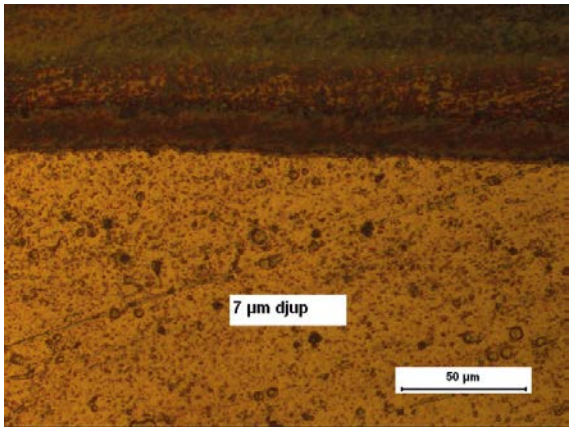
7 µm djup
50 µm

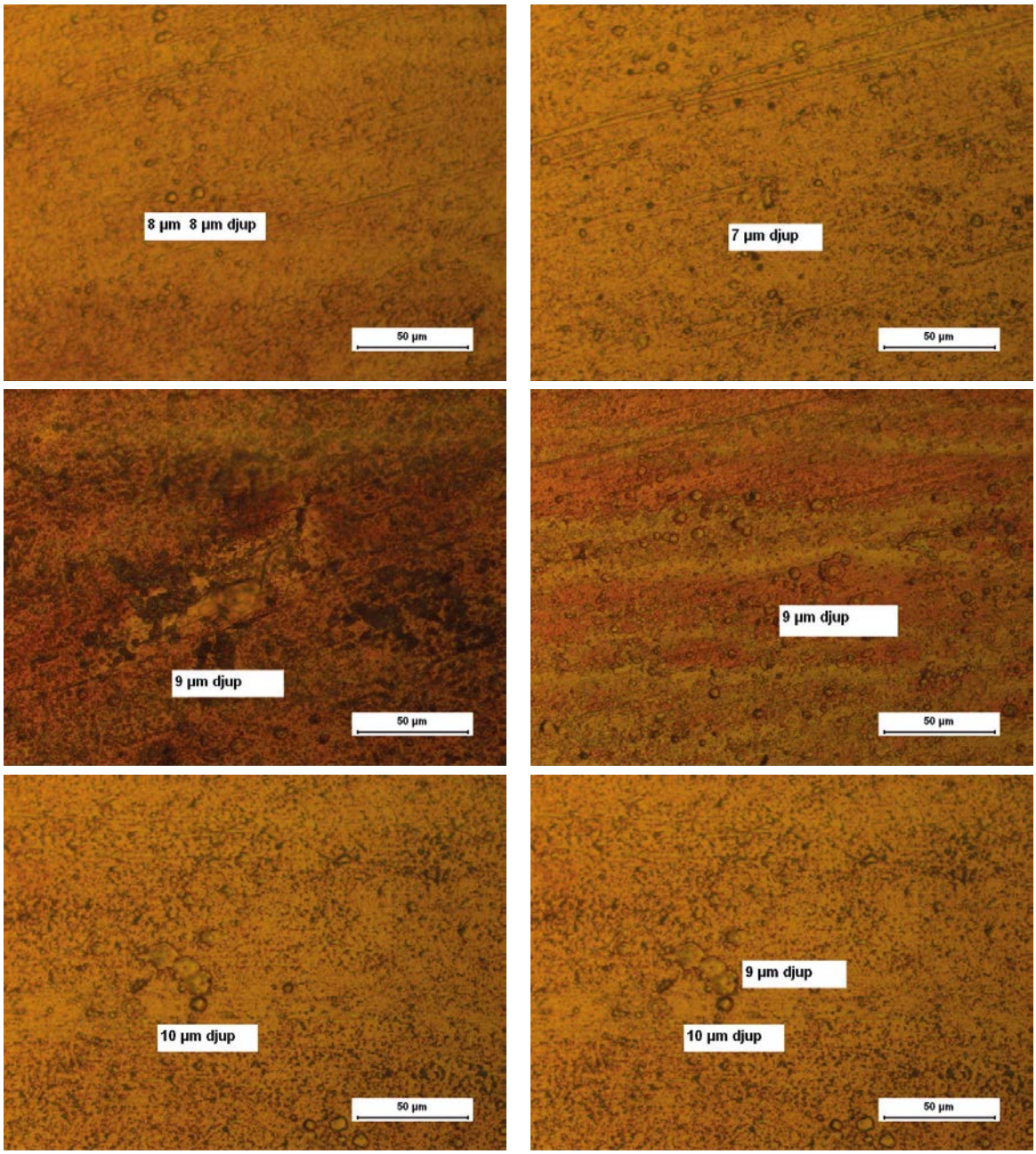
8 µm 8 µm djup
50 µm
7 µm djup
50 µm
9 µm djup
50 µm
9 µm djup
50 µm
10 µm djup
50 µm
9 µm djup
10 µm djup
50 µm

SRB exposures – Control G coupon S8-4 side 1

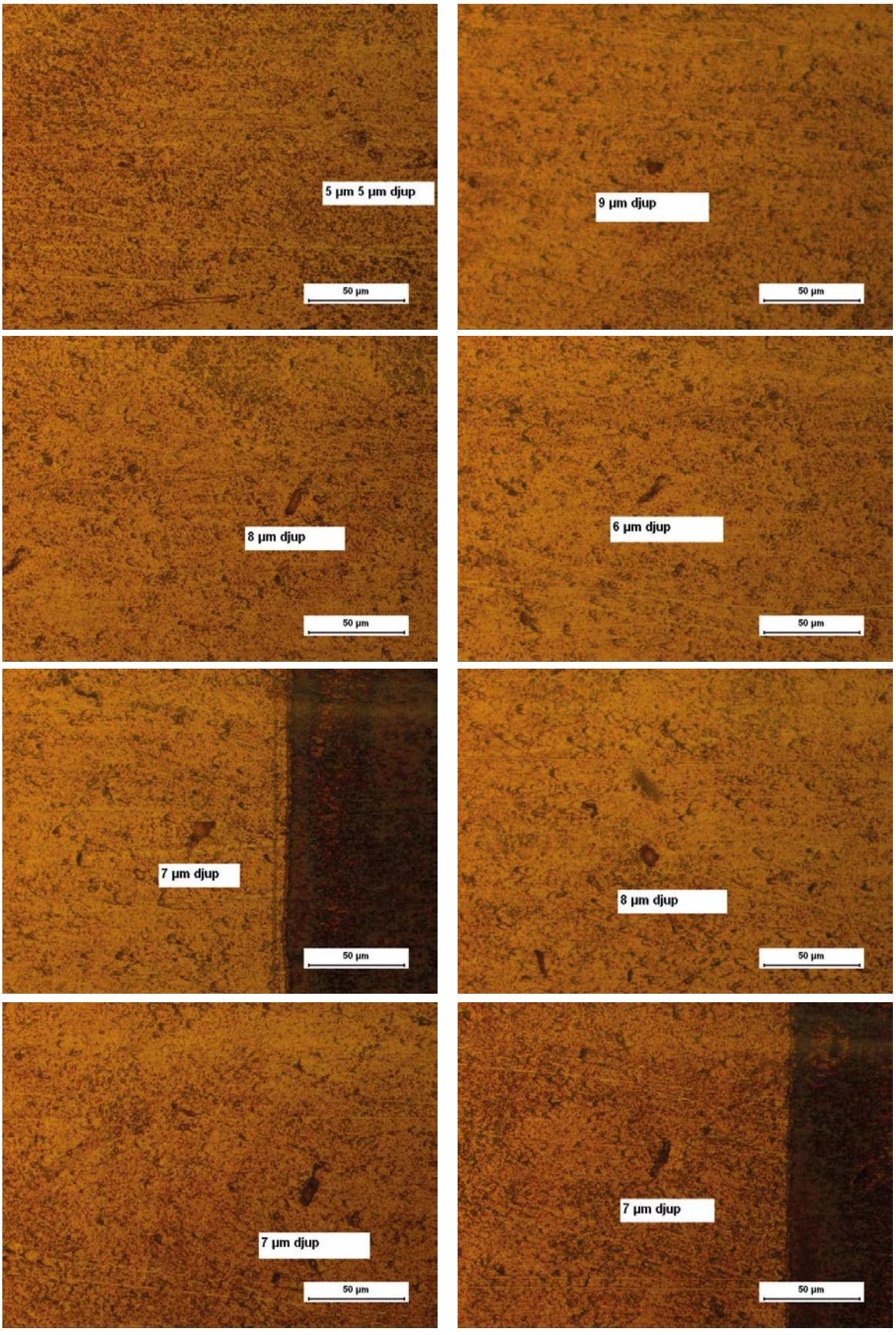

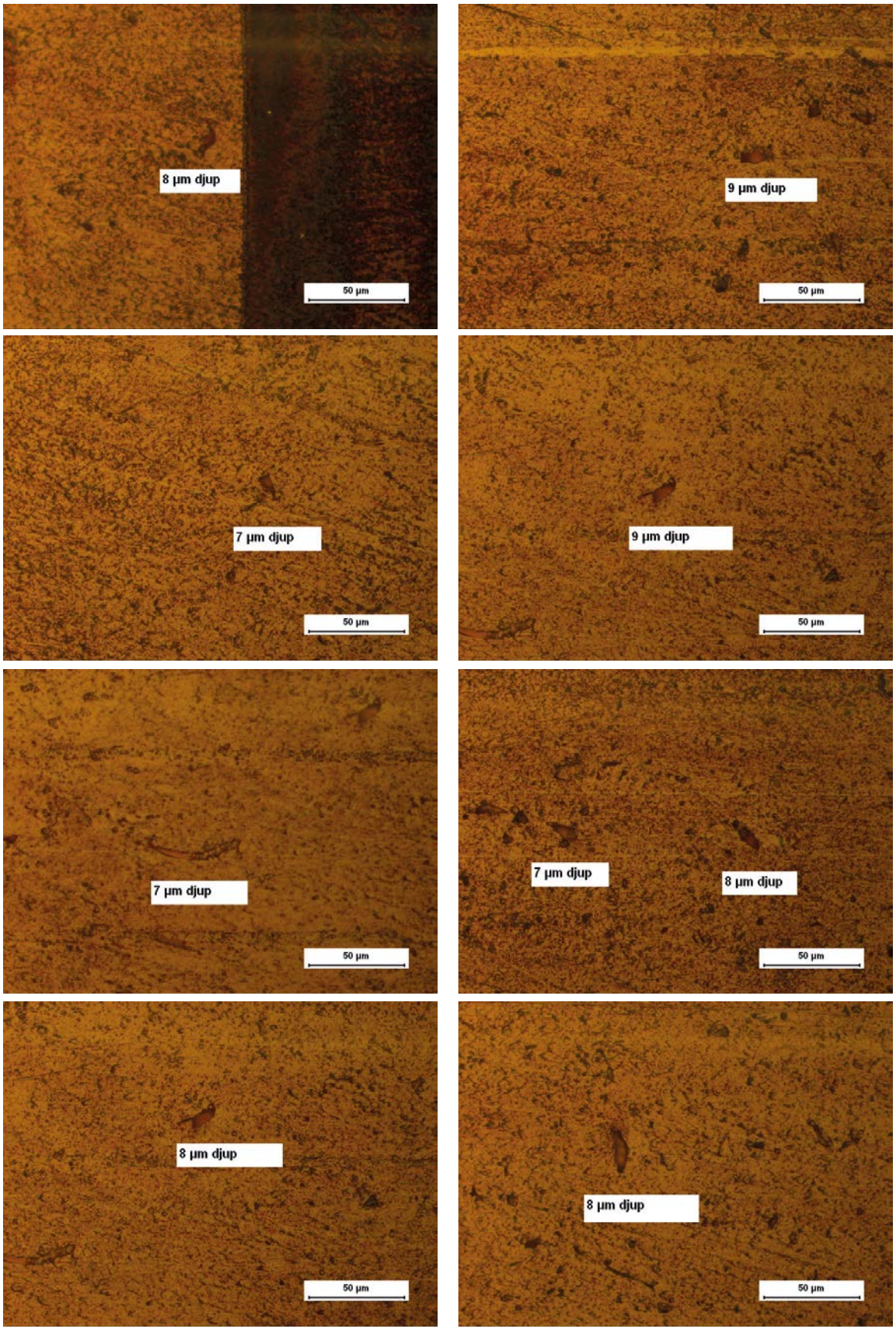
8 µm djup
50 µm
9 µm djup
50 µm
7 µm djup
50 µm
9 µm djup
50 µm
7 µm djup
50 µm
7 µm djup
8 µm djup
50 µm
8 µm djup
50 µm
8 µm djup
50 µm

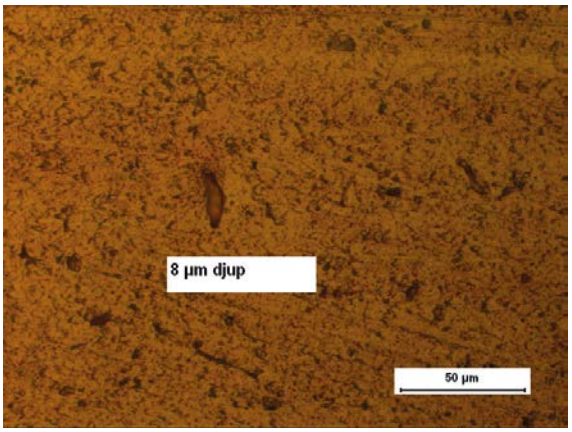
8 µm djup
50 µm

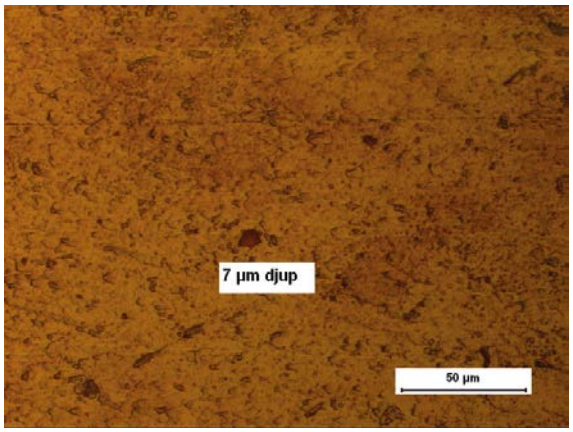
7 µm djup
50 µm

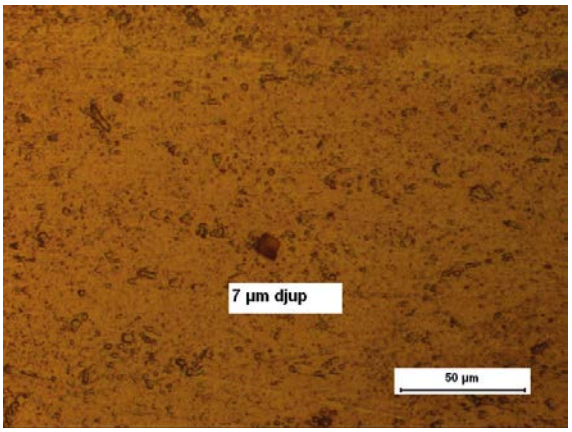
7 µm djup
50 µm

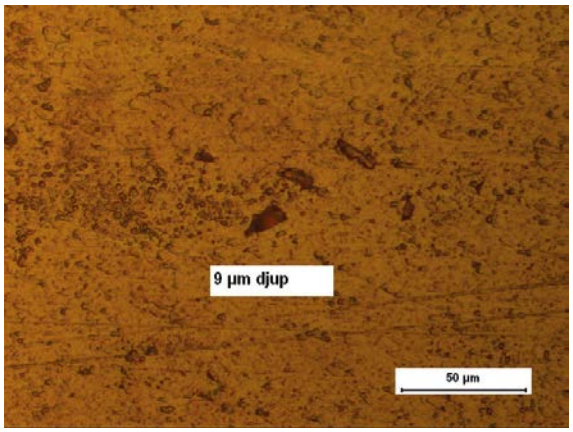
9 µm djup
50 µm

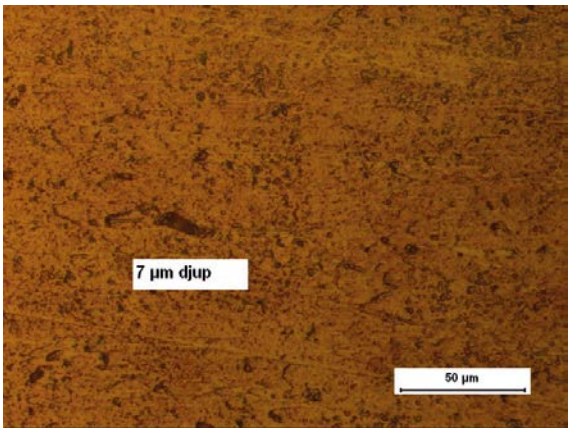
7 µm djup
50 µm

SRB exposures – Control G coupon S8-4 side 2

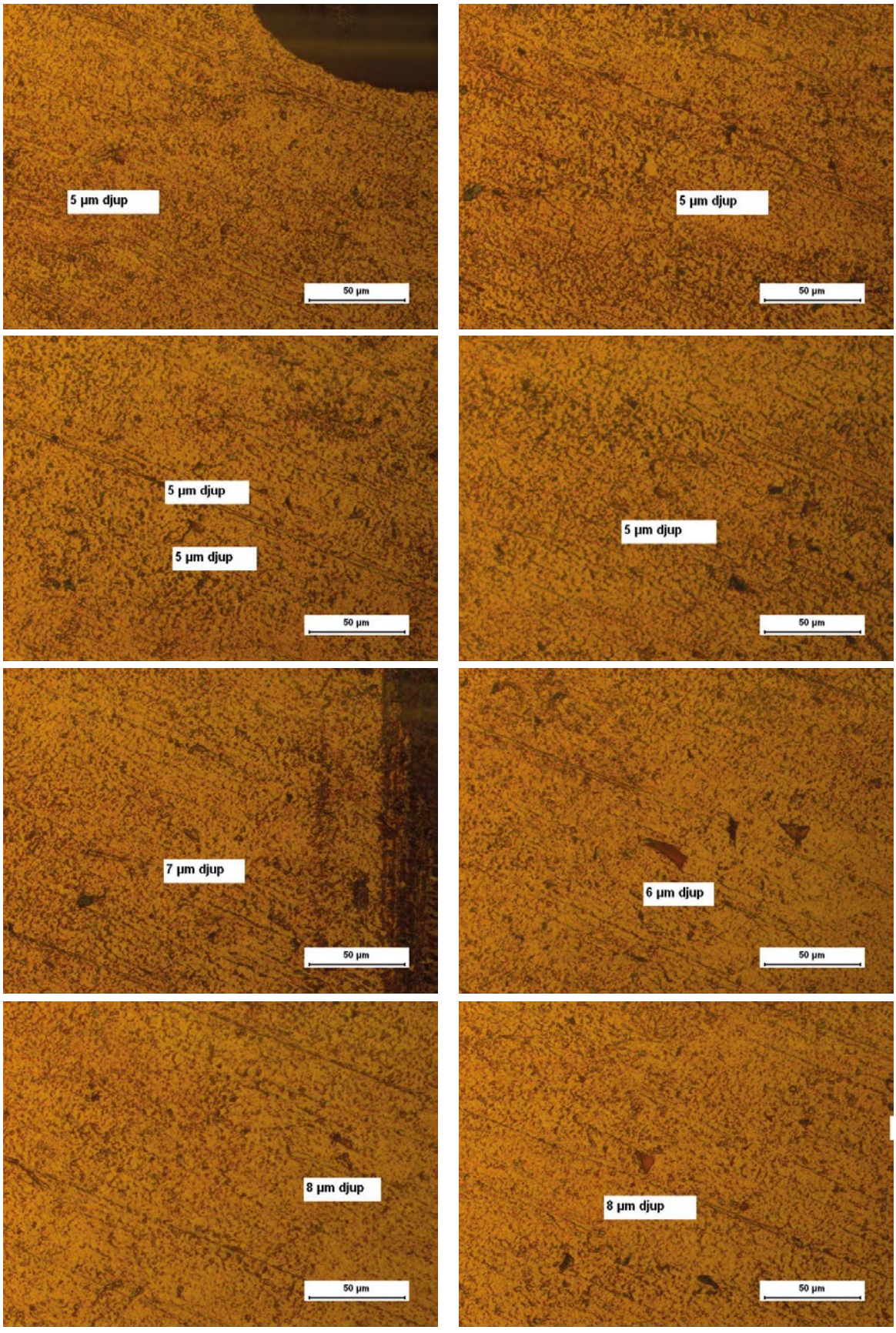

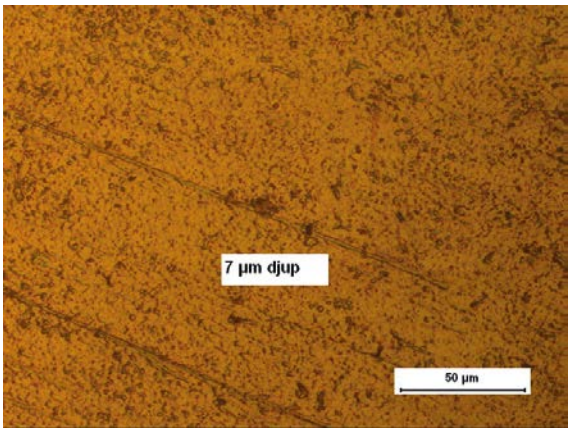
7 µm djup
50 µm

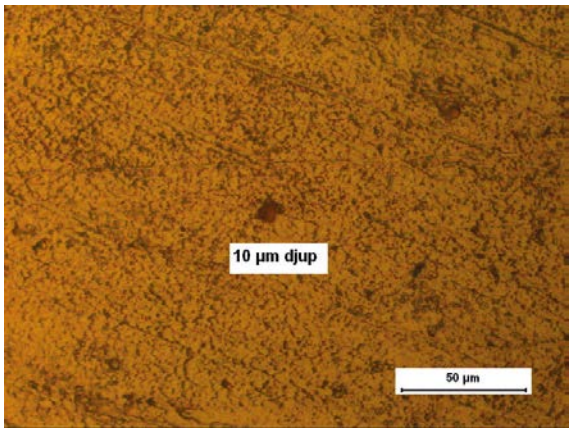
10 µm djup
50 µm

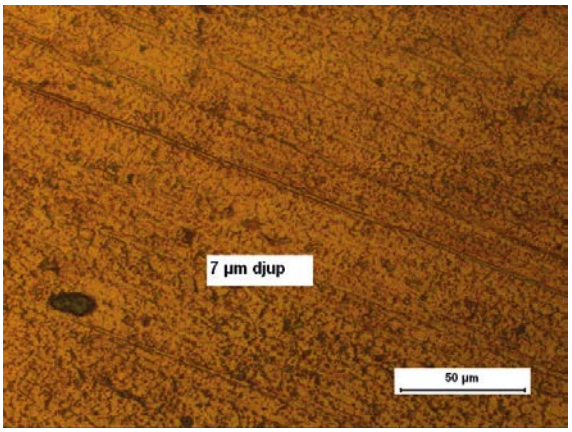
7 µm djup
50 µm

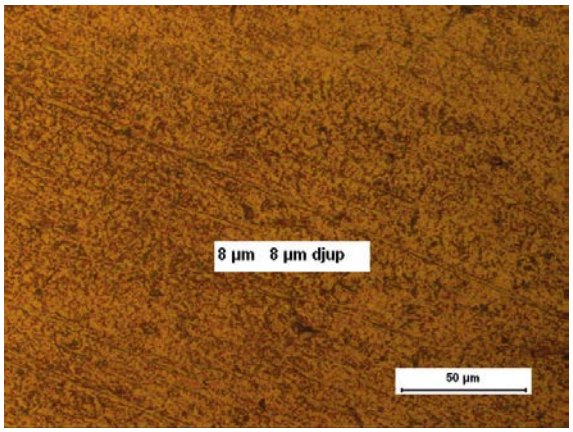
8 µm 8 µm djup
50 µm

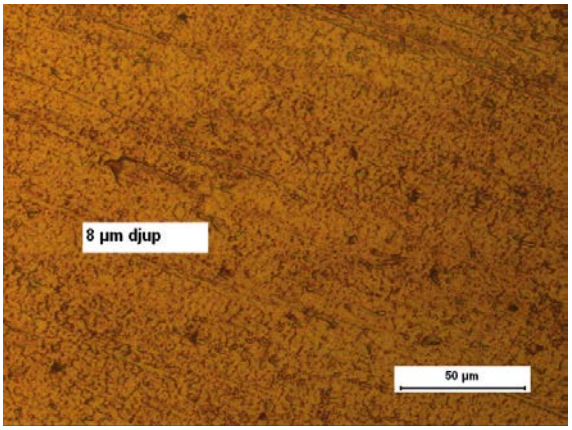
8 µm djup
50 µm

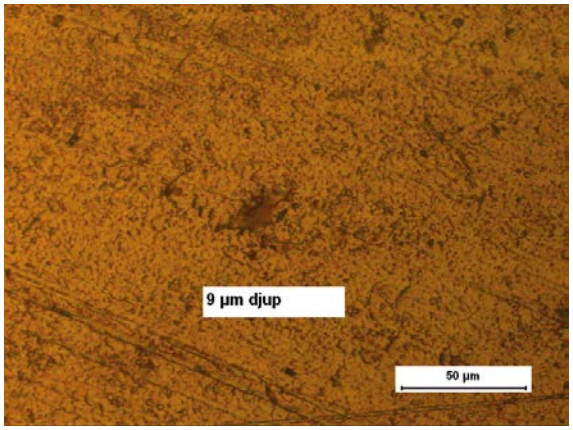
9 µm djup
50 µm

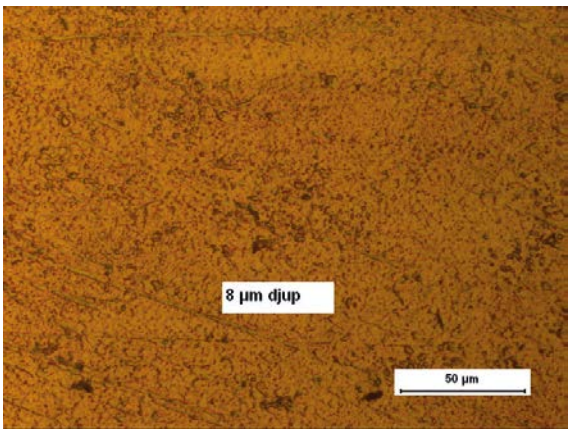
8 µm djup
50 µm

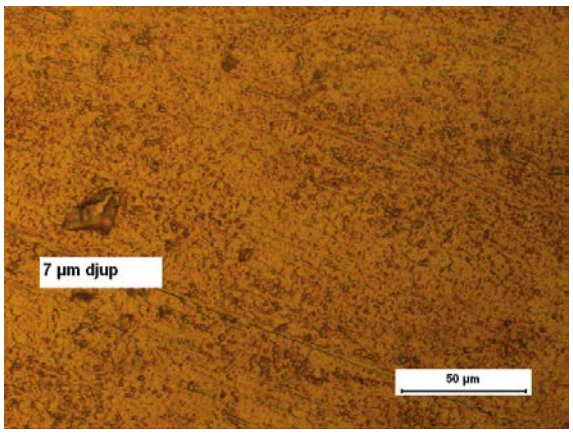
7 µm djup
50 µm

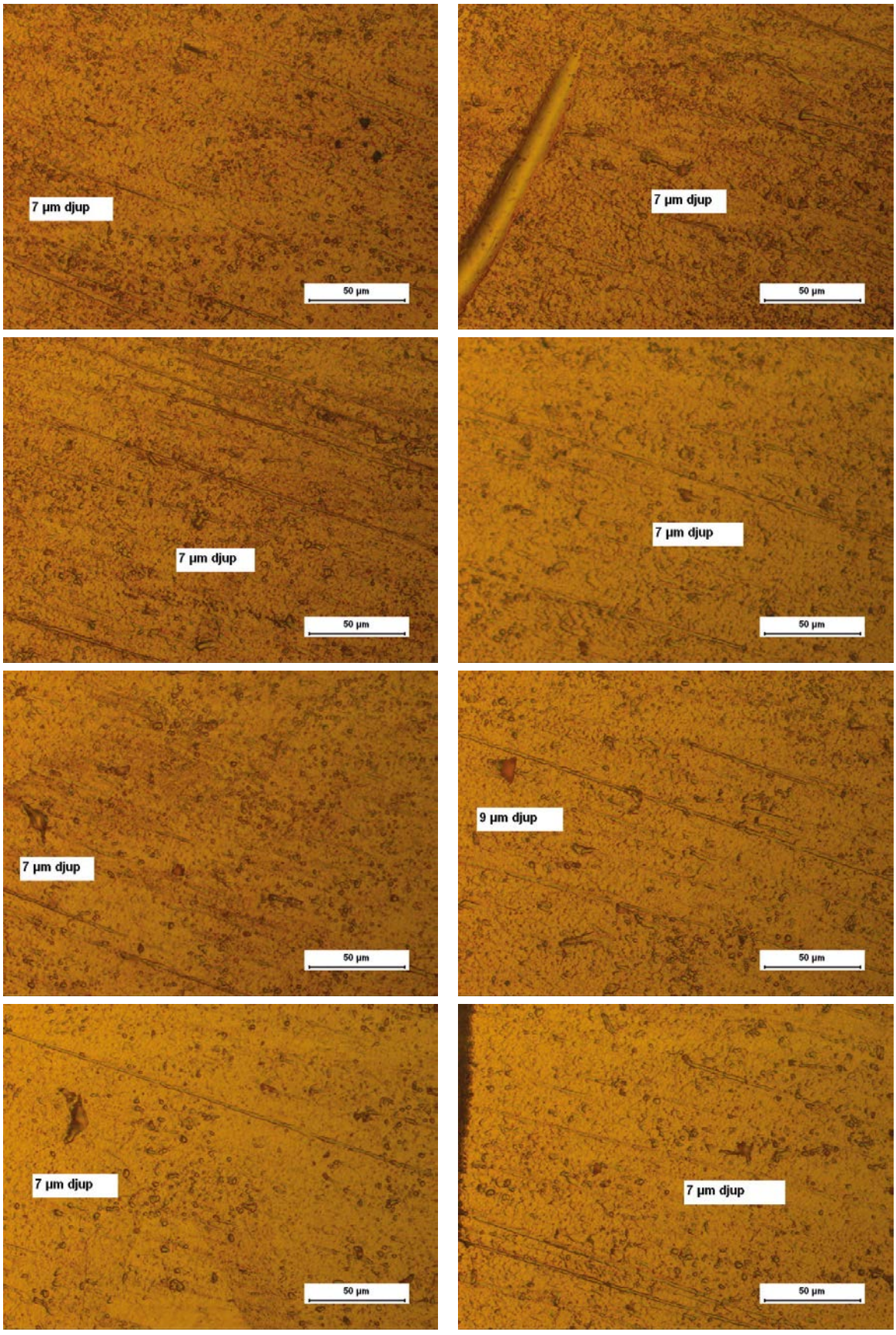
7 µm djup
50 µm
7 µm djup
50 µm
7 µm djup
50 µm
7 µm djup
50 µm
7 µm djup
50 µm
9 µm djup
50 µm
7 µm djup
50 µm
7 µm djup
50 µm

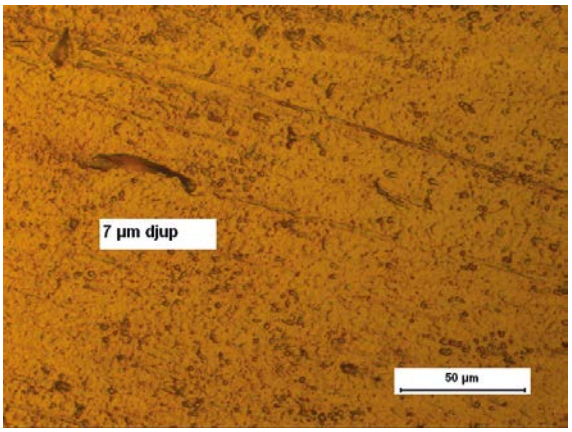
7 µm djup
50 µm

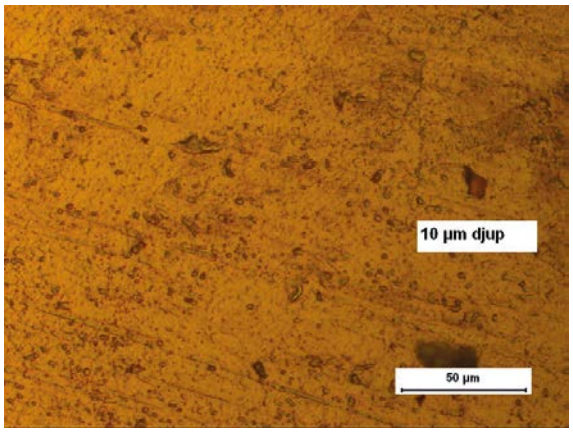
10 µm djup
50 µm

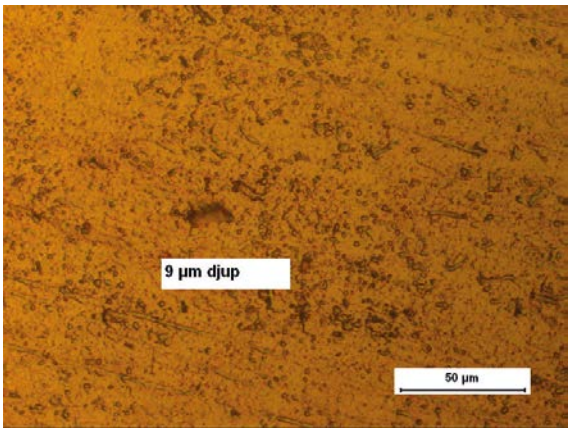
9 µm djup
50 µm

SRB exposures – Reference coupon 1 side 1 before pickling

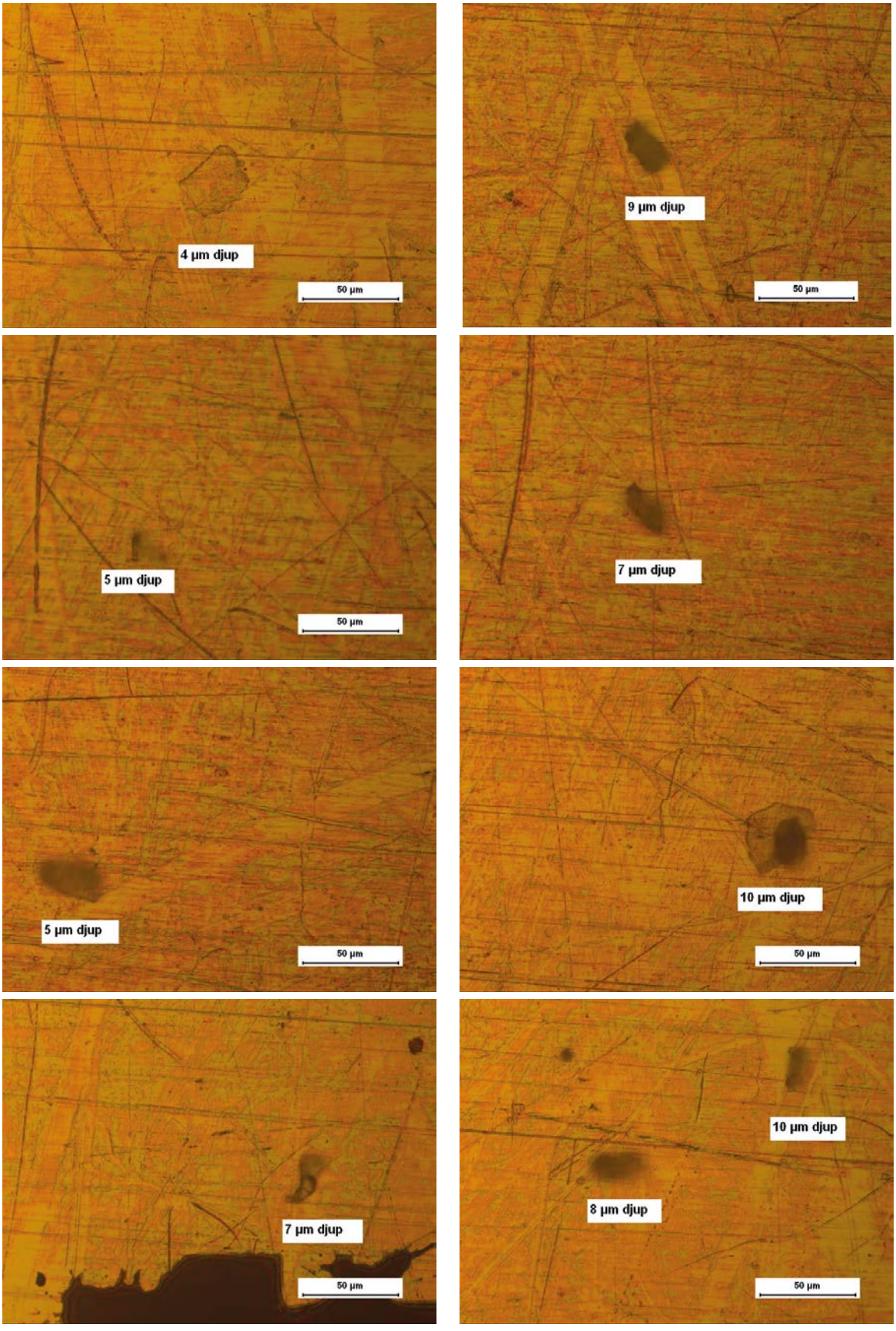

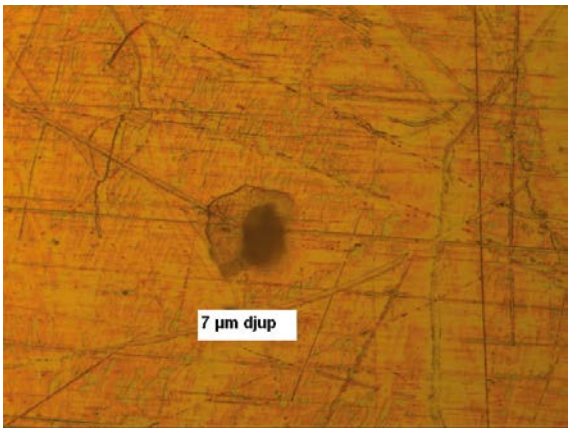
7 µm djup

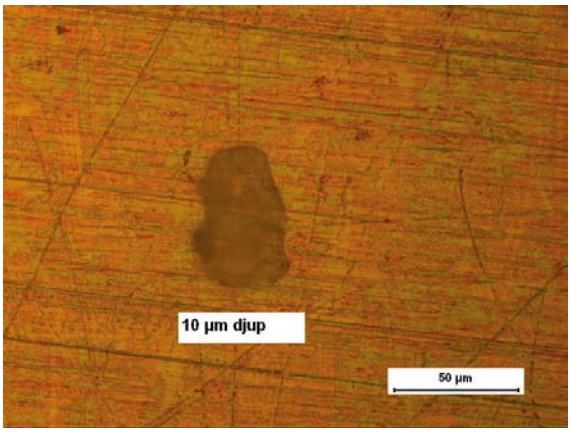
10 µm djup
50 µm

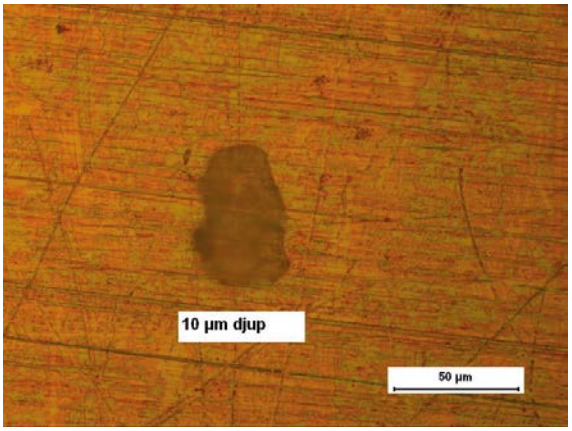
10 µm djup
50 µm

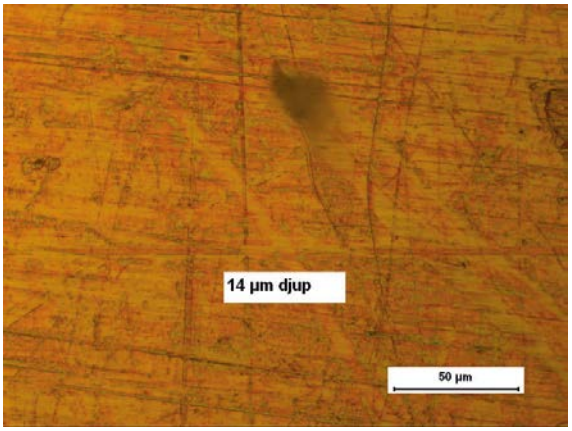
14 µm djup
50 µm

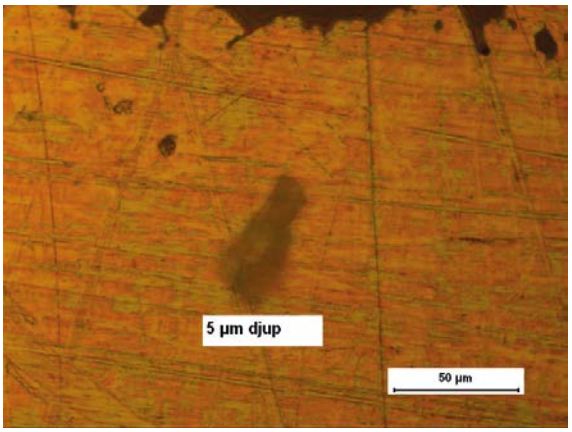
5 µm djup
50 µm

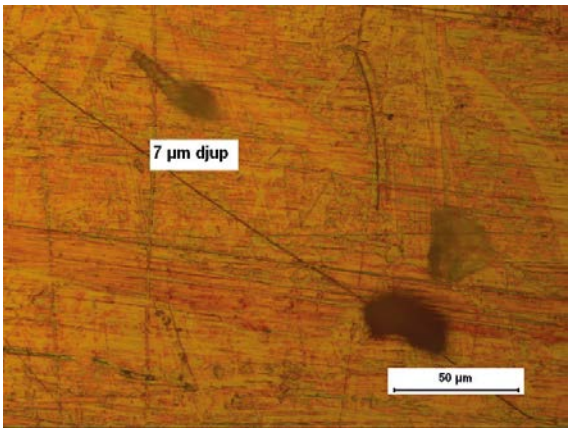
7 µm djup
50 µm

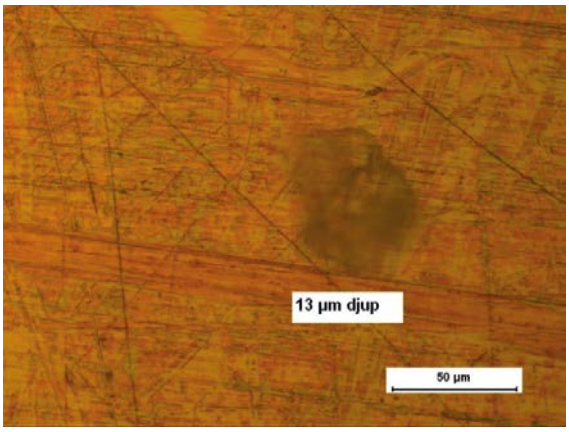
13 µm djup
50 µm

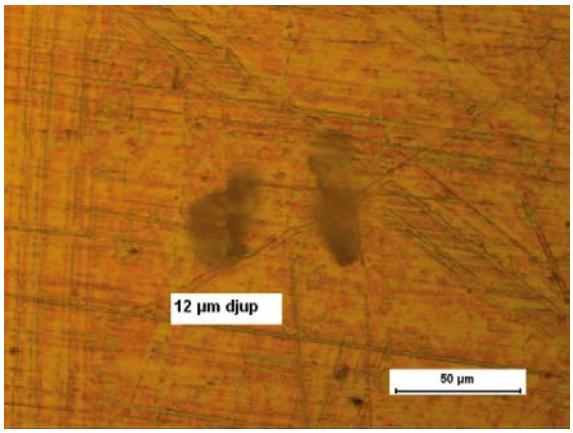
12 µm djup
50 µm

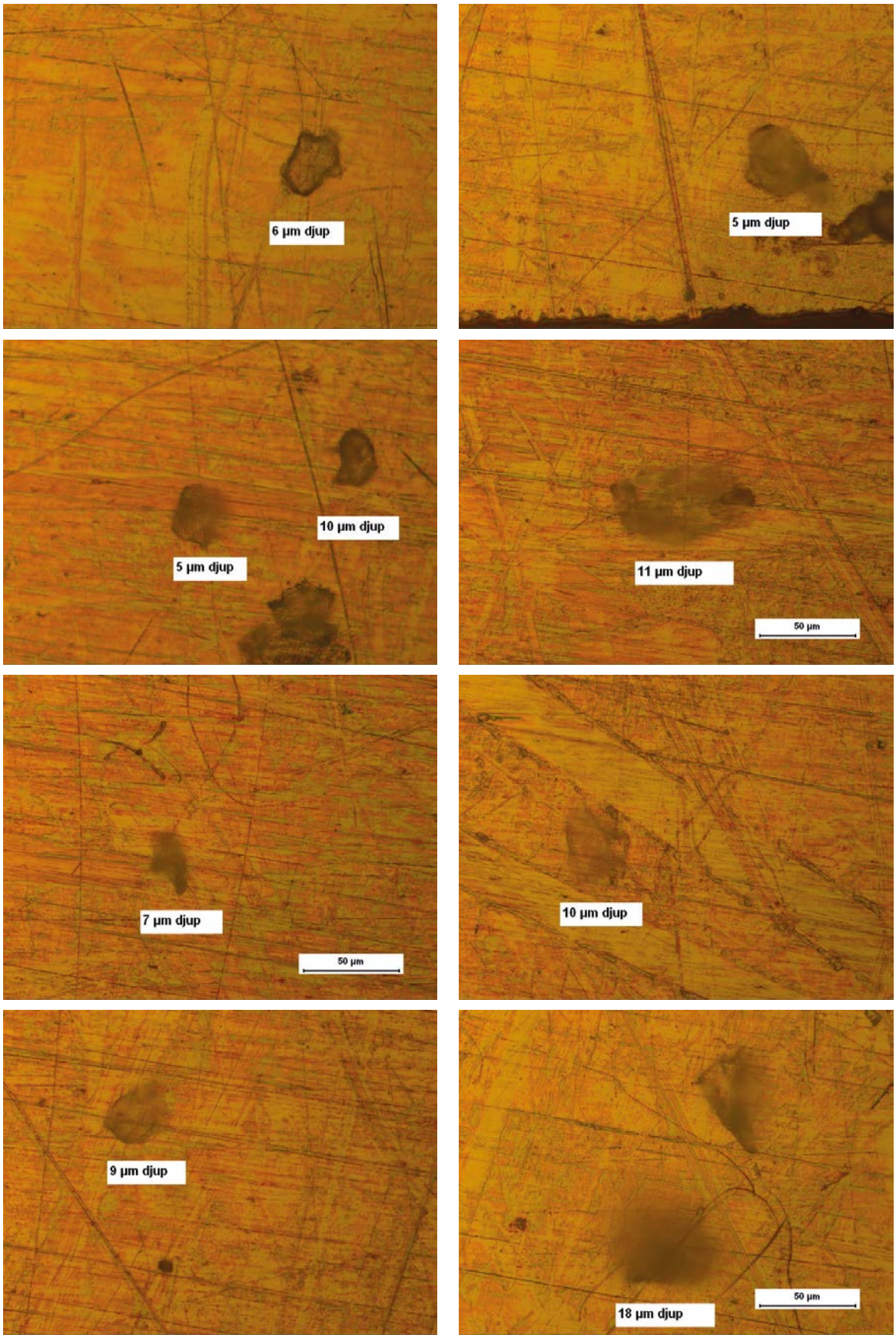
6 µm djup
5 µm djup
10 µm djup
5 µm djup
11 µm djup
50 µm
7 µm djup
50 µm
10 µm djup
9 µm djup
50 µm
18 µm djup

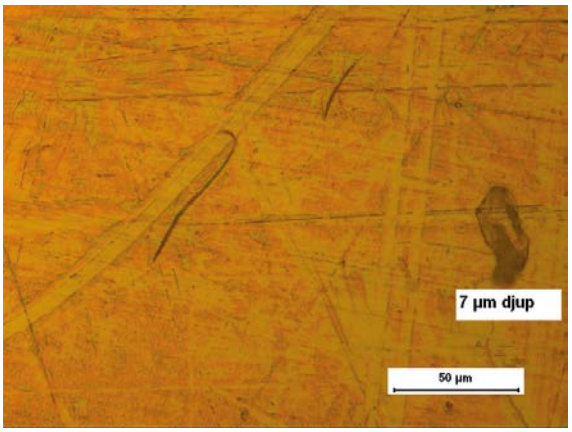
7 µm djup
50 µm

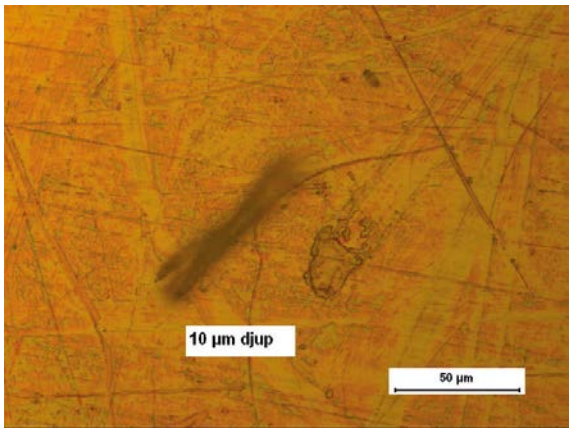
10 µm djup
50 µm

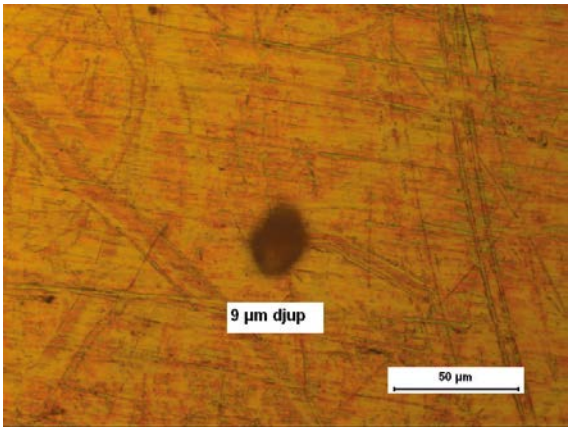
9 µm djup
50 µm

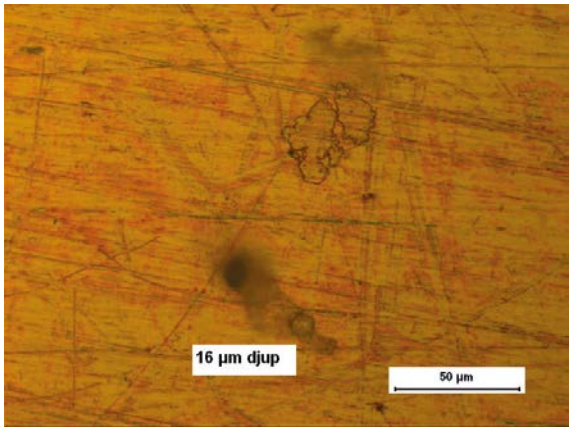
16 µm djup
50 µm

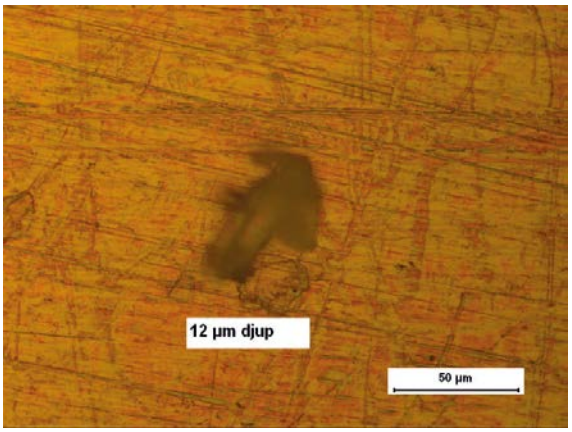
12 µm djup
50 µm

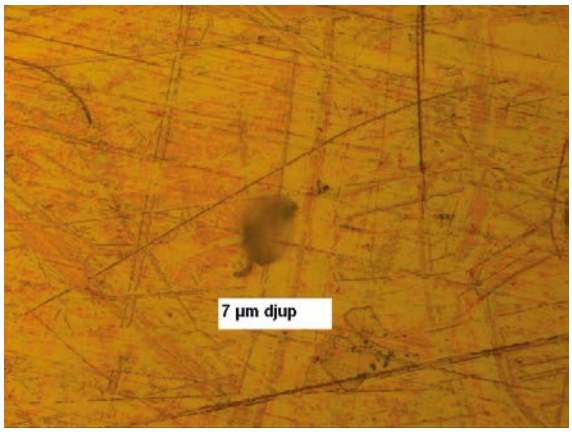
7 µm djup

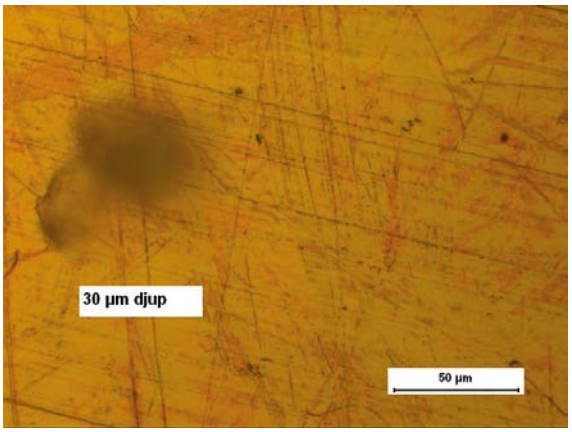
30 µm djup
50 µm

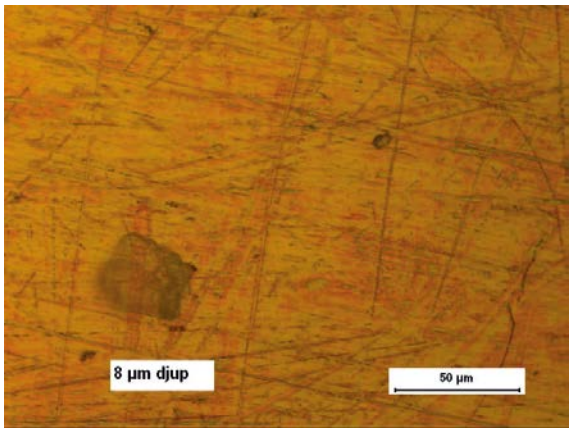
8 µm djup
50 µm

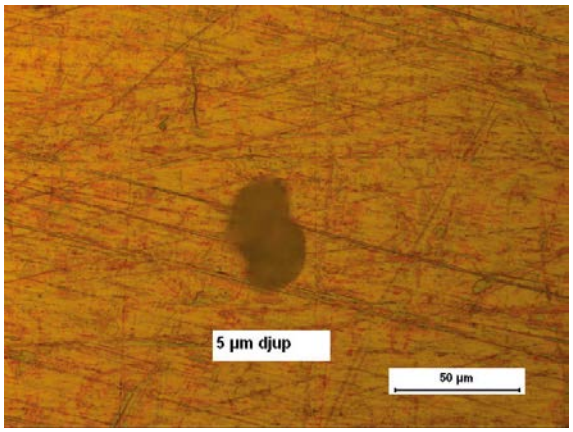
5 µm djup
50 µm

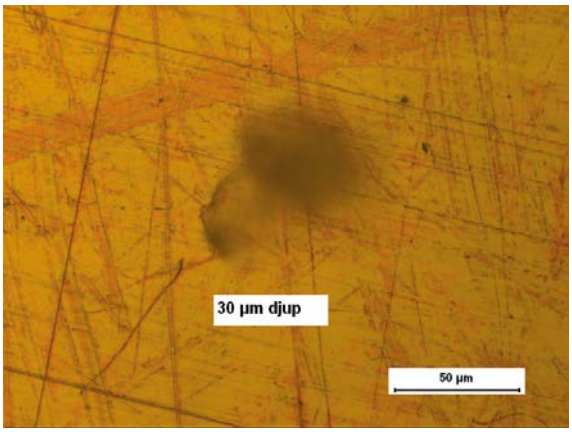
30 µm djup
50 µm

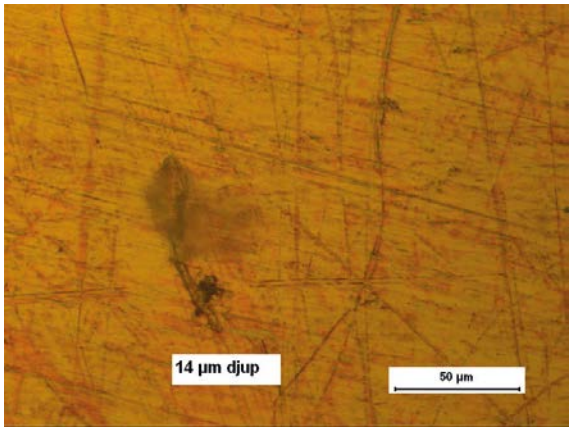
14 µm djup
50 µm

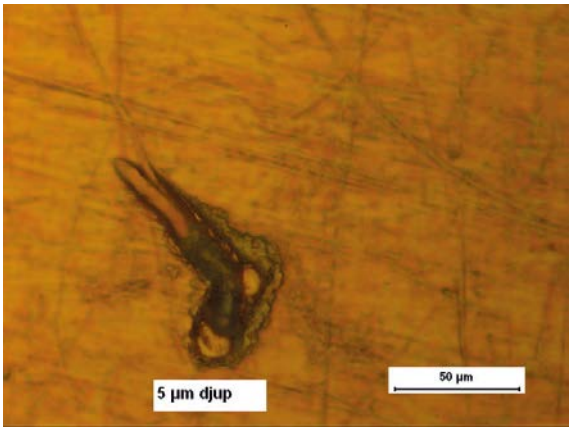
5 µm djup
50 µm

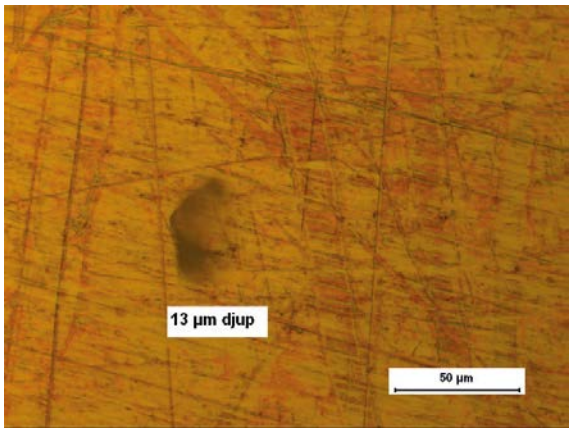
13 µm djup
50 µm

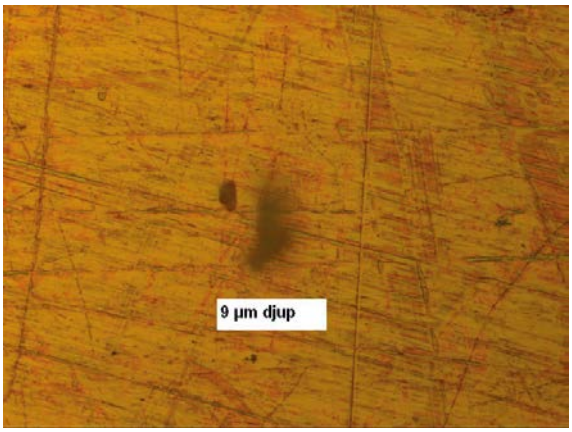
9 µm djup

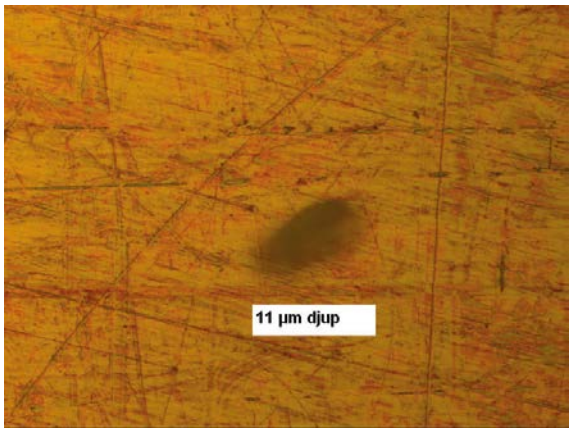
11 µm djup

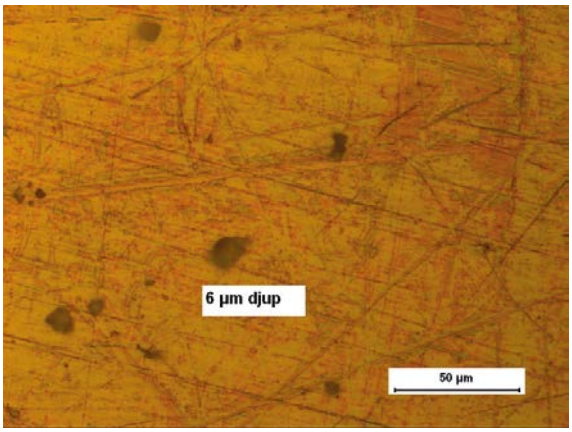
6 µm djup
50 µm

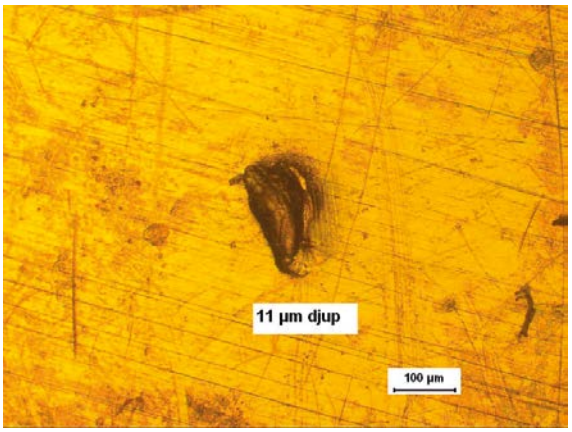
11 µm djup
100 µm

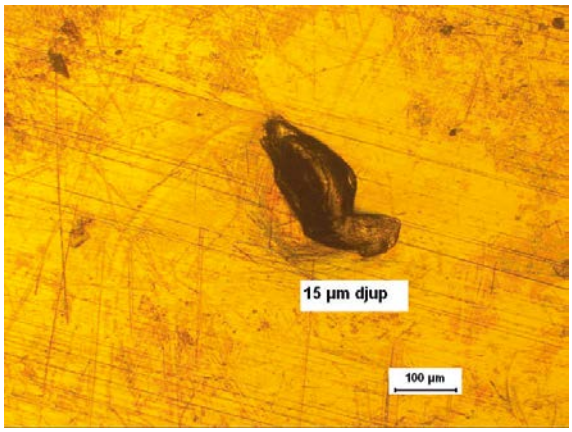
15 µm djup
100 µm

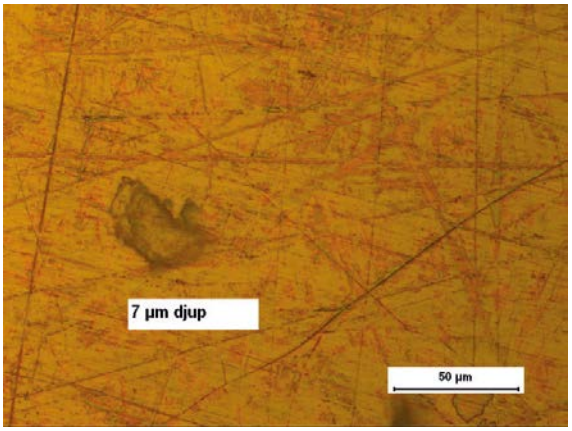
7 µm djup
50 µm

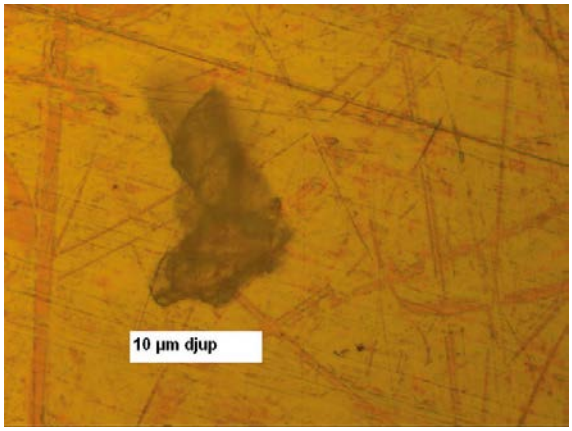
10 µm djup

SRB exposures – Reference coupon 1 side 1 after pickling

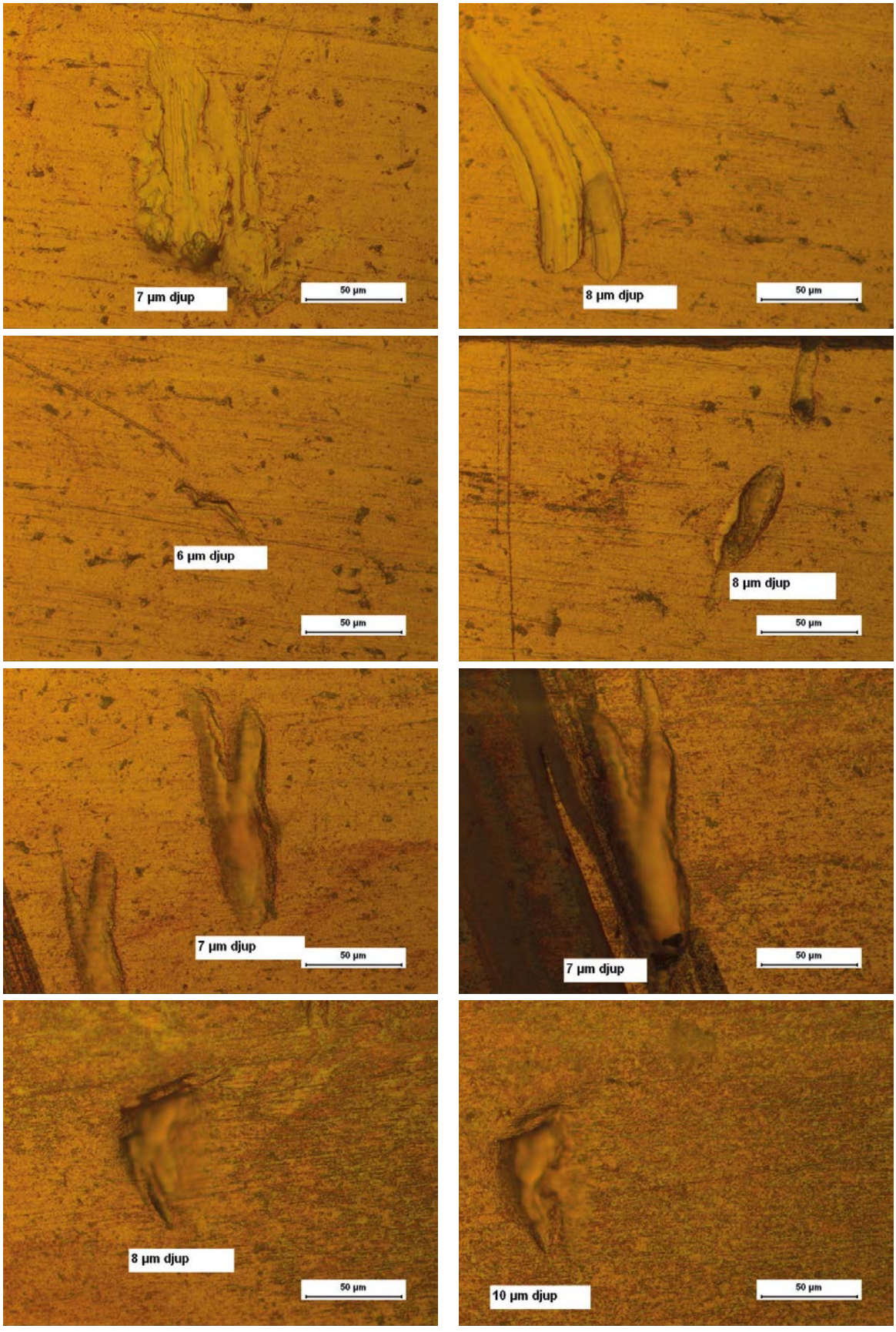

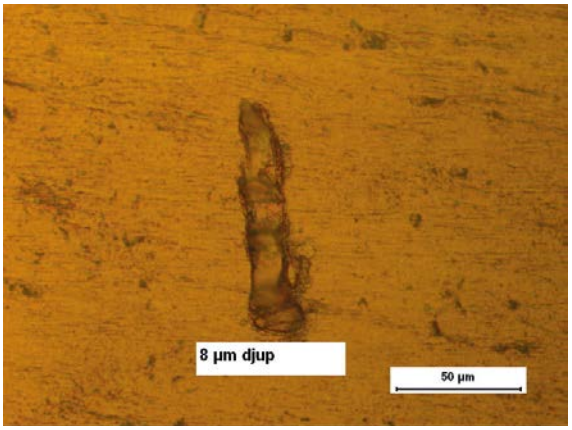
8 µm djup
50 µm

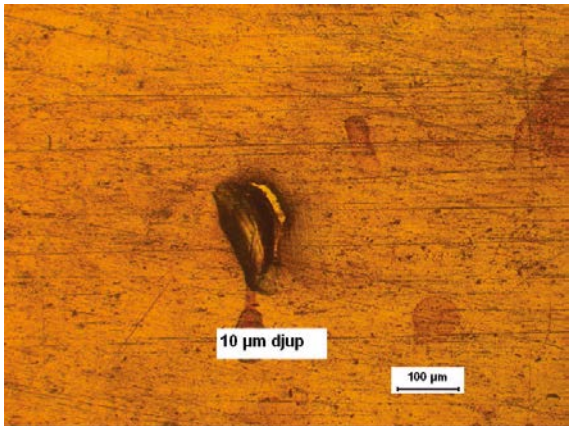
10 µm djup
100 µm

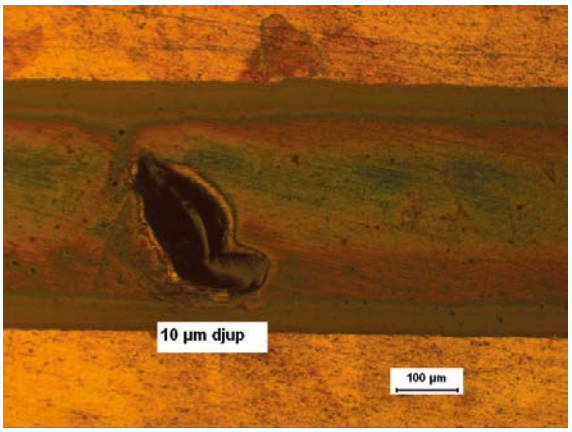
10 µm djup
100 µm

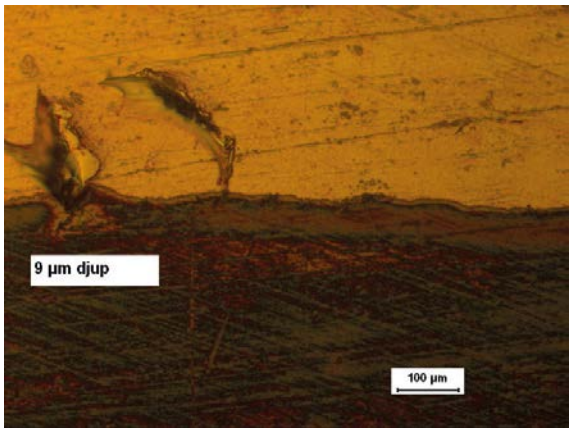
9 µm djup
100 µm

SRB exposures – Reference coupon 1 side 2 before pickling

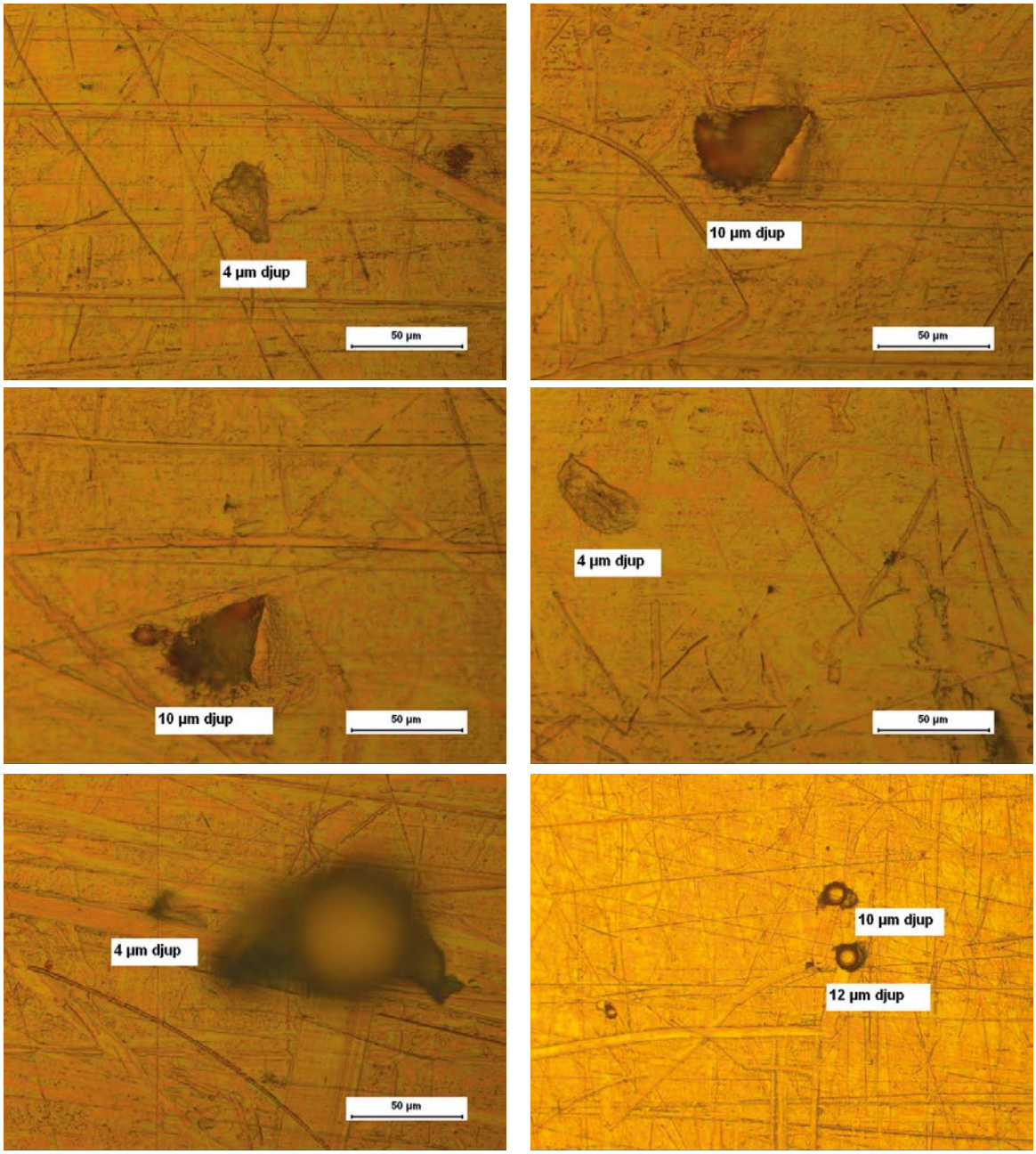

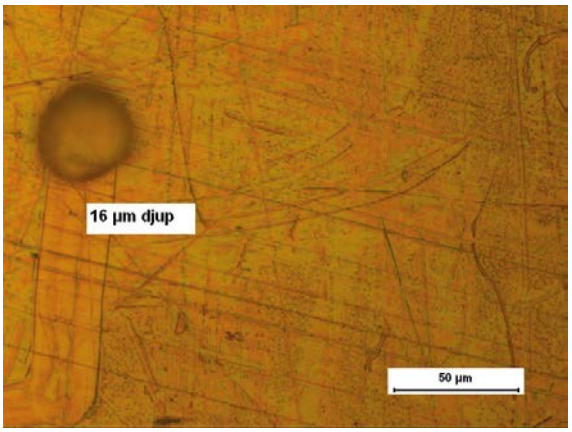
16 µm djup
50 µm

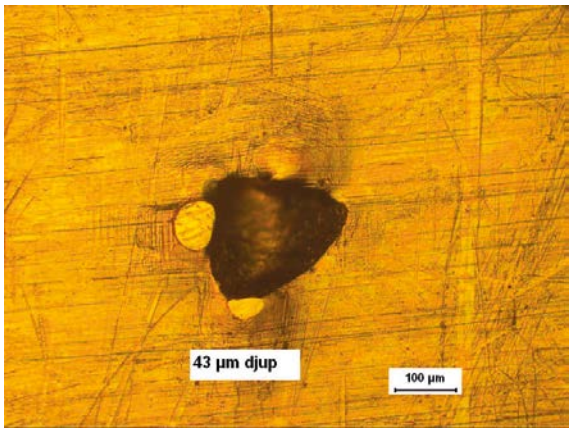
43 µm djup
100 µm

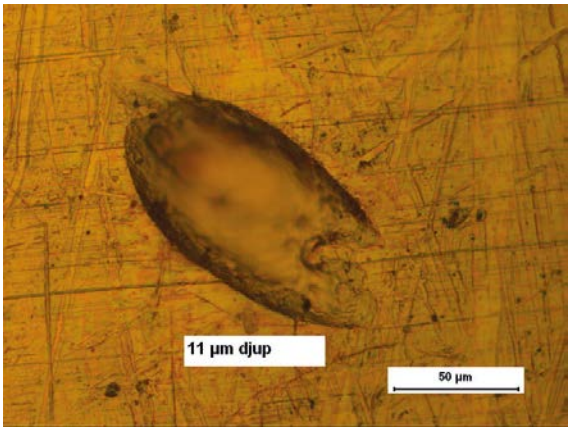
11 µm djup
50 µm

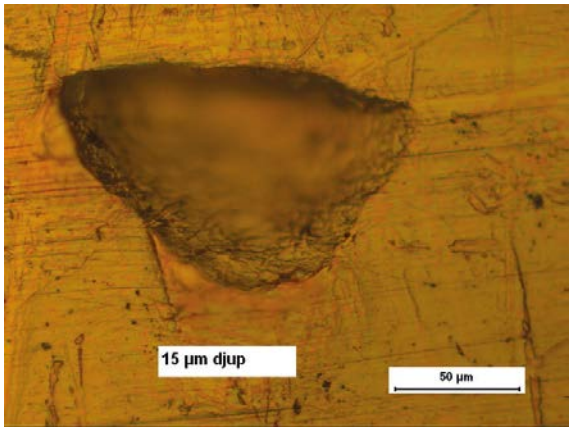
15 µm djup
50 µm

SRB exposures – Reference coupon 1 side 2 after pickling

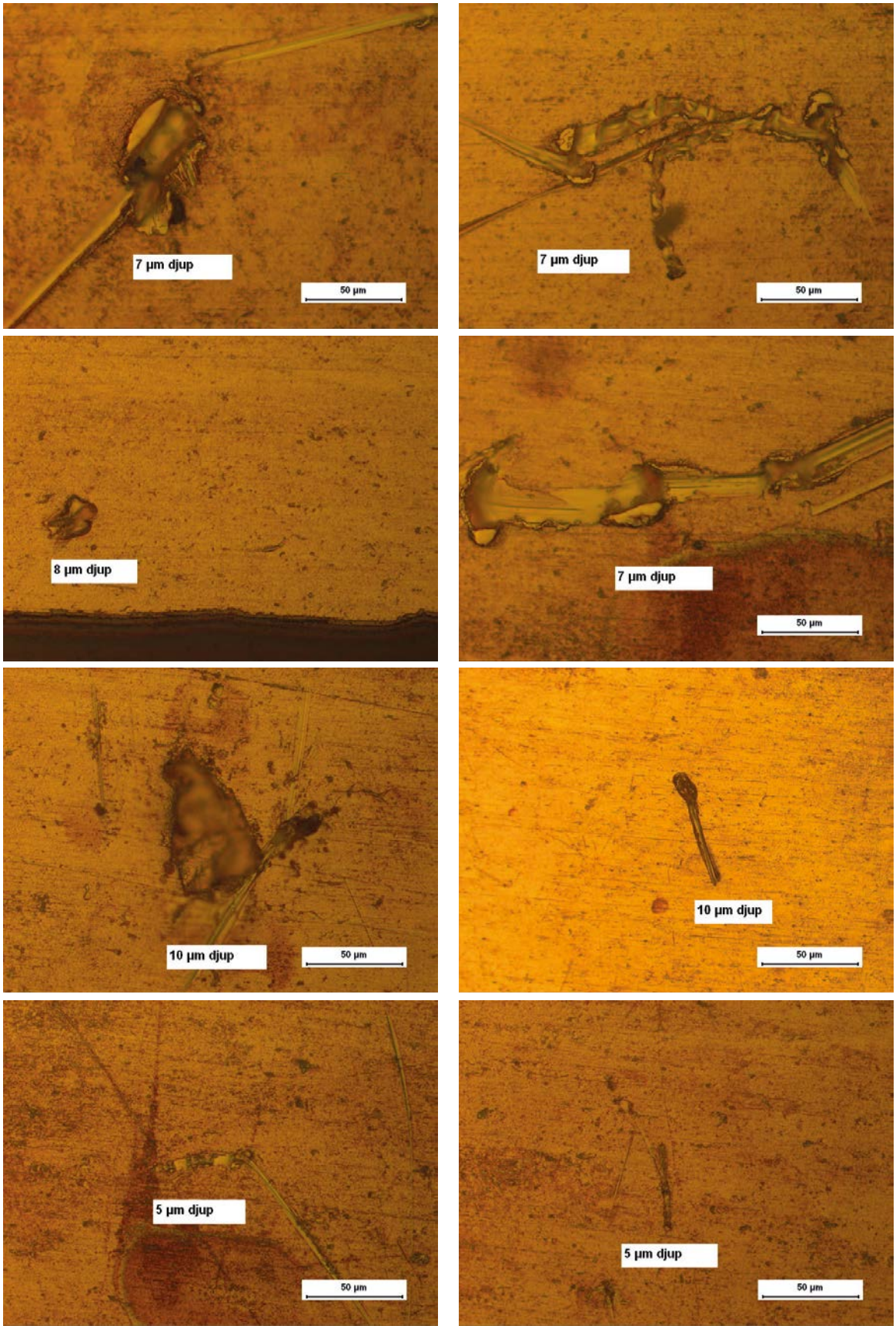

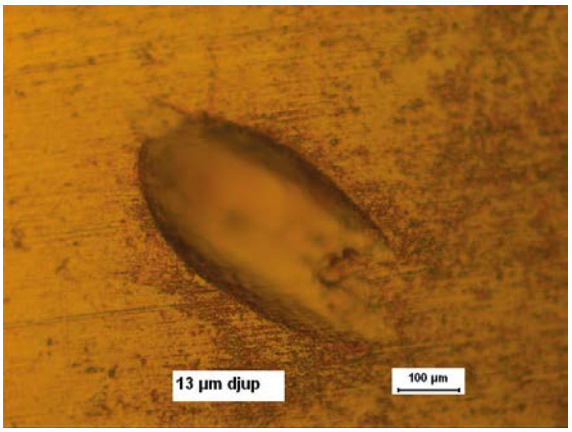
13 µm djup
100 µm

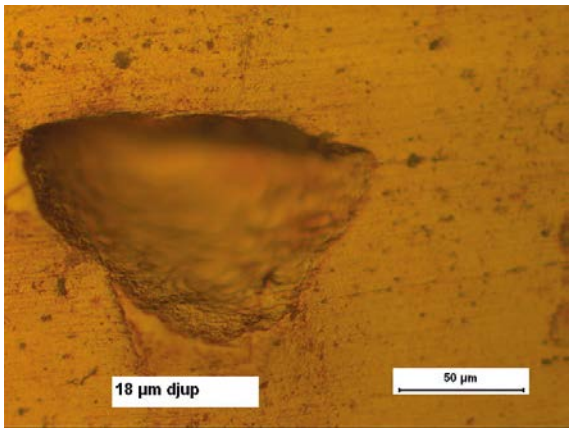
18 µm djup
50 µm

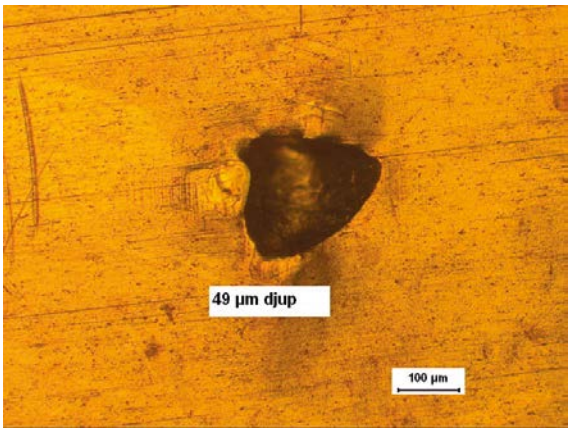
49 µm djup
100 µm

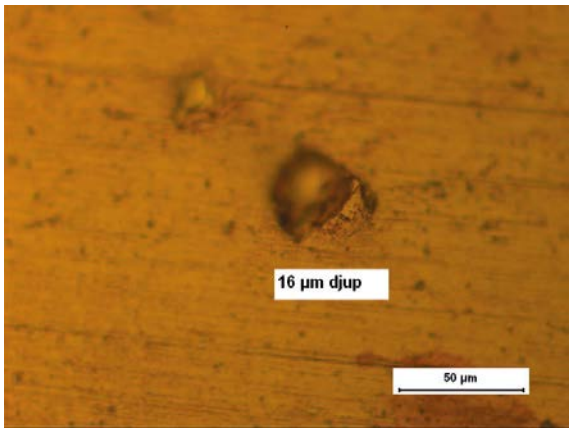
16 µm djup
50 µm

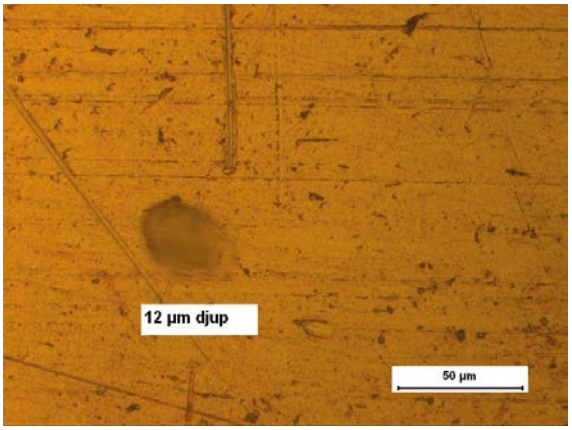
12 µm djup
50 µm

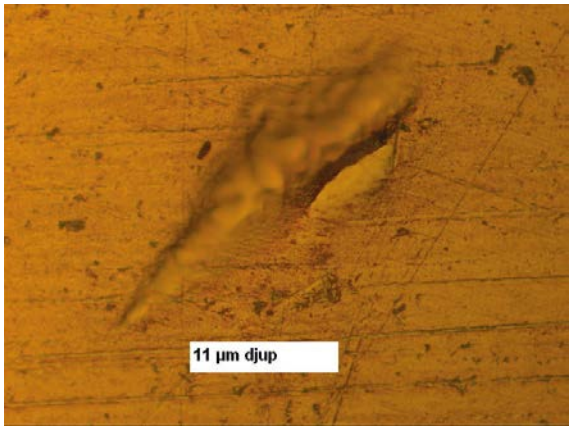
11 µm djup

SRB exposures – Reference coupon 2 side 1 before pickling

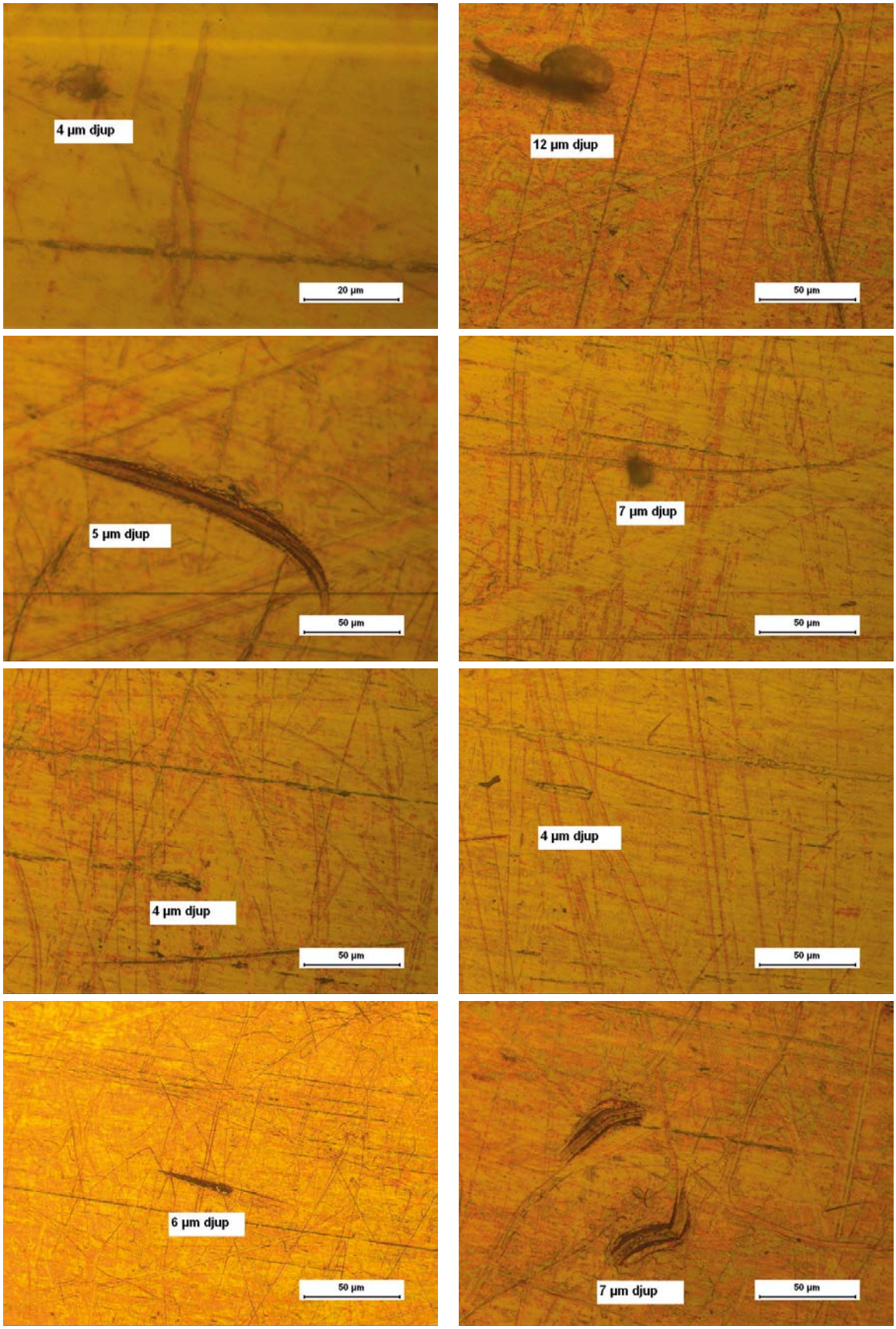

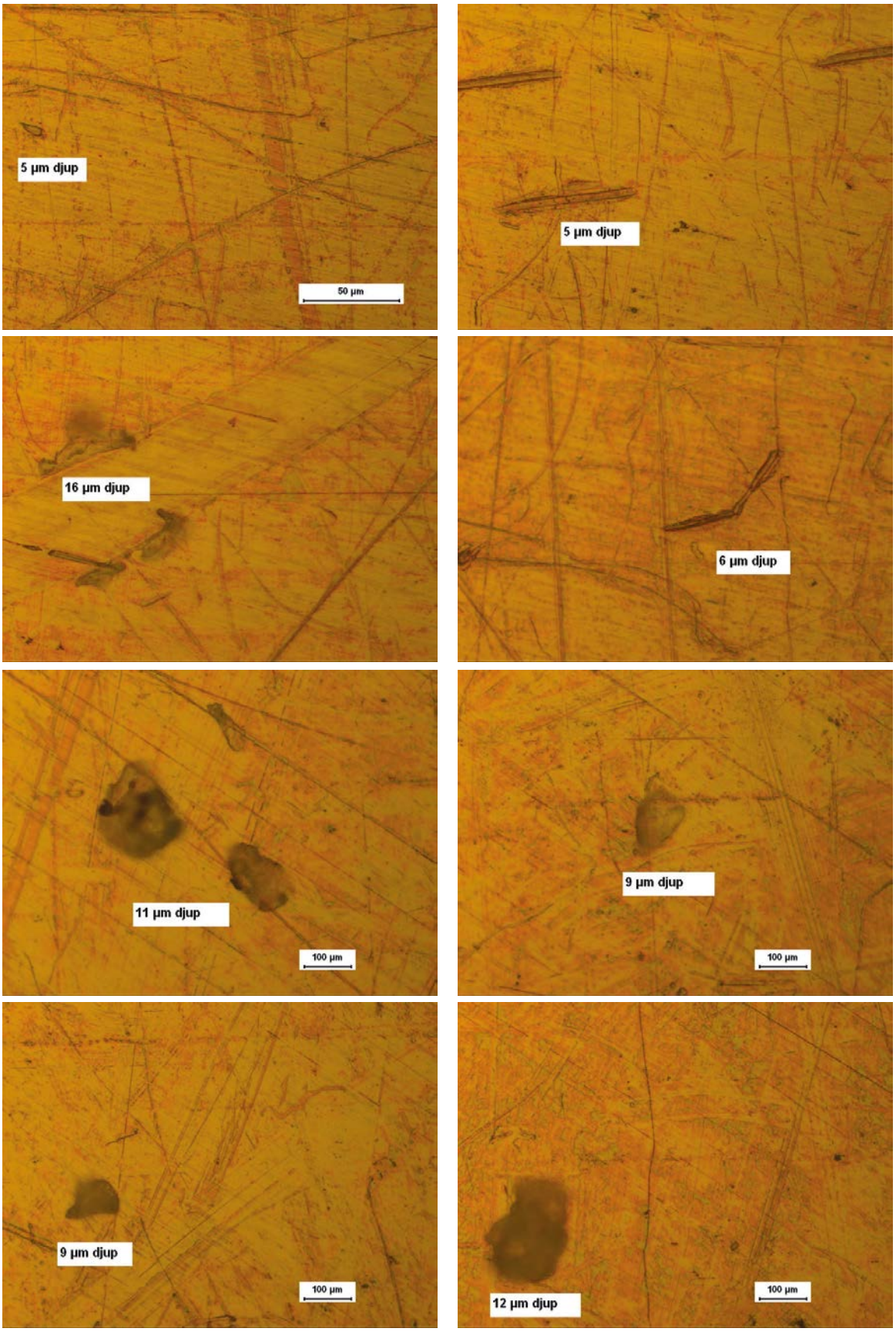
5 µm djup
50 µm
5 µm djup
16 µm djup
6 µm djup
11 µm djup
100 µm
9 µm djup
100 µm
9 µm djup
100 µm
12 µm djup
100 µm

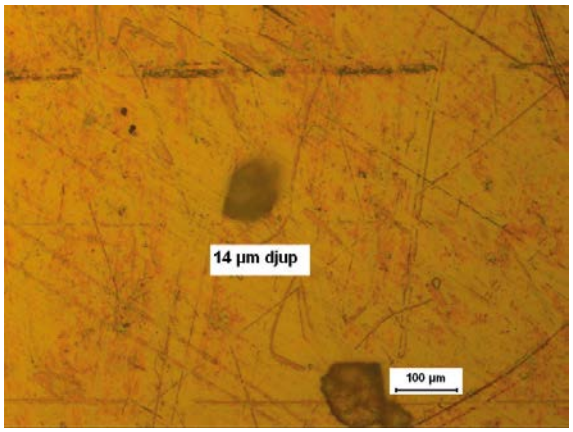
14 µm djup
100 µm

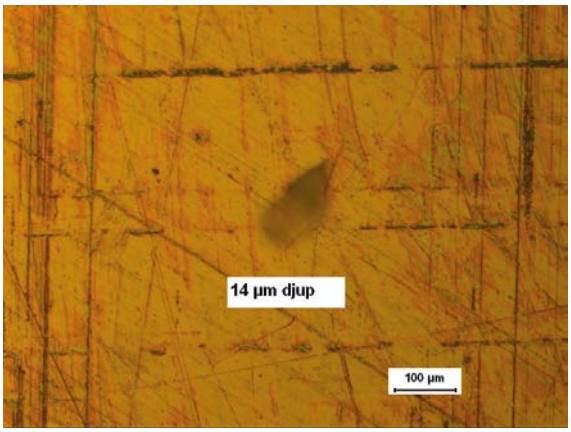
14 µm djup
100 µm

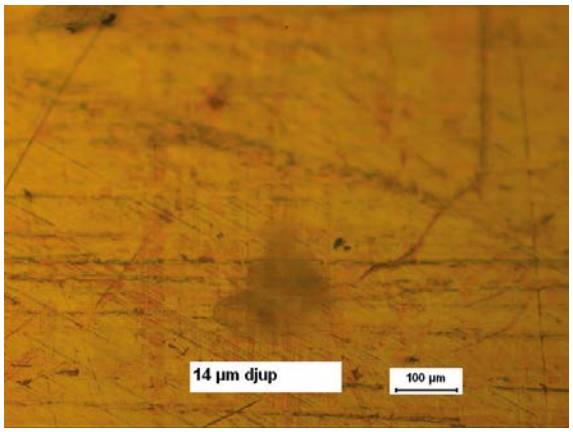
14 µm djup
100 µm

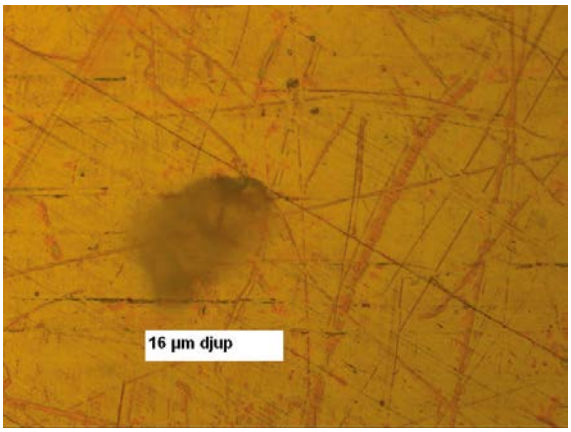
16 µm djup

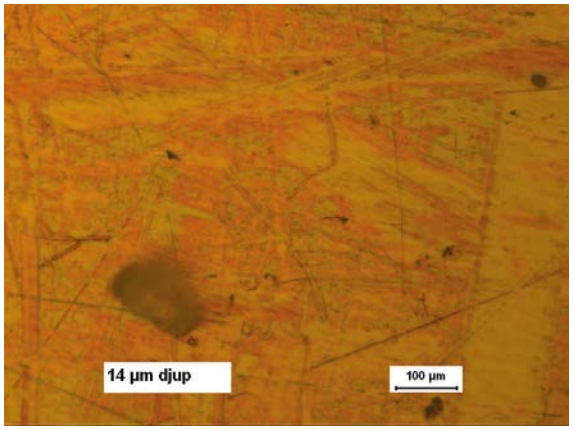
14 µm djup
100 µm

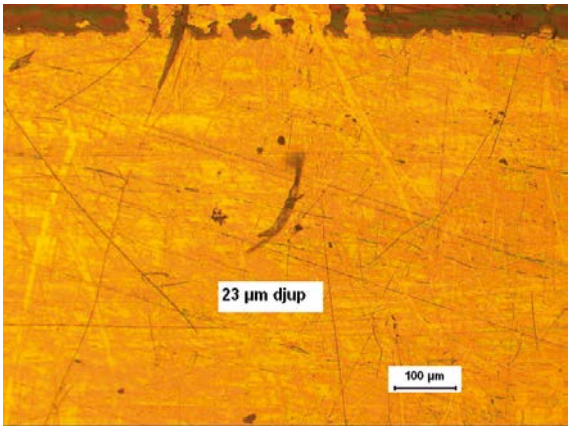
23 µm djup
100 µm

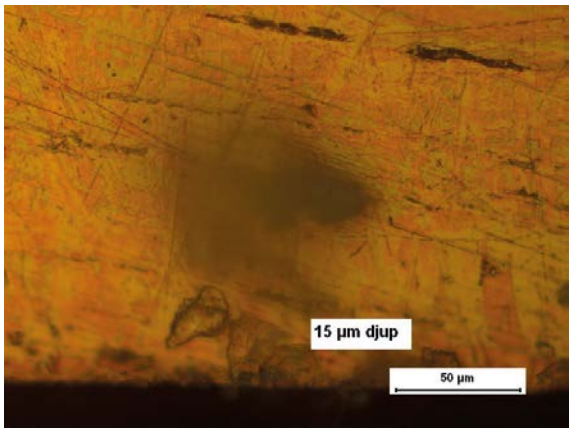
15 µm djup
50 µm

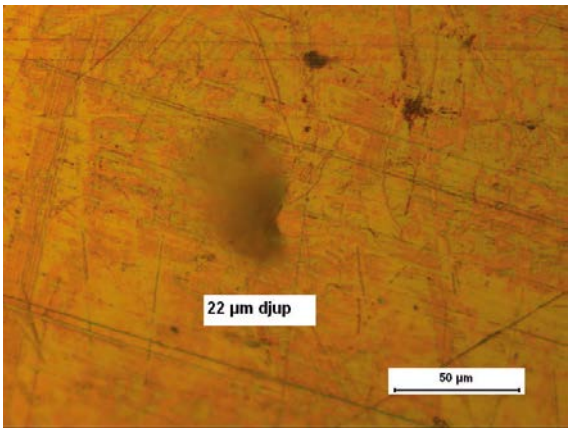
22 µm djup
50 µm

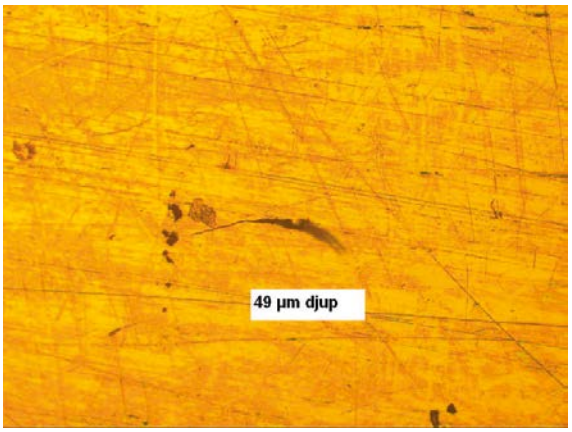
49 µm djup

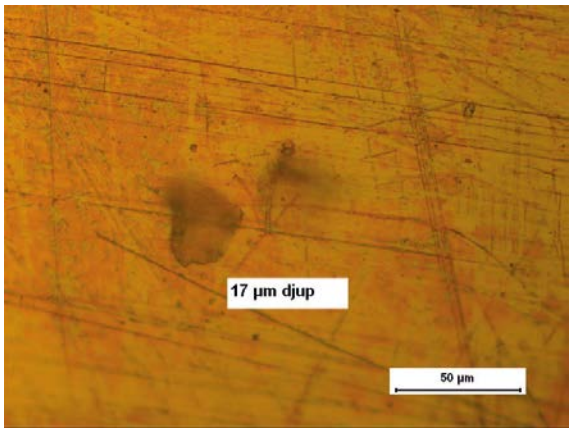
17 µm djup
50 µm

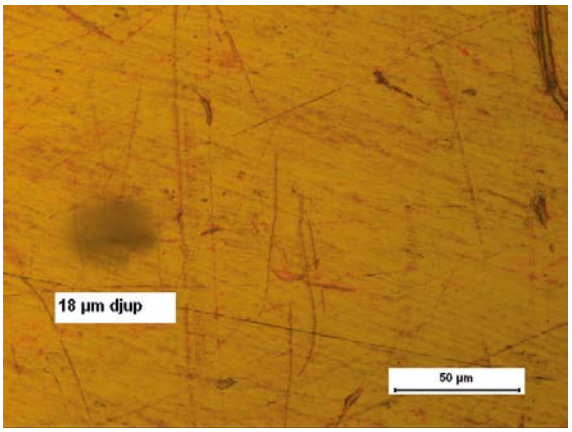
18 µm djup
50 µm

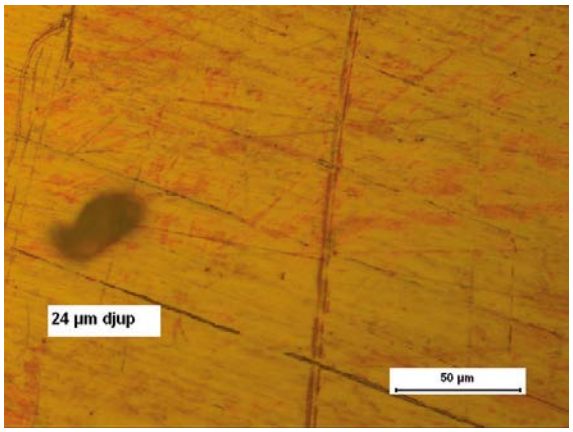
24 µm djup
50 µm

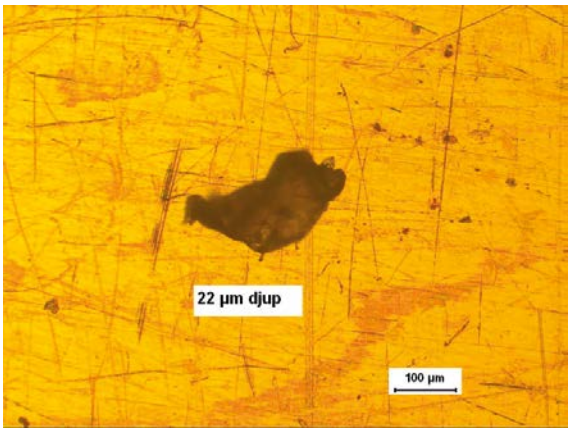
22 µm djup
100 µm

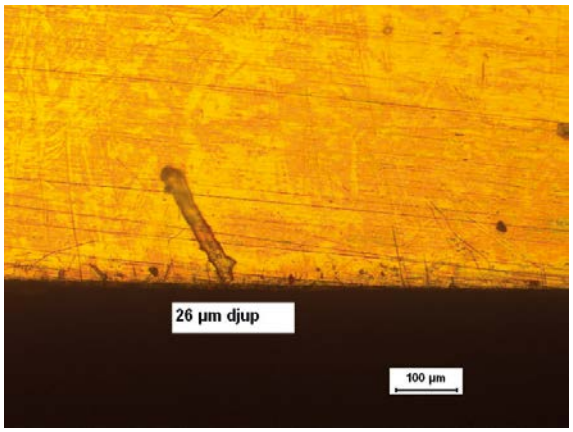
26 µm djup
100 µm

SRB exposures – Reference coupon 2 side 1 after pickling

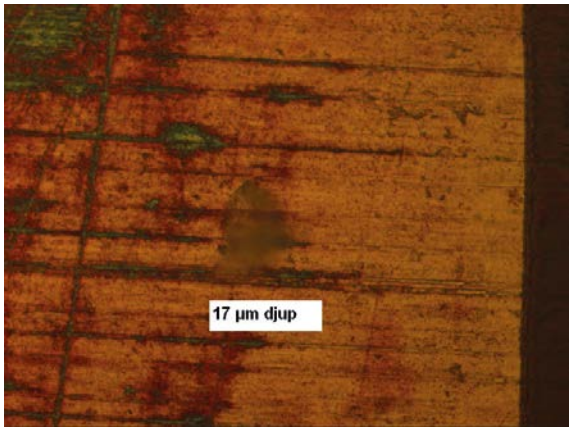

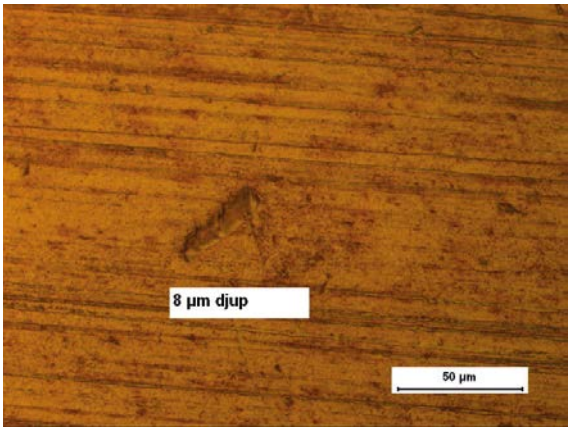

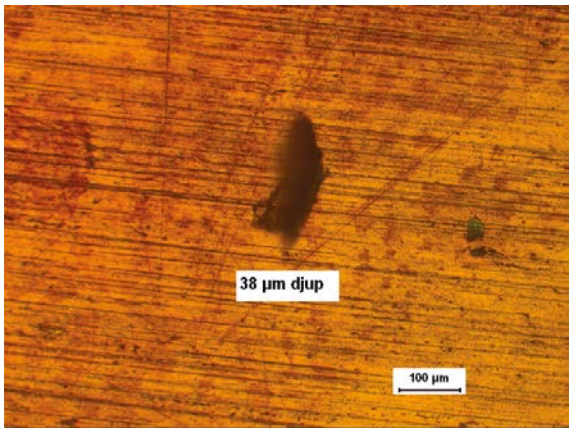

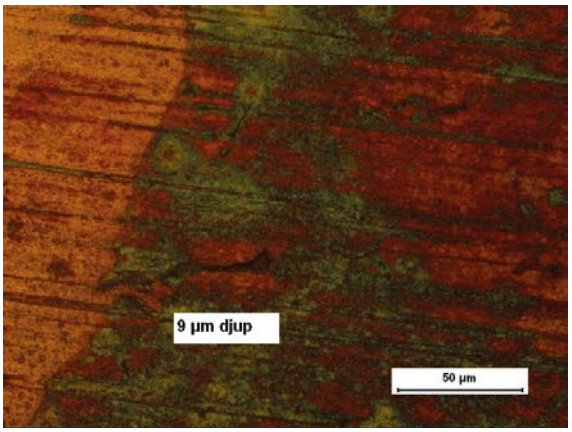

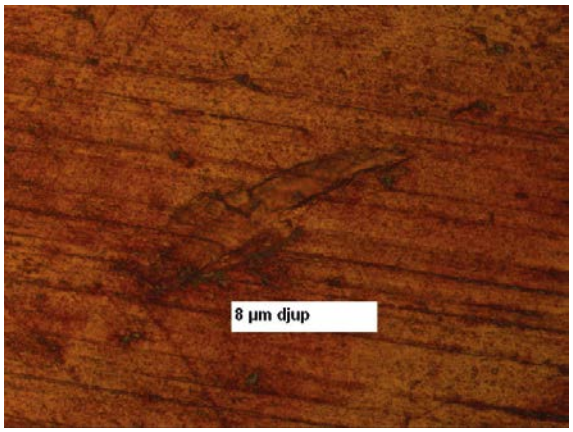

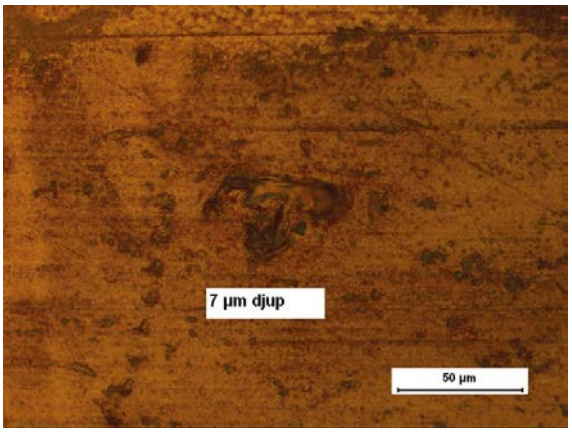

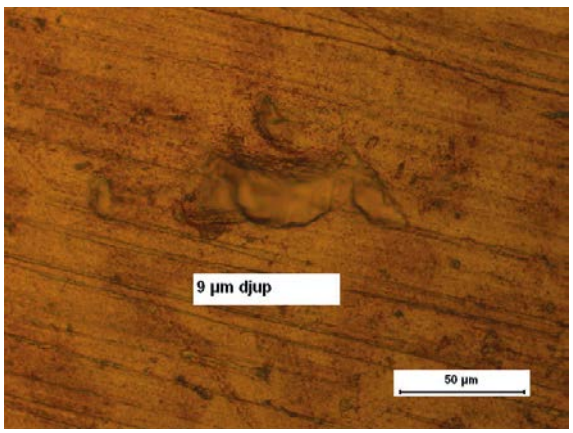

SRB exposures – Reference coupon 2 side 2 before pickling

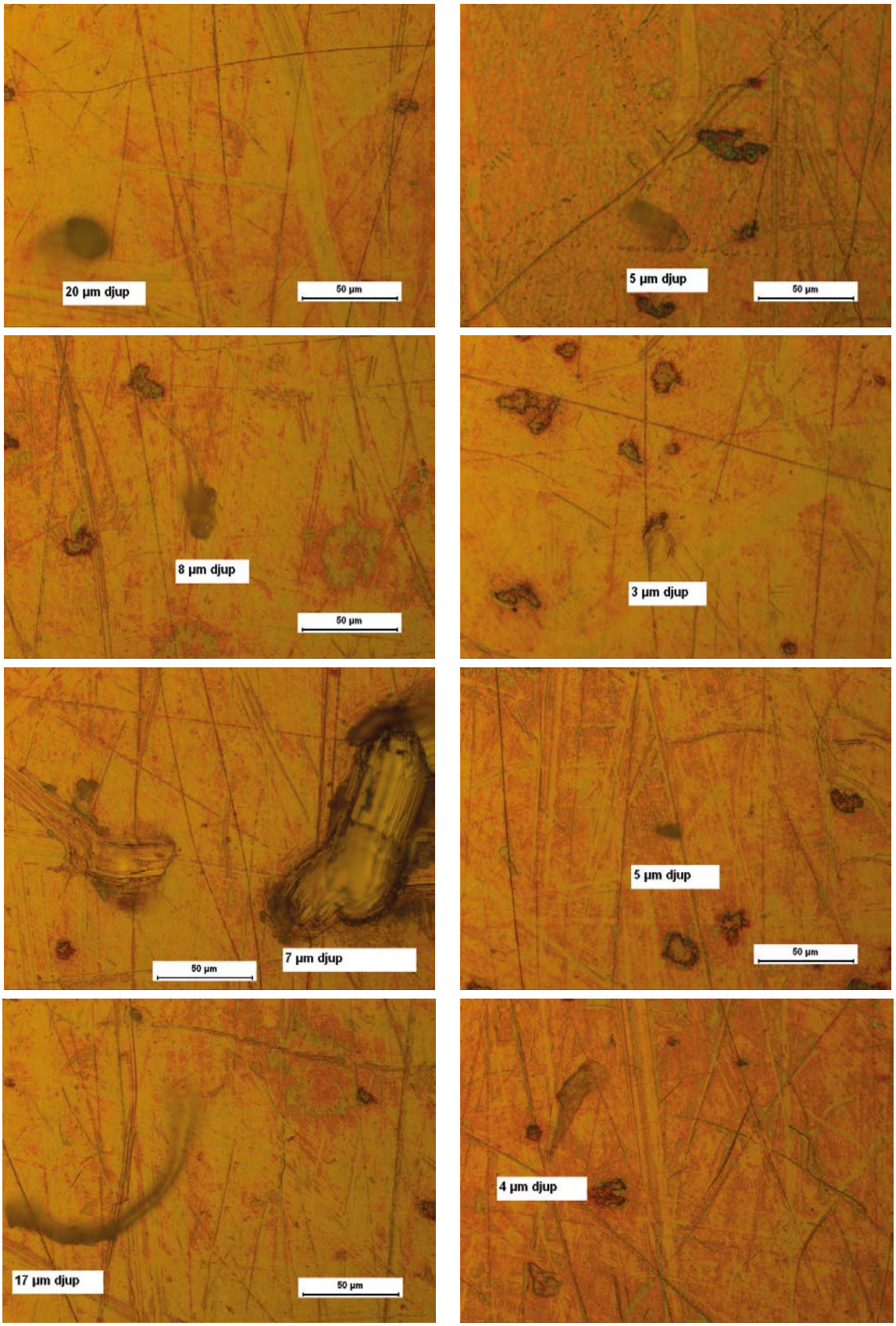

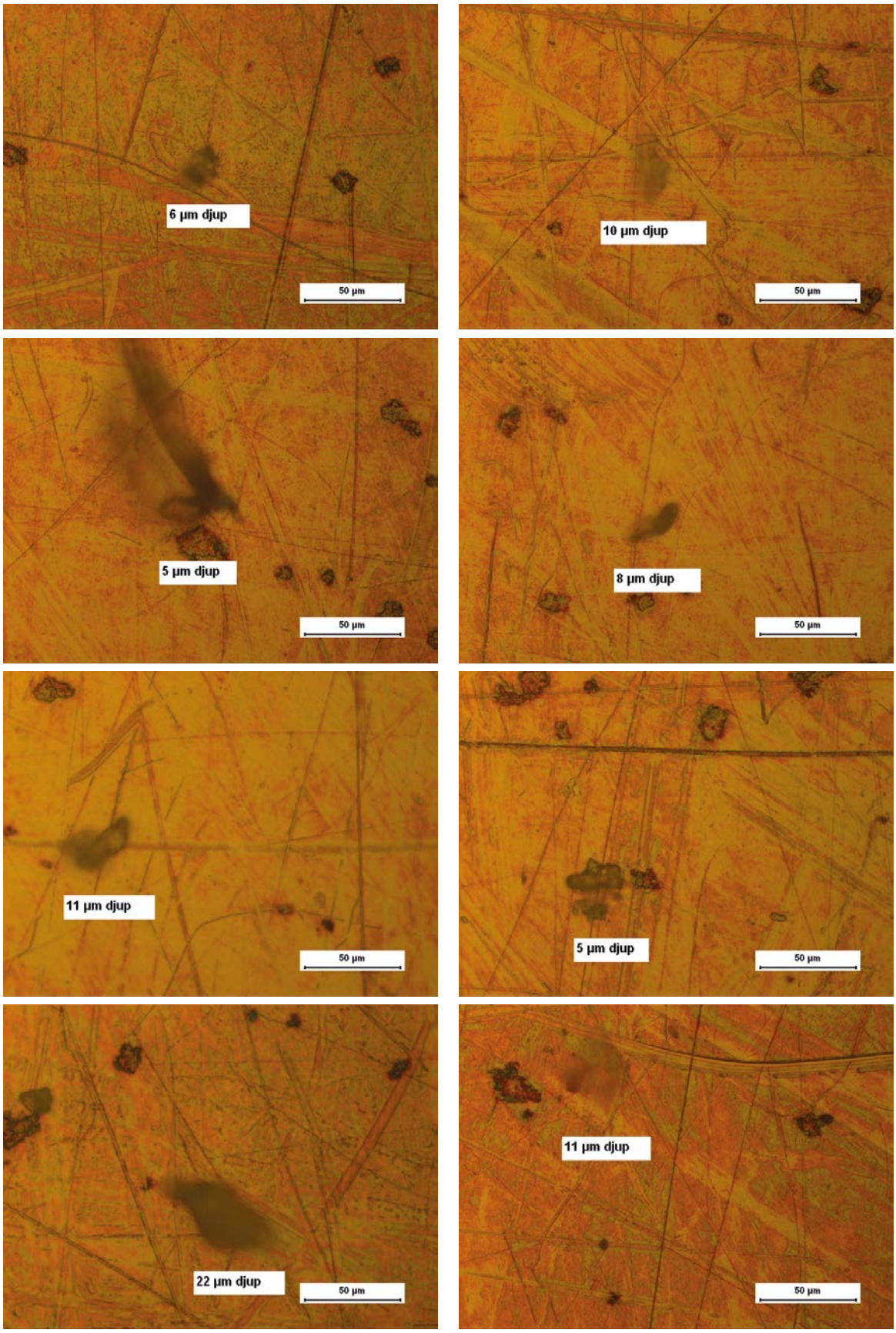
6 µm djup
50 µm
10 µm djup
50 µm
5 µm djup
50 µm
8 µm djup
50 µm
11 µm djup
50 µm
5 µm djup
50 µm
22 µm djup
50 µm
11 µm djup
50 µm

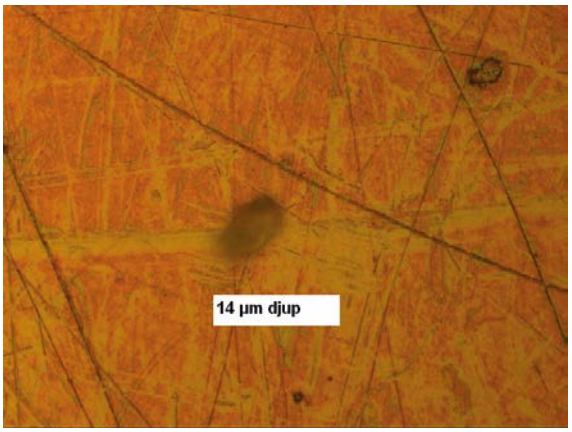
14 µm djup

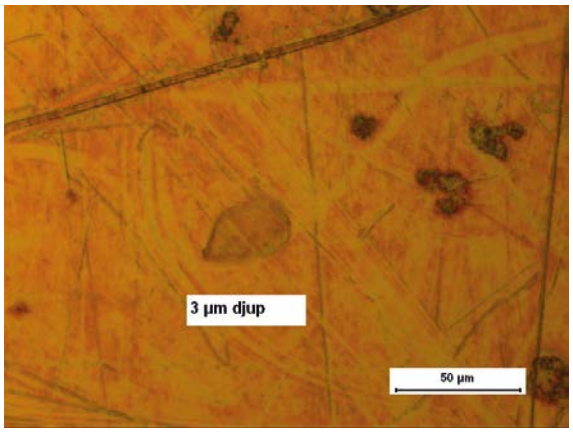
3 µm djup
50 µm

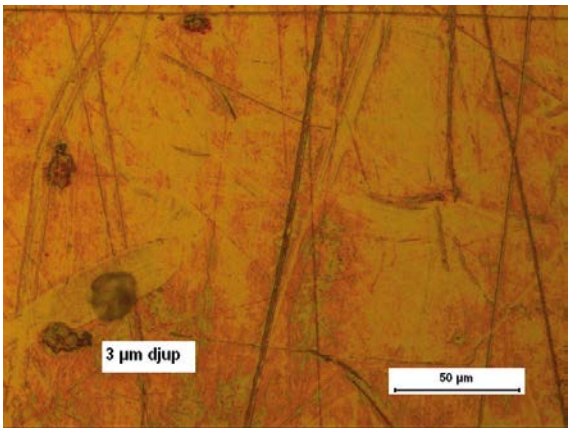
3 µm djup
50 µm

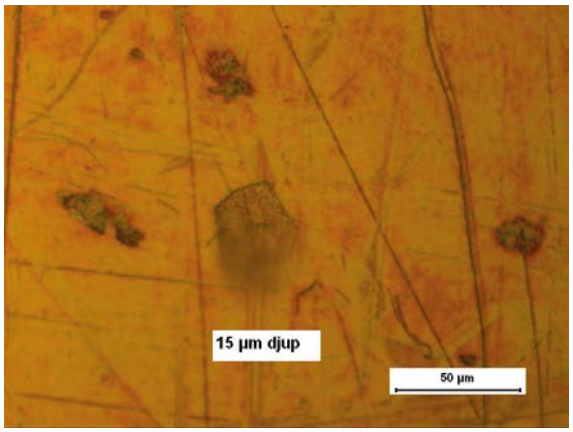
15 µm djup
50 µm

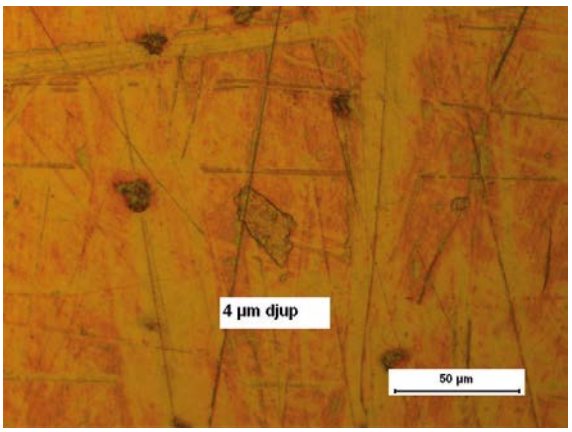
4 µm djup
50 µm

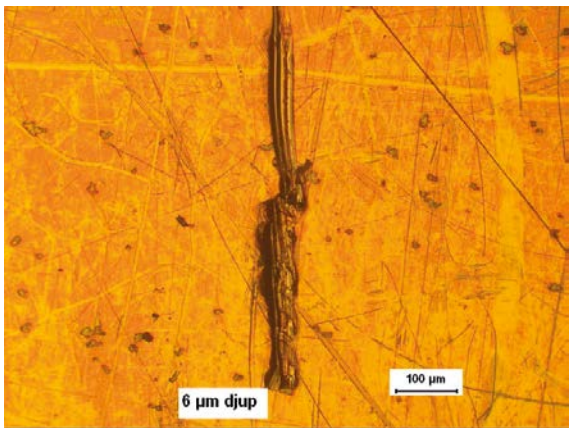
6 µm djup
100 µm

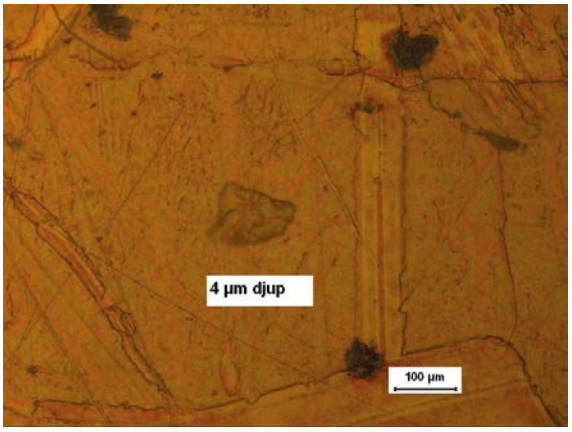
4 µm djup
100 µm

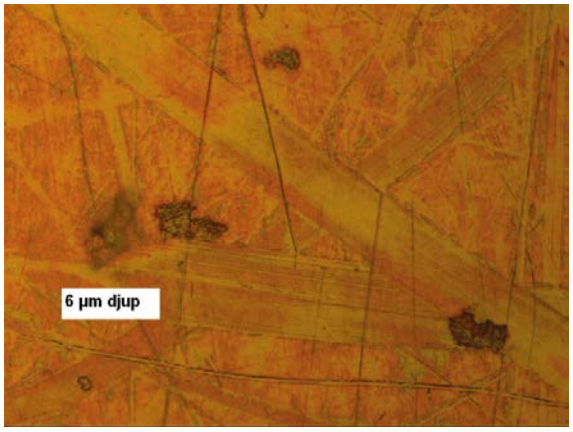
6 µm djup

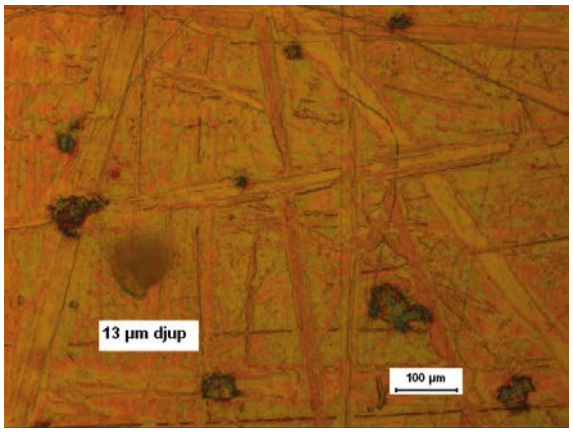
13 µm djup
100 µm

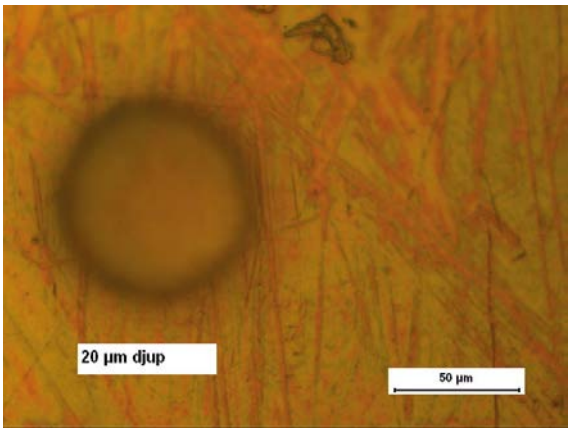
20 µm djup
50 µm

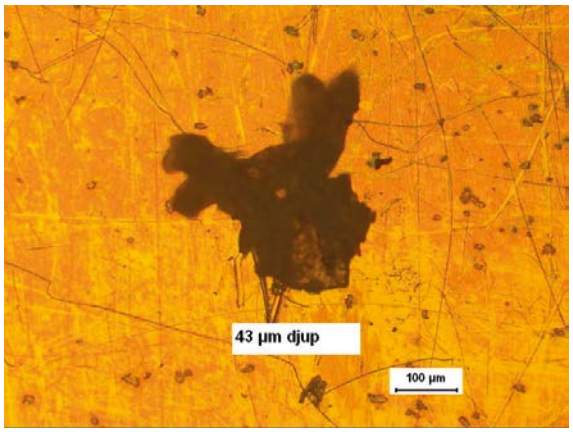
43 µm djup
100 µm

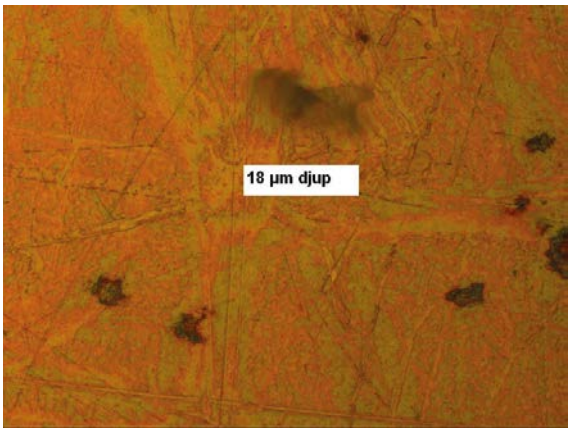
18 µm djup

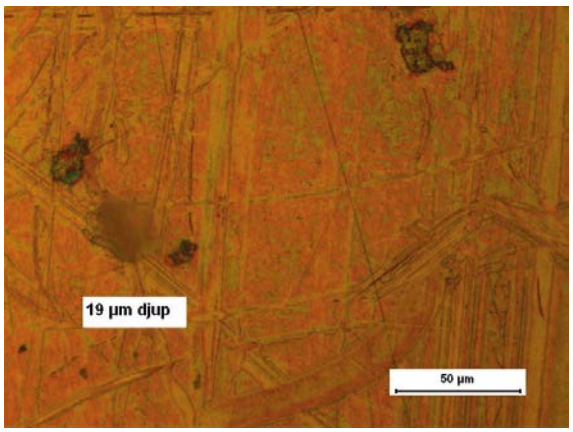
19 µm djup
50 µm

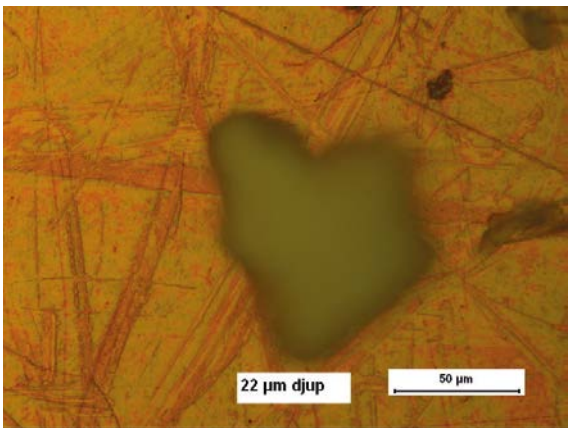
22 µm djup
50 µm

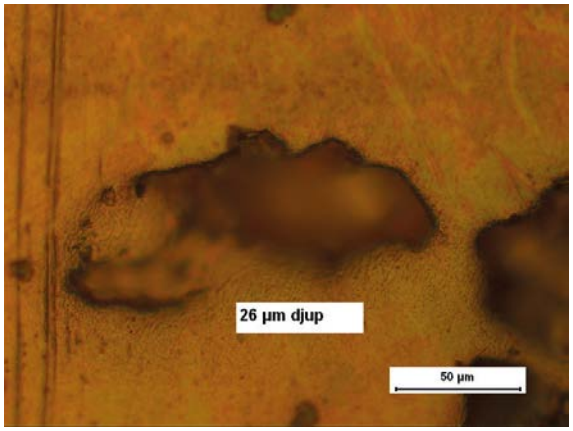
26 µm djup
50 µm

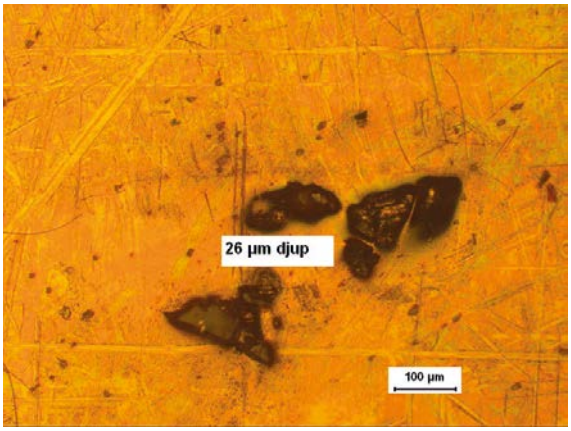
26 µm djup
100 µm

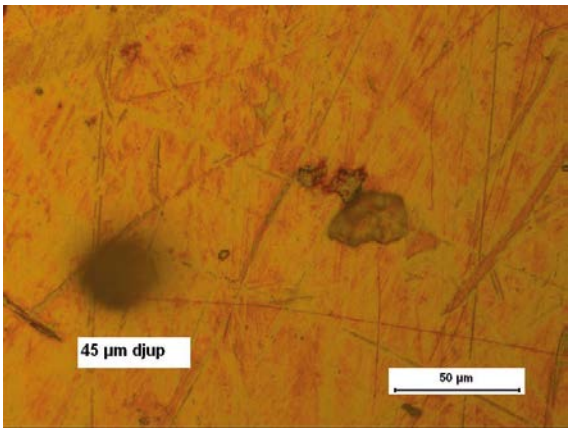
45 µm djup
50 µm

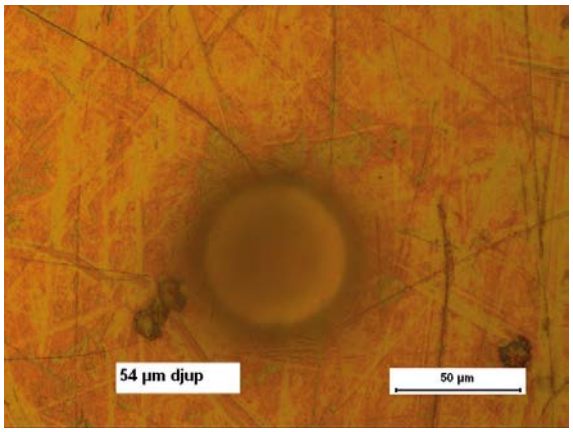
54 µm djup
50 µm

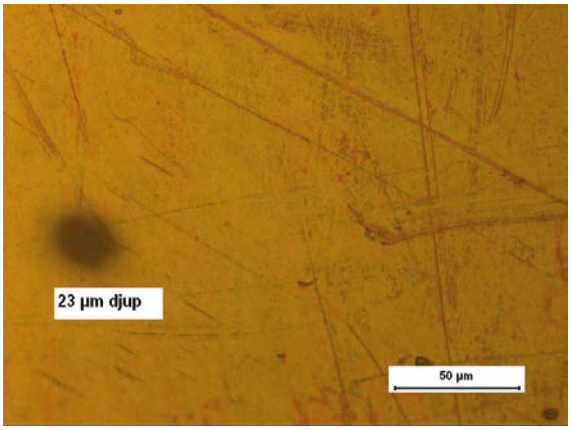
23 µm djup
50 µm

SRB exposures – Reference coupon 2 side 2 after pickling

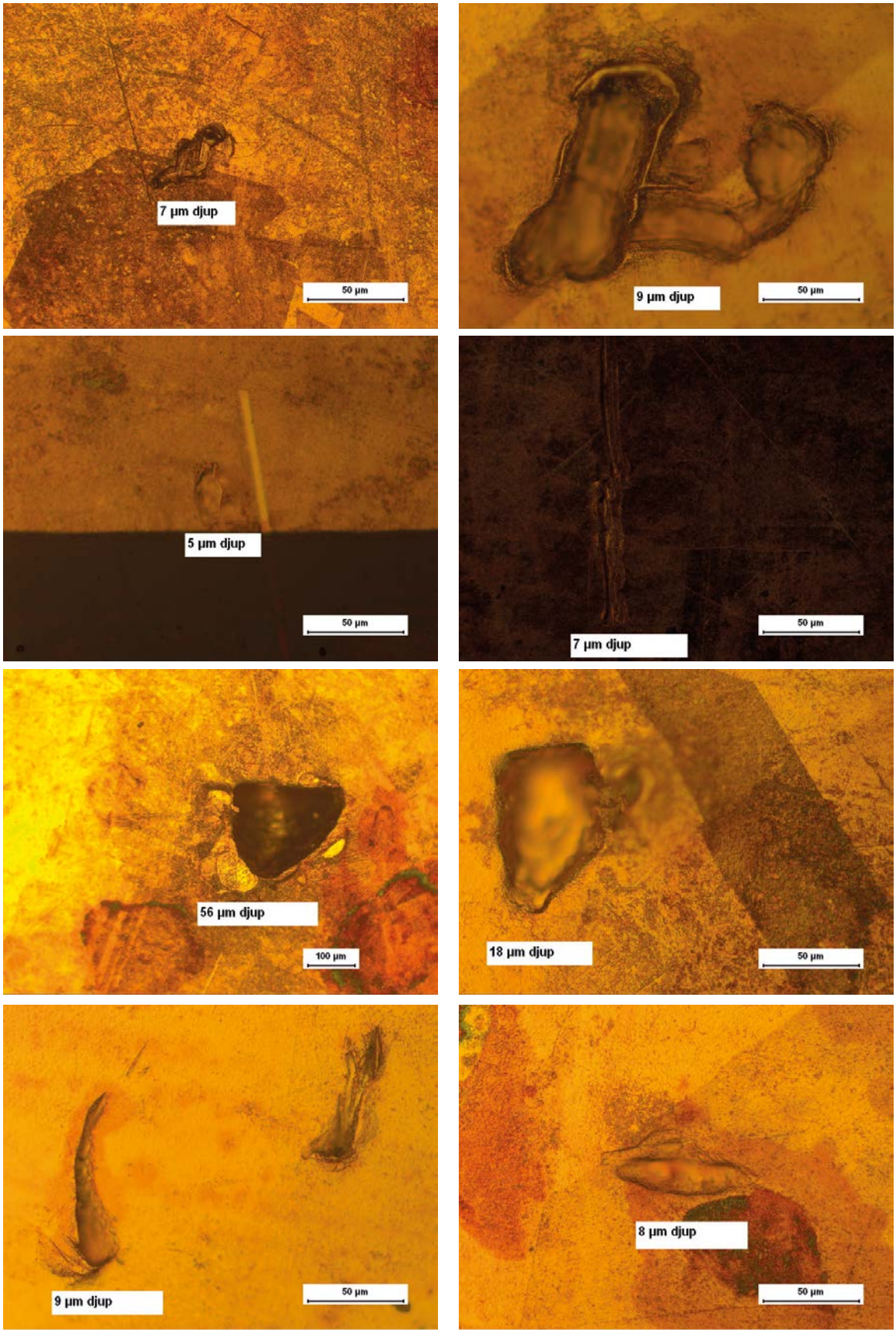

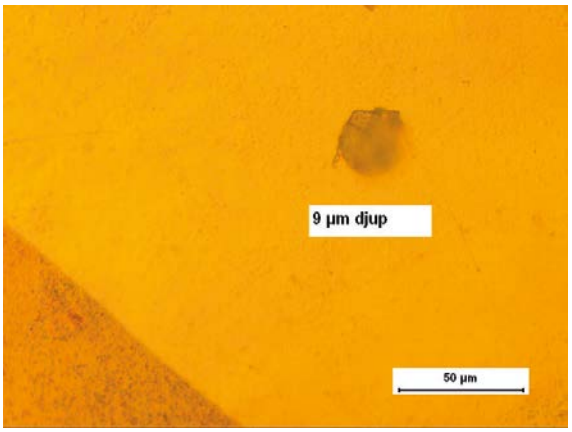
9 µm djup
50 µm

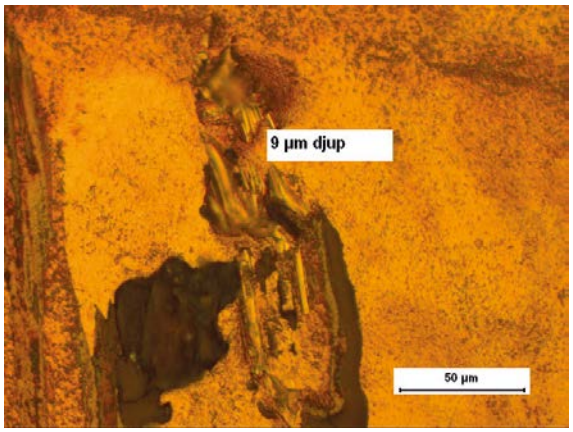
9 µm djup
50 µm

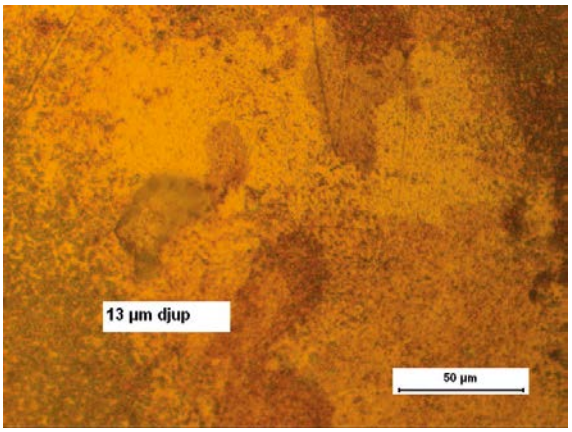
13 µm djup
50 µm

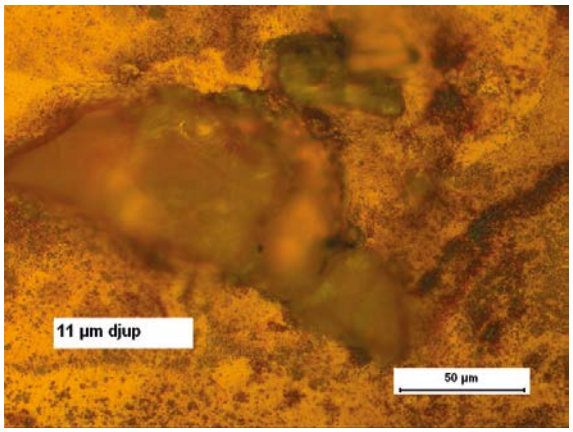
11 µm djup
50 µm

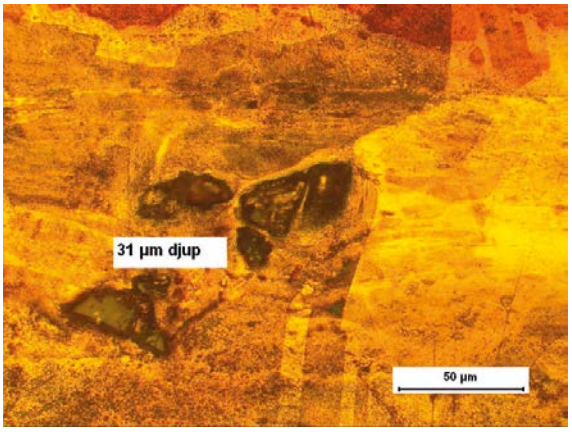
31 µm djup
50 µm

SRB exposures – Reference coupon 3 side 1 before pickling

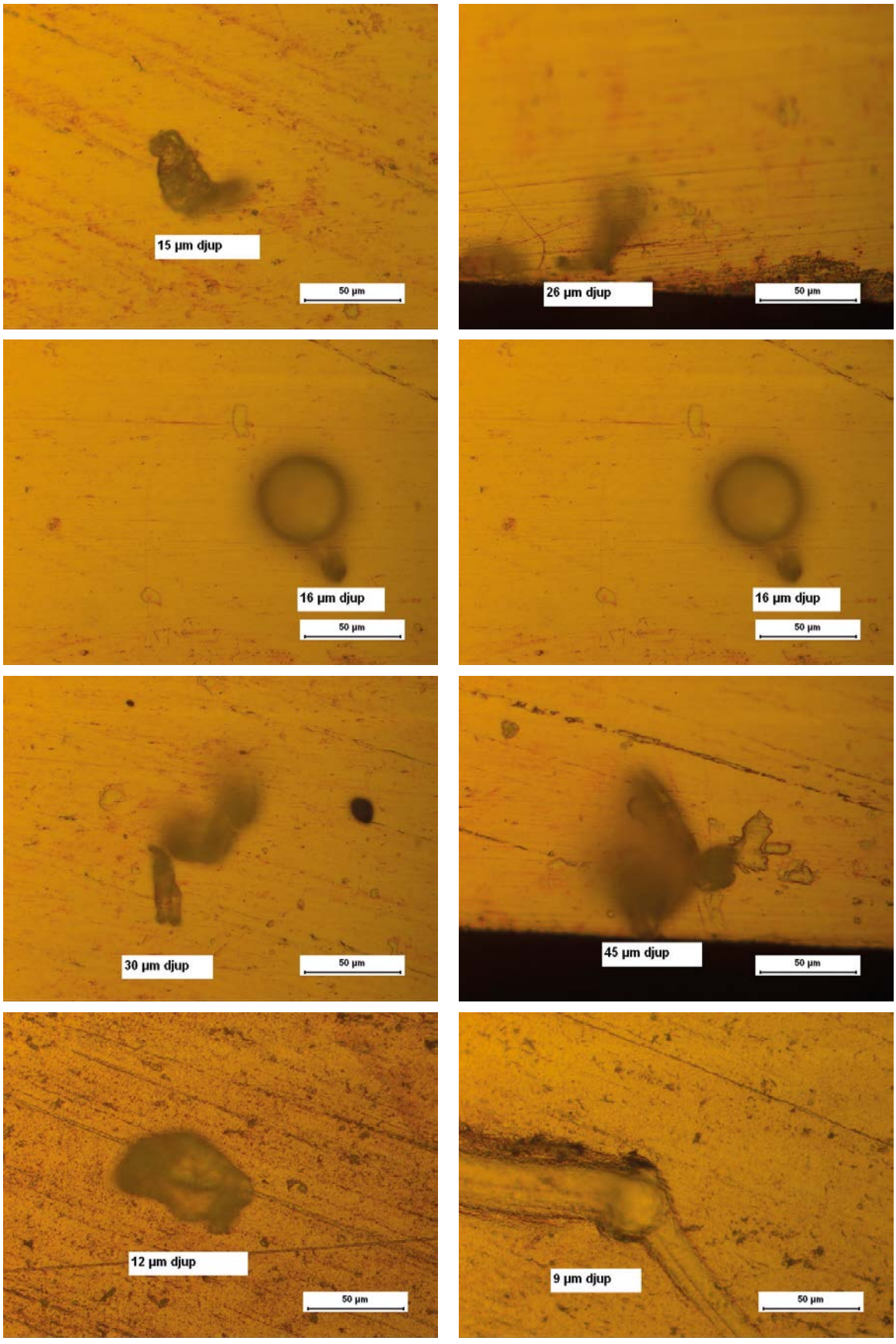

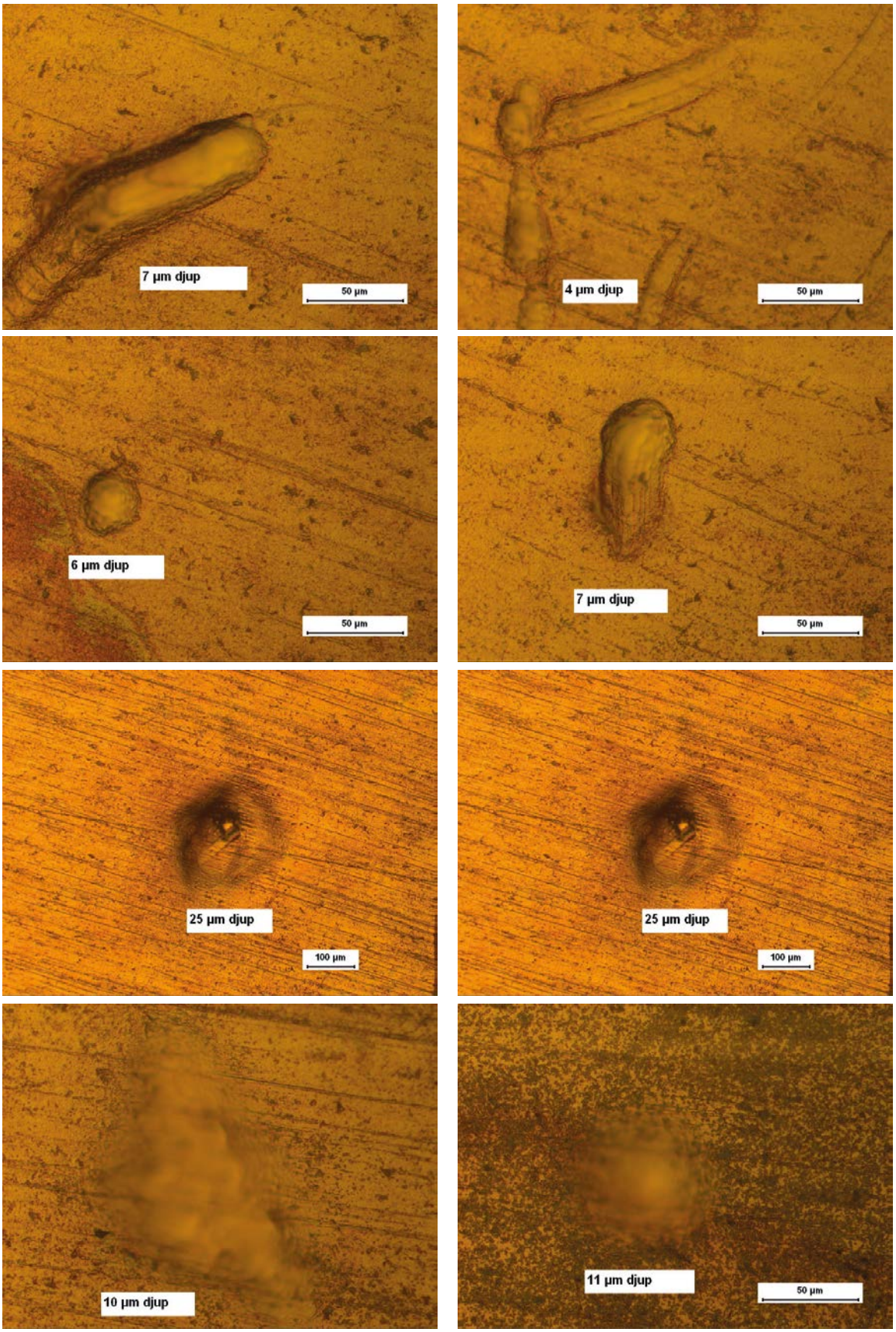
7 µm djup
50 µm
4 µm djup
50 µm
6 µm djup
50 µm
7 µm djup
50 µm
25 µm djup
100 µm
25 µm djup
100 µm
10 µm djup
11 µm djup
50 µm

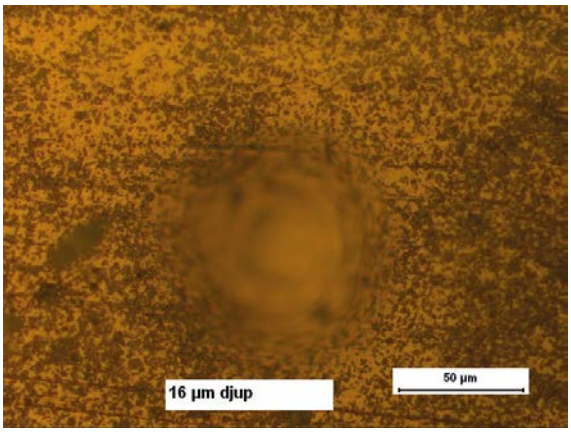
16 µm djup
50 µm

SRB exposures – Reference coupon 3 side 1 after pickling

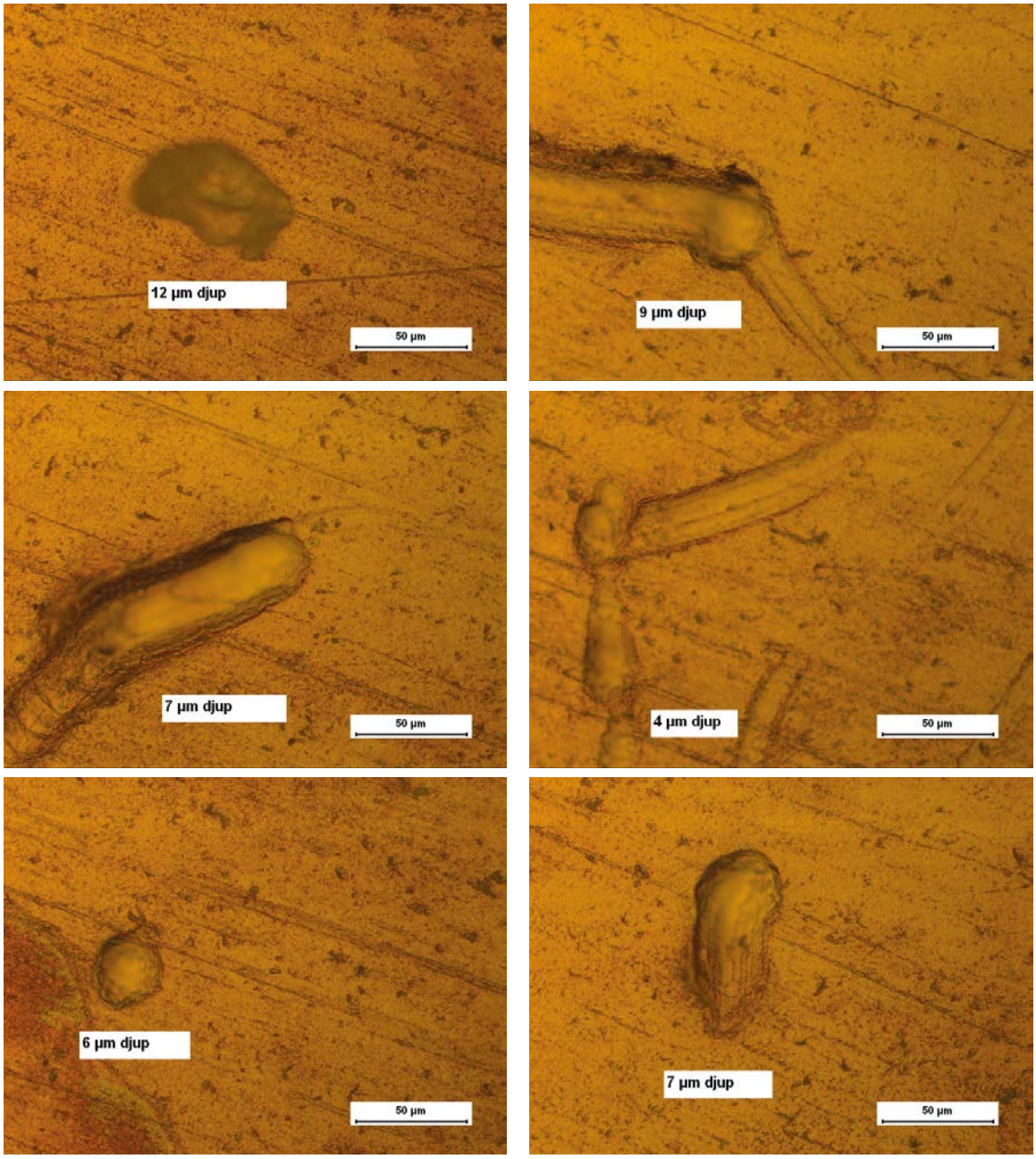

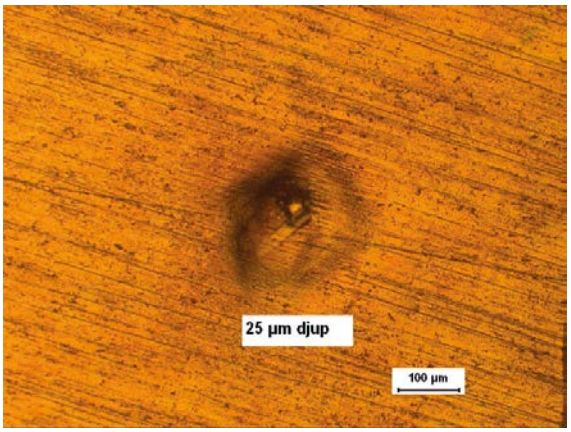
25 µm djup
100 µm

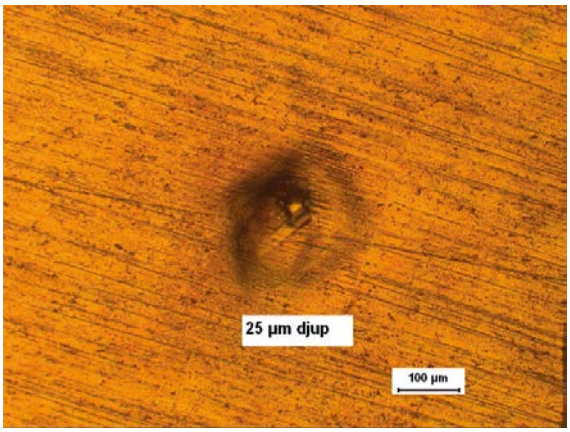
25 µm djup
100 µm

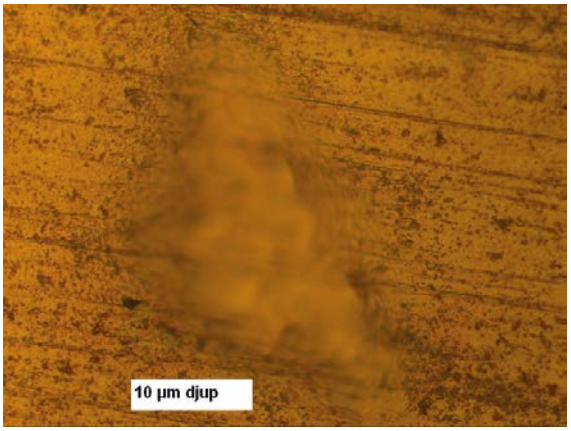
10 µm djup

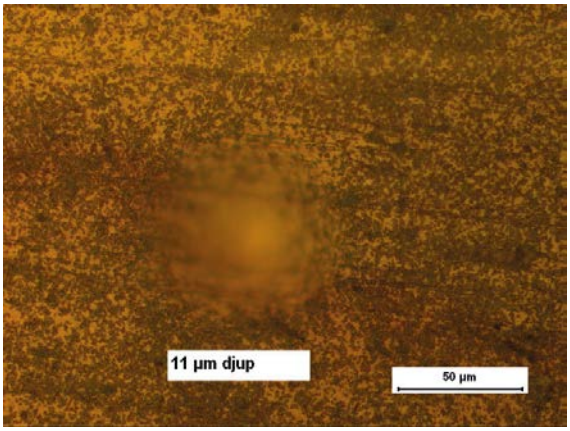
11 µm djup
50 µm

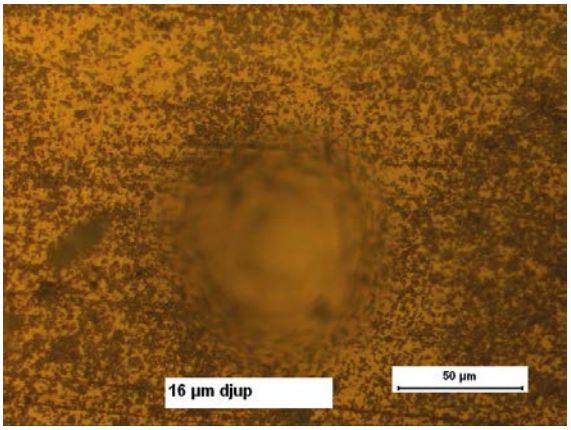
16 µm djup
50 µm

SRB exposures – Reference coupon 3 side 2 before pickling

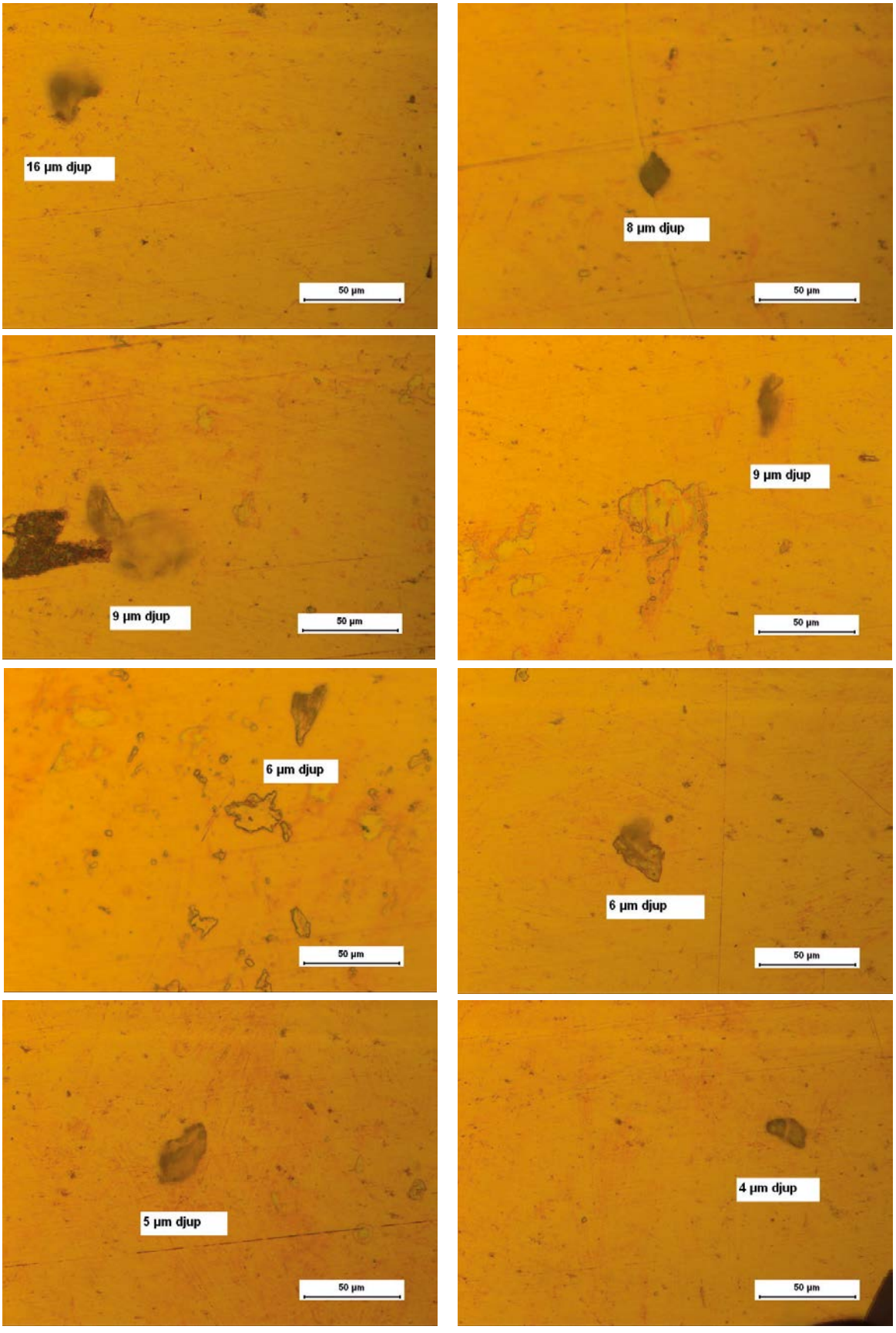

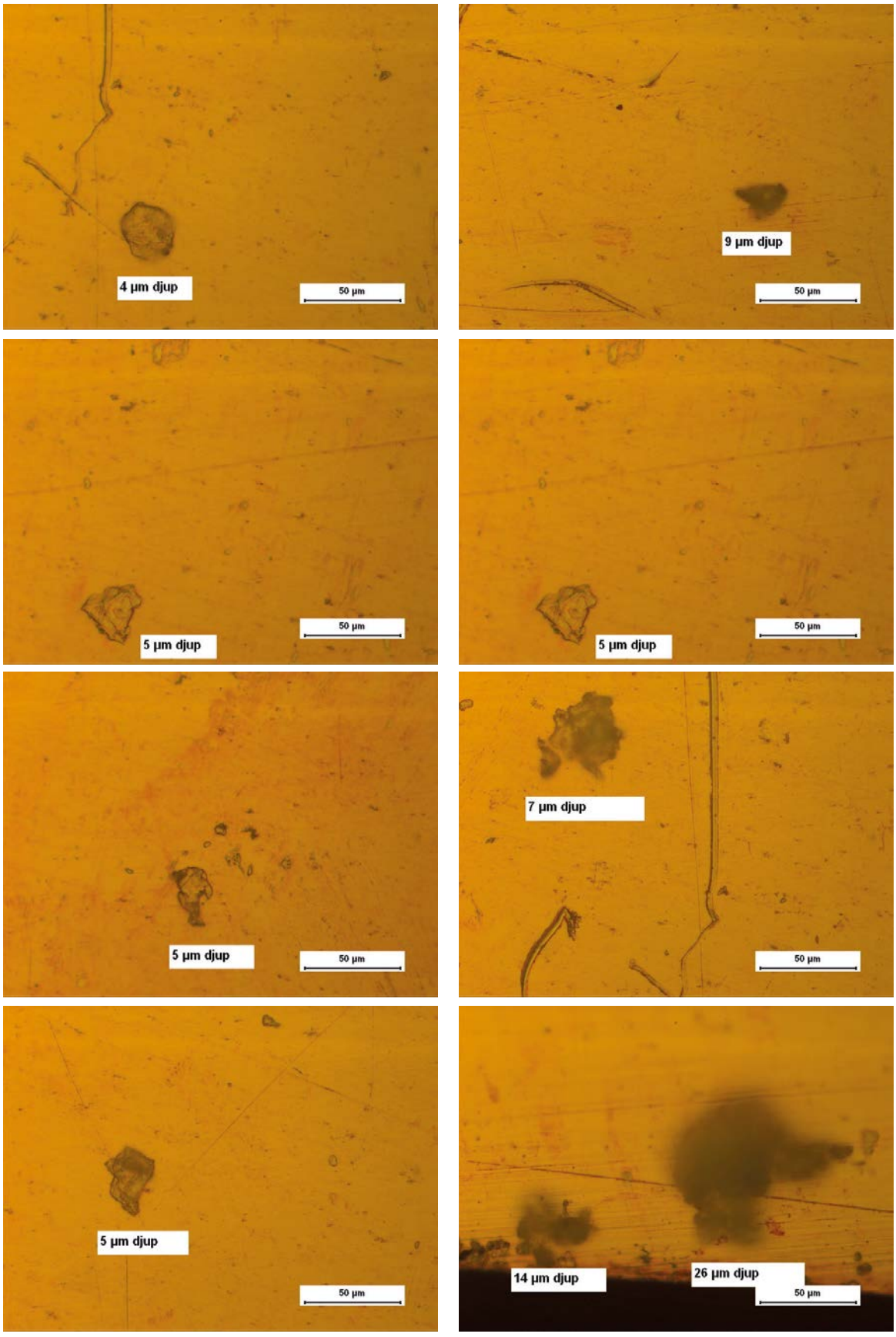
4 µm djup
50 µm
9 µm djup
50 µm
5 µm djup
50 µm
5 µm djup
50 µm
5 µm djup
50 µm
7 µm djup
50 µm
5 µm djup
50 µm
14 µm djup
26 µm djup
50 µm

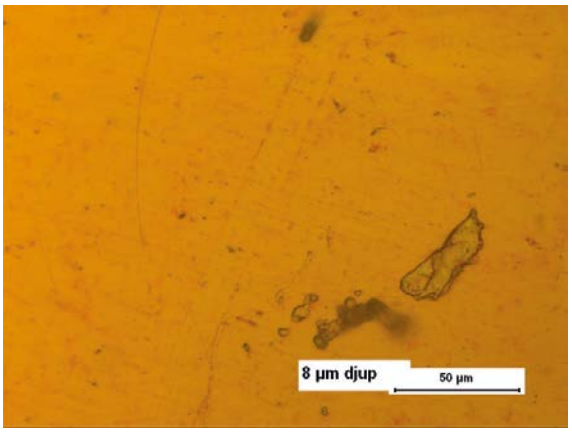
8 µm djup
50 µm

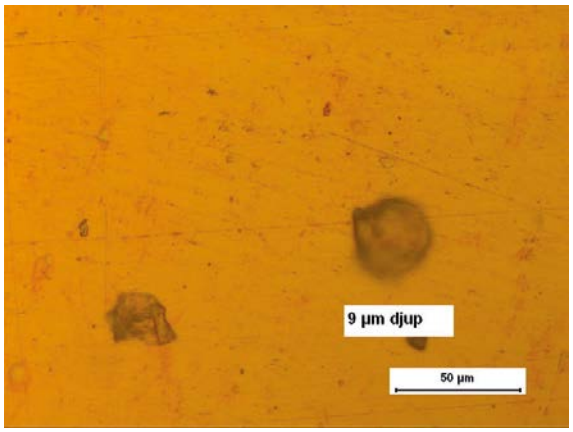
9 µm djup
50 µm

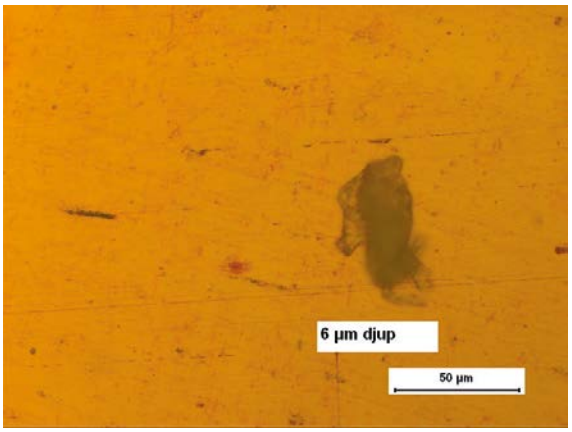
6 µm djup
50 µm

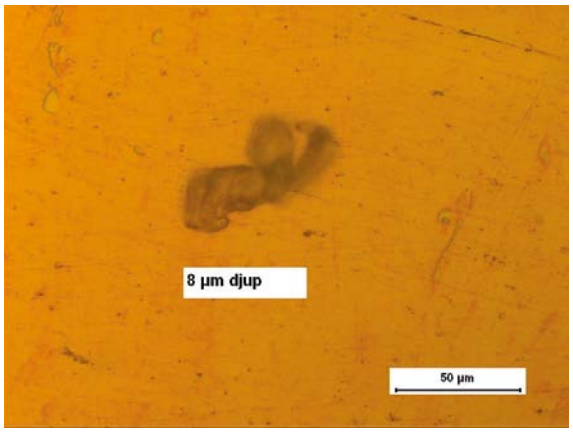
8 µm djup
50 µm

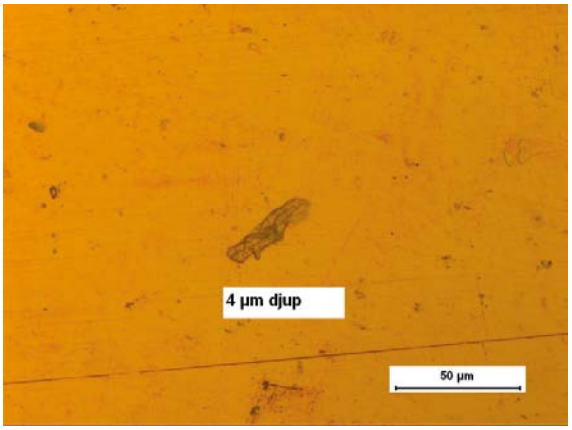
4 µm djup
50 µm

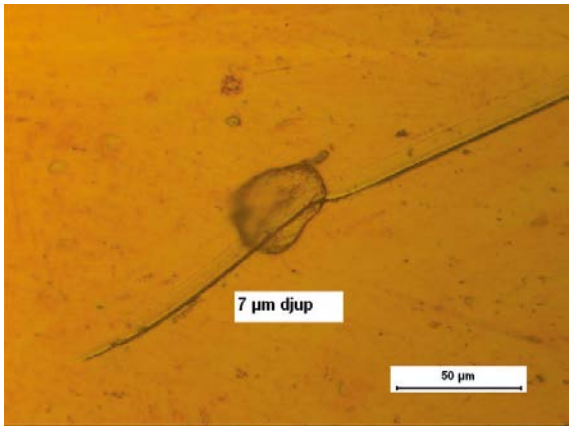
7 µm djup
50 µm

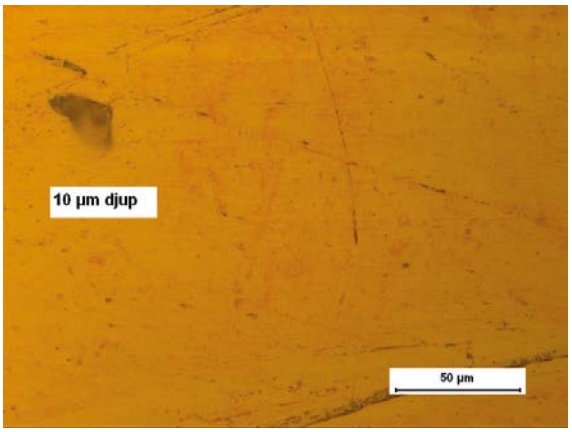
10 µm djup
50 µm

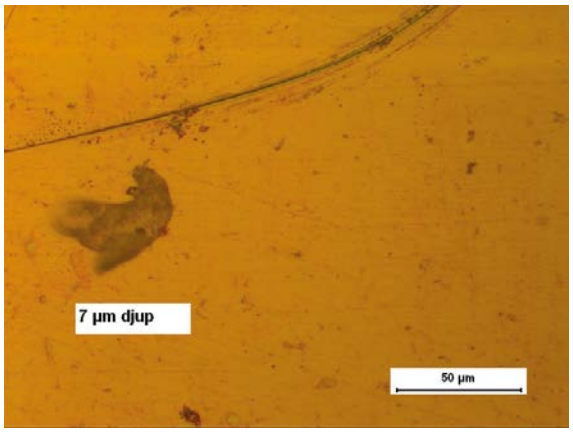
7 µm djup
50 µm

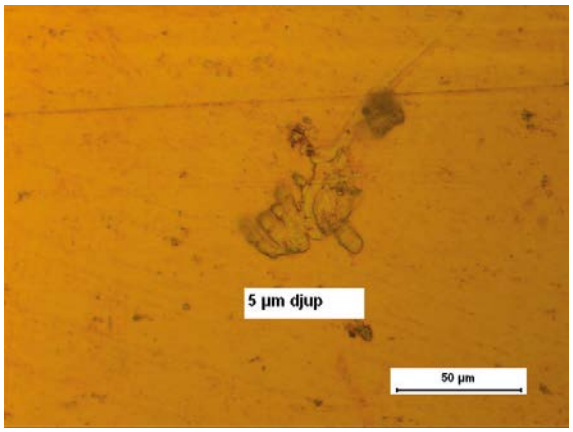
5 µm djup
50 µm

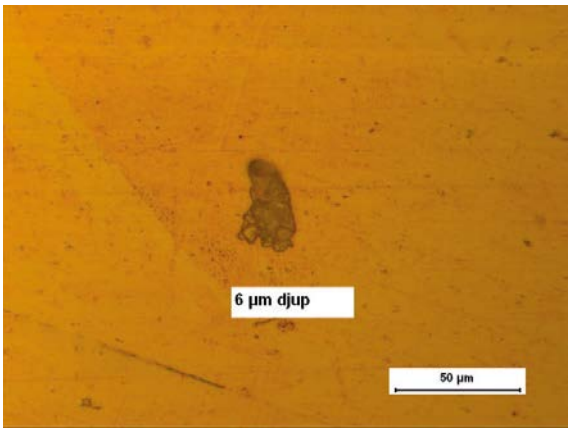
6 µm djup
50 µm

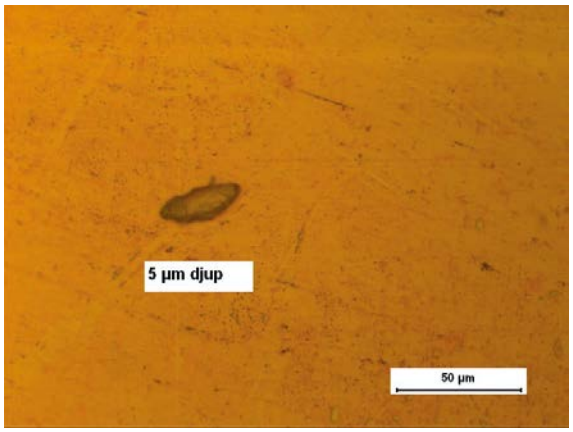
5 µm djup
50 µm

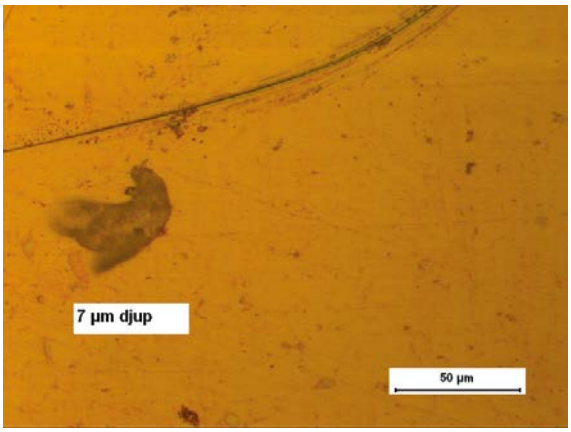
7 µm djup
50 µm

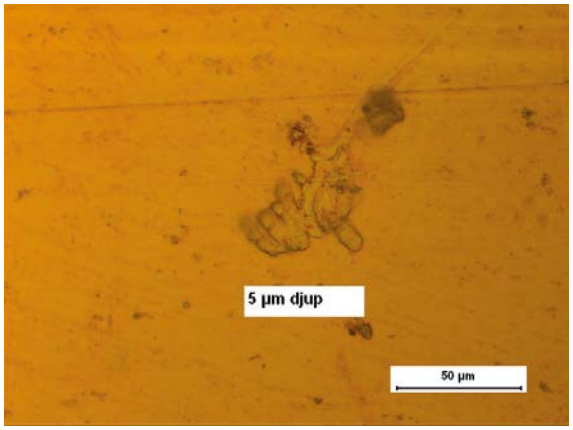
5 µm djup
50 µm

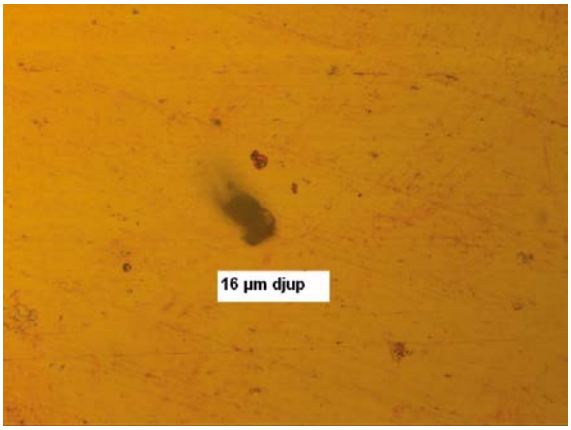
16 µm djup

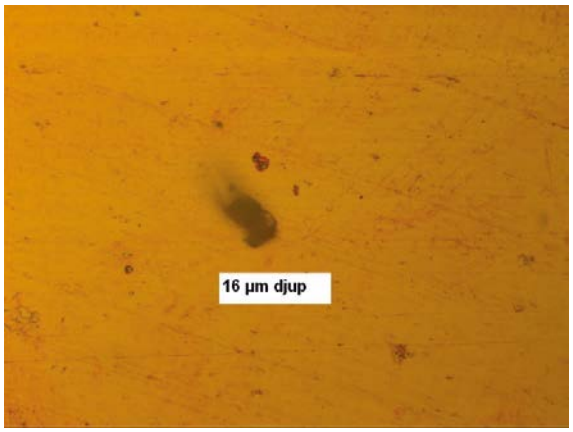
16 µm djup

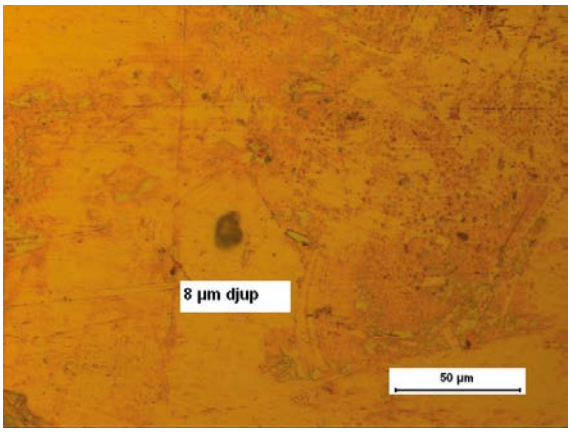
8 µm djup
50 µm

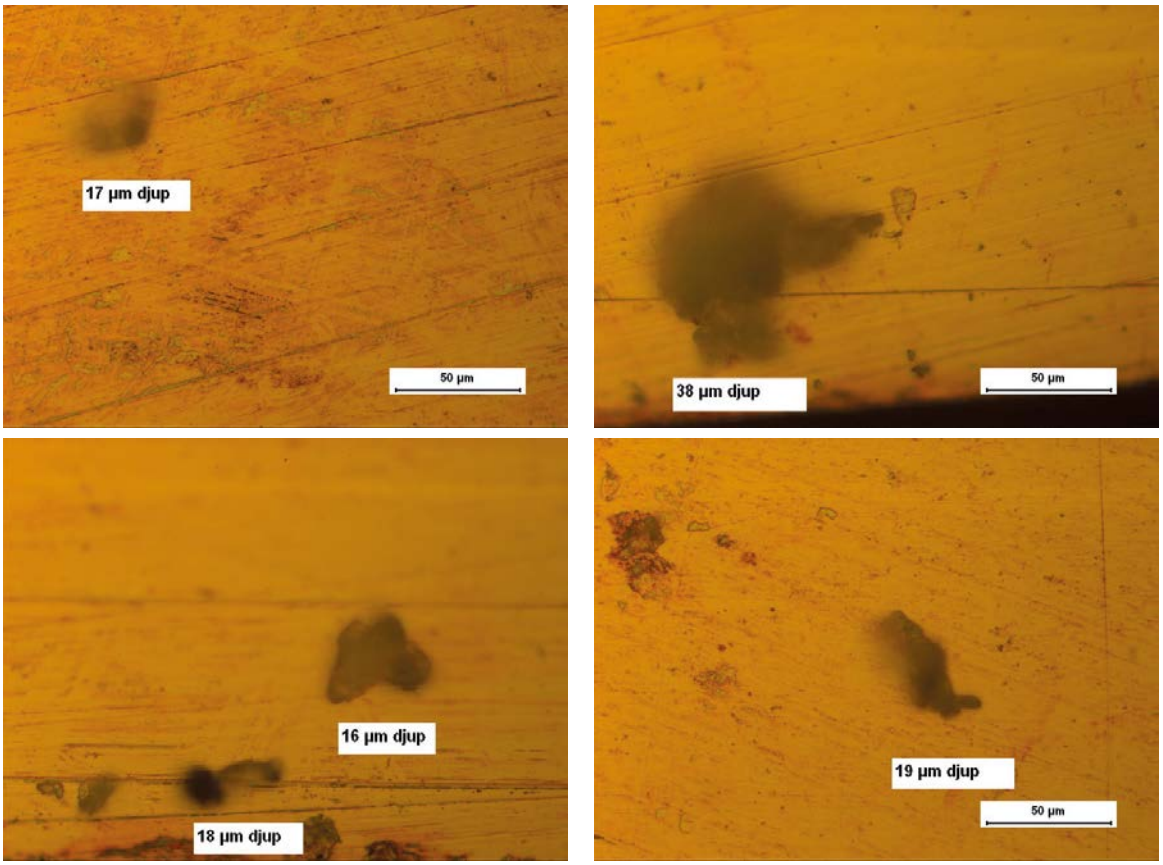
17 µm djup
50 µm
38 µm djup
50 µm
16 µm djup
18 µm djup
19 µm djup
50 µm

SRB exposures – Reference coupon 3 side 2 after pickling

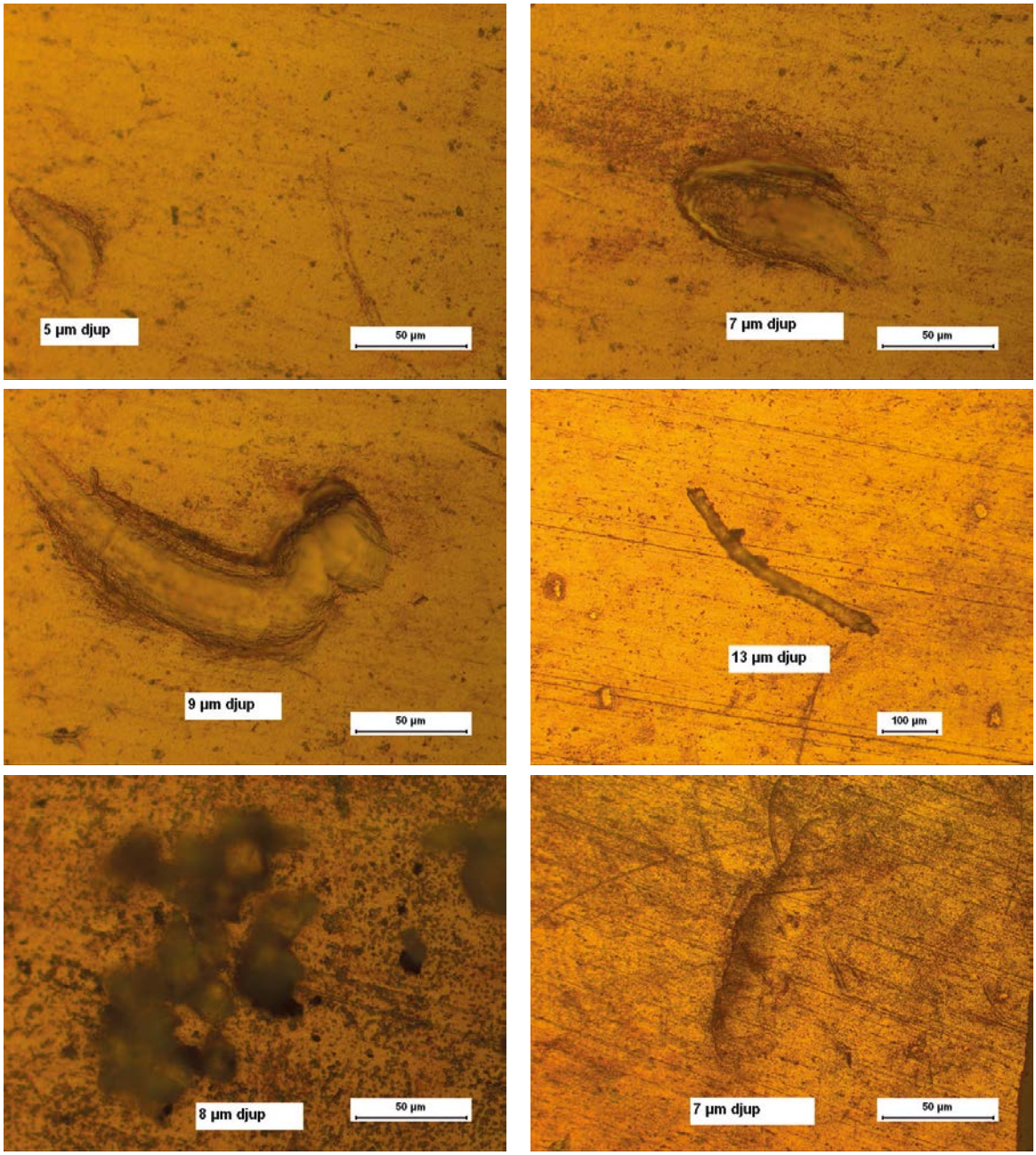

Appendix D

SEM/EDS analysis

One coupon from each exposure was cross-sectioned and analysed in the SEM in order to measure the thickness of the corrosion products on the surface after exposure. The corrosion products were also analysed with EDS in order to quantify the constituents.

D1 H_2S exposures

Gas A – coupon 6-4

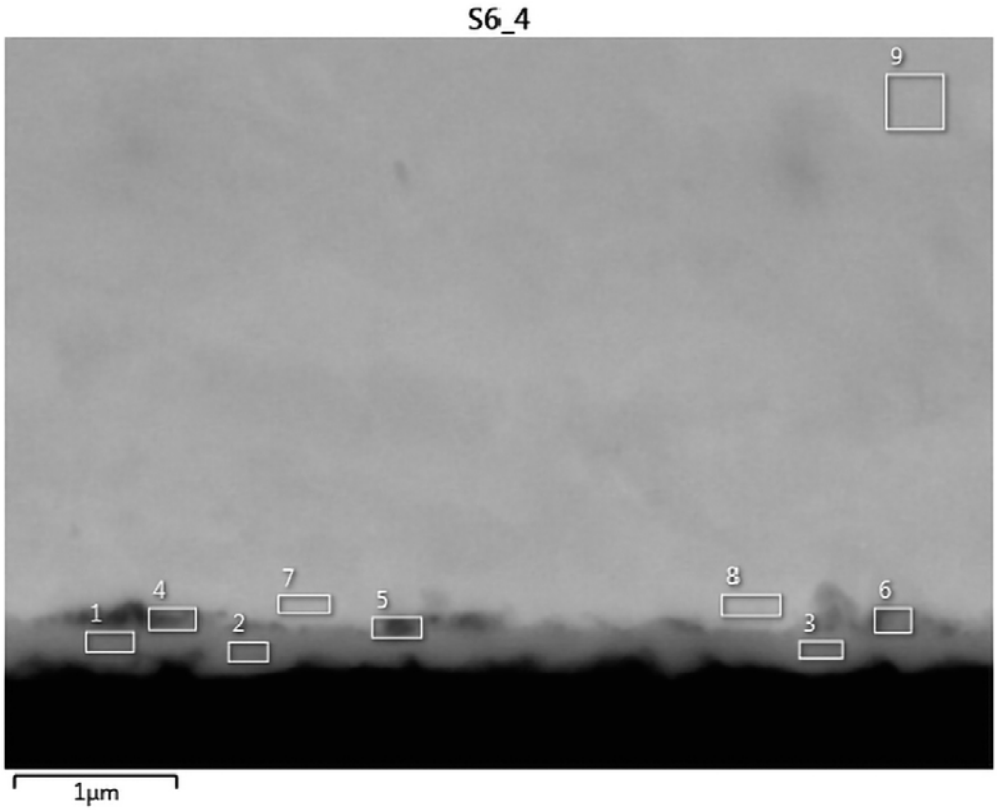

Figure D-1. *SEM image and EDS analysis on the cross section of coupon S6-4 (Gas A).*

Element (wt%)	1	2	3	4	5	6	7	8	9
S	7.99	10.77	3.90	4.60	2.06	3.76	0.90	1.36	
Cu	92.01	89.23	96.10	95.40	97.94	96.24	99.10	98.64	100.00
Total:	100.00	100.00	100.00	100.00	100.00	100.00	100.00	100.00	100.00

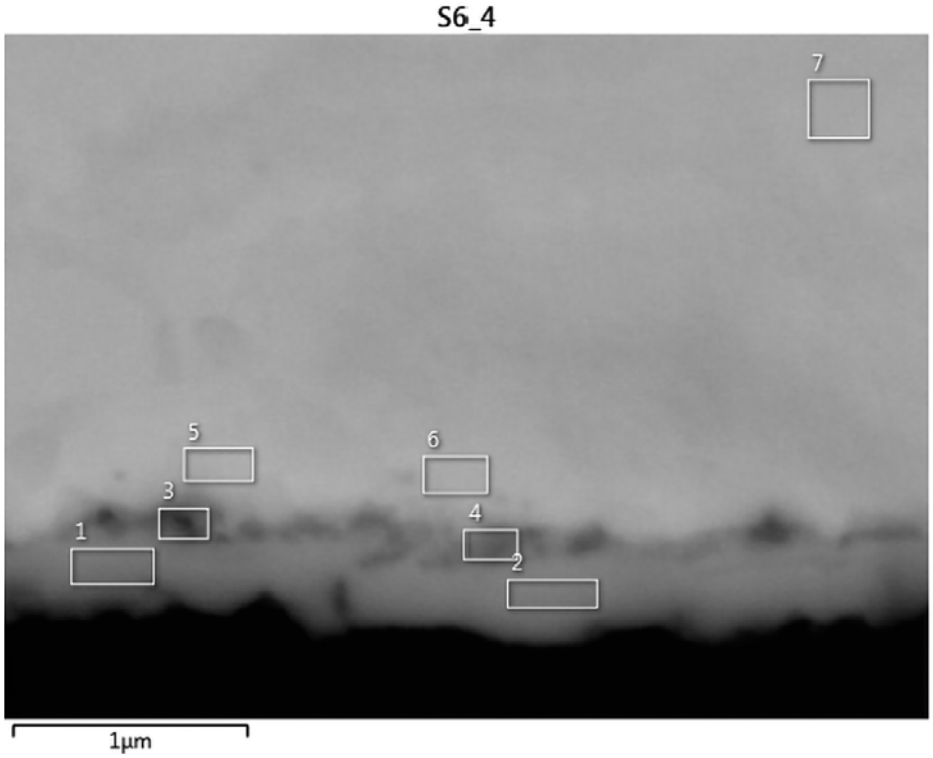

Figure D-2. *SEM image and EDS analysis on the cross section of coupon S6-4 (Gas A).*

Element (wt%)	1	2	3	4	5	6	7
S	8.05	14.04	2.52	10.45	0.41	2.07	
Cu	91.95	85.96	97.48	89.55	99.59	97.93	100.00
Total:	100.00	100.00	100.00	100.00	100.00	100.00	100.00

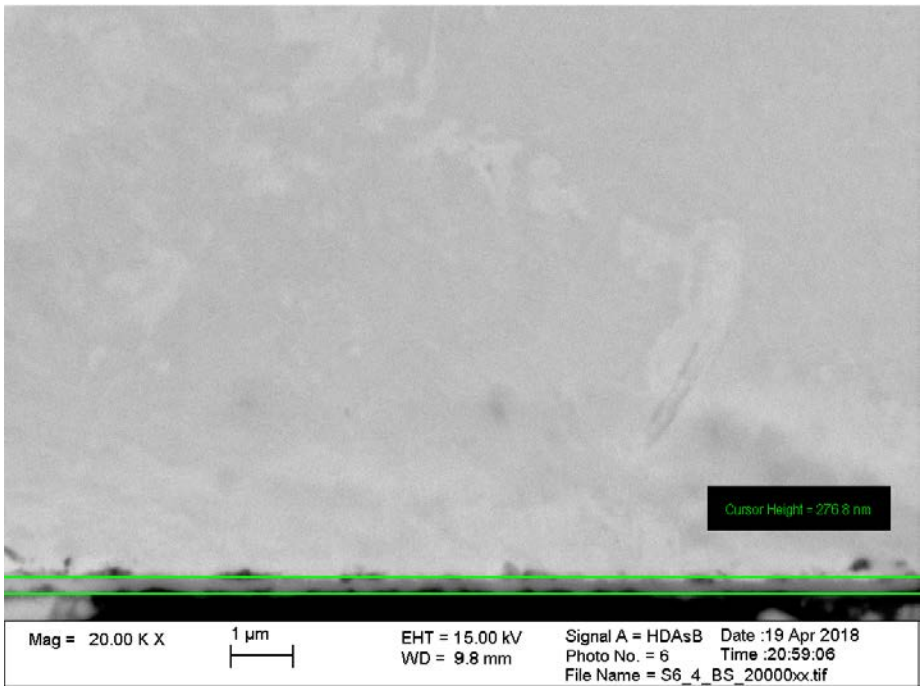

Figure D-3. *SEM image on the cross section of coupon S6-4 (Gas A) showing the sulphide layer thickness on the surface of the coupon.*

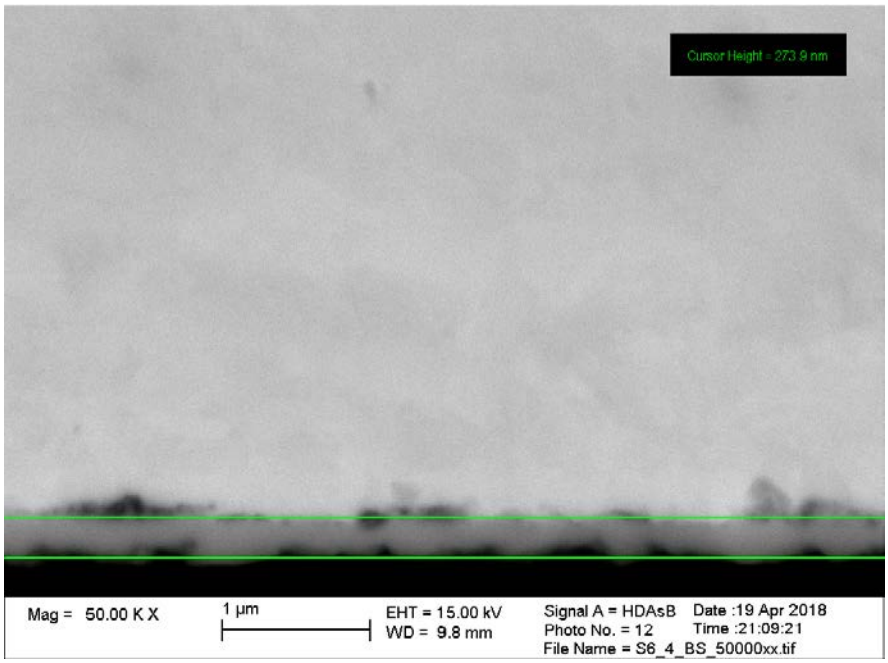

Figure D-4. *SEM image on the cross section of coupon S6-4 (Gas A) showing the sulphide layer thickness on the surface of the coupon.*

Gas B – coupon 2-4

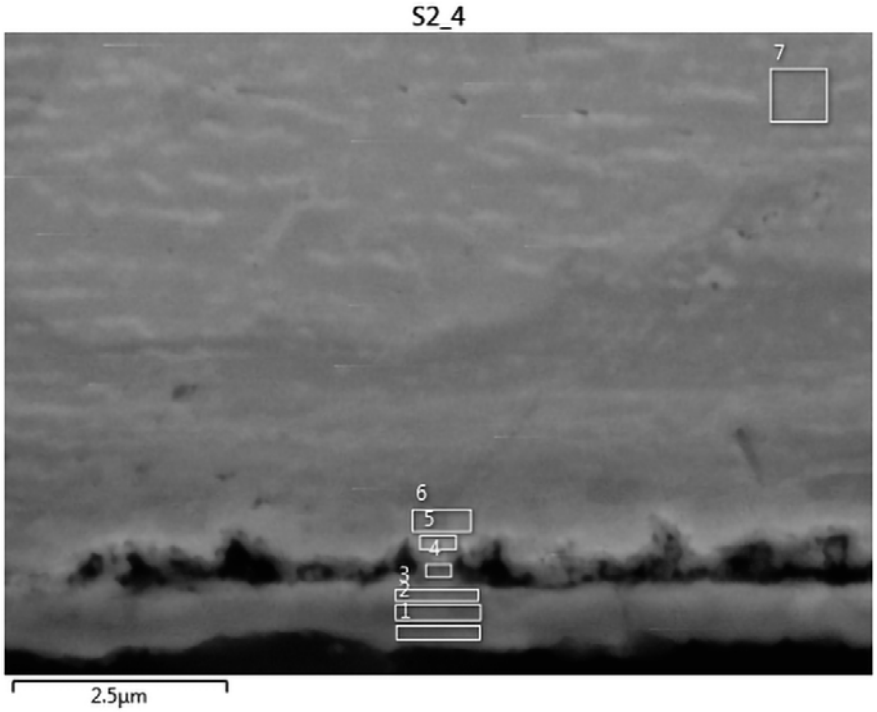

Figure D-5. *SEM image and EDS analysis on the cross section of coupon S2-4 (Gas B).*

Element (wt%)	1	2	3	4	5	6	7
S	19.95	19.06	12.14	7.27	1.16	0.17	
Cl			0.20	0.44			
Cu	80.05	80.94	87.66	92.29	98.84	99.83	100.00
Total:	100.00	100.00	100.00	100.00	100.00	100.00	100.00

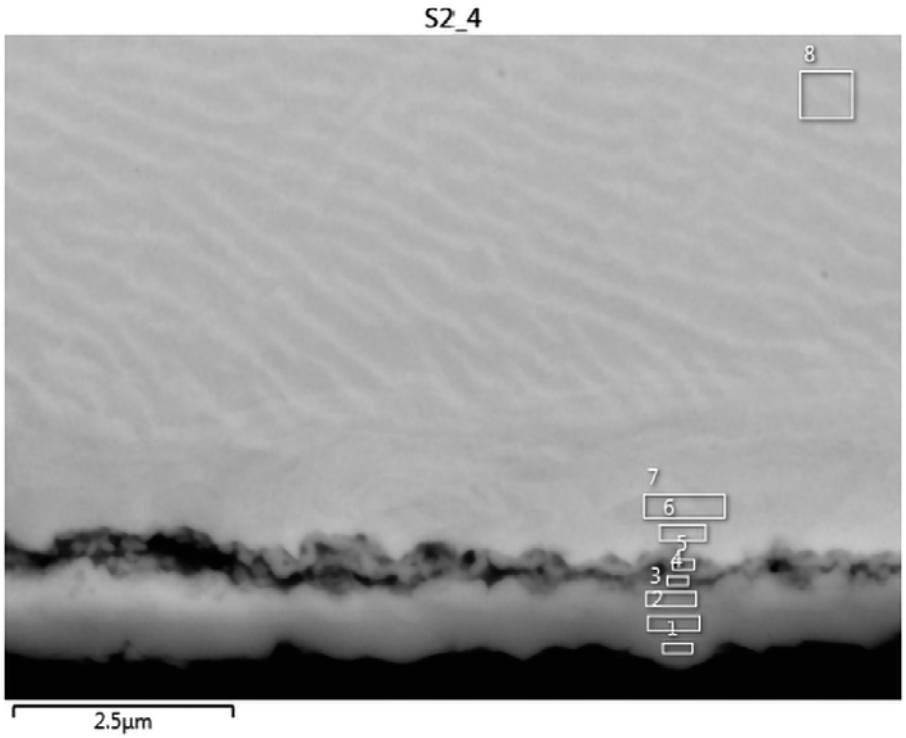

Figure D-6. *SEM image and EDS analysis on the cross section of coupon S2-4 (Gas B).*

Element (wt%)	1	2	3	4	5	6	7	8
S	17.67	20.04	12.38	12.13	3.91	0.91		
Cl			0.35	0.31	0.26	0.17		
Cu	82.33	79.96	87.27	87.57	95.83	98.92	100.00	100.00
Total:	100.00	100.00	100.00	100.00	100.00	100.00	100.00	100.00

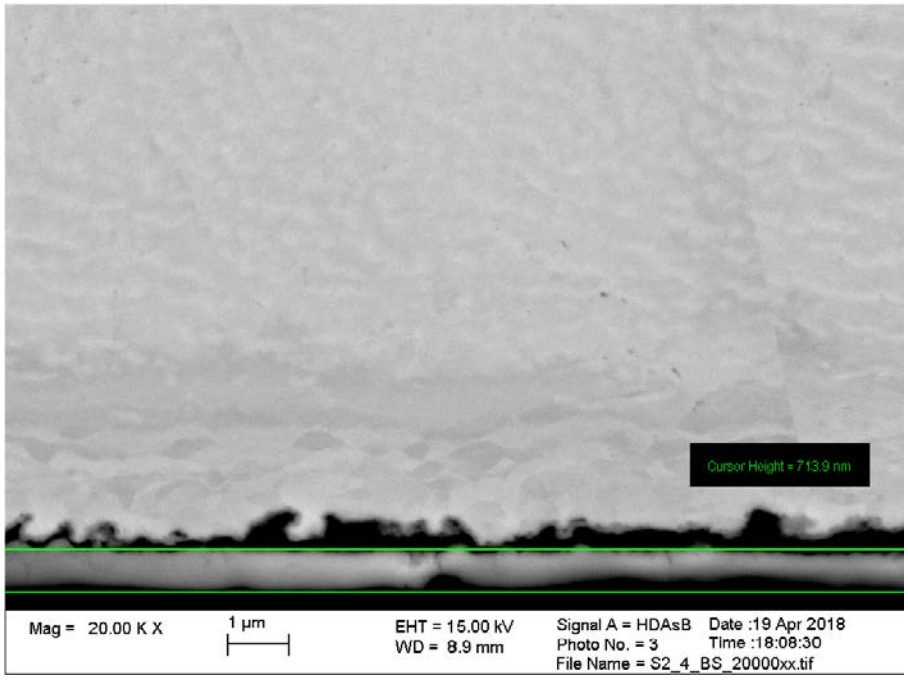

Figure D-7. *SEM image on the cross section of coupon S2-4 (Gas B) showing the sulphide layer thickness on the surface of the coupon.*

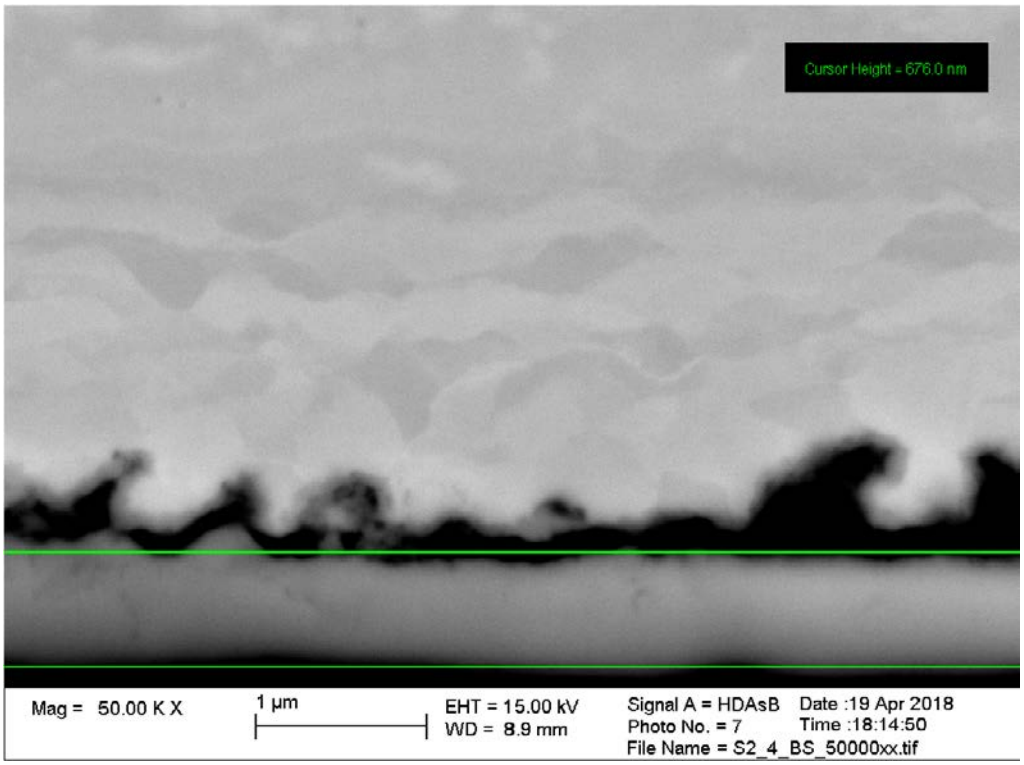

Figure D-8. *SEM image on the cross section of coupon S2-4 (Gas B) showing the sulphide layer thickness on the surface of the coupon.*

Gas C – coupon 1-10

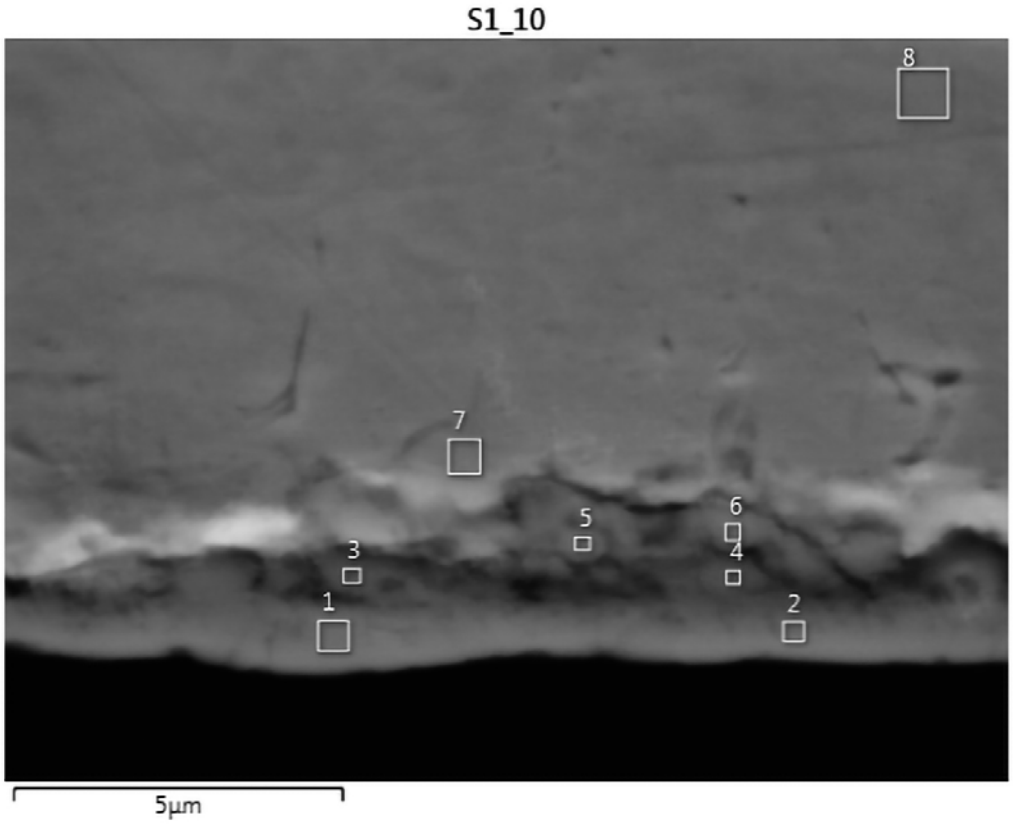

Figure D-9. *SEM image and EDS analysis on the cross section of coupon S1-10 (Gas C).*

Element (wt%)	1	2	3	4	5	6	7	8
O	0.66	0.79	1.97	2.35	4.42	3.48	0.75	0.29
Si	0.28	0.23	0.34	0.45	1.34	0.42	0.31	0.18
S	18.21	17.99	16.78	15.57	14.28	13.32	0.42	
Cl			0.19	0.22	0.29	0.30		
K				0.10	0.09	0.05		
Ca	0.08	0.10	0.20	0.12	0.14	0.11	0.06	0.06
Cu	80.77	80.90	80.53	81.19	79.45	82.33	98.46	99.48
Total:	100.00	100.00	100.00	100.00	100.00	100.00	100.00	100.00

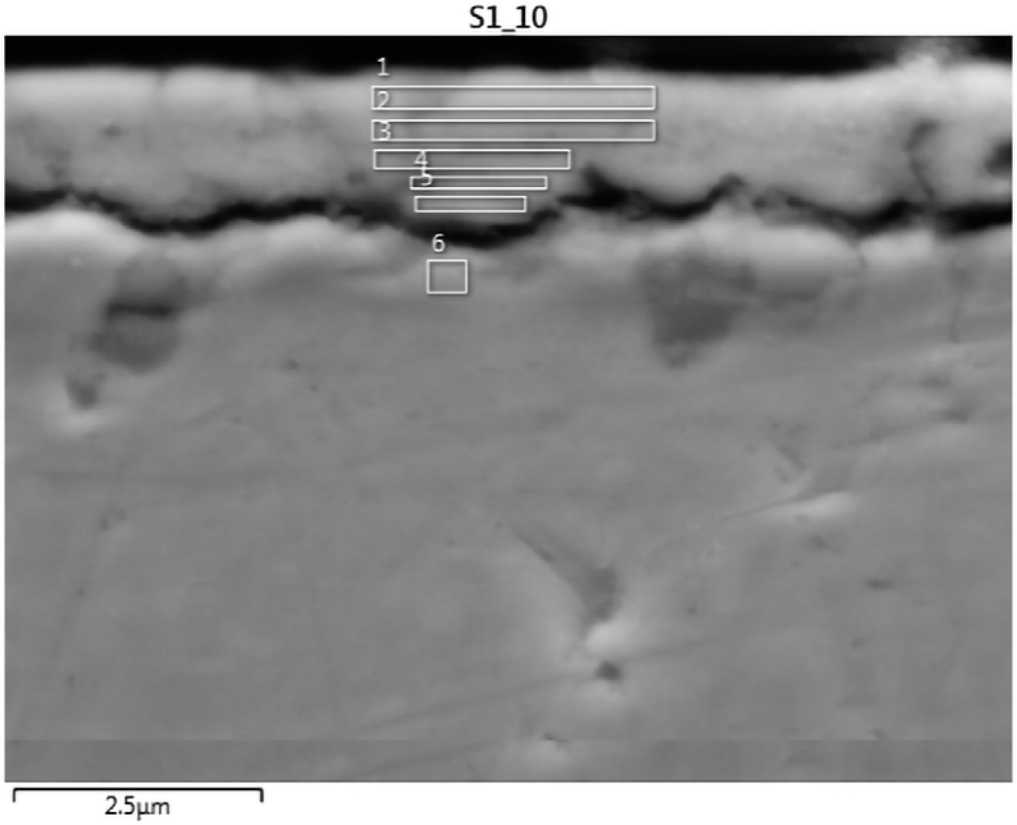

Figure D-10. *SEM image and EDS analysis on the cross section of coupon S1-10 (Gas C).*

Element (wt%)	1	2	3	4	5	6
O	3.10	2.49	2.89	3.55	4.25	1.37
Si	2.09	1.08	0.95	1.18	1.37	0.23
S	16.30	15.98	14.38	12.82	10.65	0.84
Cl		0.05	0.15	0.23	0.21	
Ca	0.39	0.21	0.21	0.24	0.32	0.14
Cu	78.12	80.19	81.41	81.99	83.20	97.42
Total:	100.00	100.00	100.00	100.00	100.00	100.00

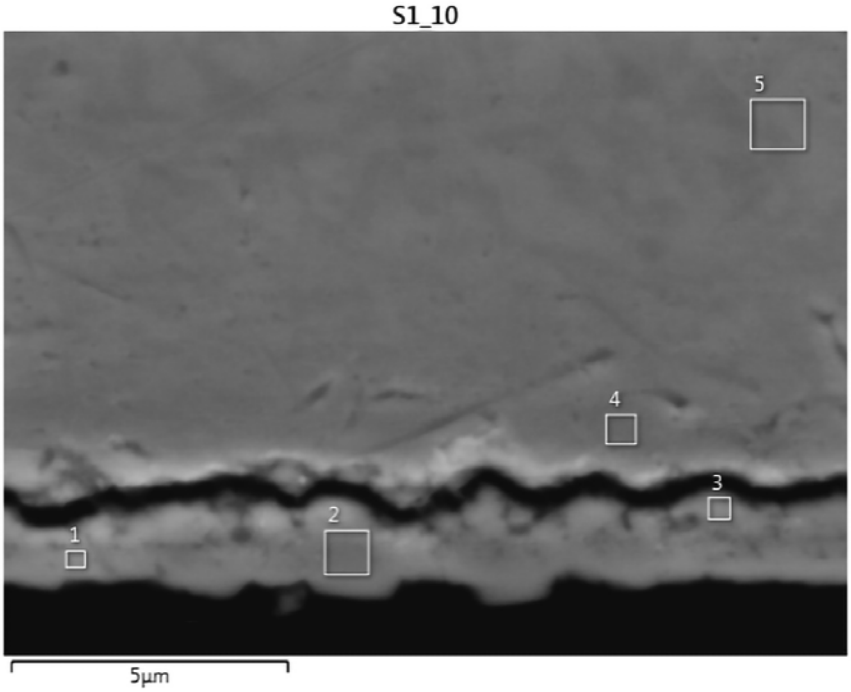

Figure D-11. *SEM image and EDS analysis on the cross section of coupon S1-10 (Gas C).*

Element (wt%)	1	2	3	4	5
O	1.35	1.10	2.75	0.31	0.30
Si	0.34	0.41	0.60	0.12	0.09
S	17.22	17.10	12.94	0.08	
Cl			0.33		
K	0.05		0.09		
Ca	0.06		0.12		
Cu	80.99	81.38	83.16	99.48	99.61
Total:	100.00	100.00	100.00	100.00	100.00

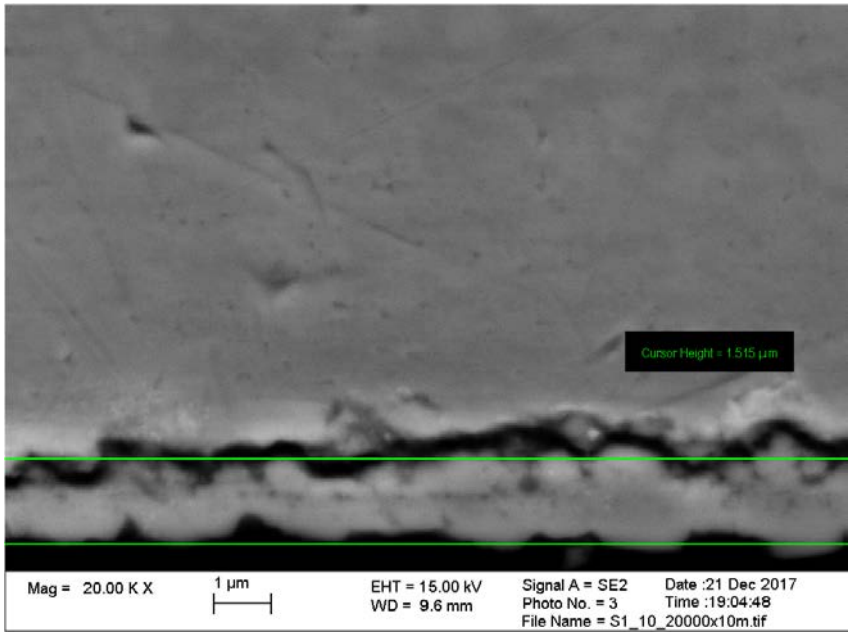

Figure D-12. *SEM image on the cross section of coupon S1-10 (Gas C) showing the sulphide layer thickness on the surface of the coupon.*

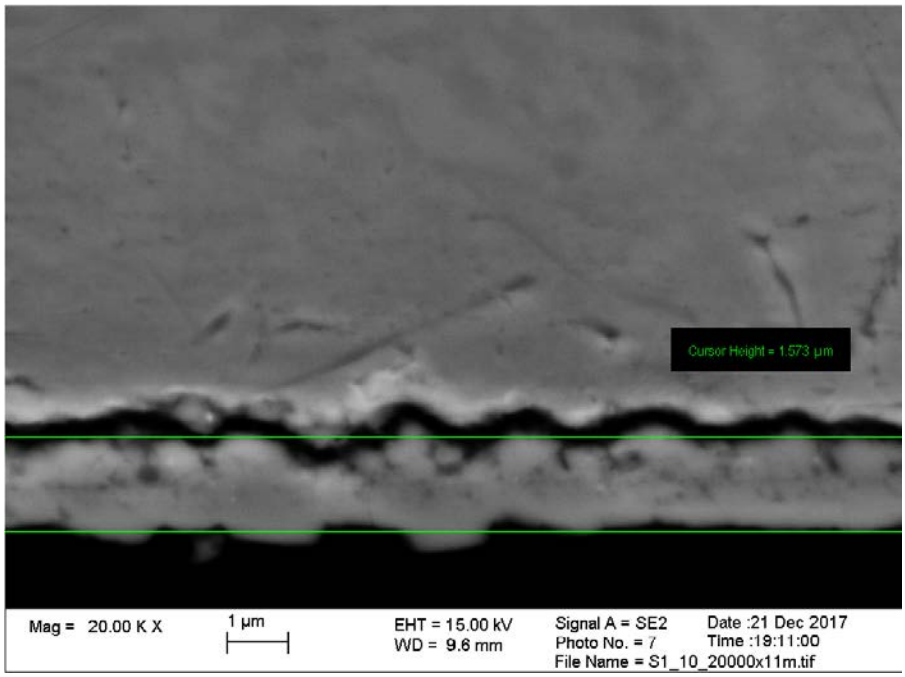

Figure D-13. *SEM image on the cross section of coupon S1-10 (Gas C) showing the sulphide layer thickness on the surface of the coupon.*

Gas D – coupon 2-10

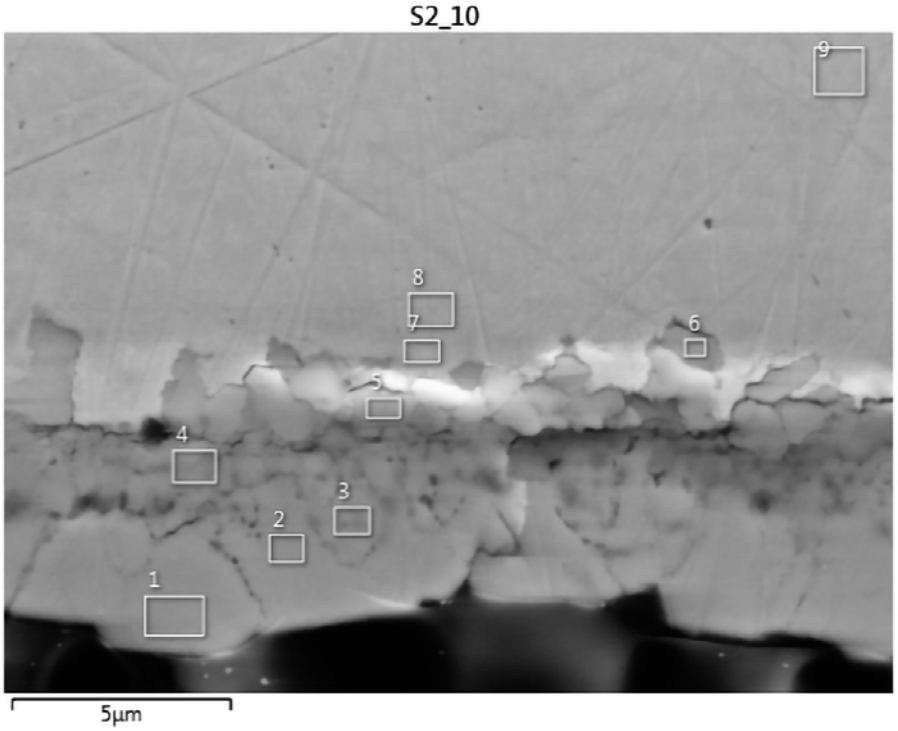

Figure D-14. *SEM image and EDS analysis on the cross section of coupon S2-10 (Gas D).*

Element (wt%)	1	2	3	4	5	6	7	8	9
S	19.46	19.27	19.51	18.95	18.39	16.89	0.24		
Cu	80.54	80.73	80.49	81.05	81.61	83.11	99.76	100.00	100.00
Total:	100.00	100.00	100.00	100.00	100.00	100.00	100.00	100.00	100.00

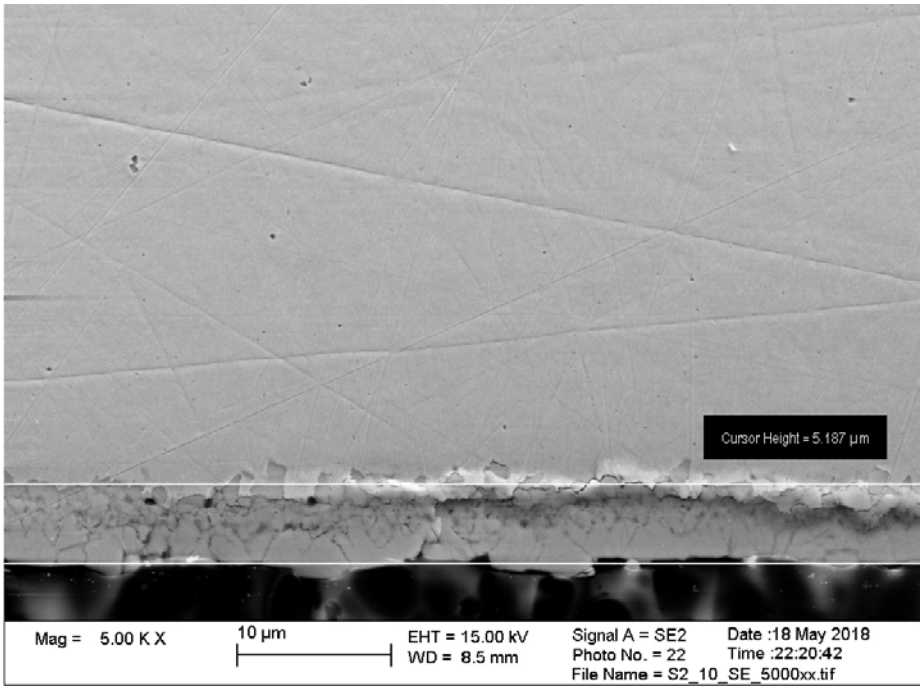

Figure D-15. *SEM image on the cross section of coupon S2-10 (Gas D) showing the sulphide layer thickness on the surface of the coupon.*

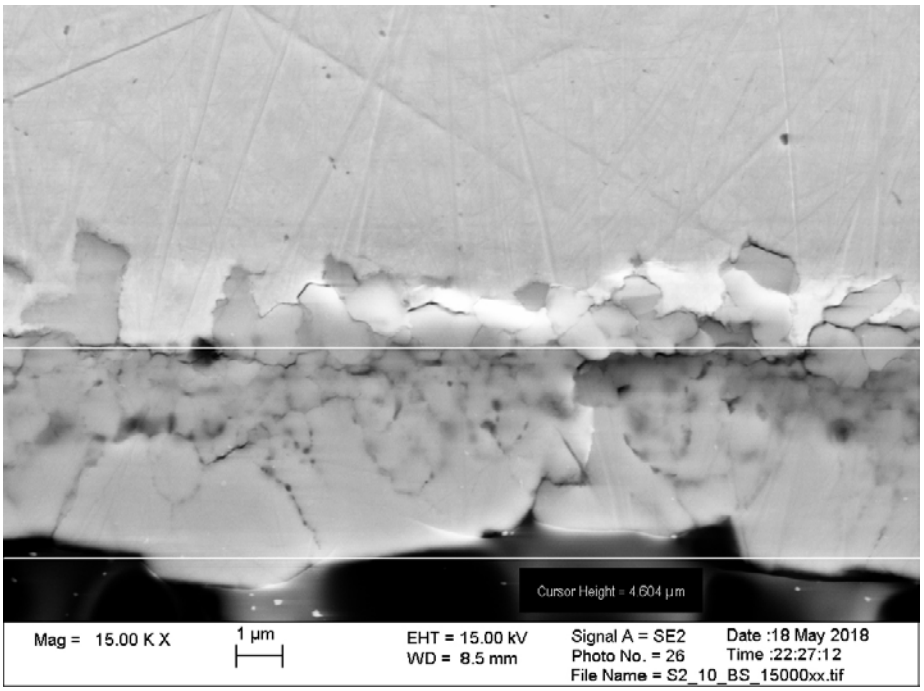

Figure D-16. *SEM image on the cross section of coupon S2-10 (Gas D) showing the sulphide layer thickness on the surface of the coupon.*

D2 SRB exposures

The cross sections were cast in conductive epoxy in pairs, with the outer surfaces placed together in order to protect the sulphide layers during coupon preparation. Therefore, each of the following images show two coupons for Bio A and B. For Bio C, Bio D and Control G cross sections of the same coupon were cast together so that only one coupon is shown in the following sections for these exposures.

Bio A and Bio B – coupons 10-2 and 7-6

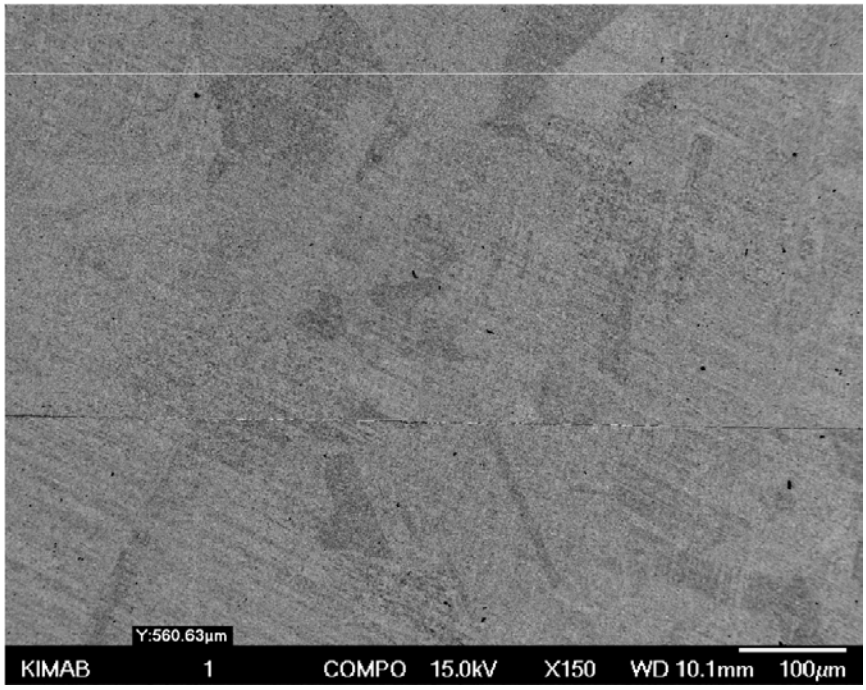

Figure D-17. *Overview of coupons Bio-B S7-6 (top) and Bio-A S10-2 (bottom) (BEI).*

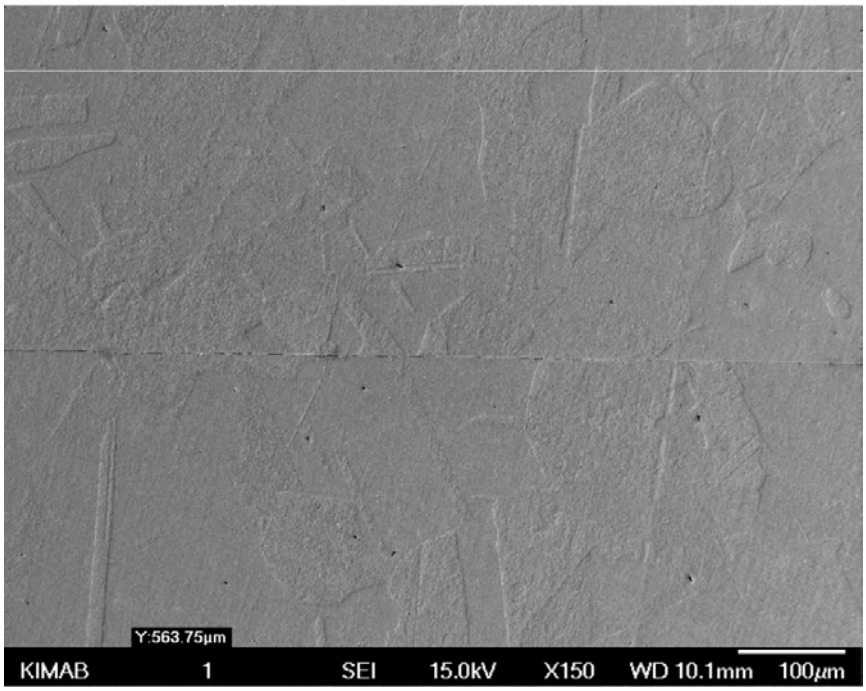

Figure D-18. *Overview of coupons Bio-B S7-6 (top) and Bio-A S10-2 (bottom) (BEI).*

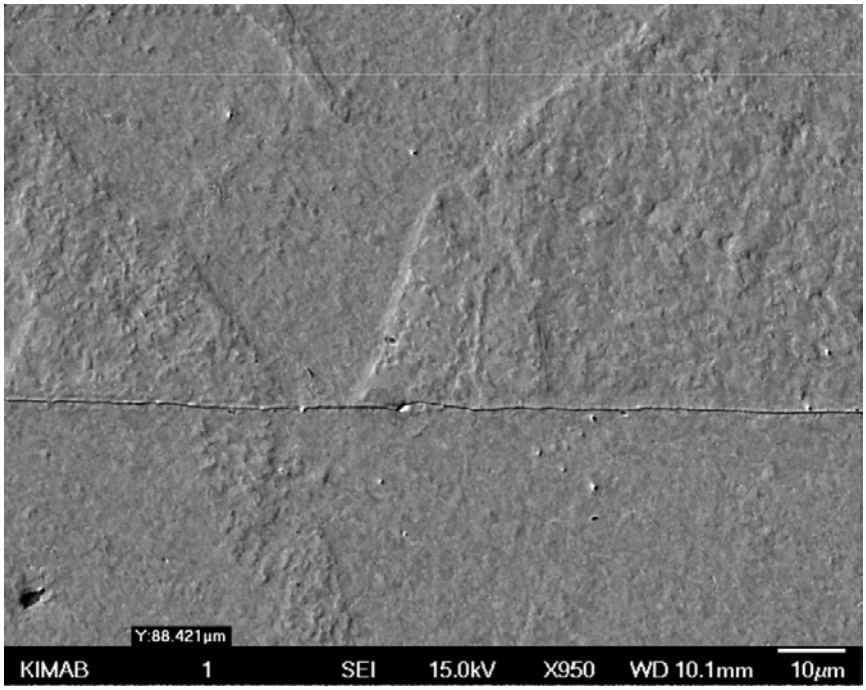

Figure D-19. *Overview of coupons Bio-B S7-6 (top) and Bio-A S10-2 (bottom) (SEI).*

Bio A – coupon 10-2

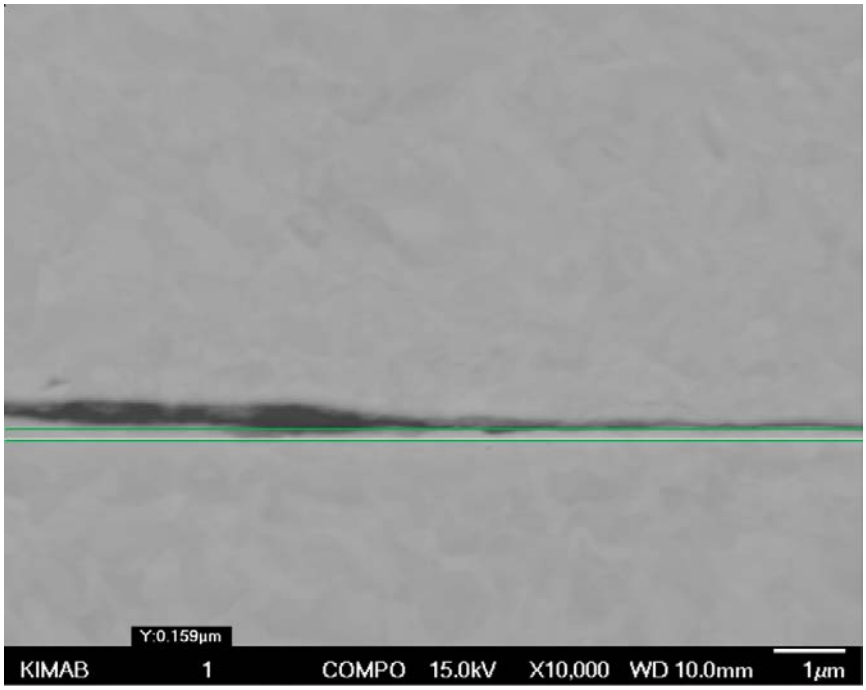

Figure D-20. *Coupon Bio-A S10-2 (bottom) (BEI). The sulphide layer was measured as being 159 nm thick.*

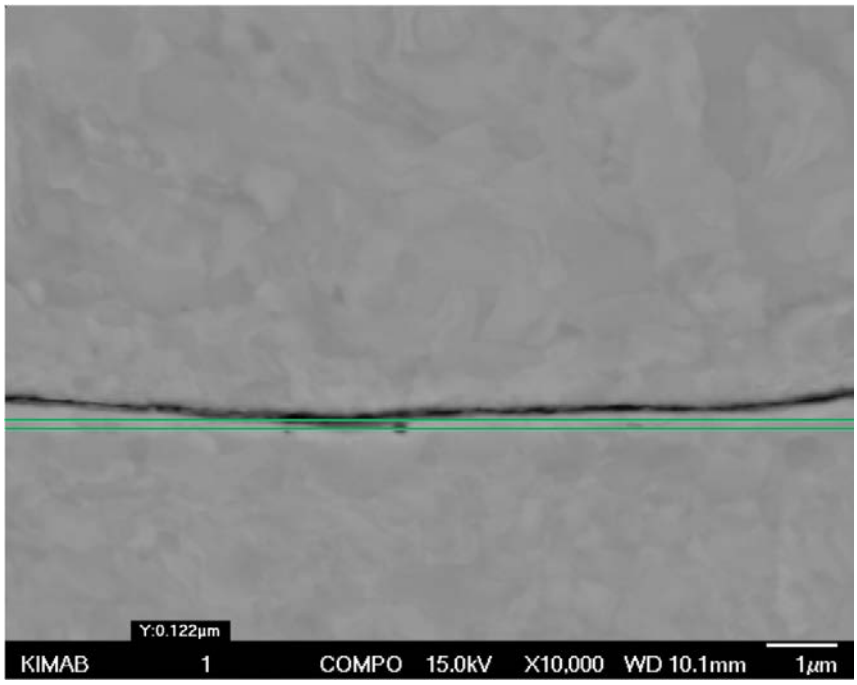

Figure D-21. *Coupon Bio-A S10-2 (bottom) (BEI). The sulphide layer was measured as being 122 nm thick.*

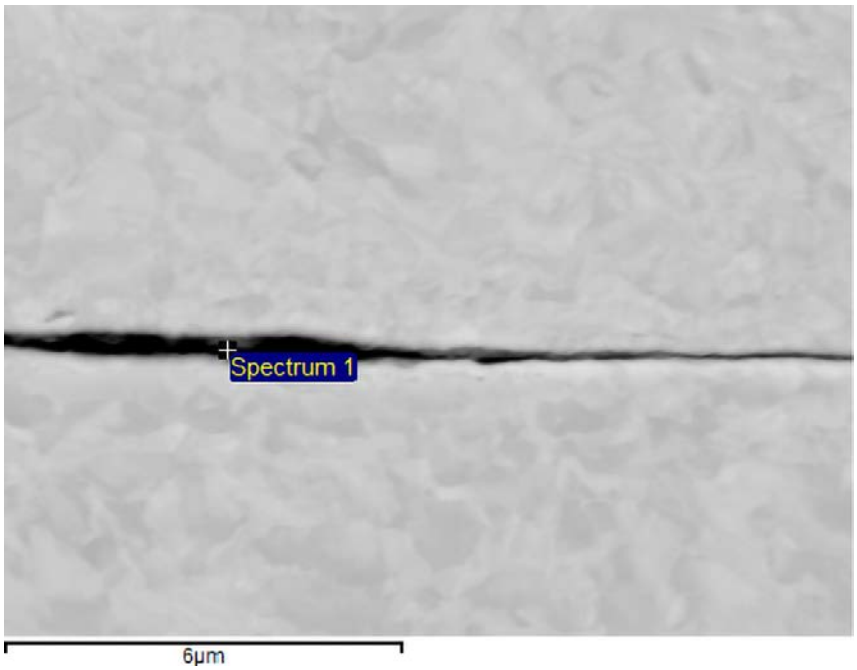

Figure D-22. *EDS analysis of sulphide layer.*

Element (wt%)	1
C	2.64
O	4.61
Si	0.49
S	1.04
Ca	0.67
Cu	90.55
Total:	100.00

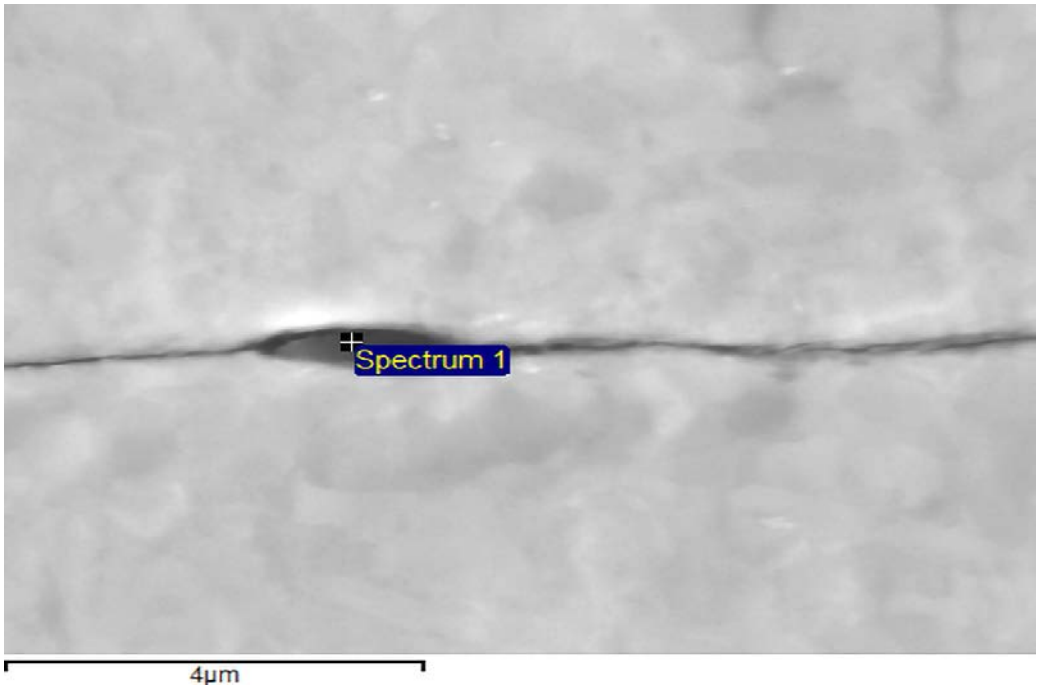

Figure D-23. *EDS analysis of sulphide layer.*

Element (wt%)	1
O	5.87
S	0.95
Cl	0.38
Cu	92.80
Total:	100.00

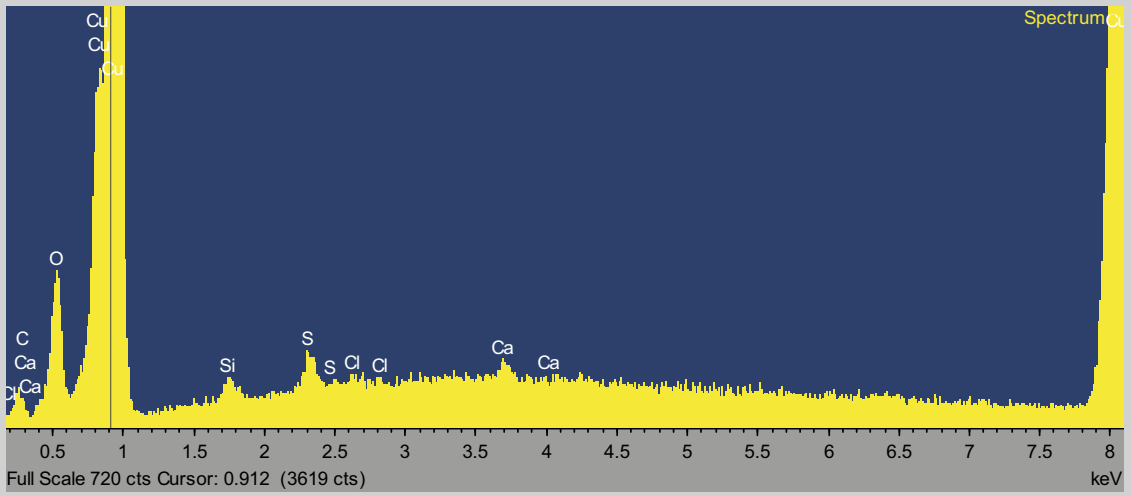

Figure D-24. *EDS spectrum for Bio A coupon 10-2, showing presence of sulphur, chlorine and calcium. Silicon is also present but is most likely residue from the coupon preparation (SiO_2 in polishing paste).*

Bio B – coupon 7-6

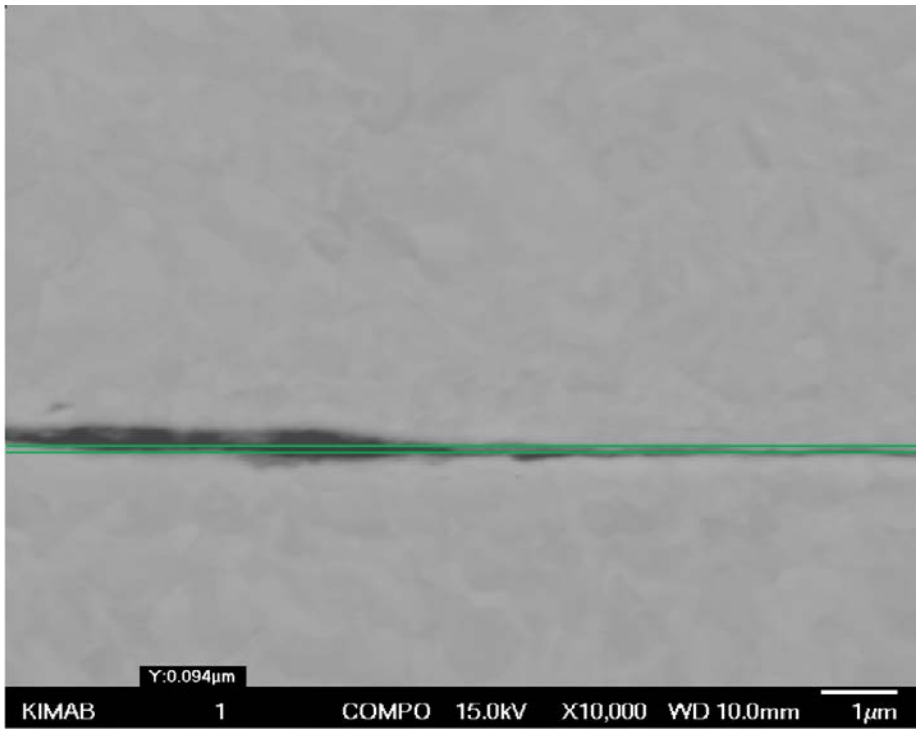

Figure D-25. *Coupon Bio-B S7-6 (top) (BEI). The sulphide layer was measured as being 94 nm thick.*

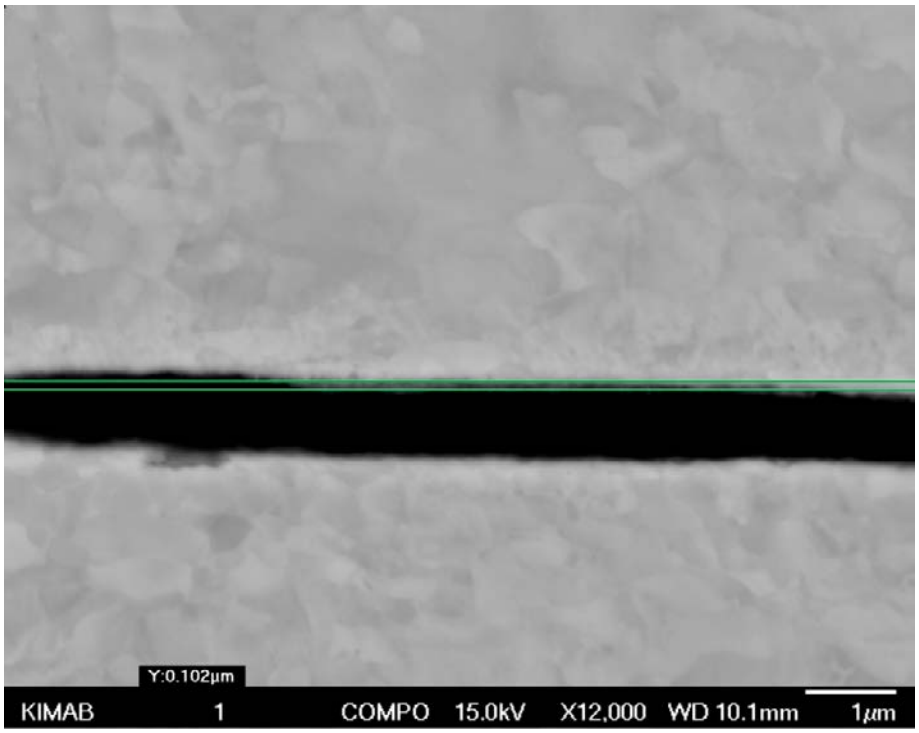

Figure D-26. *Coupon Bio-B S7:6 (top) (BEI). The sulphide layer was measured as being 102 nm thick.*

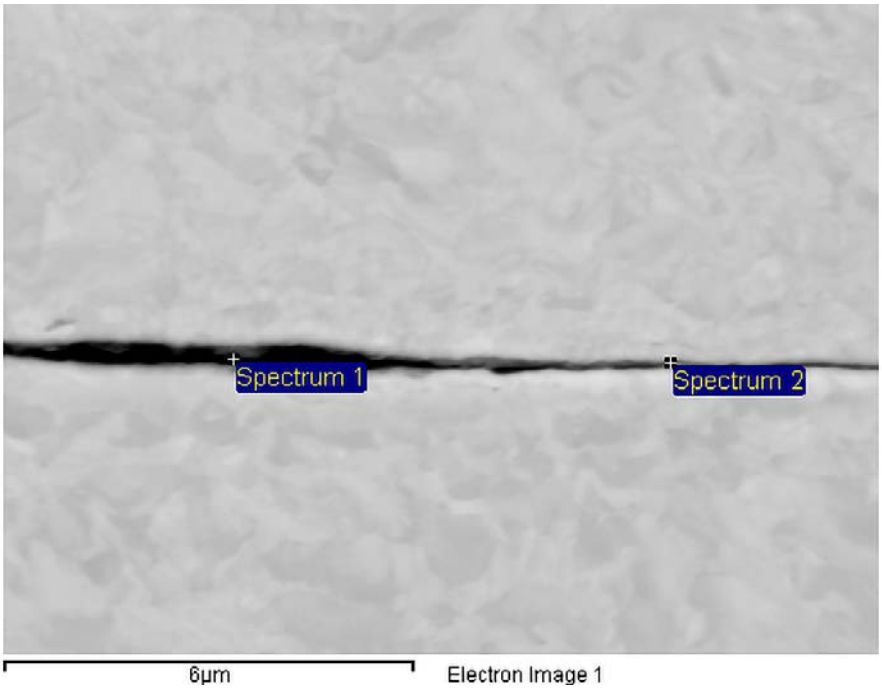

Figure D-27. *EDS analysis point for sulphide layer.*

Element (wt%)	1	2
O	3.13	0.92
S	0.74	0.32
Cl	0.27	0.13
Ca	0.35	0
Cu	95.52	98.65
Total:	100	100

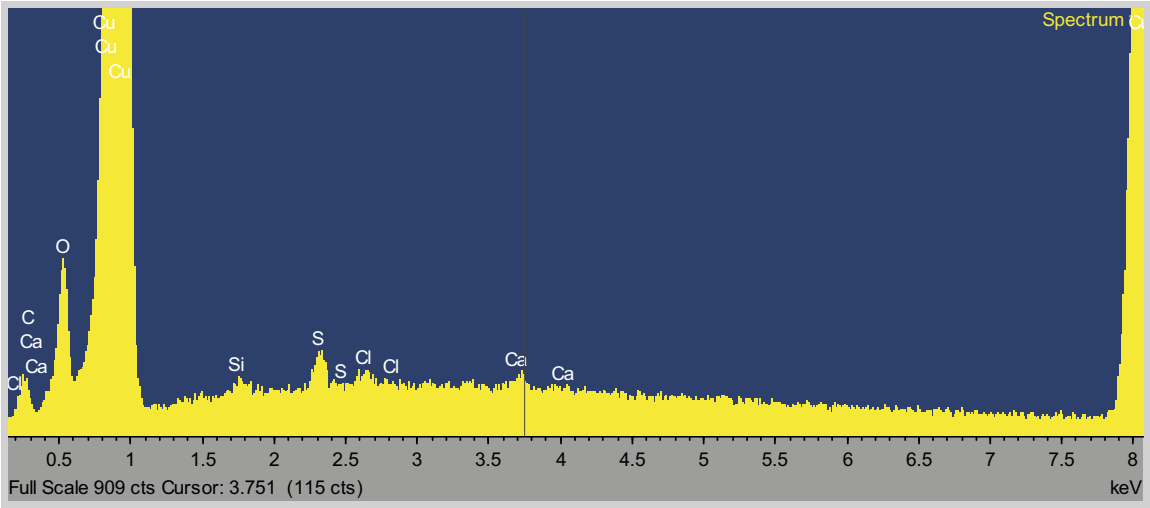

Figure D-28. *EDS spectrum for Bio B coupon 7-6, showing presence of sulphur, oxygen, chlorine and calcium. Silicon is also present but is most likely residue from the coupon preparation (SiO2 in polishing paste).*

Bio C – coupon 8-6

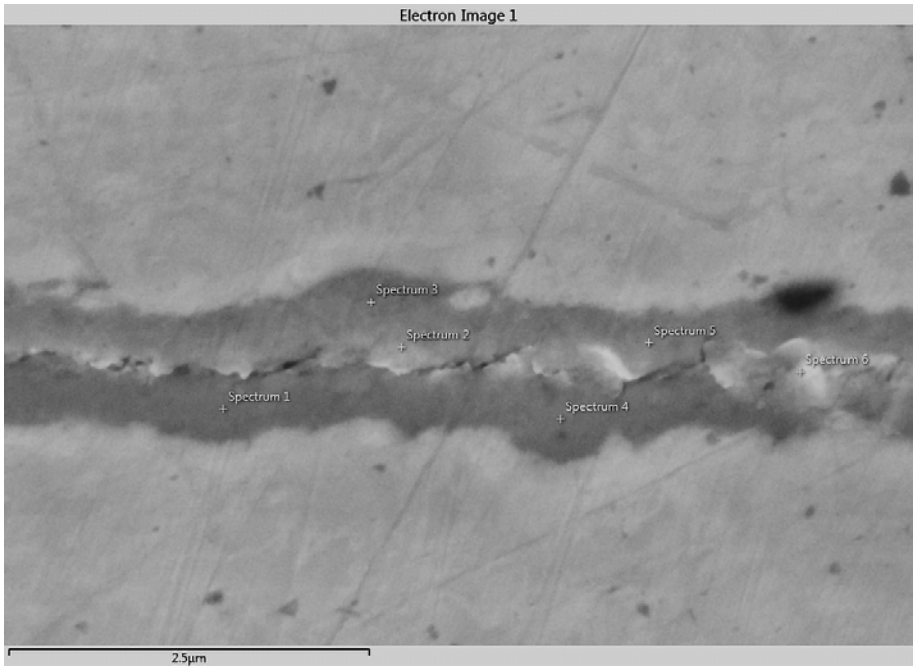

Figure D-29. *SEM image and EDS analysis on the cross section of coupon 8-6 (Bio C).*

Element (wt%)	1	2	3	4	5	6
O	2.58	2.63	0.39	0.88	0.34	0.34
S	15.4	16.26	1.27	4.61	0.42	1.15
Cl	0.54	0.59	0	0	0	0
Ca	0.14	0.15	0	0	0	0
Cu	81.34	80.36	98.34	94.51	99.23	98.51
Total:	100	100	100	100	100	100

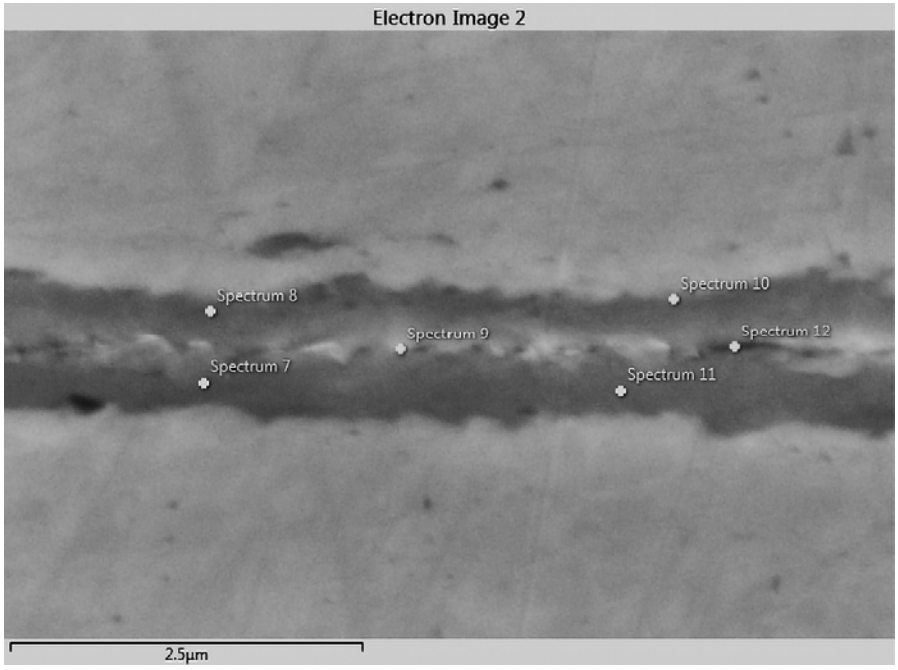

Figure D-30. *SEM image and EDS analysis on the cross section of coupon 8-6 (Bio C).*

Element (wt%)	7	8	9	10	11	12
O	2.35	2.23	2.5	4.61	0	1.63
S	16.76	16	15.05	14.15	1.96	15.42
Cl	0.59	0.47	0.5	0.91	0	0
Ca	0.15	0.19	0	0	0	0
Cu	80.15	81.11	81.94	80.34	98.04	82.96
Total:	100	100	100	100	100	100

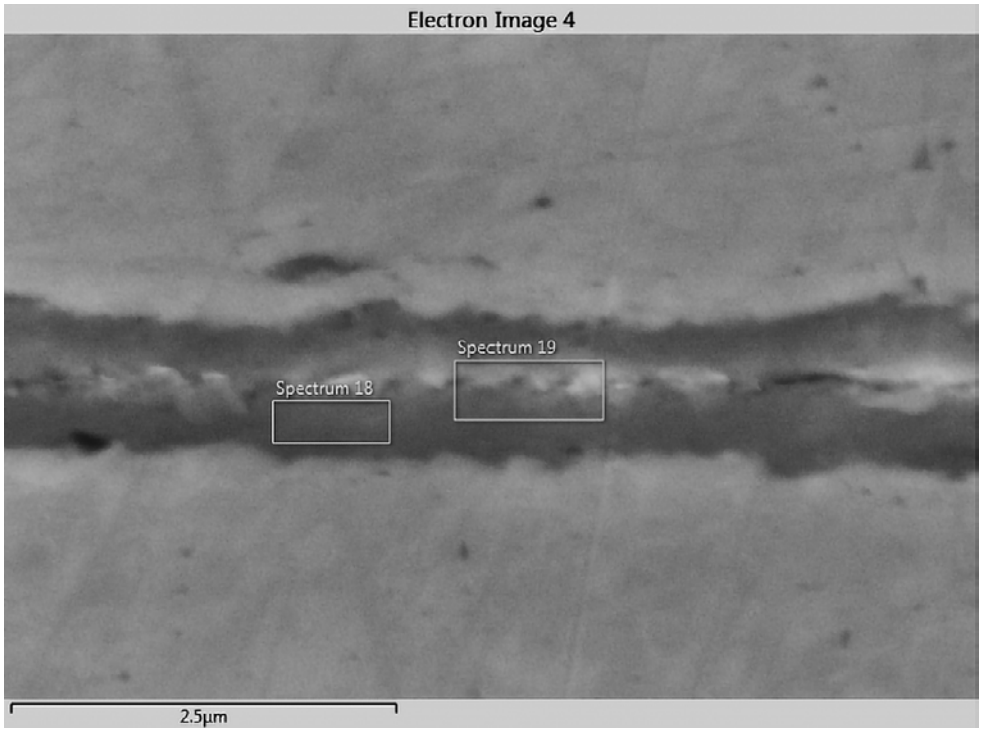

Figure D-31. *SEM image and EDS analysis on the cross section of coupon 8-6 (Bio C).*

Element (wt%)	18	19
O	2.14	3.85
S	16.92	13.98
Cl	0.5	0.71
Ca	0	0.16
Cu	80.43	81.3
Total:	100	100

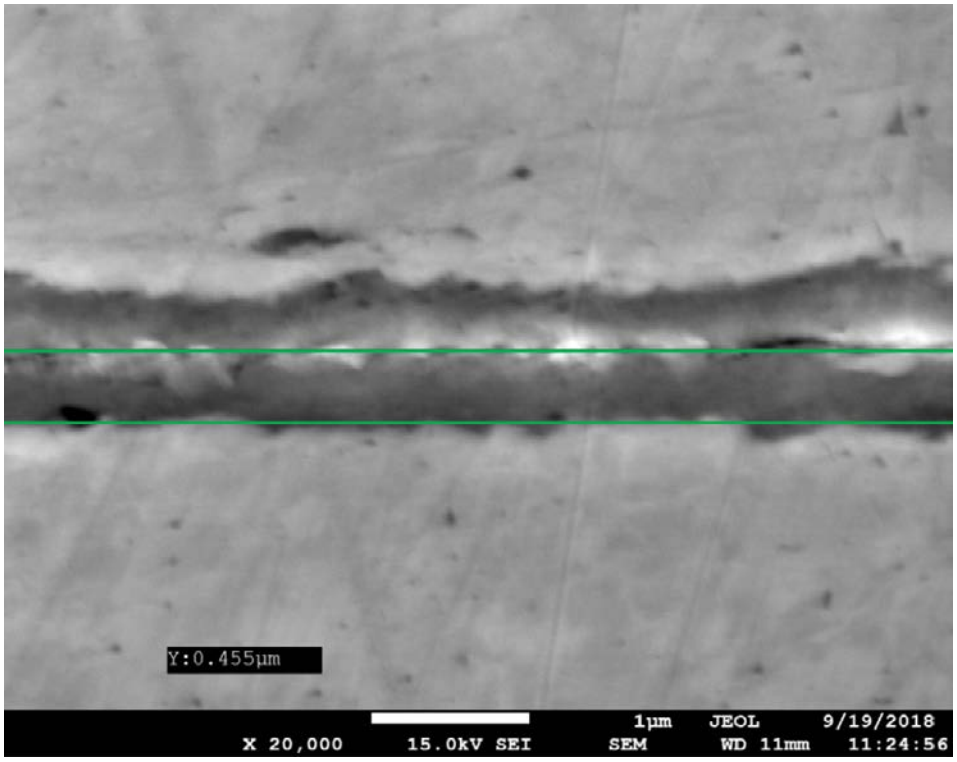

Figure D-32. *SEM image on the cross section of coupon S8-6 (Bio C). The sulphide layer was measured as being 0.46 µm thick.*

Bio D – coupon 8-1

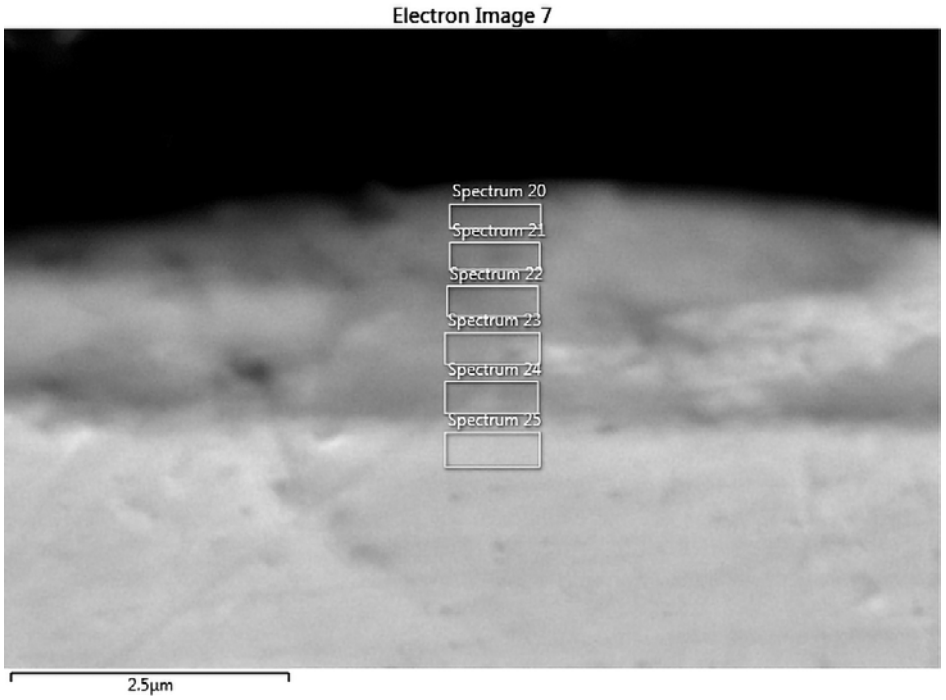

Figure D-33. *SEM image and EDS analysis on the cross section of coupon 8-1 (Bio D).*

Element (wt%)	20	21	22	23	24	25
O	9.41	7.02	5.28	4.23	3.34	1.39
Si		0.52	0.22	0.23	0.8	
S	17.65	20.38	20.48	19.02	14.5	2.63
Cl	0	0.19	0.3	0.2	0.25	0
K	0.48	0.34	0.19	0	0	0
Ca	3.17	2.32	1.54	0.74	0.4	0
Cu	69.29	69.22	72	75.58	80.71	95.99
Total:	100	100	100	100	100	100

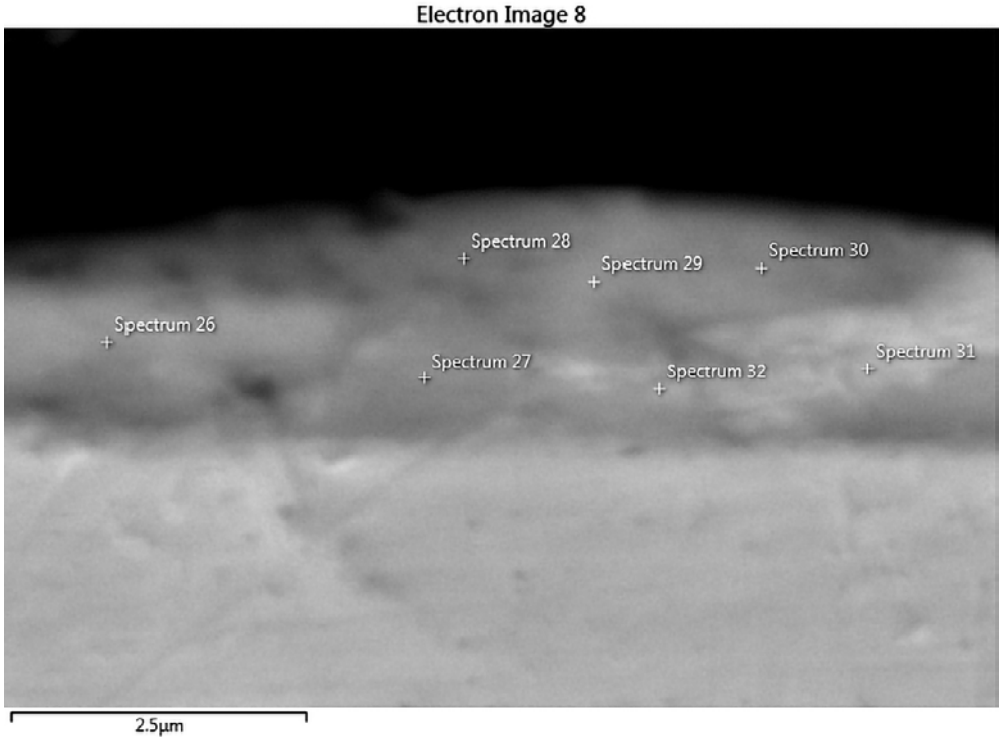

Figure D-34. *SEM image and EDS analysis on the cross section of coupon 8-1 (Bio D).*

Element (wt%)	26	27	28	29	30	31	32
O	4.06	3.78	7.66	5.39	5.08	4.22	5.2
Si	0.15	0	0.44	0.24	0.28	0.16	0.51
S	21.04	19.52	19.73	21.36	21.87	14.7	14.07
Cl	0.13	0	0.18	0.19	0.15	0.2	0.17
K	0	0	0.21	0.21	0.2	0	0
Ca	0.82	0.64	2.51	1.56	1.16	0.43	0.8
Cu	73.79	76.05	69.27	71.06	71.28	80.29	79.25
Total:	100	100	100	100	100	100	100

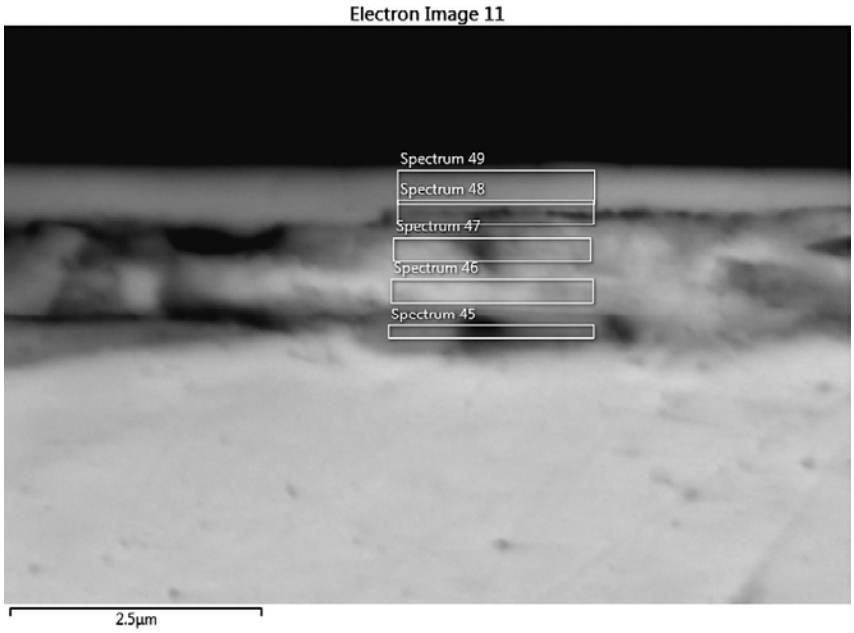

Figure D-35. *SEM image and EDS analysis on the cross section of coupon 8-1 (Bio D).*

Element (wt%)	45	46	47	48	49
O	2.82	4.37	4.83	4.36	4.27
Si	4.35	1.11	0.22	0.2	
S	12.56	7.2	10.38	18.79	22.47
Cl	0	0.29	0.2	0.21	0
K	0	0	0	0.17	
Ca	0.21	0.37	0.69	0.75	0.52
Cu	80.05	86.67	83.66	75.53	72.73
Total:	100	100	100	100	100

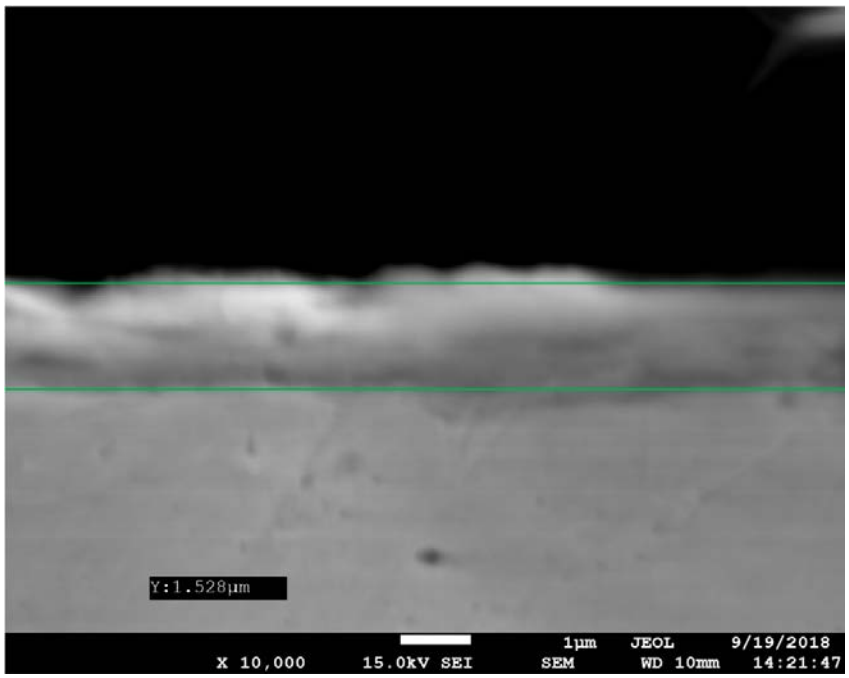

Figure D-36. *SEM image on the cross section of coupon S8-1 (Bio D). The sulphide layer was measured as being 1.5 µm thick.*

Control G – coupon 7-8

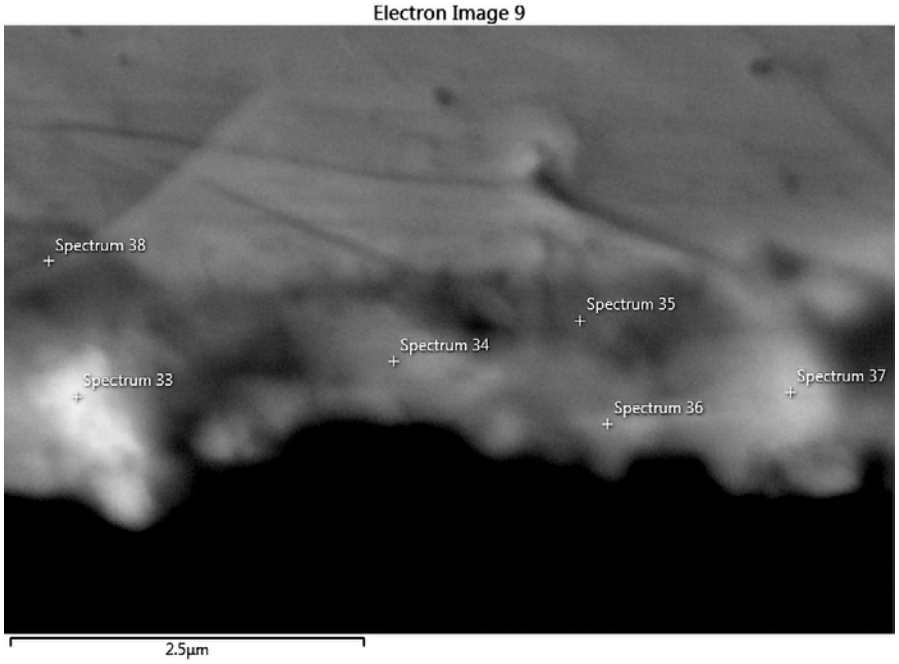

Figure D-37. *SEM image and EDS analysis on the cross section of coupon 7-8 (Control G).*

Element (wt%)	33	34	35	36	37	38
O	9.39	6.81	7.23	12.03	8.88	5.86
S	10.56	13.19	6.27	7.39	7.35	9.75
Cl	0.46	0.43	0.53	0.46	0.45	0.43
K		0	0.27	0.42	0.19	
Ca	2.86	2.04	2.62	5.52	3.71	1.73
Cu	76.74	77.52	83.07	74.2	79.42	82.24
Total:	100	100	100	100	100	100

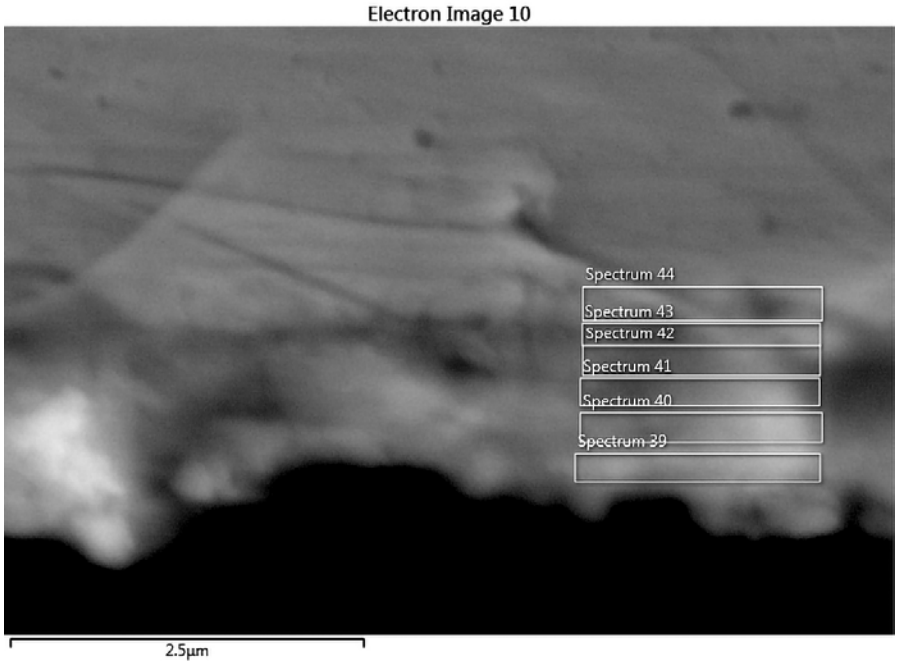

Figure D-38. *SEM image and EDS analysis on the cross section of coupon 7-8 (Control G).*

Element (wt%)	39	40	41	42	43	44
O	11.71	9.61	8.01	6.95	5.31	3.06
S	7.97	6.55	8	7.91	5.81	2.18
Cl	0.49	0.36	0.56	0.55	0.32	0.21
K	0.43	0.29	0.21	0.16	0	0
Ca	5.27	4.81	3.99	2.9	1.95	0.98
Cu	74.13	78.38	79.22	81.53	86.62	93.58
Total:	100	100	100	100	100	100

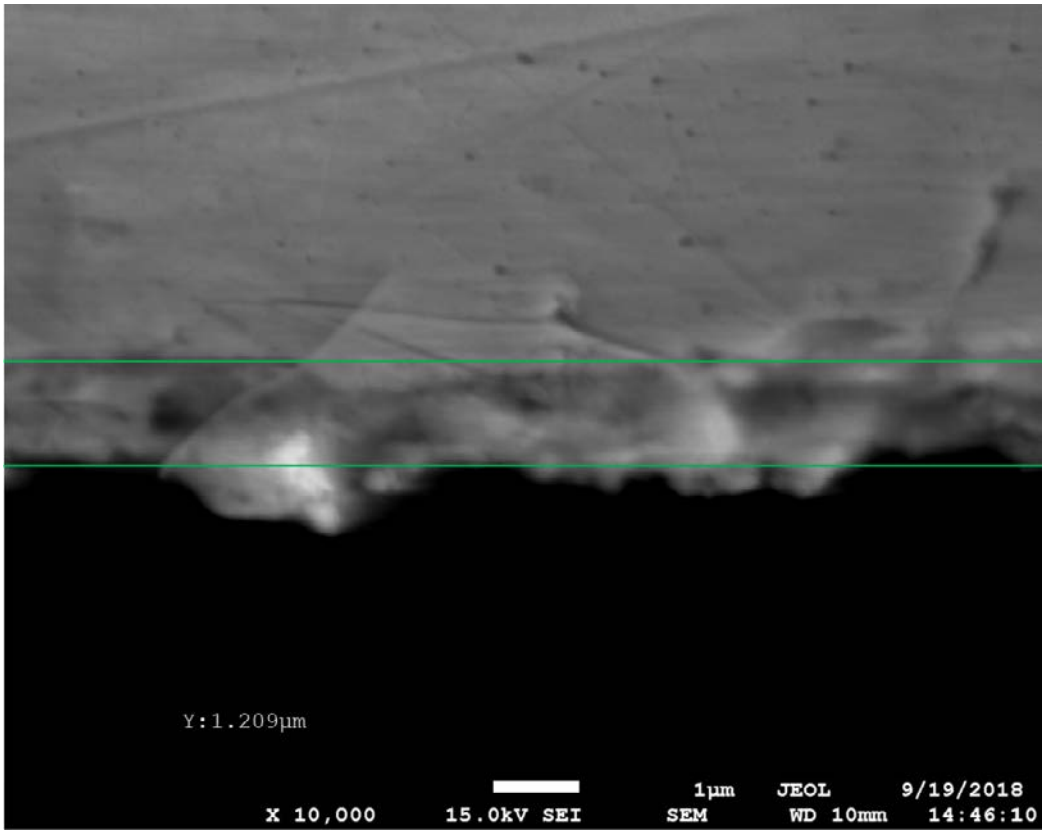

Figure D-39. *SEM image on the cross section of coupon S7-8 (Control G). The sulphide layer was measured as being 1.2 µm thick.*

D3 Surface analyses of coupons from Gas C and Gas D exposures

One coupon each from Gas C and Gas D were analysed using SEM/EDS on the surfaces. The following images and EDS analysis results are included only for information and are not discussed in the main body of the report. The EDS analyses show that the surface deposits mainly consist of Cu and S. The presence of Na and Cl could be due to the salts used in the experiments to control the humidity in the test chamber.

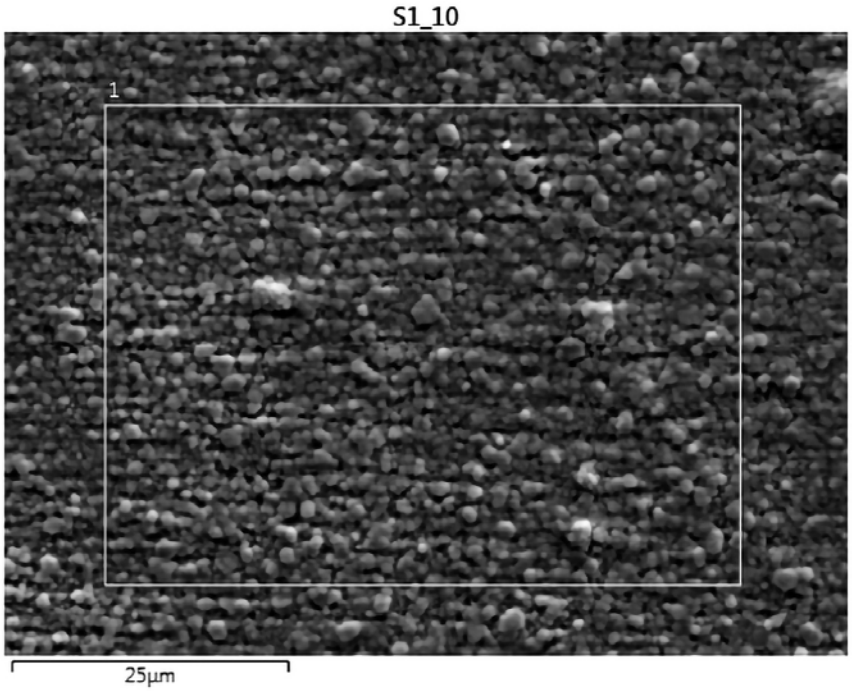

Figure D-40. *SEM backscatter image of surface of coupon S1-10 (Gas C).*

Element (wt%)	1
O	0.49
Si	0.16
S	17.47
Cl	0.50
Cu	81.38
Total:	100.00

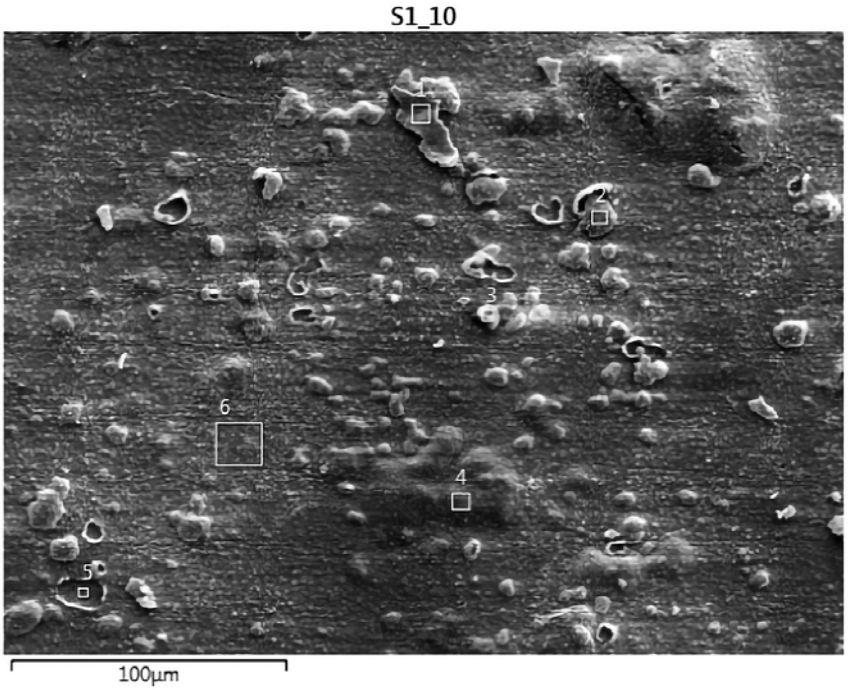

Figure D-41. *SEM backscatter image of surface of coupon S1-10 (Gas C).*

Element (wt%)	1	2	3	4	5	6
O	0.42	0.42	0.80	0.35	0.22	0.31
Na	1.10	1.13	0.43		7.76	
Si	0.08	0.04	0.06	0.02	0.05	0.07
S	18.91	17.64	17.96	17.89	16.14	18.57
Cl	1.55	3.05	1.25	0.15	4.90	0.63
Cu	77.94	77.71	79.50	81.59	70.92	80.42
Total:	100.00	100.00	100.00	100.00	100.00	100.00

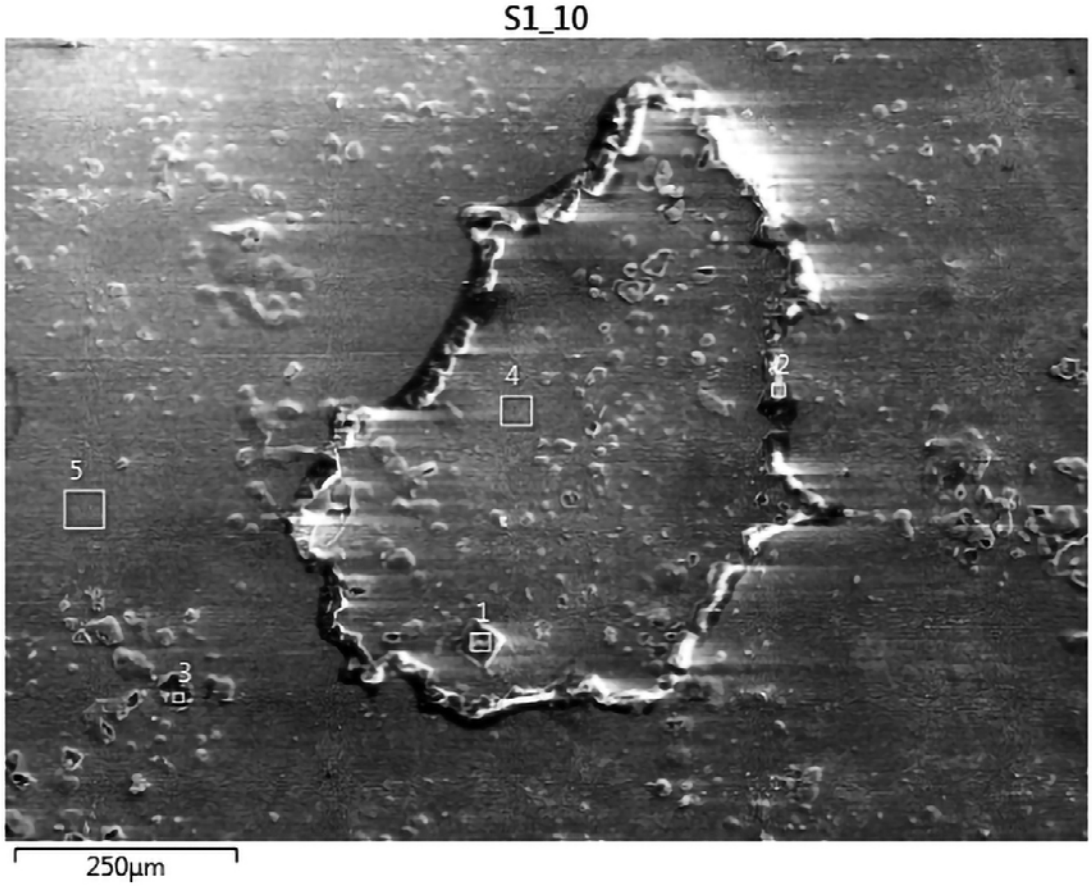

Figure D-42. *SEM backscatter image of surface of coupon S1-10 (Gas C).*

Element (wt%)	1	2	3	4	5
O	0.44	0.75	0.25	0.49	0.38
Na	38.45	38.80	33.12	2.53	
Si	0.07	0.11	0.08	0.06	0.06
S	0.53	0.85	5.99	17.93	18.59
Cl	60.09	57.89	33.48	2.05	0.30
Cu	0.42	1.60	27.08	76.94	80.67
Total:	100.00	100.00	100.00	100.00	100.00

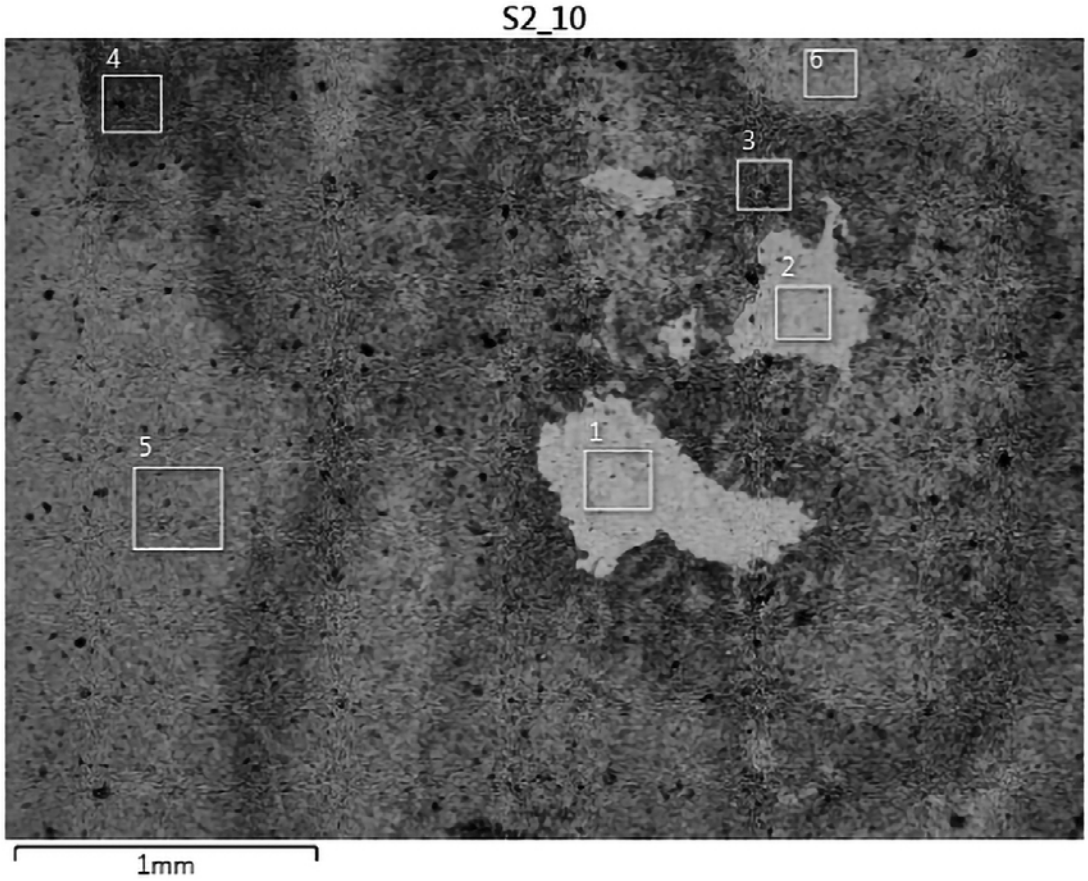

Figure D-43. *SEM backscatter image of surface of coupon S2-10 (Gas D).*

Element (wt%)	1	2	3	4	5	6
O	0.52	0.60	1.04	0.73	0.80	0.71
Al	0.25	0.23	0.18	0.18	0.20	0.20
S	6.13	6.02	19.54	19.41	19.25	19.22
Cu	93.10	93.14	79.24	79.68	79.75	79.87
Total:	100.00	100.00	100.00	100.00	100.00	100.00

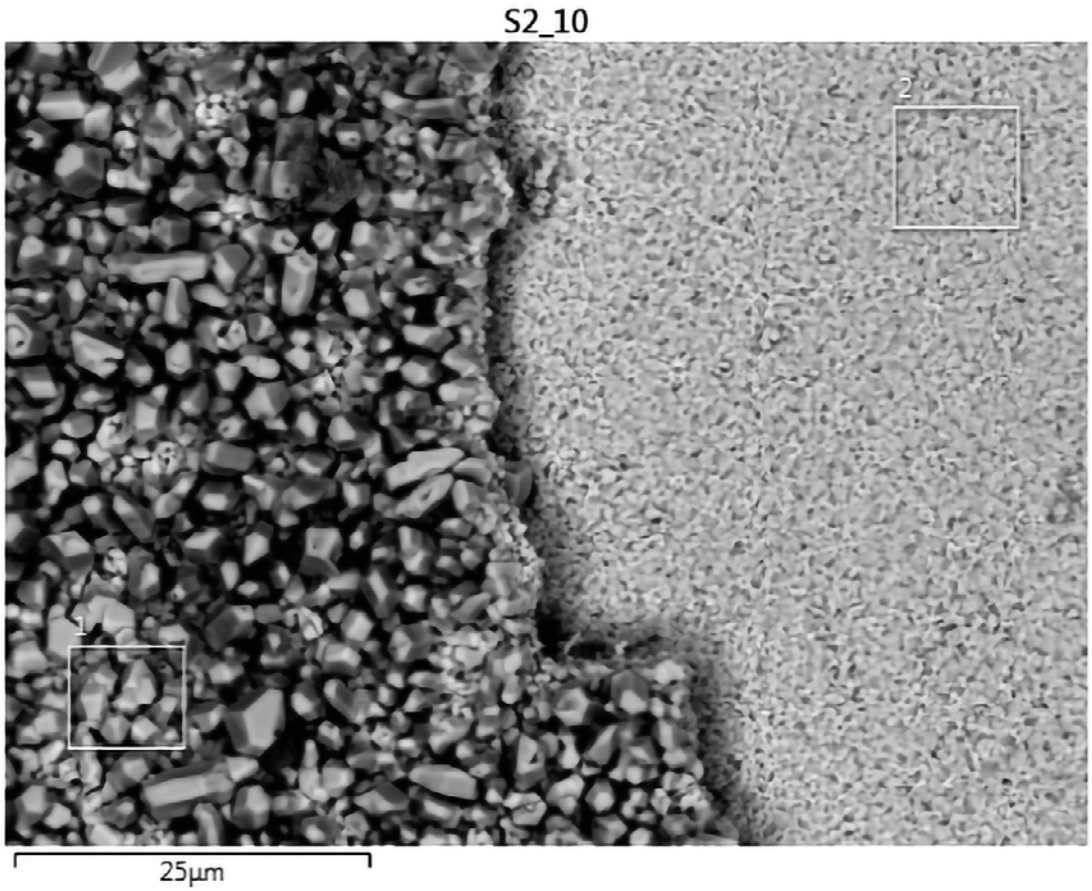

Figure D-44. *SEM backscatter image of surface of coupon S2-10 (Gas D).*

Element (wt%)	1	2
O	0.42	0.28
S	19.13	6.07
Cu	80.45	93.65
Total:	100.00	100.00